Advanced power converters for universal and flexible power management in future electricity network - Report on Control Strategies

Ciobotaru, Mihai; Iov, Florin; Zanchetta, Pericle; Biffarette, Steffano

Publication date:
2008

Document Version
Publisher's PDF, also known as Version of record

UNIFLEX-PM

019794 (SES6)

Advanced Power Converters for
Universal and Flexible Power Management in
Future Electricity Networks

DELIVERABLE D5.1

<Report on Control Strategies >

Report Version:	First Issue	
Report Preparation Date:		
Classification:	**Public**	
Contract Start Date:	01.03.2006	Duration: 3 years

Project Co-ordinator:	**Areva T&D Technology Centre**
Partners:	**University of Notthingham**
	Aalborg University
	Ecole Polytechnique Federale de Laussane
	Universita degli Studi di Genova
	ABB (Secheron)
	Dynex Semiconductor
	European Power Electronics and Drives Association

Project co-funded by the European Community under the Sixth Framework Programme – Priority 6.1.ii (Sustainable Energy Systems)

DELIVERABLE EXECUTIVE SUMMARY

Project Number: **019794 (SES6)**
Project Acronym: **UNIFLEX-PM**
Title: **Advanced Power Converters for Universal and Flexible Power Management in Future Electricity Network**

Deliverable No. D5.1
Due date: 30 May 2008
Delivery date: 31 May 2008

Short Description
The present document summarizes the work that has been done in Work Package 5 (WP5) where the focus is on modelling and control of the Uniflex-PM system. The models used in the WP5 are described in detail. Since the grid synchronization and monitoring techniques play an important role in the control of the Uniflex-PM system, a special attention is paid to this topic. The events in the electrical networks are treated in detail in terms of definitions and classifications from standards, origins, and surveys in different countries. A summary of the grid synchronization and monitoring methods is also given with a special focus on Phase Locked Loop systems. The response of the single and three phase PLLs is analyzed under different grid events. Four control strategies are studied in the WP5, namely: synchronous reference frame control, predictive control stationary reference frame control with Proportional Resonant current controllers and natural reference frame control with Proportional Resonant current controllers. These control strategies are evaluated under different grid conditions such as voltage excursions, voltage unbalances, phase jumps and short-circuits in the Point of Common Coupling. Finally, some conclusions and recommendations for future work are given.

Authors:
Aalborg University, Denmark
Mihai Ciobotaru
Florin Iov

University of Nottingham, UK
Yue Fan
Steffano Bifaretti
Pericle Zanchetta

Partners Contributed: Aalborg University and University of Nottingham
Made available to: PU

REPORT DETAILING CONVERTER APPLICATIONS IN FUTURE EUROPEAN ELECTRICITY MARKET

		YES	NO
Distribution List:	AREVA	✓	
	UNOTT	✓	
	AAU	✓	
	EPFL	✓	
	UGDIE	✓	
	ABB	✓	
	DSL	✓	
	EPE	✓	
	EC DIRECTORATE J – ENERGY	✓	

E					
D					
C					
B					
A					
	30.05.2008	AAU and UNOTT	AAU and UNOTT		PU
Rev.	Date	Drafted	Checked	Approved	Status*

* I: Internal; PP: Restricted to Programme participant; RE: Restricted to specified group; CO: Confidential; PU: Public

UNIFLEX-PM REFERENCE	W5 AU	DV	2001		30/05/08
Internal partner reference:	Filing N°	Doc.Type	Order N°	Rev. N°	Date

REVISION

CONTENTS

LIST OF FIGURES

LIST OF TABLES

ACRONYMS AND ABBREVIATIONS

AC	Alternating Current
CHB	Cascaded H-Bridge
DC	Direct Current
DSC	Delay Signal Cancellation
IM	Isolation Module
PCC	Point of Common Coupling
PI	Proportional Integral
PLL	Phase Locked Loop
PR	Proportional Resonant
PWM	Pulse Width Modulation
SOGI	Second Order Generalized Integrator
THD	Total Harmonic Distortion

1 INTRODUCTION

1.1 BACKGROUND

In 2001 the Green paper “Towards a European strategy for the security of energy supply”, the European Commission stressed the weaknesses of the European economy regarding energy dependence: “If no measures are taken, in the next 20 to 30 years 70 % of the Union’s energy requirements, as opposed to the current 50 %, will be covered by imported products. This dependence can be witnessed in all sectors of the economy. For example transport, the domestic sector and the electricity industry depend largely on oil and gas and are at the mercy of erratic variations in international prices. Enlargement will exacerbate these trends. In economic terms, the consequences of this dependence are heavy. It cost the Union some EUR 240 billion in 1999, or 6 % of total imports. In geopolitical terms, 45 % of oil imports come from the Middle East and 40 % of natural gas from Russia. The European Union does not yet have all the means to change the international market. The European Union’s long-term strategy for energy supply security must be geared to ensuring, for the well-being of its citizens and the proper functioning of the economy, the uninterrupted physical availability of energy products on the market, at a price which is affordable for all consumers (private and industrial), while respecting environmental concerns and looking towards sustainable development, as enshrined in Articles 2 and 6 of the Treaty on European Union. Security of supply does not seek to maximise energy self-sufficiency or to minimise dependence, but aims to reduce the risks linked to such dependence. Among the objectives to be pursued are those balancing between and diversifying the various sources of supply (by product and by geographical region).”

Those words are still relevant and the World Energy Council envisages that by 2050, the global energy mix will be made up of at least eight energy sources (coal, oil, gas, nuclear, hydro, biomass, wind and solar) with none expected to have more than a 30% share of the market. To address these issues, considerable effort is now being expended in the development of sustainable energy systems (PTA 1.1.6.1), which brings with it a wholesale re-organisation of the electricity network both technologically and in terms of the market.

The approach is summed up in [1] where Ph. Busquin states: “In addition to acting on the demand side and improving efficiency, ensuring the security of supply of clean energy requires the complete development of new sustainable energy generation and transformation technologies, such as renewable energies and fuel cells. Energy grids will need to be reinforced and managed by innovative supervisory systems, enhancing reliability and minimizing risks of major disruptions, such as the recent blackouts that occurred on both sides of the Atlantic. The final goal is to develop a sustainable system where hydrogen and electricity will be the main interchangeable energy carriers, with fuel cells having the ability to transform one into the other.” Further, it is stated: “The integration of renewable and other efficient distributed power generation sources into existing and future unified electricity systems represents an enormous technological challenge.”

To meet these challenges, a complex reorganisation of the electricity power industry has started in Europe, encouraging competition in both the wholesale and retail sectors of the market. "To facilitate the creation of an open single market in electricity, further effective interconnection of

Member State national grids is needed. In the near future, power utilities may still operate regulated distribution systems, but in the longer term the production, brokerage and sale of electricity and new power services will be a competitive function of the unified electricity market. This will require the transformation of conventional electricity transmission and distribution grid into an interactive and unified power supply network. Major technological and regulatory changes will be the basis of this new electricity service paradigm, which is itself a prime driver for the substantial European research effort in this area. Removing the geographical constraints on the delivery of power supplies will lead to increased competition and enhanced quality, reliability, security and safety".

Distributed generation (DG) will play a key role in this novel concept. This covers a broad range of technologies, including many renewable technologies that provide small-scale power at sites close to users. The greatest potential market for DG is displacing power supplied through the grid. On-site production minimises the transmission and distribution losses as well as the transmission and distribution costs, a significant part (above 30%) of the total electricity cost. As the demand for more and better quality electric power increases, DG can provide alternatives for reliable, cost-effective, premium power for homes and business. It can also offer customers continuity and reliability of supply, when a power outage occurs at home or in the neighbourhood, by restoring power in a short time.

1.2 ELECTRICITY NETWORK: PRESENT AND FUTURE

Today's electricity network is the result of technological and institutional development over many years, with most of the electricity generated in large power stations and transmitted through high-voltage transmission systems [1] as shown in Fig. 1.1

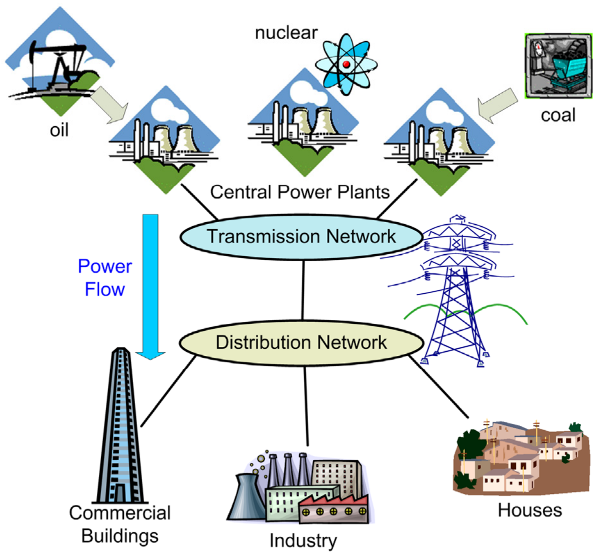

Fig. 1.1. General layout of the existing electricity network.

The power is delivered through a passive infrastructure to consumers. Then, it is delivered to consumer via medium and low-voltage distribution system [1]. The power flow in this arrangement is only in one direction: from the central power stations to the consumers. Typically, such a layout for the electricity network leads to a national or regional monopoly of the supplier acting both at the transmission and distribution level.

Since most of the European countries have started to liberalize the electricity market, this monopoly will disappear. In order to enable the electricity market multiple transmission system operators (TSOs) as well as distribution system operators (DSOs) will operate the electricity network transparently and without discrimination under the governance of a regulator [1]. This scenario requires an increase penetration of the renewable energy resources (RES) and other distributed generation (DG) and an active role for DSOs in controlling the network stability, optimising central and distributed power inputs into the network, interconnection, etc.

Moreover, in order to reach this goal, the entire architecture of the electricity network must be redesigned and the information and communication technologies (ICT) will be the key factor [1]. New features added by ICT and ICT-based applications as universal connectivity, services over internet and web, distributed intelligence, advanced fault handling, intelligent load shedding etc will transform the existing electrical grid into a smart one.

Among the different architectures of the future electricity systems three conceptual models are of interest [1]: Micro-grids, an "Internet" model and Active Networks supported by ICT.

In [1] is stated that "the active networks are envisaged as a possible evolution of the current passive distribution networks and technically and economically may be the best way to facilitate DG initially in a deregulated market". A possible layout of such an electricity network is shown in Fig. 1.2.

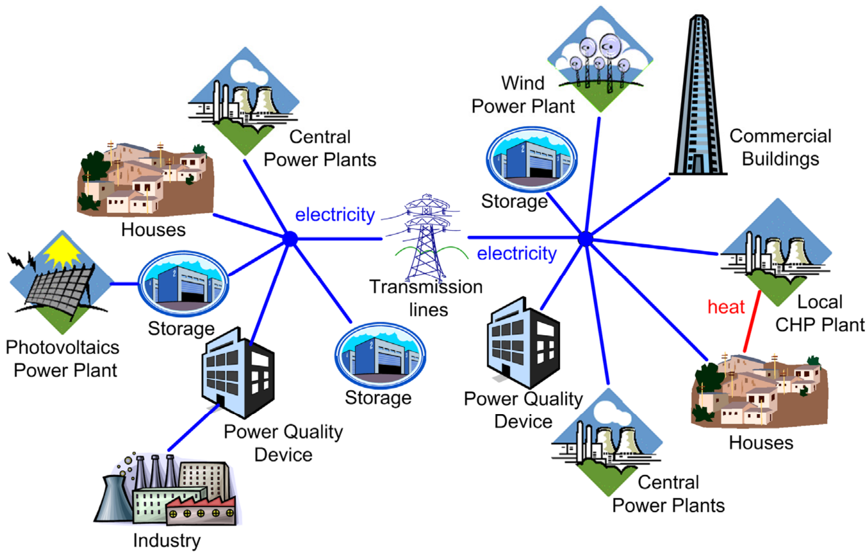

Fig. 1.2. Possible architecture of an active network with distributed/on-site generation and fully integrated network management.

"The structure of this model is based on increased interconnection as opposed to the current mostly linear/radial connection, relatively small local control areas, and the charging of system services based on connectivity" [1].
"With increased distribution of power input nodes as a result of DG, bi-directional energy flow is possible and new technologies are emerging that can enable the direct routing of electricity. New

power electronics systems offer ways of controlling the routing of electricity and also provide flexible DG interfaces to the network". [1]

1.3 UNIFLEX-PM PROJECT

1.3.1 General objectives

The UNIFLEX Project is concentrating on the development of key enabling technologies to reach the DG objectives. Among the key technologies required to make these new network concepts a reality, Power Electronics is to play a major role as 100% of electricity produced by renewable energy sources has to be converted by power electronic equipments. Additionally, power flow control using power electronic converters will be needed to ensure proper and secure work of the grid when submitted to the economical laws of the liberalized market. Without increased intelligence in power flow management, it will be impossible to secure a stable network with large numbers of small to medium sized dispersed generators. This is recognised in [1] under "The challenges", where it is stated "Power electronics: Devices such as FACTS are critical components of a future grid control infrastructure".

Implementation of the vision for a "Future European Electricity Grid" in which the conventional electricity transmission and distribution grid is transformed into an "interactive and unified power supply network" [1] is critically dependent on the development of power converters that have greater functionality, higher reliability, higher efficiency, lower cost and more sophisticated control than the state of the art. Power converters are absolutely central to the new network concepts in which innovative supervisory energy control systems are fundamental. Existing projects under FP5/FP6 (for example DG-FACTS, CRISP, DISPOWER, EU-DEEP) are defining new connection philosophies and the roles of power converters. Without innovation in power converters, attempts to realise the visions outlined in [3] and enshrined in these projects will fail.

The UNIFLEX-PM project brings together research in power converter topology and control with that in applications of new semiconductor devices. UNIFLEX-PM is highly flexible converter architecture, using advanced components and advanced control strategies that can be applied universally to meet the needs of the "Future European Electricity Grid". UNIFLEX-PM converters will have the functionality, performance, reliability and cost to allow the widespread penetration of power electronics, without which the desired network concepts cannot be realised. UNIFLEX-PM will deliver a key enabling technology within the Priority Thematic Area 1.1.6.1 "Sustainable Energy Systems"

1.3.2 Strategic impact

Establishment of a new paradigm for electricity networks in Europe in which there is large-scale integration of distributed energy resources is major element of the key strategic objective of the EU to secure a supply of energy that is clean sustainable and economical [1]. The impact of this will be to reduce dependence on fossil fuels and reduce climate change and pollution, which are of concern to all European citizens. In the new system, large numbers of small and medium sized generators and energy storage elements are interconnected through a fully interactive intelligent electricity network. It is well accepted that advanced power electronics is a key enabling technology for the new system [1] without which it has no future. ***This is why UNIFLEX-PM is needed, as the technology does not exist at present***. UNIFLEX-PM will provide the power electronics technology required and it therefore has the potential to make tremendous impact upon the implementation of DG which brings with it major benefits to European society such as:

- Reduced dependence on fossil fuels
- Reduction in climate change
- Reduction in pollution
- Sustainable energy supply
- Secure supply of energy
- Economic energy supply

1.4 GENERAL OBJECTIVES IN WP5

This workpackage focuses on research, through analysis and numerical simulation, of global control strategies for UNIFLEX-PM converter interactions with the system/load/sources to meet the requirements derived in WP2. There is a close interaction with WP3 since the tasks of local control (energy balance within the converter and modulation, for example) and global control are not decoupled if the system is to operate with high power quality and high efficiency. The global control strategy will determine the performance of the converter in the power system. Suitable control strategies will be established and will be tested in the hardware technology validation workpackage (WP7). Energy storage will play a very important part in power systems where the intermittent sources, such as wind and solar systems, have high penetration percentage, therefore, the energy management of storage elements integrated with a UNIFLEX-PM modular power conversion system will be investigated to realise a secured power supply system. Furthermore, the operation and performance of control strategies for converters in the transmission and distribution systems will be identified.

2 UNIFLEX-PM CONVERTER STRUCTURE

The Uniflex-PM converter structure is multi cellular and modular and it is based on the multi-level cascaded H-bridge topology with a DC-DC isolation stage [3].

This Chapter will present the general structure as well as the particular topologies used in WP5 for the Uniflex-PM system.

2.1 GENERAL STRUCTURE

The general layout of the Uniflex-PM system is shown in Fig. 2.1.

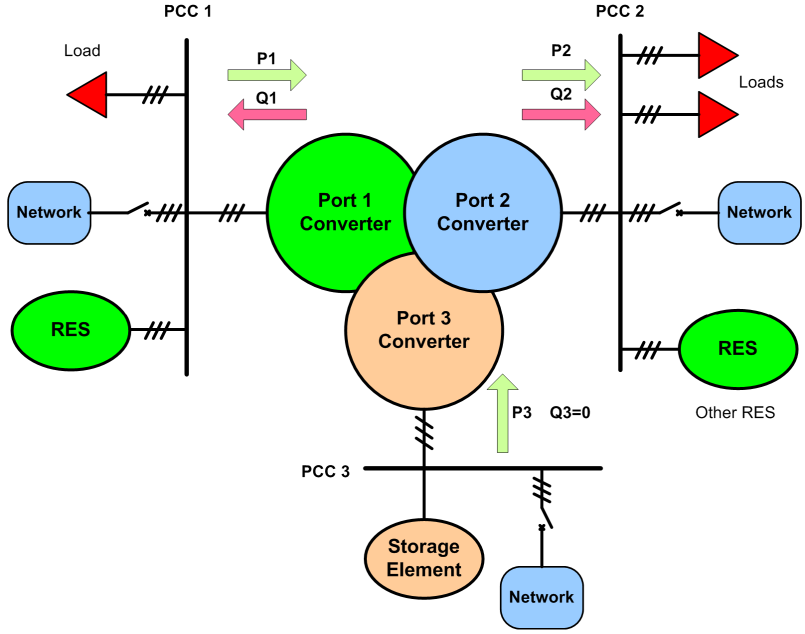

Fig. 2.1. General structure of the Uniflex-PM used in WP5.

The power converter is connected to medium voltage electrical networks on Port One and Port Two, while the Port Three is used for connection of an energy storage system. However, a connection to the low voltage electricity network is also possible in Port Three.

Each port is based on the multilevel cascaded H-bridge power converter with a DC-DC isolation module (VSI based module) [3]. Thus, a medium voltage operation and low harmonic distortion is achieved [4].

2.2 TWO PORT SYSTEM

A two port based structure with three series power modules per phase is considered in the analysis presented in §5 as shown in Fig. 2.2.

Since the Isolation Module (IM) for each branch has an independent control an equivalent capacitor is used instead in WP5 [4]. Thus, just the AC to DC modules are used in this work package.

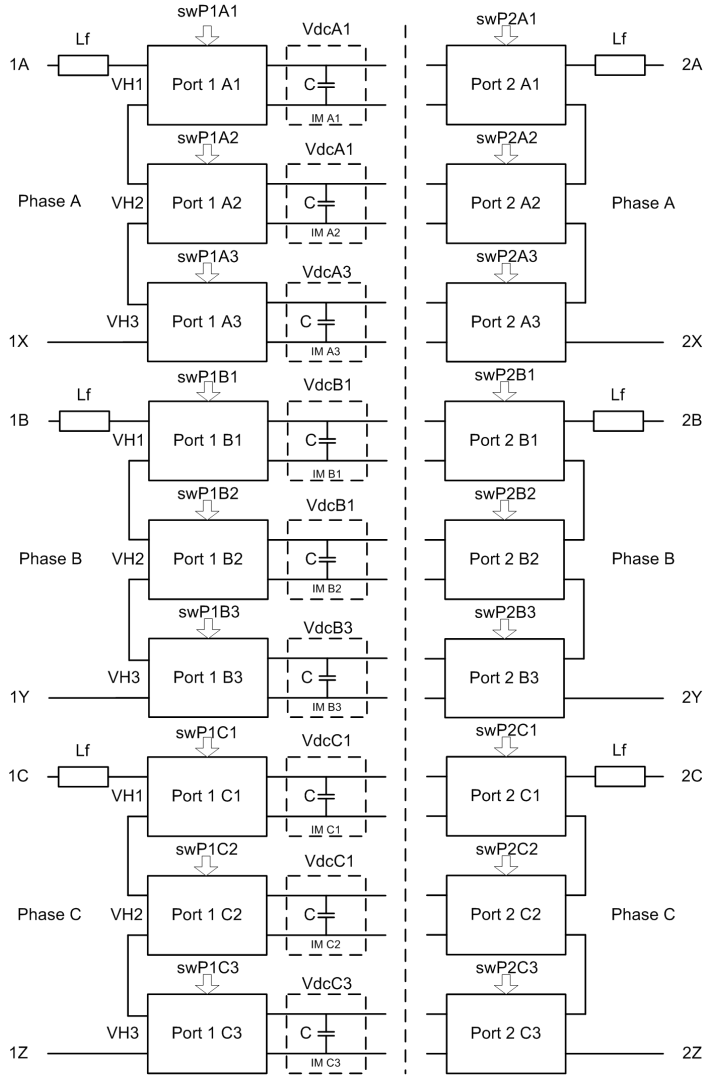

Fig. 2.2. Equivalent model per phase for the two port Uniflex-PM system.

The structure of a single phase H-bridge cell is shown in Fig. 2.3

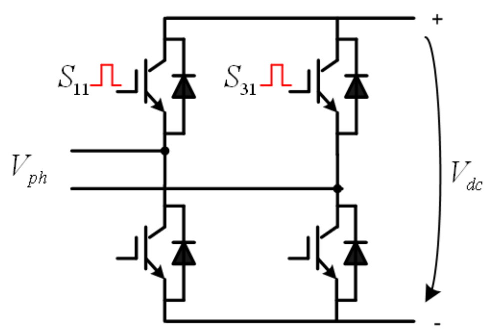

Fig. 2.3. Simplified diagram of a single-phase H-bridge cell.

The interleaving of the dc-link circuits is also considered for this system. A chart with the connection of the DC-link circuits for Port 1 and Port 2 is given in Table 2.1.

Table 2.1. Connection chart of the DC-link circuits for the two port system

Port 1	**Connection**	**Port 2**
Port 1 A1	→	Port 2 A1
Port 1 A2	→	Port 2 B1
Port 1 A3	→	Port 2 C1
Port 1 B1	→	Port 2 A2
Port 1 B2	→	Port 2 B2
Port 1 B3	→	Port 2 C2
Port 1 C1	→	Port 2 A3
Port 1 C2	→	Port 2 B3
Port 1 C3	→	Port 2 C3

2.3 MODULATION STRATEGY

A horizontally phase-shifted multicarrier modulation is used for the Uniflex-PM system in WP5 [3].

The multilevel cascaded H-bridge converter with H-bridge cells per phase leg has ***m*** voltage levels:

$$m = 2H + 1 \qquad (2.1)$$

Hence, a number of (m-1) triangular carriers are necessary [3] and [4]. These triangular carriers have the same frequency and the same amplitude. There is a phase shift between any two adjacent carriers [4]:

$$\varphi_{carrier} = \frac{2\pi}{m-1} \qquad (2.2)$$

This modulation strategy has as input three-phase reference signals for the phase voltages that are provided by the control strategy. In order to obtain the gate signals for the power switches these references are compared with the triangular carriers.

The principle of generating these gate signals is illustrated in Fig. 2.4 for a seven level CHB converter. The carriers one, two and three are used to generate gate signals for the upper switches in the left legs of the H-bridge cells The inverted signal of theses carriers will produce the gate signals for the upper switches in the right leg.

The output voltage of the module one v_{H1} is switched between zero and V_{dc} during the positive cycle of the reference signal or between zero and -V_{dc} during the negative cycle respectively as shown in Fig. 2.5.

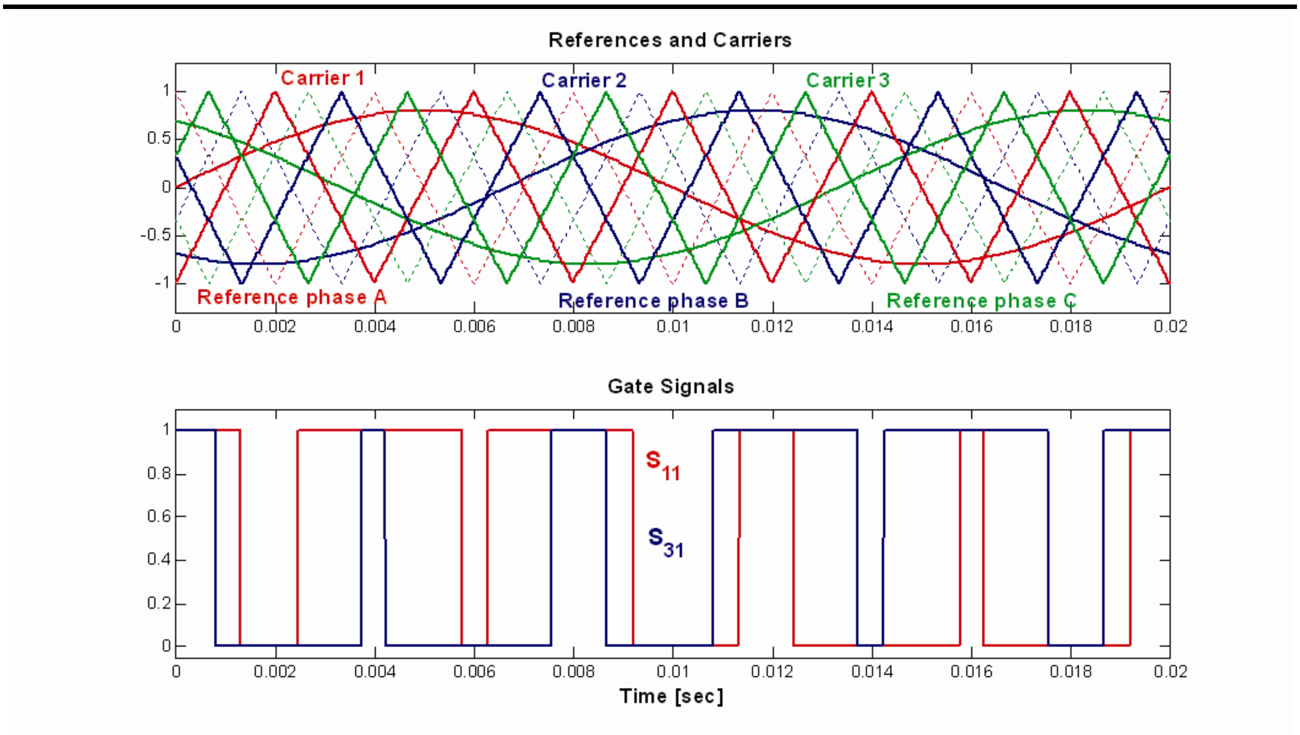

Fig. 2.4. Gate signal generation for a seven level CHB inverter.

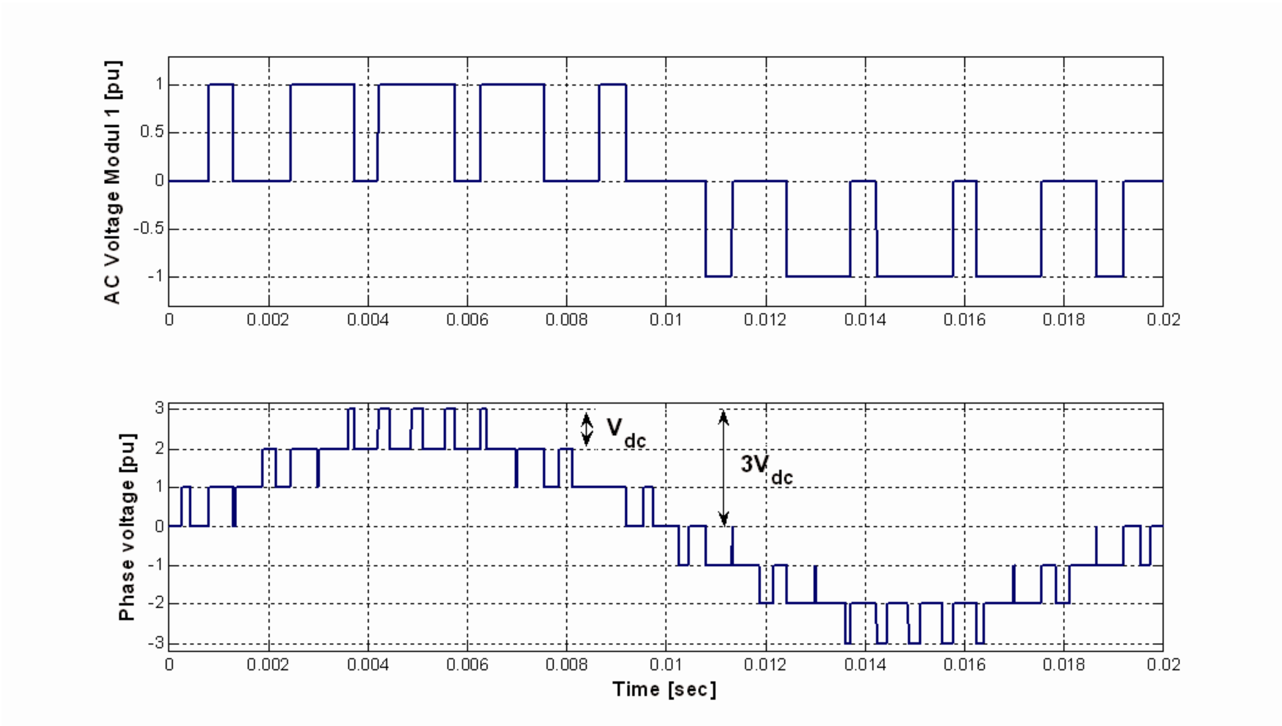

Fig. 2.5. AC voltages for a seven level CHB inverter.

In this example the frequency modulation index m_f is 5 and the amplitude modulation index m_a is 0.8 where:

$$m_f = \frac{carrier\ frequency}{fundamental\ frequency} \tag{2.3}$$

and

$$m_a = \frac{peak\ amplitude\ of\ reference}{peak\ amplitude\ of\ carrier} \tag{2.4}$$

The inverter phase voltage is equal with the sum of the individual AC voltage per module as shown in Fig. 2.5. Thus, a seven level voltage is obtained.

Notice that the frequency of the carrier depends on the fundamental frequency. Thus, in grid connected application where the grid frequency varies, the carrier frequency must be modify so that a constant frequency modulation index is maintained during the converter operation.

Considering a switching frequency for the power semiconductor devices $f_{sw,SCR}$ the inverter switching frequency is obtained as:

$$f_{sw,Inv} = (m-1)\cdot m_f \cdot f_{fundamental} = (m-1)\, f_{sw,SCR} \tag{2.5}$$

Thus, using a relatively low switching frequency per device, it is obtained a switching frequency for the converter that depends on the level number. In the considered case for a 50 Hz fundamental frequency and a frequency modulation index of 5, the switching frequency for each semiconductor device is 250 Hz while the switching frequency of the inverter is 1500 Hz.

2.4 SYSTEM MODELLING

2.4.1 Grid model

A grid model based on Thevenin equivalent is used as specified in [6] and [7]. A complete structure of this model is shown in Fig. 2.6.

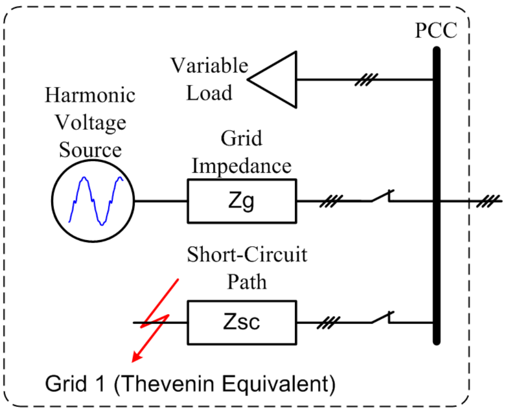

Fig. 2.6. Structure of the grid model used in WP5.

The grid model is characterized by a short-circuit power and a grid impedance with a ratio R_g / X_g of 0.1. This impedance ratio corresponds to a value of 83.4° for the grid voltage angle in the PCC while the short circuit power is ten times grater then the rated power of the Uniflex-PM system as recommended in [7]. A passive load with a rated power of 5% from the short circuit power of the grid and a power factor of 0.86 is also connected in the PCC. The short circuit path has an impedance ratio R_f / X_f of 0.2 [8]. Modifying the short-circuit resistance different voltage dips can be obtained.

The model implements also different harmonic contents and asymmetries in the grid voltages. The following standards for harmonic content up to the 25th harmonic order are considered:

- Voltage harmonic content in the PCC according to the Danish requirements for wind turbines connected to electrical networks with voltages below 100 kV [6];
- Standard EN 50160 [9];
- Standard EN 61000 [10];
- User defined levels.

The short-circuit path is modelled based on the equivalent electrical circuit approach.

2.4.1.1 Three-phase to ground short-circuit

The equivalent electrical diagram of a three-phase to ground short-circuit is given in Fig. 2.7.

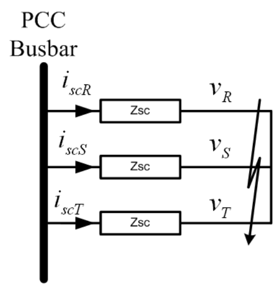

Fig. 2.7. Equivalent diagram of a 3-phase to ground short-circuit.

This short circuit can be described by the following equations for voltages and currents:

$$\begin{aligned} v_R &= v_S = v_T = 0 \\ i_R + i_S + i_T &= 0 \end{aligned} \quad (2.6)$$

2.4.1.2 Two-phase to ground short-circuit

The equivalent electrical diagram of a 2-phase to ground short-circuit is given in Fig. 2.8.

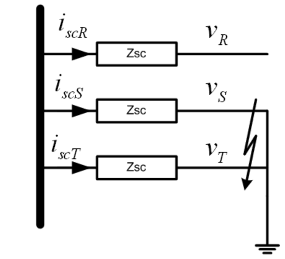

Fig. 2.8. Equivalent diagram of a 2-phase to ground short-circuit.

This short circuit can be described by the following equations for voltages and currents:

$$v_S = v_T = 0$$
$$i_R = 0 \tag{2.7}$$
$$i_S + i_T = 0$$

2.4.1.3 Two-phase short-circuit

The equivalent electrical diagram of a 2-phase short-circuit without ground is presented in Fig. 2.9

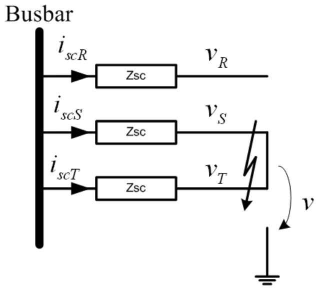

Fig. 2.9. Equivalent diagram of a 2-phase short-circuit.`

This short circuit can be described by the following equations for voltages and currents:

$$v_S = v_T \neq 0$$
$$i_R = 0 \tag{2.8}$$
$$i_S + i_T = 0$$

2.4.1.4 Single-phase to ground short-circuit

The equivalent electrical diagram of a 1-phase to ground short-circuit is given in Fig. 2.10.

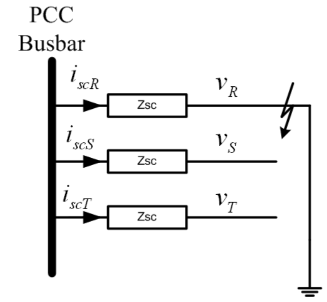

Fig. 2.10. Equivalent diagram of a 1-phase to ground short-circuit.

This short circuit can be described by the following equations for voltages and currents:

$$v_R = 0$$
$$i_R \neq 0 \qquad (2.9)$$
$$i_S = i_T = 0$$

2.4.2 Uniflex-PM system

All the modelling and simulation work done in WP5 is made using Matlab/Simulink environment. This tool offers a flexible platform for building and testing dynamic systems including their control. Different approaches have been used for modelling of the Uniflex–PM system using Matlab/Simulink

2.4.2.1 SimPowerSystems Blockset

SimPowerSystems is a design tool in the Simulink environment that allows to rapidly and easily build models that simulate power systems. The Uniflex-PM model used in this tool is based on the average model for the H-bridge as shown in Fig. 2.11 [3].

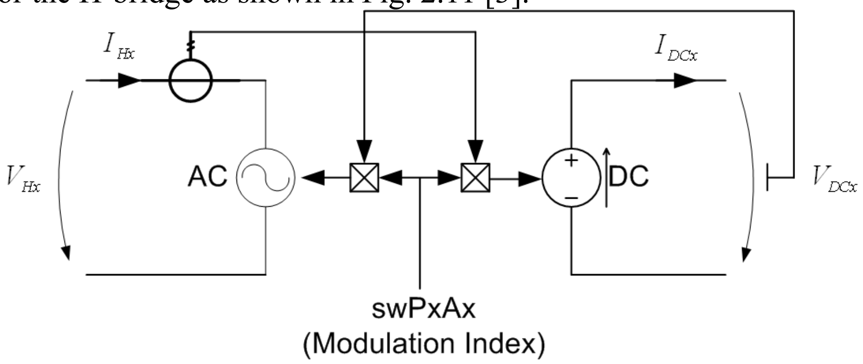

Fig. 2.11. Average model of the H-bridge.

2.4.2.2 PLECS

PLECS is a Simulink toolbox used for simulation of electrical circuits within the Simulink environment. Simulations are fast, due to the fact that components are taken to be ideal [11].

As shown on Fig. 2.12, circuits made with PLECS include resistors, inductors, capacitors, switches, and voltage and current sources all taken as ideal components. Voltages and currents can be measured using probes. These measurements can be used as feedback for the control within the Simulink environment or just viewed online using scopes.

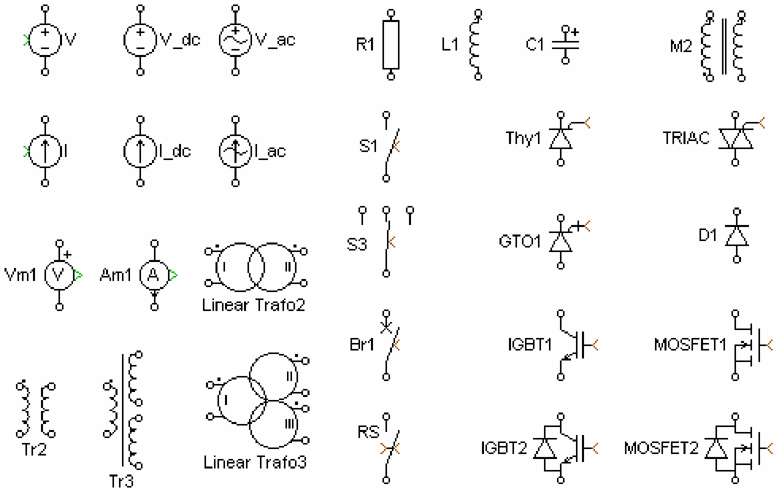

Fig. 2.12. Some of PLECS components used for circuit simulation.

Voltages and currents can only be viewed in graph windows using special probes. Matlab Simulink is very good in post processing of simulation results. Actually most of the simulation tools provide an interface for Simulink.

Using this toolbox it is possible to implement the power converter and other electrical circuits as a PLECS subsystem and the control as standard Simulink subsystem. In this tool only switching models can be used for the power converters.

2.4.2.3 C S-Function

An S-function is a computer language description of a Simulink block. S-functions can be written in MATLAB, C, C++ or Ada, These S-functions are compiled as MEX-files using the mex utility. As with other MEX-files, they are dynamically linked into MATLAB when needed. S-functions use a special calling syntax that enables the user to interact with Simulink's equation solvers. This interaction is very similar to the interaction that takes place between the solvers and built-in Simulink blocks. The form of an S-function is general and can accommodate continuous, discrete, and hybrid systems. S-functions allow the user to add new models to the Simulink built-in models. These new blocks can be written in MATLAB®, C, C++, Fortran, or Ada. An algorithm or model can be implemented in an S-function and then customize a user interface by using masking.

The main advantage of using this approach is that the user can interact in an efficient way with Simulink environment. As a result the models are usually faster than other implementation methods.

Since the Uniflex-PM system is very complex and some analysis requires long simulation time frames this approach may be very useful. Moreover, the model created in this format can be used for both average and switching models. The only difference is the inclusion of the PWM generator.

3 GRID SYNCHRONIZATION AND MONITORING

3.1 INTRODUCTION

This Chapter starts with an overview of events in the electrical networks both medium and high voltage mainly based on [12]. The main idea is to highlight the importance of the grid synchronization and monitoring techniques for a power converter connected to the electrical network.

Afterwards, a state of the art regarding the synchronization and monitoring techniques will be presented. Moreover, the impact of these grid monitoring methods on the accuracy of the power converter control will be discussed.

3.2 EVENTS IN ELECTRICAL NETWORKS

3.2.1 Definitions and Classifications

Various events can occur in the electrical networks and most of them are related with the network voltage. These voltage events usually are characterized by a change in the magnitude of the voltage and they can have different time durations from milliseconds up to hours [12], [13]. Based on these two main characteristics, namely magnitude and duration the voltage events are classified by standards in different ways [13].

The standard EN 50160 [9] is focused on characterisation of voltage in low and medium voltage networks while IEEE Std. 1159 states that "there is no implied limitation on the voltage rating of the power system being monitored" [14]. The momentary voltage disturbances are classified in IEEE Std. 1250 [15] for duration up to a few seconds.

Moreover, the terminology used in these standards is very different. For example the same event in EN 50160 is called "voltage dip" while in IEEE Std 1159 it is referred as "voltage sag". However, the magnitude of this event is defined different in these standards.

In order to illustrate these differences the definitions of voltage magnitude events from both standards are presented in Fig. 3.1 based on [9], [12], [13], [14] and [15].

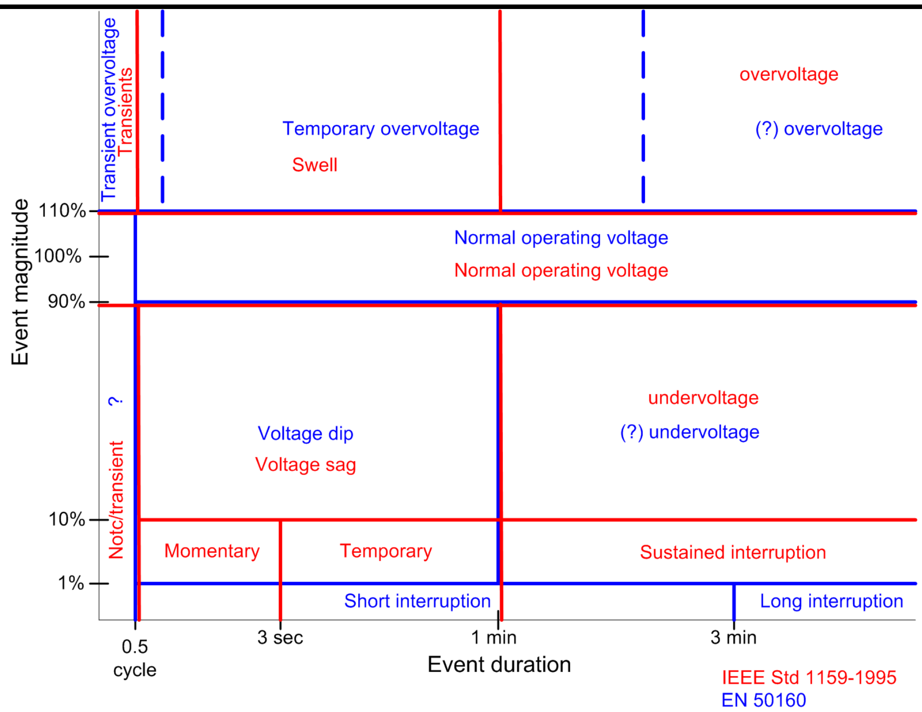

Fig. 3.1. Definition of voltage magnitude events based on standards (source [12]based on [9], [13], and [14]).

Note: the question mark is used in Fig. 3.1 because the standard does not specify a term/name for that type of event. This method of events classification in the electrical network based on magnitude and duration has advantages and drawbacks. In [13] it is stated that the following items are of concern when using this method:

- The RMS voltage during the event is not always constant and therefore this method might lead to ambiguities in defining the magnitude and duration of the event.
- Fast events with duration of less that one cycle cannot be defined very well because the RMS voltage cannot be calculated precisely.
- Repetitive events can give erroneous results. In this case the numbers of events can either be underestimated or overestimated.

In the present analysis the focus is on network events characterized by a voltage drop down to 0.1 pu or less and durations up to 1 second. Based on [13] two types of events are characterized by this magnitude and duration namely short interruptions and voltage sags. These events can mainly be related with short-circuits in the electrical networks. In most of the cases these events will trip the power generation based renewable sources and will cause an important loss of power generation into the faulted network. However, currently some grid codes require up to 100% reactive current injection [16] and [17]. Hence, it is required that these sources must stay connected during faults.

Longer network events have a relatively low frequency of occurrence and are typically associated with black-out or other severe events in the network.

3.2.2 Short interruptions

3.2.2.1 Terms and definitions

The definitions for this class of events as defined in the standards [9], [14] and [15] are summarized in Table 1 [3].

Table 3.1. Definitions for short interruption in various standards

Standard	Definition	Magnitude	Duration	Applicability
EN 50160	Short interruption	< 1%	Up to 3 min	LV and MV (up to 35 kV)
IEEE Std 1159-1995	Momentary interruption	< 10%	0.5 cycles to 3 sec	LV, MV, HV
IEEE Std 1250-1995	Instantaneous interruption	Complete loss of voltage	0.5 cycles to 0.5 sec	LV, MV, HV
	Momentary interruption		0.5 sec to 2 sec	LV, MV, HV

As it can be observed in Table 3.1 only the IEEE Std 1159-1995 covers the whole range of voltages while EN 50160 is limited to 30 kV networks.

3.2.2.2 Origins

The origins of the voltage interruptions in general are "faults which subsequently trigger protection measure" [13]. Among other causes the following shall be mentioned [13]:

- Protection operation when there is no fault;
- Broken conductors not triggering protective measure;
- Operator intervention

"When the supply is restored automatically, the result event is called a short interruption" [13]. Based on the network layout between the location of the fault and the point where the voltage is measured and the protection schemes used, the event is "seen" in a different way as shown in Fig. 3.2.

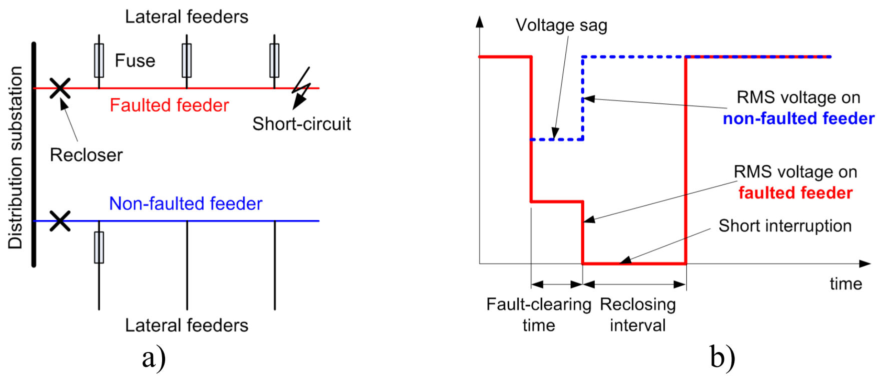

Fig. 3.2. Fault in a distribution network: a) network layout and b) RMS voltages on feeders

The voltage on the faulted feeder will drop to zero while the non-faulted feeder will "see" a voltage sag/dip.

3.2.3 Voltage sags/dips

3.2.3.1 Terms and definitions

A summary of different terms and definitions for voltage sags/dips as given in standards is presented in Table 3.2 [12].

Table 3.2. Definitions of voltage sags/dips in various standards

Standard	Magnitude	Duration	Applicability
EN 50160	1% - 90%	0.5 cycles to 1 min	LV and MV (up to 35 kV)
IEEE Std 1159-1995	10% - 90%	0.5 cycles to 1 min	LV, MV, HV
IEEE Std 1250-1995	Reduction of voltage	0.5 cycles to few sec	LV, MV, HV

3.2.3.2 Origin

According to [13] the voltage sags/dips "are short duration reductions in RMS voltage, caused by short circuits, overloads and starting of large motors. Since voltage sags/dips are caused by short-circuit faults located at hundreds of kilometres away in the transmission system these events are a more "global" problems than an interruption [13].

The magnitude of the voltage sags/dips is determined by the following factors [13]:

- Distance to fault;
- Cross section of the lines and cables;
- Connection type of transformers between the location of fault and the recording point;
- Type of the network (radial or loops);
- Short-circuit impedance of the network, etc

An overview regarding the influence of transformer winding connections on the propagation of voltage sags/dips is given in [18].

For example different short-circuit types on the high-voltage windings of an Dy1 or Dy11 transformer, which is very common in wind turbine systems, leads to different voltage sags/dips on the low voltage side of it as shown in Fig. 3.3. However, when several cascaded transformers are present between the fault location and the "reading" point of voltage, the voltage sag/dip will be determined by the connection types of all these transformers.

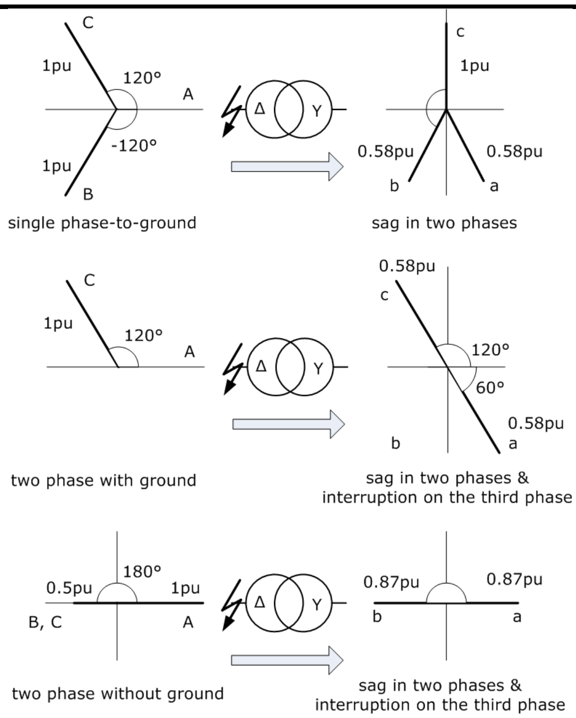

Fig. 3.3. Propagation of voltage sags caused by asymmetrical faults on a Dy1 transformer

3.2.4 Events survey in different countries

3.2.4.1 US and Canada

A very comprehensive investigation regarding power quality for US and Canada is presented in [19] and [20]. This study is based on three surveys conducted by National Power Laboratory (NPL), the Canadian Electrical Association (CEA) and the Electric Power Research Institute (EPRI).

The CEA survey of power quality has run for three years since 1991 and 22 utility companies have participated. The main focus was on residential, commercial and industrial customer sites which have been monitored at their low voltage connection.

The NPL survey had also focused on low voltage networks and it has been running for a five years beginning with 1990. The main goal was to monitor single-phase normal-mode electrical disturbances.

The EPRI survey run between June 1993 and September 1995 aimed to "perform the most thorough study …. to describe power quality levels on primary distribution system in the US" [20]. During this survey the medium voltage networks ranged between 4.16 kV and 34.5 kV and lengths from 1 to 80 km were monitored. "One third of the monitors were located at substations just down line from the feeder circuit breaker, while the remaining monitors were randomly placed along three-phase sections of the feeder primary" [20]. The data presented in [19] and [20] are also used in [13].

Since in the focus in WP5 is on the network events at the medium and high voltage levels, only some results from the EPRI survey will be highlighted.

The EPRI low RMS event data for substation monitors with a 5 min filter are shown in Fig. 3.4 while the survey for feeder monitors is given in Fig. 3.5. Both data are filtered with a 5-min filter. The reason of using this filter is that "from a critical process perspective, it is likely that once a process drops out, other events within a 5 min period are probably not going to impact that process" [20]. However, using this filter "it is expected that the numbers …. are 50 – 70 % lower than if no filters was used" [20].

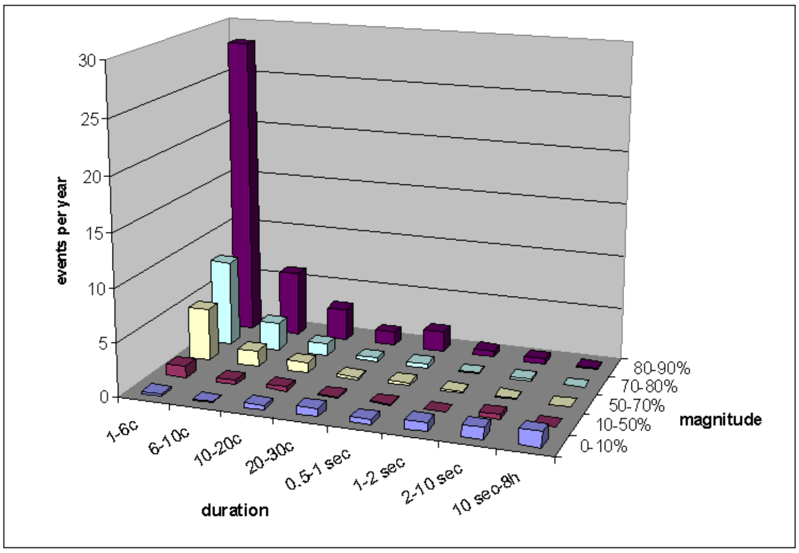

Fig. 3.4. EPRI data for substations monitors with a 5-min filter.

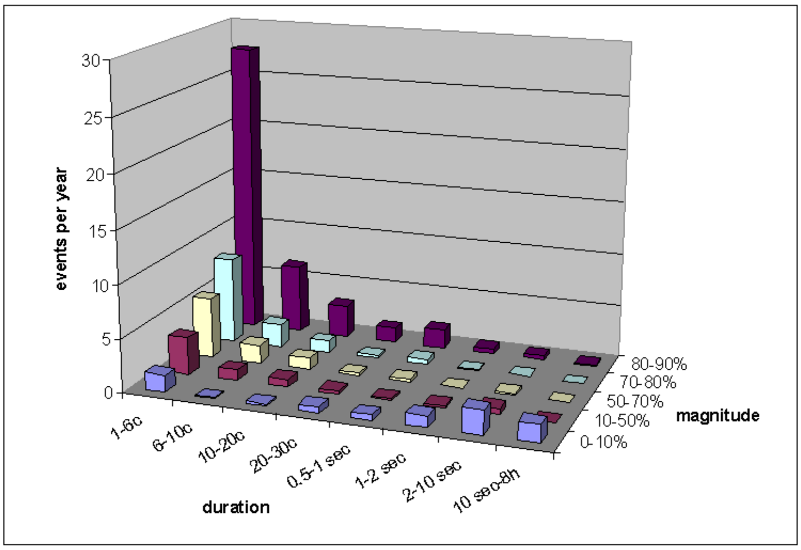

Fig. 3.5. EPRI data for feeder monitors with a 5-min filter.

As it can be observed from Fig. 3.4 and Fig. 3.5 the highest number of the events is characterized by drops in magnitude down to 0.8 pu from the rated voltage and with duration of maximum 6 cycles. Also, most of the events have duration up to 6 cycles especially on the feeder monitors.

3.2.4.2 France

A statistic regarding the number of faults per year in the whole French transmission and sub-transmission systems is presented in [21]. Here, based on the duration of the events, the faults are mainly divided in two categories, namely momentary and permanent fault. According to [21], the momentary fault has duration on the order of several hundreds of milliseconds and it is related to the operating time of a recloser. On the other hand a permanent fault “lasts several minutes to several hours and it requires human intervention” [21].

A summary of this fault statistic is shown in Fig. 3.6 (source [12] based on [21]).

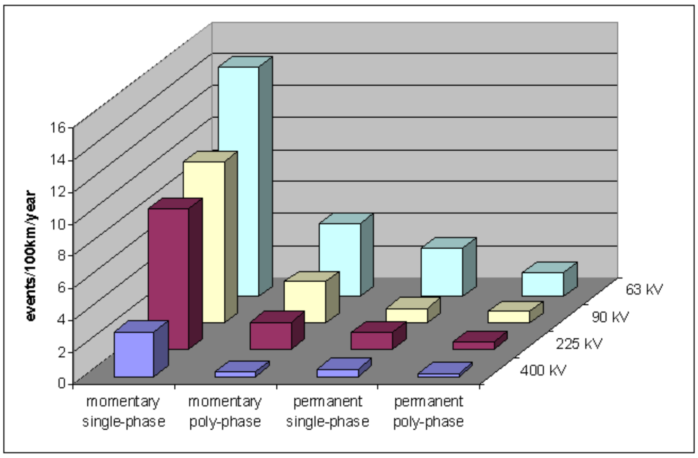

Fig. 3.6. Fault statistics in the France’s transmission and sub-transmission lines (source [3] based on [21]).

It is obviously that most of the faults are located in MV networks especially momentary ones. Moreover, the frequency of the momentary single phase faults is dominant in the entire network, while the permanent poly-phase faults have the lowest occurrence.

3.2.4.3 Nordel

Statistics regarding the faults in the transmission system of the Nordic countries are available on Nordel’s web-page [22]. Each year a document summarizing the faults in the transmission systems of the members is available from Nordel. This very comprehensive document gives in details the number of faults on each voltage level, per subcomponents, etc.

According to [22], more than 50% from the total number of faults per year in the period 2000-2005 in Denmark, Finland and Sweden are located on overhead lines as shown in Fig. 3.7. Exception is Norway where faults located in substations are predominant compared with faults on overhead lines.

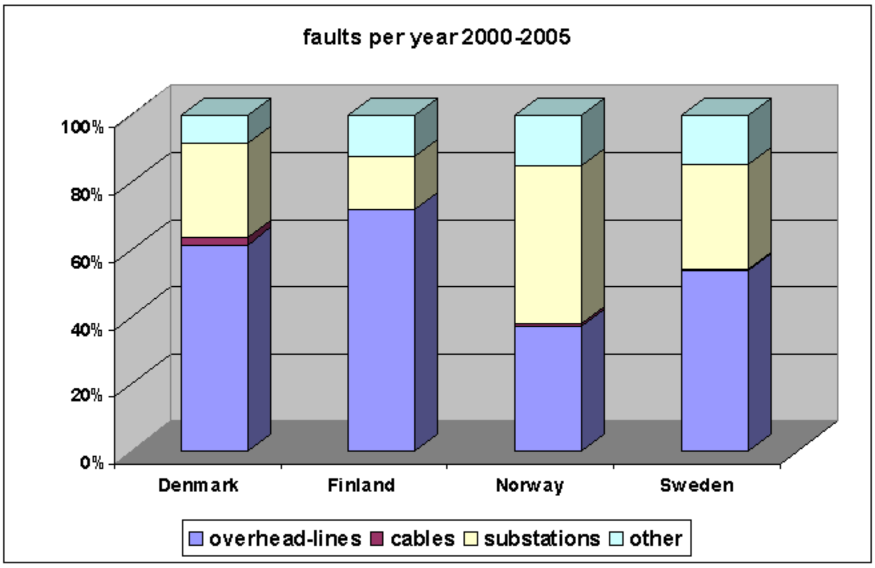

Fig. 3.7. Sharing of faults on the transmission systems of Nordic countries in the period 2000-2005.

In all Nordic countries the number of faults located on cables is less than 2.5% from the total number of faults in the considered period.

In all considered countries most of the faults on overhead lines in the last ten years are on 132 kV lines, while 400 kV lines are less susceptible to faults as shown in Fig. 3.8. Exception is Norway where the number of faults on 400 kV lines as well as on 132 kV ones are almost equal.

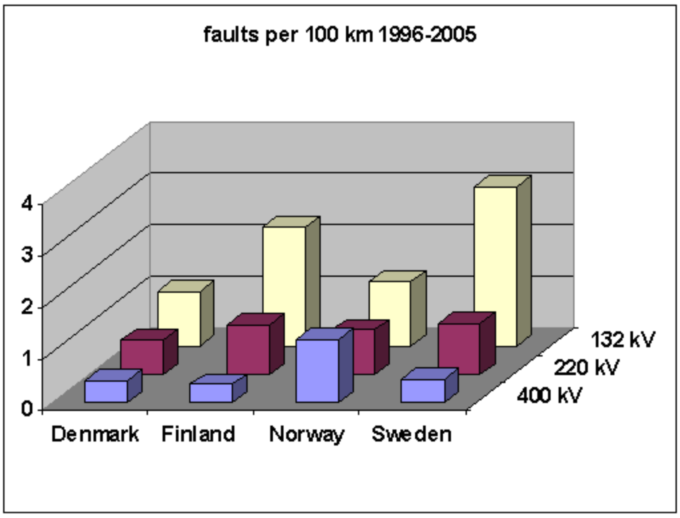

Fig. 3.8. Number of faults per 100km of overhead lines in the last ten years in the Nordic Countries.

An analysis of the fault type on all voltage levels in the considered Nordic Countries is given in Fig. 3.9, Fig. 3.10 and Fig. 3.11.

This analysis reveals that the highest number of faults is of single phase type in all considered Nordic countries.

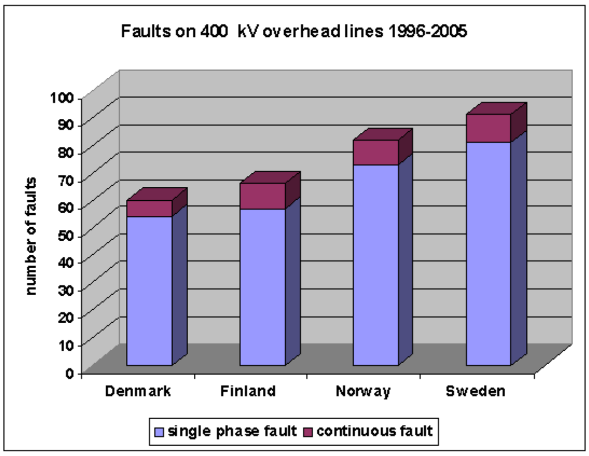

Fig. 3.9. Sharing of fault types on 400 kV overheads lines.

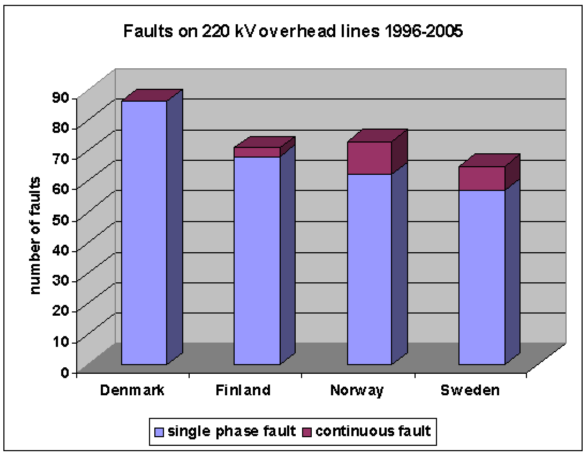

Fig. 3.10. Sharing of fault types on 220 kV overheads lines.

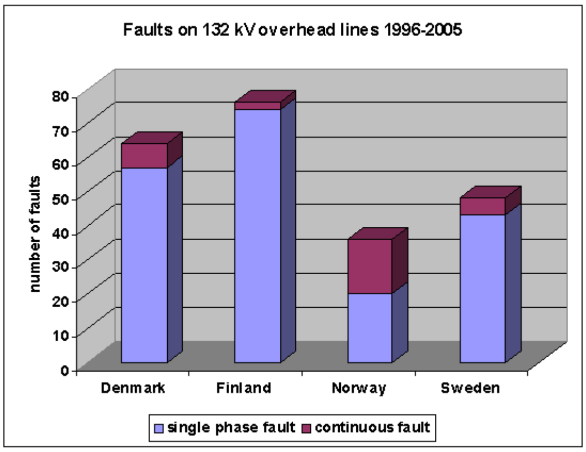

Fig. 3.11. Sharing of fault types on 132 kV overheads lines.

Denmark has the highest number of events on the 220 kV lines, while Sweden on the 400 kV systems. Continuous faults have a relative low sharing in all considered countries.

3.2.4.4 Summary

Based on the presented survey regarding faults on the electrical network the following conclusions can be drawn:

- Most of the events are located on overhead lines
- Most of the faults are located on 132 kV networks.
- The single phase fault has the highest probability to occur compared with other types of faults
- Voltage drops down to 0.75 pu have a duration of several cycles while voltage drops down to 0.25 pu from the rated voltage have duration of several seconds up to minutes.

It is obvious that an accurate estimation of the grid voltage magnitude and angle is very important during network events especially for grid connected converters. Therefore, a special attention was paid in this workpackage to the grid synchronization and monitoring techniques.

3.3 GRID SYNCHRONIZATION AND MONITORING METHODS

Initially, the synchronization of the delivered current with the utility network voltage was a basic requirement for interconnecting distributed power generators with the power system [16], [24]. In case of wind turbines, reactive power control at the point of common coupling is requested [24]. Consequently, the wind turbine control should accommodate an algorithm capable of detecting the phase angle of grid voltage in order to synchronize the delivered current. Moreover, the phase angle plays an important role in control, being used to transform the feedback variables to a suitable reference frame in which the control structure is implemented. Hence, phase angle detection has a significant role in control of the grid side converter in a wind turbine.

Numerous research papers report several algorithms capable of detecting the grid voltage phase angle, i.e. zero crossing detection, the use of arctan function or Phase-Locked Loop (PLL) technique.

An overview of the grid synchronization and monitoring methods is presented in the following, based on [16] and [24].

3.3.1 Zero crossing method

A simple method of obtaining the phase and frequency information is to detect the zero-crossing point of the grid voltage [25], [27]. This method has two major drawbacks as described in the following.

Since the zero crossing point can be detected only at every half cycle of the utility frequency, the phase tracking action is impossible between the detecting points and thus the fast dynamic performance can not be obtained [28]. Some work has been done in order to alleviate this problem using multiple level crossing detection as presented in [29].

Significant line voltage distortion due to notches caused by power device switching and/or low frequency harmonic content can easily corrupt the output of a conventional zero-crossing detector

[30]. Therefore, the zero-crossing detection of the grid voltage needs to obtain its fundamental component at the line frequency. This task is usually made by a digital filter. In order to avoid the delay introduced by this filter numerous techniques are used in the technical literature. Methods based on advanced filtering techniques are presented in [30]-[34]. Other methods use Neural Networks for detection of the true zero-crossing of the grid voltage waveform [35]-[37]. An improved accuracy in the integrity of the zero-crossing can also be obtained by reconstructing a voltage representing the grid voltage [38]-[41].

However, starting from its simplicity, when the two major drawbacks are alleviated by using advanced techniques, the zero-crossing method proves to be rather complex and unsuitable for applications which require accurate and fast tracking of the grid voltage.

3.3.2 Arctangent method

Another solution for detecting the phase angle of grid voltage is the use of *arctan* function applied to voltages transformed into a Cartesian coordinate system such as synchronous or stationary reference frames as shown in Fig. 3.12 and Fig. 3.13 respectively.

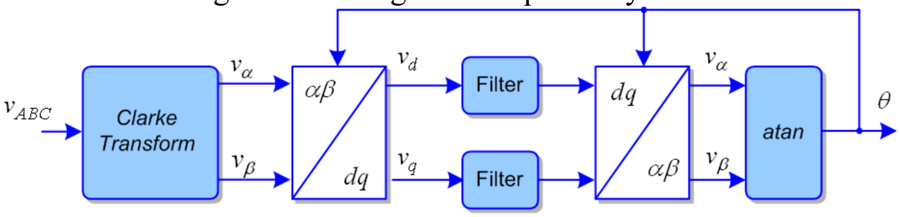

Fig. 3.12. Synchronization method using filtering in synchronous reference frame.

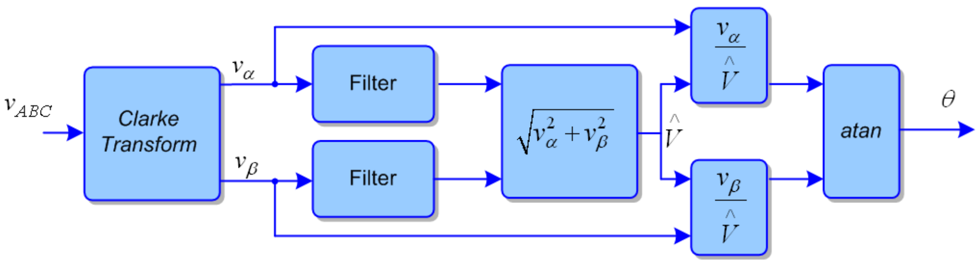

Fig. 3.13. Synchronization method using filtering in stationary frame.

This method has been used in drives applications [59], for transforming feedback variables to a reference frame suitable for control purposes. However, this method has the drawback that requires additional filtering in order to obtain an accurate detection of the phase angle and frequency in the case of a distorted grid voltage. Therefore, this technique is not suitable for grid-connected converter applications.

3.3.3 PLL technique

Phase-Locked Loop (PLL) is a phase tracking algorithm widely applied in communication technology [25], being able to provide an output signal synchronized with its reference input in both frequency and phase.

Nowadays, the PLL technique is the state of the art method to extract the phase angle of the grid voltages [28], [29], [43]and [44]. The PLL is implemented in dq synchronous reference frame and its schematic is illustrated in Fig. 3.14. As it can be noticed, this structure needs the coordinate transformation form *abc* to *dq* and the lock is realized by setting the reference to zero. A controller, usually PI, is used to control this variable. This structure can provides both the grid frequency as well as the grid voltage angle.

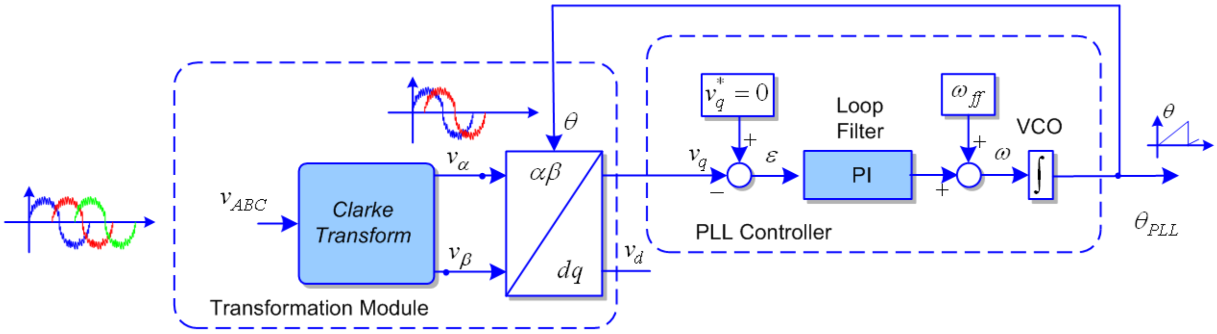

Fig. 3.14. Basic structure of a PLL system for grid synchronization.

After the integration of the grid frequency, the utility voltage angle is obtained, which is fed back into the P*ark* Transform module in order to transform into the synchronous rotating reference frame

This algorithm has a better rejection of grid harmonics, notches and any other kind of disturbances but additional improvements have to be done in order to overcome grid unbalance [45]-[49]. In the case of unsymmetrical voltage faults, the second harmonics produced by the negative sequence will propagate through the PLL system and will be reflected in the extracted phase angle. In order to overcome this, different filtering techniques are necessary such that the negative sequence is filtered out. As a consequence, during unbalance conditions, the three phase *dq* PLL structure can estimate the phase angle of the positive sequence of the grid voltages.

3.3.4 Grid Monitoring

Grid requirements applying to utility connected power generation units impose the operation conditions in respect to voltage and frequency values. The demands are country specific. A graphical representation of allowed operation area in respect to the grid voltage amplitude and grid frequency as specified in the Danish Grid code for wind turbines connected to the distribution system [17] is illustrated in Fig. 3.15.

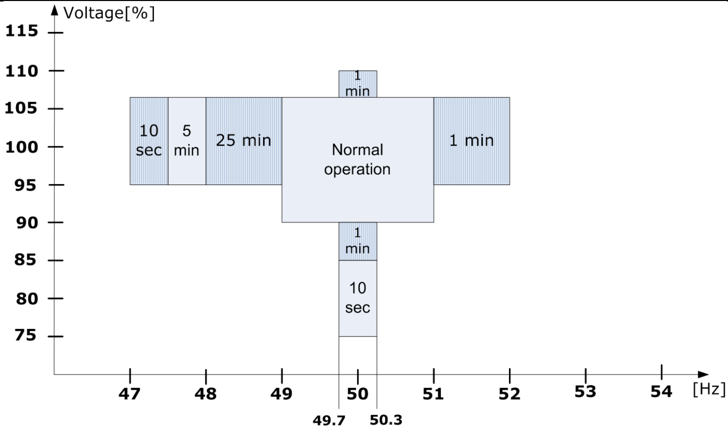

Fig. 3.15. Voltage and frequency operational ranges for wind turbines connected to the Danish distribution system [17].

A normal operation area between 95 and 105% of the nominal grid voltage and ±1 Hz around the nominal frequency is defined. Either frequency or voltage exceeds the predefined limits, the wind turbine should disconnect within the specified time interval. Therefore, in order to be able to disconnect in time, the wind turbine should accommodate a fast and reliable grid monitoring unit.

The PLL structures are used in the grid monitoring techniques. In a three-phase system, the grid voltage information can easily be obtained through the Clarke Transform as shown in Fig. 3.16.

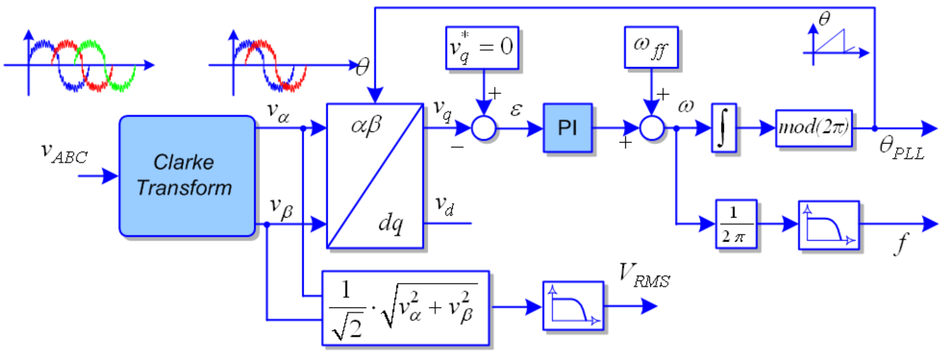

Fig. 3.16. General structure of a grid monitoring system based on three-phase PLL.

The same structure as presented in Fig. 3.16 can be used for single phase systems (Fig. 3.17). However, in this case, the orthogonal voltage system is much more difficult to acquire [27]. Therefore, more attention should be paid for the generation of the orthogonal voltage system.

In the technical literature, some techniques for generating the orthogonal voltage components from a single-phase input signal are described, some of which are compared in [42] and [50].

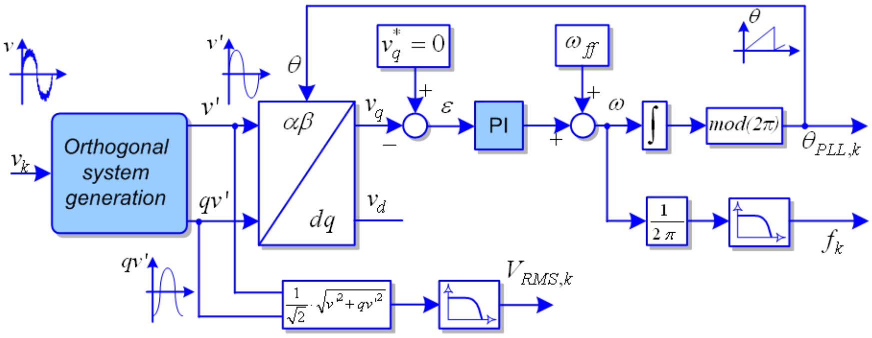

Fig. 3.17. General structure of a grid monitoring system based on single-phase PLL.

An easy technique of generating the orthogonal voltage system in a single-phase system incorporates a transport delay function (Fig. 3.18), which is responsible for introducing a phase shift of 90 degrees with respect to the fundamental frequency of the input signal [52].

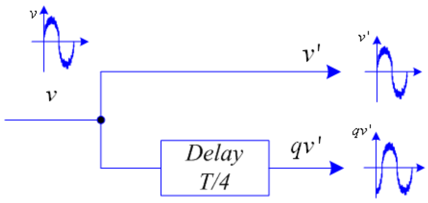

Fig. 3.18. Generating orthogonal voltage system using the transport delay function.

This method is easy to implement because it requires a FIFO buffer with a size equal to quarter of number of the fundamental frequency samples and it is also easy to tune. However, it is frequency dependent and creates an unfiltered orthogonal system.

A related method, but more complex of creating a phase shift of 90 degrees, uses the Hilbert Transform [50] and [53] as shown in Fig. 3.19.

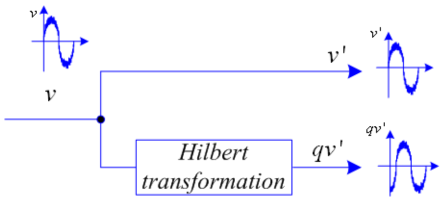

Fig. 3.19. Generating orthogonal voltage system using the Hilbert Transform.

Another method of generating the orthogonal voltage system is based on the inverse Park Transform [42], [50], [52] and [54], as presented in Fig. 3.20.

The method requires an inverse Park Transform and two first order low pass filters. Though, it is difficult to select the time constant of the filters and also to tune the PI controllers because two independent non-linear loops are involved in this structure.

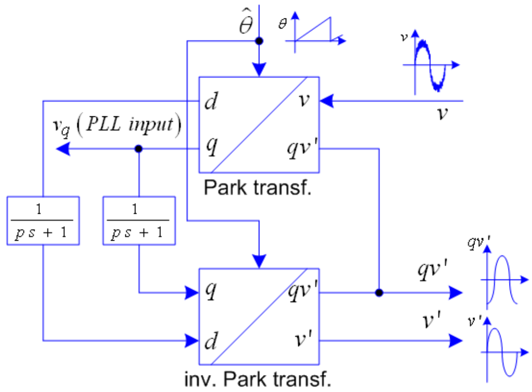

Fig. 3.20. Generating orthogonal voltage system using the inverse Park transform.

The orthogonal voltage system can also be obtained using resonant structures such as the Second Order Generalized Integrator (SOGI) [55], as presented in Fig. 3.21.

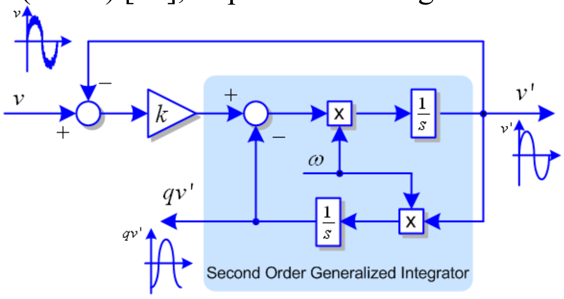

Fig. 3.21. Generating orthogonal voltage system using a Second Order Generalized Integrator (SOGI).

This method has the following advantages: easy implementation on DSPs, very good dynamic performances; fast or accurate response based on the tuning; filtering of orthogonal voltages without delay and it is frequency independent. However, this approach is very sensitive to the discretization method of the integrators [55].

In [56], a method for generating the orthogonal voltage system based on Kalman estimator is proposed.

A new three-phase PLL structure for grid monitoring under unbalanced voltages into the grid is proposed in [57] as shown in Fig. 3.22.

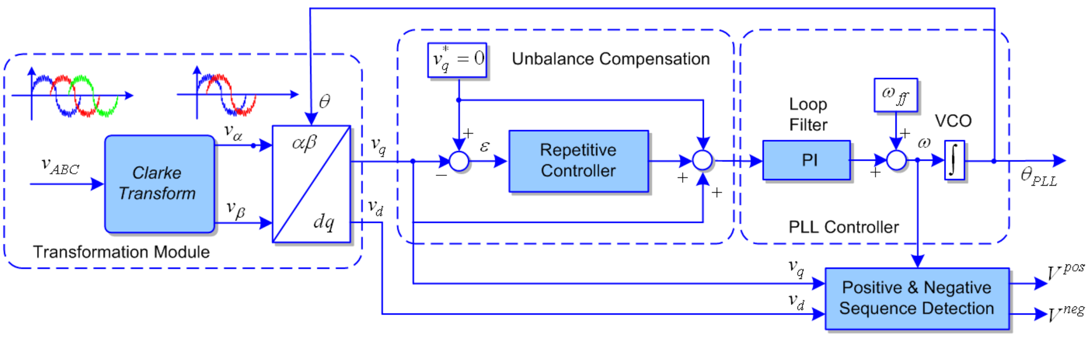

Fig. 3.22. Advanced grid monitoring structure based on PLL [57].

The transformation module is used to transform the grid voltages from *abc* to *dq* synchronous rotating reference frame. The unbalance compensation algorithm is based on a repetitive controller [57]. The role of unbalance compensation unit is to allow only the positive sequence component to pass through the PLL controller, hence reducing the unbalance effect on the frequency and phase angle estimation.

The positive negative sequence detector extracts the negative sequence component of grid voltage while the positive sequence component is determined using delay signal cancellation (DSC) filter [57]. Having the information about both positive and negative sequence components, the value of grid unbalance can be further estimated. Using these four parts, the proposed system is able to estimate the phase angle of the positive sequence voltage component, the grid frequency and the magnitude of positive and negative sequence components. The algorithm has been extensively tested under different grid disturbances [57] and provides fast and accurate grid variables in case of balanced and, unbalanced faults as well as in case of frequency deviation conditions. Comparing the response time of the proposed algorithm with the disconnection times suggested by the grid interconnection requirements, the algorithm is proving to be a suitable solution for grid monitoring in case of distributed power generation systems [57].

3.4 PLL RESPONSE UNDER GRID DISTURBANCES

In this paragraph the dynamic performances of the three-phase PLL and the single-phase one will be analyzed under different grid disturbances. The structure of the considered three-phase PLL is shown in Fig. 3.16 while the single phase one is based on the SOGI structure (see Fig. 3.17 and Fig. 3.21). Both PLLs have the same parameters for the PI controllers namely a settling time of 0.04 sec and a damping factor of 0.707.

The short-circuits are characterized as in the Danish grid code for connecting wind turbines to the Distribution System [6], [12] and [17]: 150 msec duration of the fault and a voltage drop down to 25% from the rated voltage in the PCC are considered. The short-circuit power of the equivalent grid is 20 MVA and a grid impedance ratio R/X of 0.1 is taken into account.

3.4.1 Three-phase short-circuit

First, the dynamic performances of the considered PLLs have been analyzed during a three-phase short-circuit in the PCC as shown in Fig. 3.23.

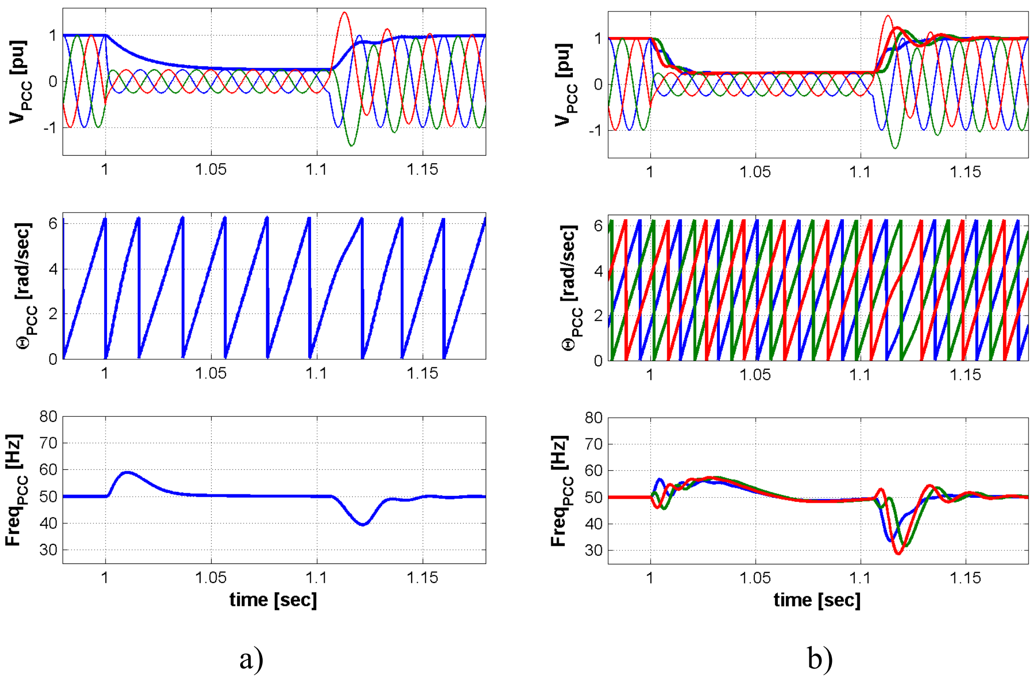

Fig. 3.23. Dynamic response of the PLLs during three-phase short-circuits: a) three-phase PLL and b) single-phase PLL.

It can be observed that both PLLs estimate the amplitude of the voltage, the grid angle as well as the frequency with good results.

3.4.2 Two-phase to ground short-circuit

In this case the response of the PLLs is shown in Fig. 3.24.

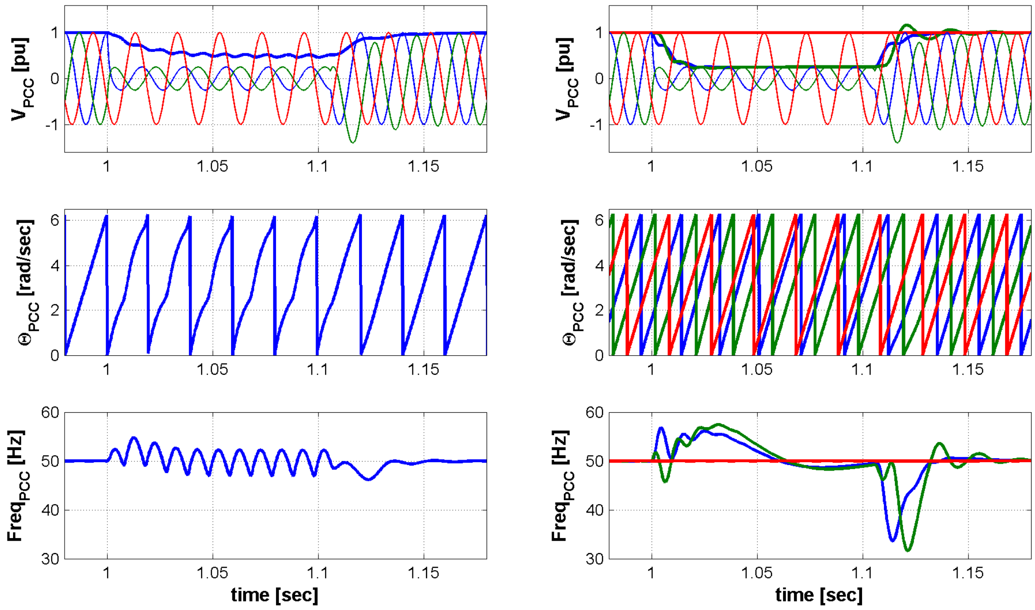

a) b)

Fig. 3.24. Dynamic response of the PLLs during a two-phase to ground short-circuits: a) three-phase PLL and b) single-phase PLL

It can be observed for the three-phase PLL the 100 Hz component in the estimated voltage amplitude as well as in the estimated grid frequency. The voltage amplitude is calculated based on the individual phase voltages; therefore, it is not estimated correctly during the fault. The single-phase PLL gives accurate voltage amplitude in each phase as well as the frequencies. A trade-of between the accuracy of the grid voltage and frequency must be made.

3.4.3 Two-phase short-circuit

Two-phase short-circuits give voltages drop down to 50% from the rated voltage in the faulted phases. The estimated grid voltage parameters in this case are shown in Fig. 3.25.

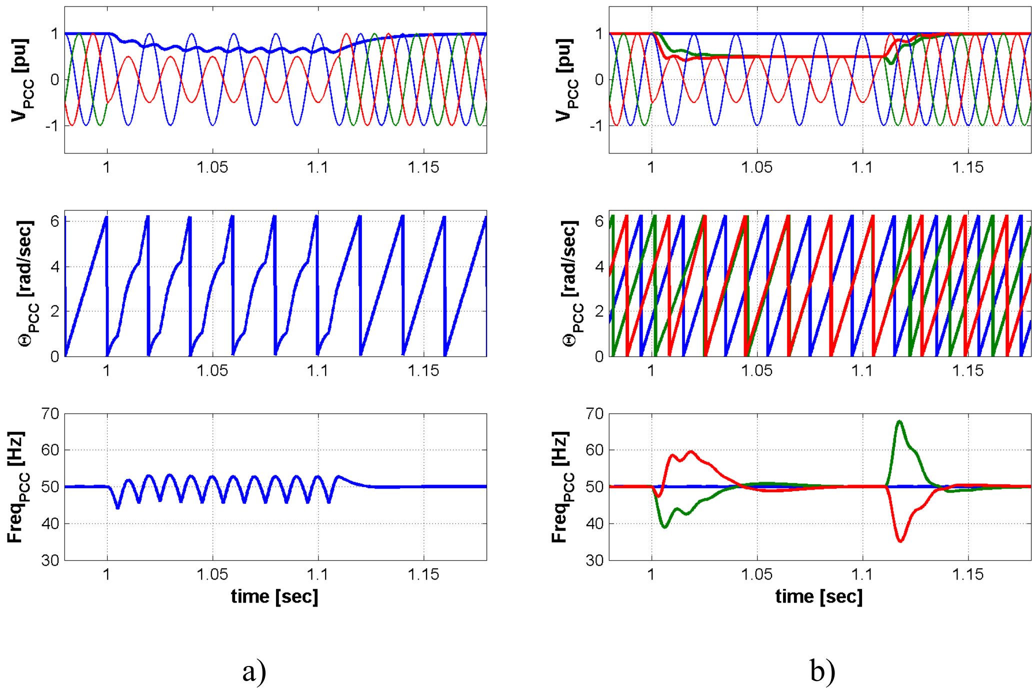

Fig. 3.25. Dynamic response of the PLLs during a two-phase short-circuit: a) three-phase PLL and b) single-phase PLL

Again, it can be observed the 100 Hz component in the output of the three-phase PLL. The grid voltage angle is also distorted. Accurate estimations of the voltage amplitude in each phase as well as grid voltage angles are provided by the single-phase PLL.

3.4.4 Single-phase short-circuit

This type of fault seems to have the highest occurrence in the distribution networks (see §3.2.4). The output of the considered PLL structures in this case is presented in

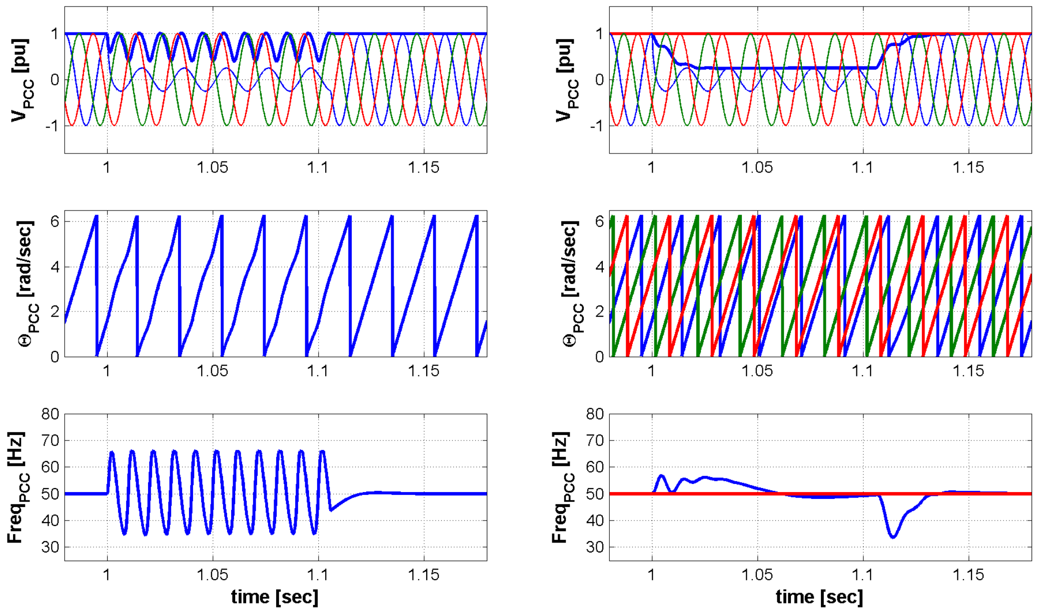

a) b)

Fig. 3.26. Dynamic response of the PLLs during a single-phase short-circuit: a) three-phase PLL and b) single-phase PLL.

Very high 100 Hz ripple is present in the estimated voltage and frequency of the three-phase PLL while the single-phase PLL provides accurate values for the grid voltage parameters.

3.4.5 Grid voltage unbalances

A 3% unbalance in the grid voltages is considered in this case. Since the standards [9] and [10] usually specify a value less than 3% for the voltage unbalances, this case can be considered as a “worst case” scenario. The output of the PLLs is given in Fig. 3.27.

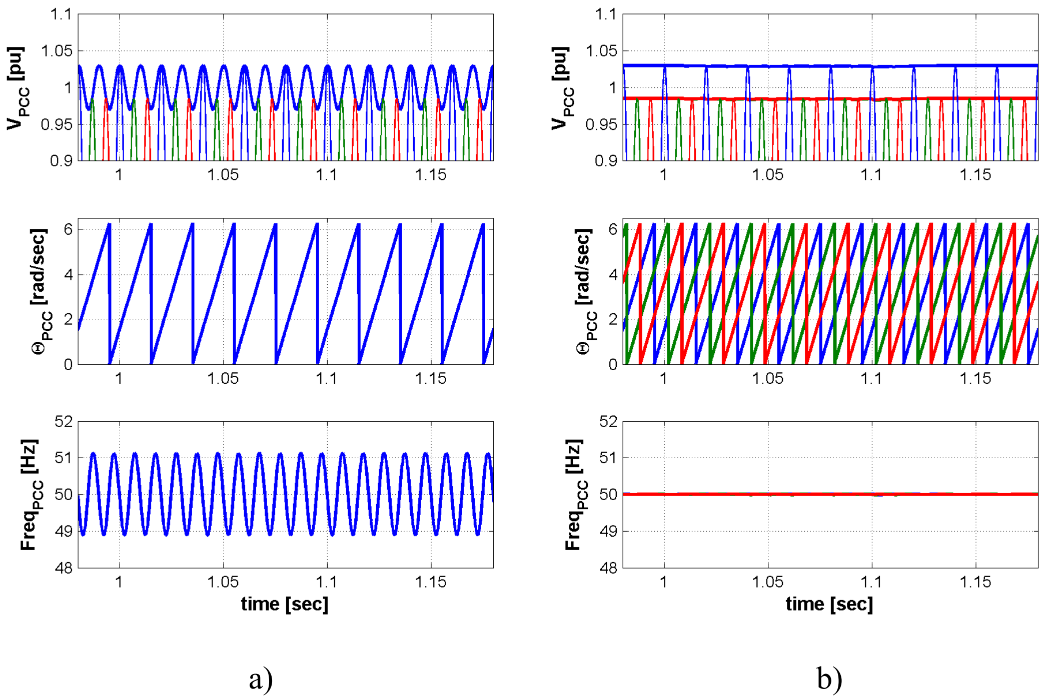

Fig. 3.27. Estimated grid voltage parameters for unbalanced grid conditions: a) three-phase PLL and b) single-phase PLL.

3.4.6 Phase jumps

Phase-jumps are typically associated with short-circuits in the network and their magnitude is influenced by the transformer connection between the fault location and the measurement point. According to [13] the maximum range for phase jumps in electrical networks is in the range +60º to -60º. Therefore, in the present analysis a phase jump of +60º is considered. The output of the PLLs in this case is presented in Fig. 3.28.

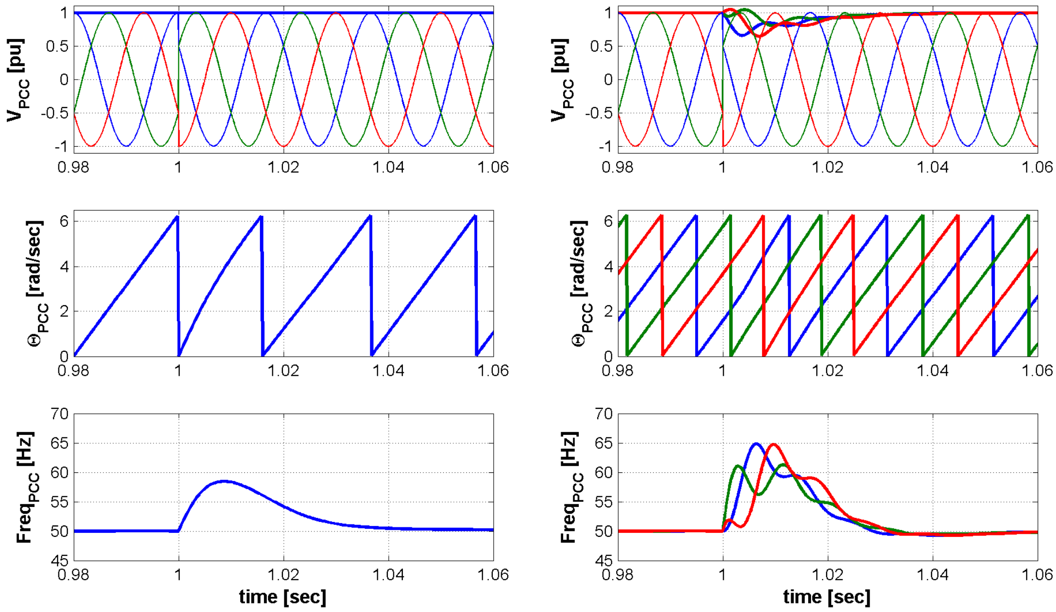

a) b)

Fig. 3.28. Estimated grid voltage parameters for a 60º phase jump: a) three-phase PLL and b) single-phase PLL.

3.5 CONCLUSIONS

Based on the above analysis it is obvious that the three-phase PLL is very sensitive to unsymmetrical and unbalanced faults compared to the single phase one. Since most of the control strategies require some transformations between different reference frames they became sensitive to the grid voltage magnitude and angle. Therefore, in case of the Uniflex-PM system that should be able to withstand to all kind of events in the networks, the PLL is one of the key components. Moreover, the information provided by the PLL is used in the supervisory control to select a suitable operation mode of the system as well as in taking decision in the control algorithm.

4 CONTROL STRATEGIES FOR UNIFLEX-PM SYSTEM

4.1 SYNCHRONOUS REFERENCE FRAME CONTROL

The overall control block of the synchronous reference frame control is presented in Fig. 4.1.

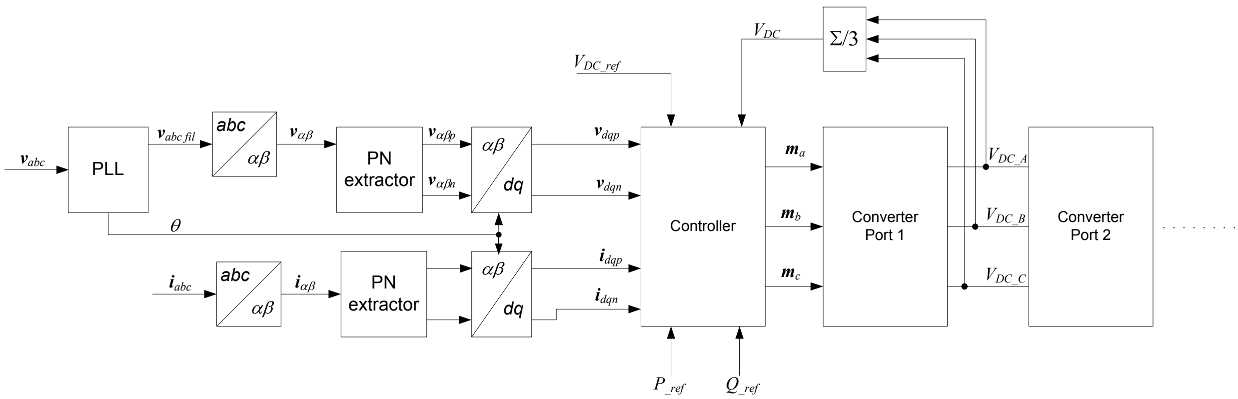

Fig. 4.1. Diagram of synchronous reference frame Control

The control scheme for Port 1 is shown in Fig. 4.2. A similar control structure is also used for Port 2 (Fig. 4.3). A cascaded control structure is selected to implement the control system to regulate the power/DC-link voltage and input line currents at the same time: the outer loop is the power/DC-link voltage loop while the inner loop is responsible for the current control.
Two *dq* frames in positive and negative coordinates are implemented to regulate the supply current taking unbalanced supply conditions into consideration [60]-[62]. Instead of a normal PI controller, a PI+Resonant controller is used to control the positive and negative *dq* currents in case of a distorted supply voltage [62].

The positive and negative signals are extracted via the delay signal cancellation method. Moreover, a PLL filter is used to obtain the phase angle that allows generating a rotating frame for voltages and currents synchronous with the grid.

In port 1, the dc-link voltage and reactive power are regulated generating the references for the current control. The reactive power and DC link voltage are regulated by PI controller. One PI controller is utilized to control the average value of the dc-link voltage. Only positive sequence current references are generated at present. The negative sequence currents are set to be zero.

In port 2, active and reactive powers are controlled. The active power control generates the current reference for the positive sequence d-axis current while the reactive power control generates the current reference for the positive sequence *q*-axis current. The negative sequence currents are regulated to be zero.

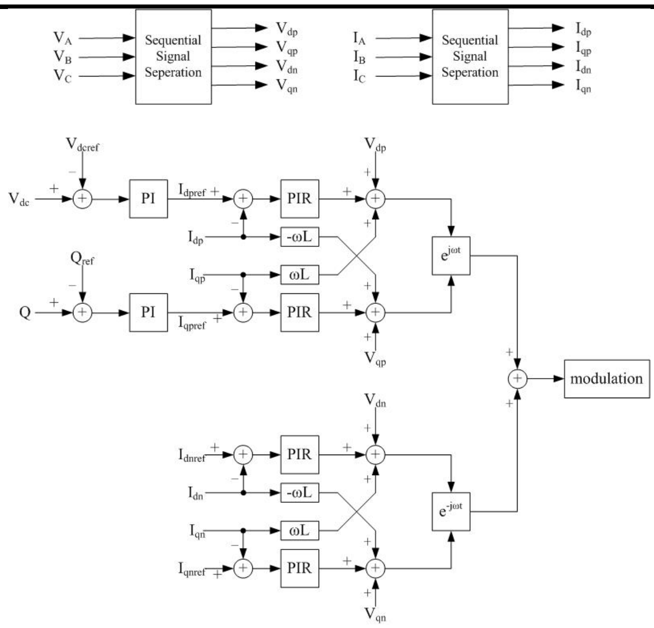

Fig. 4.2. Synchronous reference frame control for Port1 in the Uniflex-PM system.

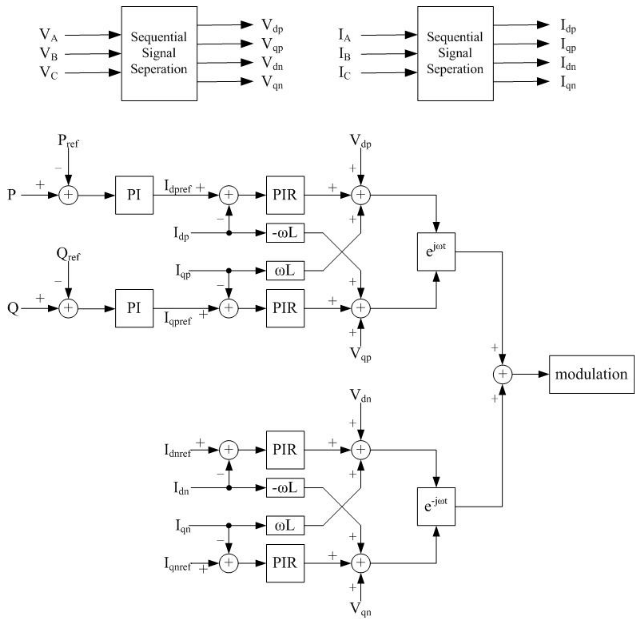

Fig. 4.3. Synchronous reference frame control for Port2 in the Uniflex-PM system.

4.2 PREDICTIVE CONTROL

4.2.1 Overall structure

The overall block diagram of the Controller is shown in Fig. 4.4, where only for Port 1 side is illustrated in detail. For Port 2, a control scheme similar to Port 1, but without the outer DC-link control loop, is used. The multi loop structure is selected to design the controller to regulate the power/DC-link voltage and input line currents at the same time. The outer loop is the power/DC-link voltage loop while the inner loop, illustrated, is responsible for the current control.

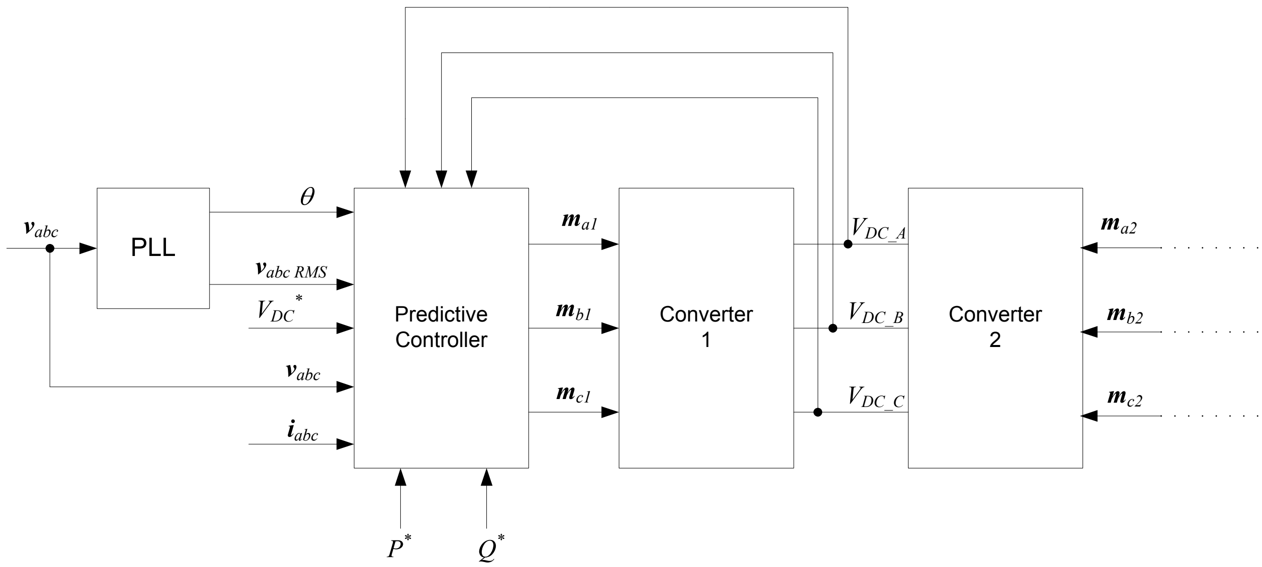

Fig. 4.4. Overall block diagram of the predictive control.

In Port 1, the regulation of active power P is obtained through the DC-link voltage balance, performed by a PI controller. Predictive controller needs the calculation of the amplitude and phase of the current references. Active power P contributes to generate only the amplitude of the current references while the reactive power Q acts on both the amplitude and phase of the current references.

For Port 2, the controller is similar to that of Port 1 except for active power regulation. In fact, both the active and reactive powers are controlled through PI controllers without any interaction of DC-link voltage. Then, the calculation of the amplitude and phase of the current references, necessary for the Predictive controller, is the same.

A detailed description of the predictive controller is shown in next paragraph.

4.2.2 Predictive Controller

This section describes the application of a predictive current control to the UNIFLEX-PM conversion structure to control the system grid currents. Predictive controllers present very fast response and are particularly suitable for an easy microprocessor implementation.

The basic equation of the Predictive control model is obtained starting from the following state equation for the input/output filter L_f:

$$i(t+t_0) = i(t_0) + \frac{1}{L_f}\int_{t_0}^{t}(v_j - v_{xj})dt \tag{4.1}$$

where j represents the phase A, B or C. Applying a time discretization to (4.1) with a sampling period T_s and supposing v_{xj} constant during T_s, the following expression for voltage v_{xj} is obtained:

$$v_{xj_k} = \frac{L_f}{T_s}(i_k - i_{k+1}) + \frac{1}{T_s}\int_{t_k}^{t_k+T_s} v_j dt \tag{4.2}$$

In order to zero the current error, the control system imposes, at each sampling period, i_{k+1} equal to the reference current. To reduce the effects of the harmonics in the grid voltages, the integral of v_j is calculated using the method proposed in [63].

The block diagram of the Predictive controller employed for Phase a of Port 1 is shown in Fig. 4.5.

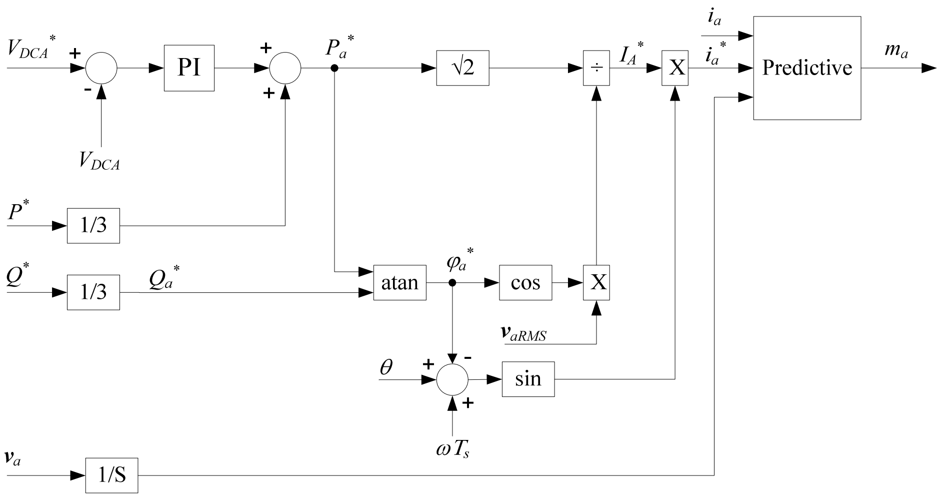

Fig. 4.5. Block diagram of Predictive Controller for Phase A Port 1.

Reference current ia*, necessary to the Predictive controller to zero the error at each sampling period, is calculated on the base of the following sinusoidal function:

$$i_a^* = I_a^* \sin\alpha = I_a^* \sin(\theta + \omega T_s - \varphi_a^*) \tag{4.3}$$

whose amplitude Ia* and phase α depends on the actual values of active power reference P*, reactive power Q* and the output a PI regulator used to control the of DC-link voltage.

In particular, amplitude Ia* is obtained on the basis of the following relationship:

$$I_a^* = \frac{\sqrt{2}P_a^*}{V_{aRMS} \cdot \cos\varphi_a^*} \quad (4.4)$$

where Pa* is the active power reference for Phase a obtained modifying the overall active power reference, divided by 3, on the basis of DC-link error on the same phase; Va_{RMS} is the RMS value of the grid voltage, provided by a PLL, and necessary in case of distorted grid.

The phase difference between voltage and current in the PCC φ_a^* is needed to produce the desired power factor and is calculated as:

$$\varphi_a^* = \mathrm{atan}\frac{Q_a^*}{P_a^*} \quad (4.5)$$

To avoid that the systems exceeds the desired apparent power, φ_a^* modifies both the values of Ia* and phase α of reference current ia*.

Phase angle α of reference current ia* is achieved by subtracting from the actual voltage grid angle θ, provided by a PLL, angle φ_a^*; moreover, a term ωT_S is added to account that ia* value, calculated at the generic sampling instant k, is applied next sampling period k+1.

Finally, integrative block (1/s) in Fig. 4.5 provides the voltage grid integral necessary to calculate the integral term in (4.2).

4.3 STATIONARY REFERENCE FRAME CONTROL WITH PR CURRENT CONTROLLERS

The stationary reference frame controller has been chosen as a possible alternative to the "classical" synchronous reference frame control due to the fast current control provided by Proportional Resonant (PR) controllers. Thus, the Uniflex-PM system can increase its dynamic response under different grid events or sudden change in the power flow.

The overall structure of this control is shown in Fig. 4.6 and it is based on PR current controllers. The PR controller has been chosen due to the fact that it gives better performances compare to the classical PI. The two well known drawbacks of the PI controller (steady-state errors and poor harmonics rejection capability) can be easily overcome by the PR controller. The PR controller is able to remove the steady-state error without using voltage feed-forward, which makes it more reliable compared with the "classical" synchronous reference frame control. However, a three-phase PLL (Phase-Locked Loop) system is used to obtain the necessary information about the grid voltage magnitude and its angle.

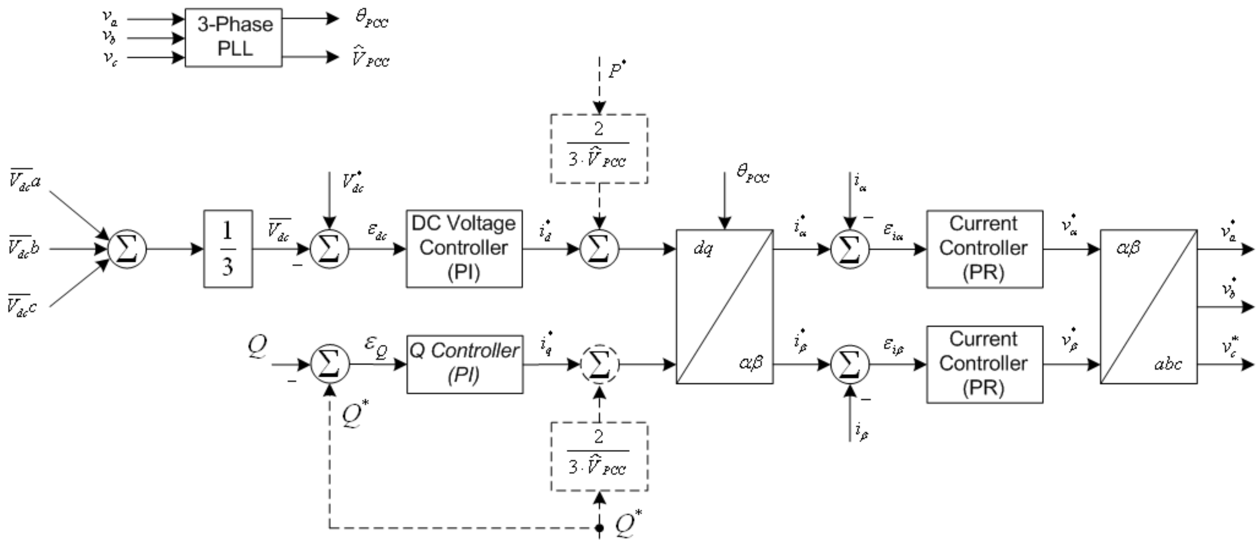

Fig. 4.6. Stationary reference frame control strategy with global DC-link voltage control for the UNIFLEX-PM system.

In order to support the bidirectional power flow through the system, the current reference in d-axis is obtained based on the active power set-point and the average voltage (provided by PLL) and a correction given by the DC-link voltage control loop. This controller controls the average value of the nine DC links of the Uniflex-PM system. The reactive power is controlled using a PI controller which provides the current reference in the q-axis. One of the drawbacks of this control is the transformation of the control variables from synchronous reference frame to the stationery one. Based on the grid voltage angle the current references in synchronous reference frame are transformed into the stationary frame and then applied to the PR current controllers. It is also worth to notice that this control does not require a neutral connection.

4.4 NATURAL REFERENCE FRAME CONTROL WITH PR CURRENT CONTROLLERS

The natural reference frame controller has been chosen in order to give to the Uniflex-PM system more flexibility in controlling the currents individually on each phase. Thus, the Uniflex-PM system can increase its ride-through capabilities and it can provide a better power flow management, especially under unbalance situations. However, the natural reference frame controller requires neutral connection.

As it can be noticed from Fig. 4.7, the natural reference frame control includes an individual PR current controller for each phase.

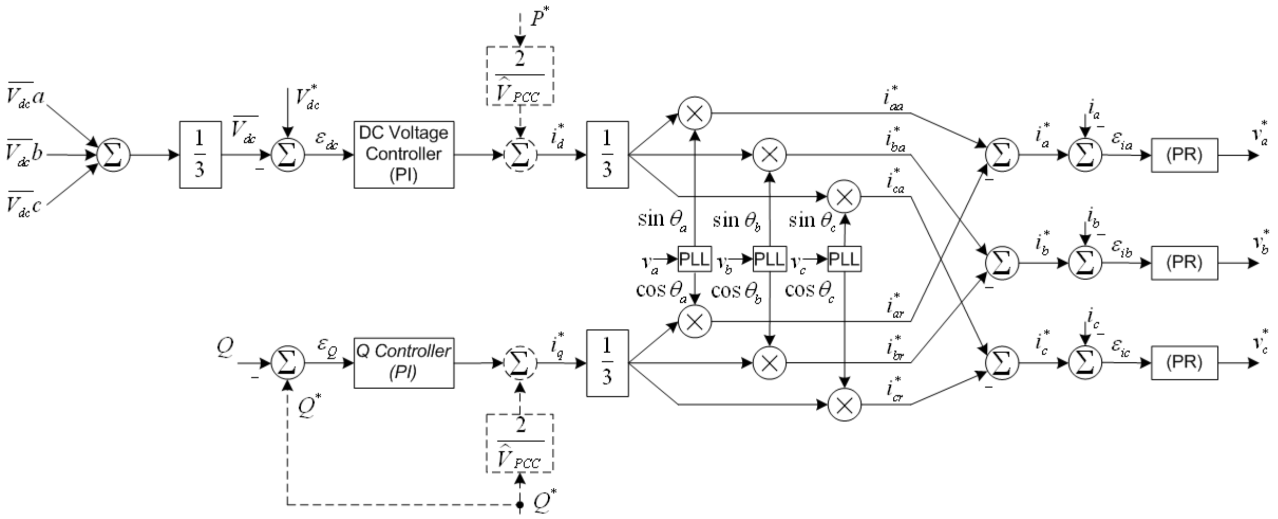

Fig. 4.7. Natural reference frame control strategy with DC control per global.

The PR controller has been chosen due to the fact that it gives better performances compare to the classical PI, as it is demonstrated in [15]. The two well known drawbacks of the PI controller (steady-state errors and poor harmonics rejection capability) can be easily overcome by the PR controller. The PR controller is able to remove the steady-state error without using voltage feed-forward, which makes it more reliable. Moreover, the proposed control strategy does not require a cross-coupling as the classical synchronous reference frame control.

The structure presented in Fig. 4.7 includes three independent single-phase PLLs (Phase-Locked Loop) based on the second order generalized integrator (SOGI), as presented in [16] and [17]. The advantage of using a PLL for each phase is that the voltage amplitude and phase in the Point of Common Coupling (PCC) can be provided for every phase of the three-phase system, thus improving the ride-through capabilities.

As shown in Fig. 4.7, the active power is controlled by a DC voltage PI controller which controls the DC voltage per global. The reactive power is controlled using a PI controller which provides the reactive currents for each phase of the system. The way it is presented, the structure shown in Fig. 4.7 can not provide active and reactive control for each phase individually. However, the DC and the Q controllers can easily be split per each phase leading to a more flexible solution for the Uniflex-PM system.

5 EVALUATION OF CONTROL STRATEGIES

5.1 SYSTEM PARAMETERS

The considered control strategies (§4) are evaluated in different grid conditions and situations. The basic parameters presented in Table 5.1 are used for the Uniflex-PM model and its control.

Table 5.1. Parameters for Uniflex-PM system.

Parameters		Units	Val.	Obs
Grid short-circuit power	S_{sc}	[MVA]	20	
Rated voltage (line-to-line)	U_{ll}	[kV]	3.3	
Grid impedance ratio	R/X	-	0.1	
Rated apparent power / converter	S_{nc}	[kVA]	300	
Rated output current / module	I_{nm}	[A]	52.63	
Input filter reactance [pu]	x_f	[pu]	0.14	16 mH
DC-link voltage	V_{dc}	[V]	1100	
DC-link capacitor	C	[mF]	6.2	WP4PL_TN_3005.pdf
Switching frequency of H-bridge	f_{sw}	[Hz]	300	
Switching frequency for Converter	$f_{sw,conv}$	[Hz]	1800	
Deadtime	T_{dead}	[µs]	-	-
Sampling frequency for control	$f_{sampling}$	[kHz]	5	

5.2 STUDY CASES

In order to evaluate the selected control strategies for the Uniflex-PM system some simulation study cases have been designed. A detailed description of these study cases is provided in the following paragraphs.

5.2.1 Harmonic content

This analysis considers that the power modules deliver 100% active power into the PCC while the reactive power is set to zero. The grid voltages are "clean" which means no harmonic content is present in the PCC.

The harmonic spectrum is computed for phase current as follows:

- 10 fundamental periods are used for the Fast Fourier Transform;
- The resolution is 512 points per 20 ms fundamental period, thus a 12 kHz bandwidth for the spectra is provided.
- Interharmonics (if any) are removed from the original spectra.
- Individual harmonics for currents up to 50th harmonic plotted vs. EN 61000-2-4 [10].
- Current THD calculated for harmonics up to 50th order are compared with the maximum value of 8% permitted in EN 61000-2-4 (Class 2) [10].

It has been selected the standard EN 61000-2-4 because it provides harmonic levels for multiple of the 3rd harmonic. The standard EN 50160 does not provide this value. Thus, the control strategies that require a neutral connection such as the predictive control can be evaluated even for these harmonics.

5.2.2 Bi-directional power flow

A bi-directional power flow is simulated with a profile as shown in Fig. 5.1.This corresponds to a leading/lagging operation at 0.9 power factor.

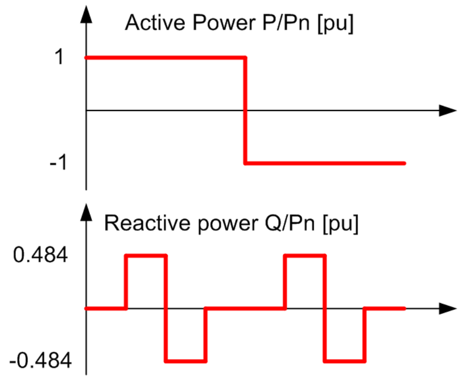

Fig. 5.1. Power profile for studying the bi-directional power flow.

5.2.3 Voltage excursions

Voltage excursions of 75% and 120% from the rated voltages in the PCC of the Port 1 are considered as shown in Fig. 5.2.

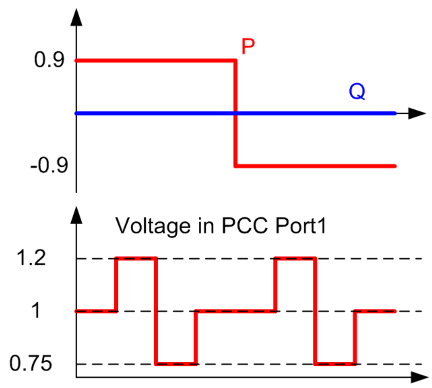

Fig. 5.2. Time profile for voltage excursions in Port 1.

5.2.4 Voltage unbalances

An unbalance of 3% is considered in the grid voltages at Port 1. This unbalance is defined as the ratio between the negative and the positive sequence of the voltage (V_{neg}/V_{pos}) in the PCC. During the unbalances the active power is reversing through the Uniflex-PM system while the reactive power in both ports is kept at zero as shown in Fig. 5.3.

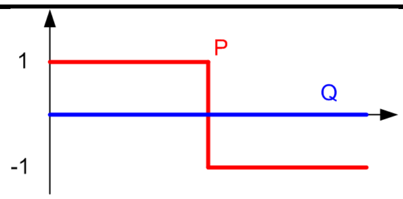

Fig. 5.3. Power references in Port 1 during unbalanced voltages.

5.2.5 Voltage asymmetries/Phase jumps

The considered control strategies are evaluated for phase jumps of ± 60º in all phases at Port 1 as shown in Fig. 5.4.

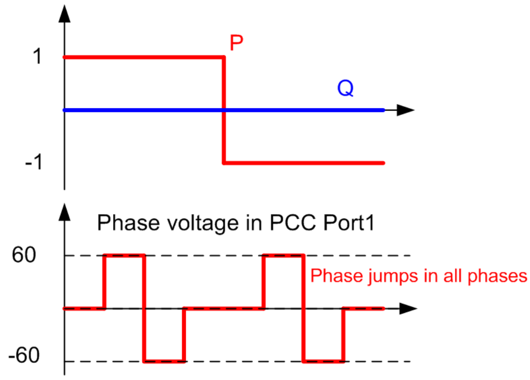

Fig. 5.4. Time profile for phase jumps in PCC voltages for Port 1.

It should be noticed here that the phase jump from +60° to -60° is an extreme situation that cannot occur in real operation. Typically the phase jumps are from zero to ±60° [13]. However, this case has been selected to evaluate the proposed control strategies under extreme conditions.

5.2.6 Frequency excursions

The control strategies are evaluated for frequency excursions in Port 1. There is a reverse in active power while the reactive power is kept constant at zero during these frequency excursions as presented in Fig. 5.5.

Again, this case can be considered as an extreme one. In normal operation of a power system such sudden changes in the grid frequency cannot occur.

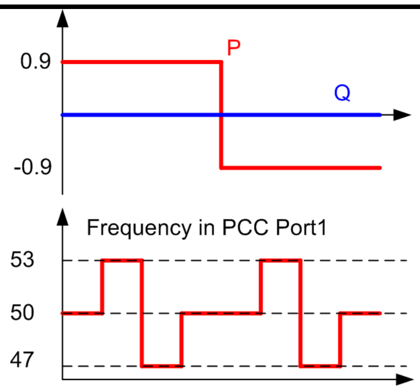

Fig. 5.5. Profile for frequency excursions in PCC of Port 1.

5.2.7 Short-Circuits

All types of short-circuits namely three-phase, two-phase with ground, two-phase without ground and single-phase one are studied. The short-circuit resistance is selected so that the voltage dip is down to 10% of the rated voltage in the PCC where possible.

Table 5.2. Specifications for short-circuit analysis

Short-Circuit Type	Acronym	Voltage level in PCC
Three-phase	3-ph SC	0.1 [pu] in phase A,B,C
Two-phase with ground	2-ph gnd SC	0.1 [pu] in phase A,B
Two-phase without ground	2-ph SC	0.5 [pu] in phase A and B
Single-phase	1-ph SC	0.1 [pu] in phase A

These events will occur at the PCC of Port 1. The system is operating at 100% active power and 0% reactive power. The voltage dip will have duration of 100 msec as shown in Fig. 5.6.

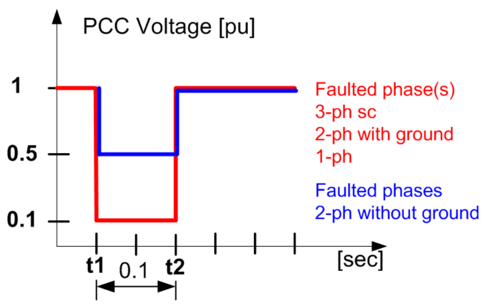

Fig. 5.6. Voltage profile used in short-circuit analysis.

Before the event the power converter will operate at 100% active power and 0% reactive power. During and after the fault the active power reference is set to zero, while the power converter delivers 100% reactive current in the faulted port.

5.3 SIMULATION RESULTS

In this paragraph the simulation results are presented for the following control strategies:

- Synchronous reference frame *dq* control as presented in §4.1;
- Predictive control as presented in §4.2;
- Stationary reference frame $\alpha\beta$ control as presented in §4.3;
- Natural reference frame *abc* control as presented in §4.4.

The simulation results are organized as follows:

- Synchronous reference frame *dq* control
  - Voltage and current waveforms in Port 1.
  - Active and reactive power in Port 1.
  - Voltage and current waveforms in Port 2.
  - Active and reactive power in Port 2.
- Predictive control
  - Voltage and current waveforms in Port 1.
  - Average DC-link voltage in Phase B of the system.
  - Active and reactive power in Port 1.
  - Active and reactive power in Port 2.
- Stationary reference frame control
  - Reference signals for the considered study case.
  - Currents in Port 1 and Port 2.
  - Average DC-link voltage used in control.
  - Active and reactive power in Port 1
  - Active and reactive power in Port 2
- Natural reference frame control
  - Reference signals for the considered study case.
  - Currents in Port 1 and Port 2.
  - Average DC-link voltage used in control.
  - Active and reactive power in Port 1
  - Active and reactive power in Port 2

For each control strategy some conclusions are provided after the study cases.

5.3.1 Synchronous reference frame control

5.3.1.1 Current Harmonic Compatibility Levels

The current harmonic compatibility levels for the synchronous reference frame control compared with the standard are given in Fig. 5.7.

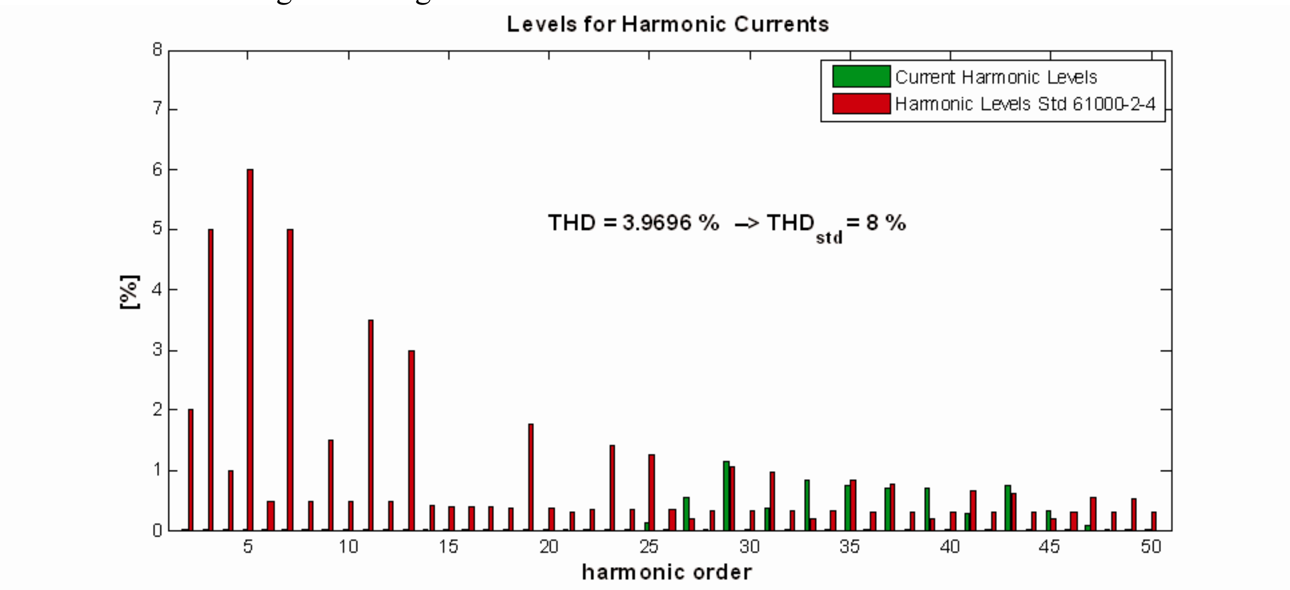

Fig. 5.7. Current harmonic compatibility levels for synchronous reference frame control.

Most of the current harmonic levels exceed the standard values for harmonic orders greater than the 27^{th} harmonic. It should be noticed that the switching frequency is around 1.8 kHz that corresponds to the 36^{th} harmonic in the spectrum. The current THD is below 4% in this case.

5.3.1.2 Bi-directional Power Flow

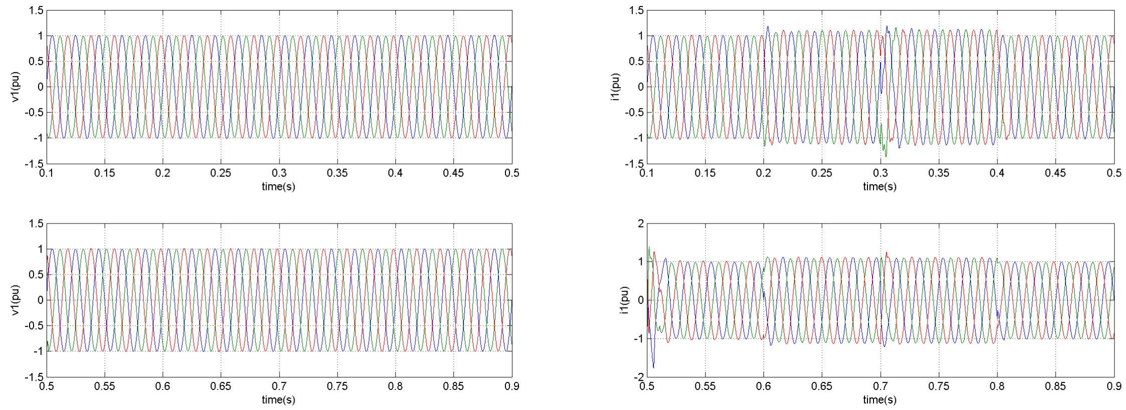

a) b)

Fig. 5.8. Simulation results in Port 1 for bidirectional power flow: a) voltage and b) current.

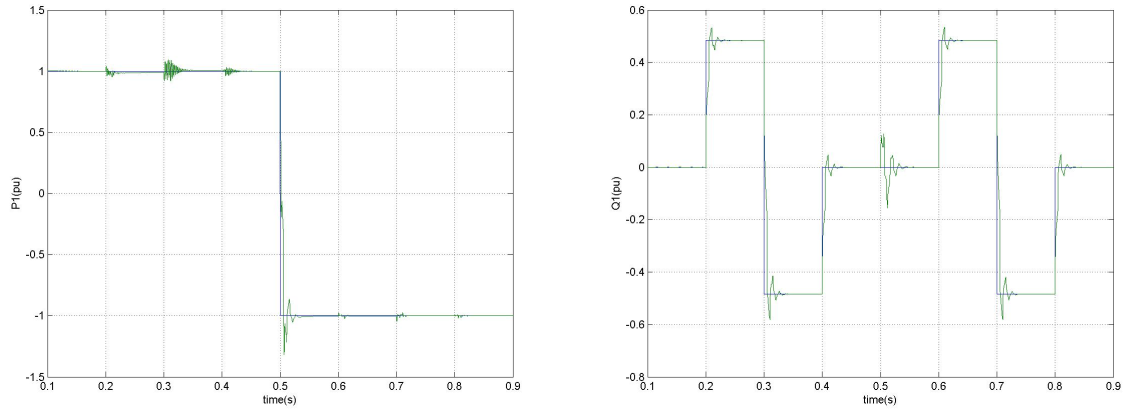

a) b)

Fig. 5.9 Simulation results in Port 1 for bidirectional power flow: a) active power and b) reactive power.

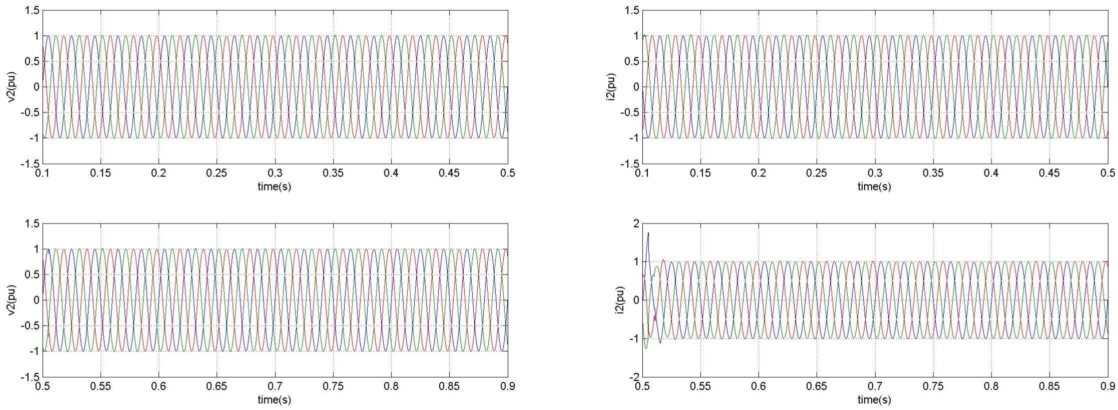

a) b)

Fig. 5.10. Simulation results in Port 2 for bidirectional power flow: a) voltage and b) current.

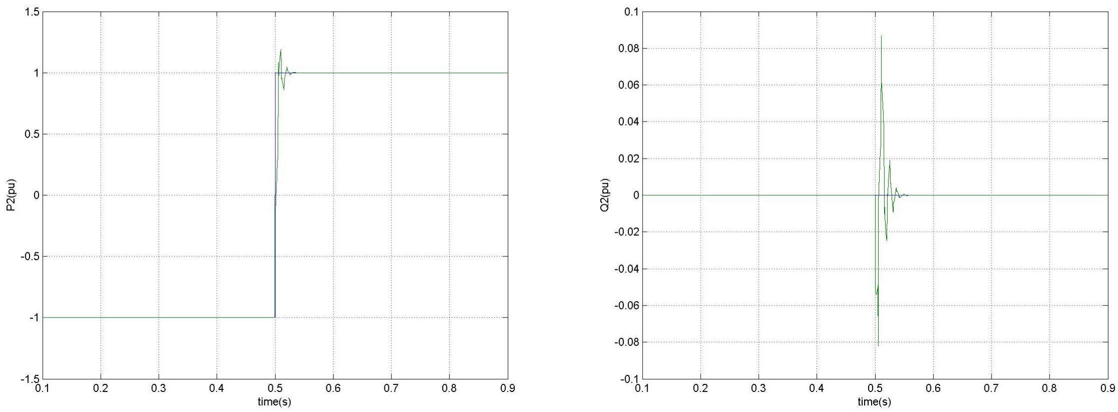

a) b)

Fig. 5.11. Simulation results in Port 2 for bidirectional power flow: a) active power and b) reactive power.

5.3.1.3 Voltage Excursions

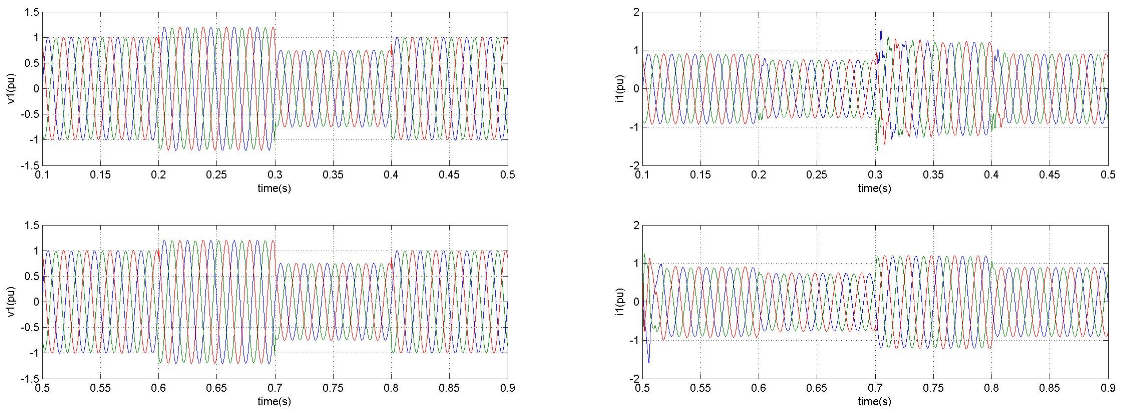

a) b)

Fig. 5.12 Simulation results in Port 1 for voltage excursions:
a) voltage and b) current.

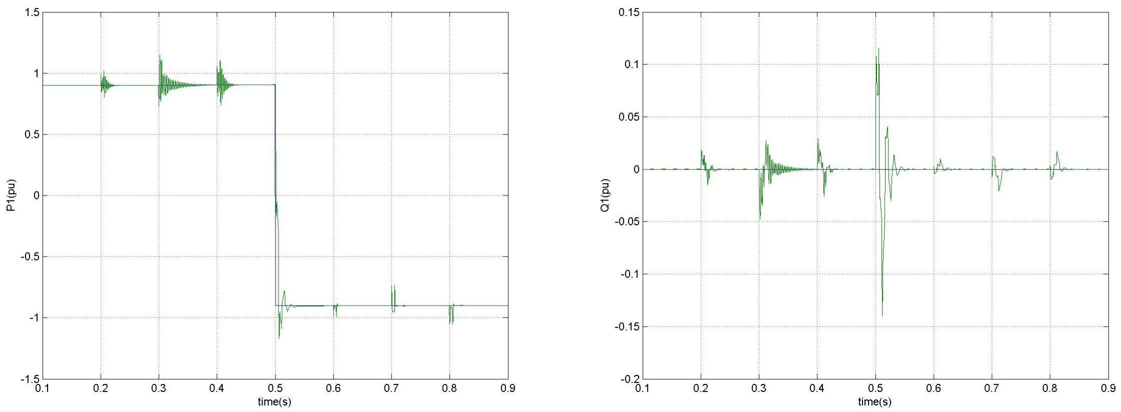

a) b)

Fig. 5.13. Simulation results in Port 1 for voltage excursions:
a) active power and b) reactive power.

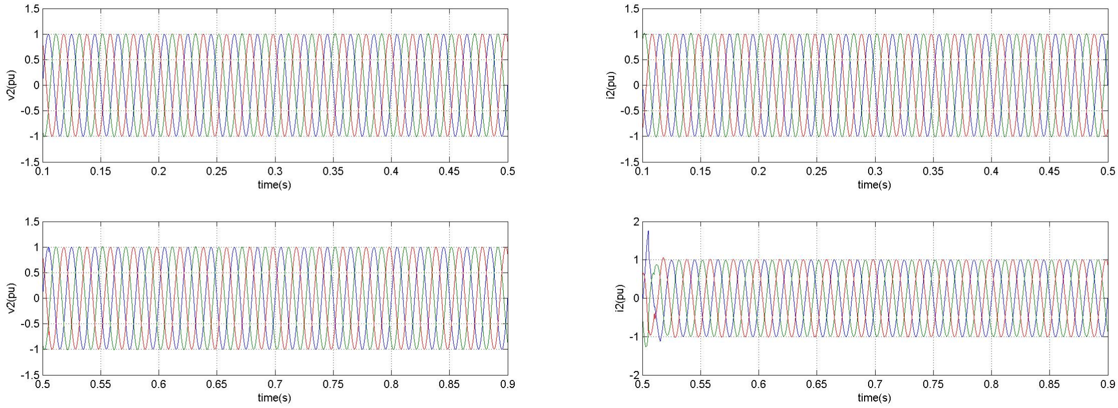

a) b)

Fig. 5.14. Simulation results in Port 2 for voltage excursions: a) voltages and b) currents.

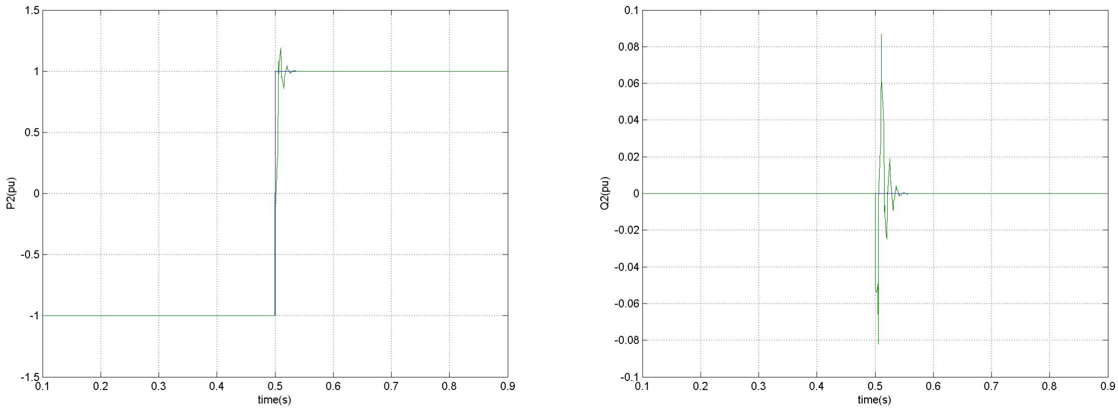

a) b)

Fig. 5.15. Simulation results in Port 2 for voltage excursions: a) active power and b) reactive power.

5.3.1.4 Voltage unbalances

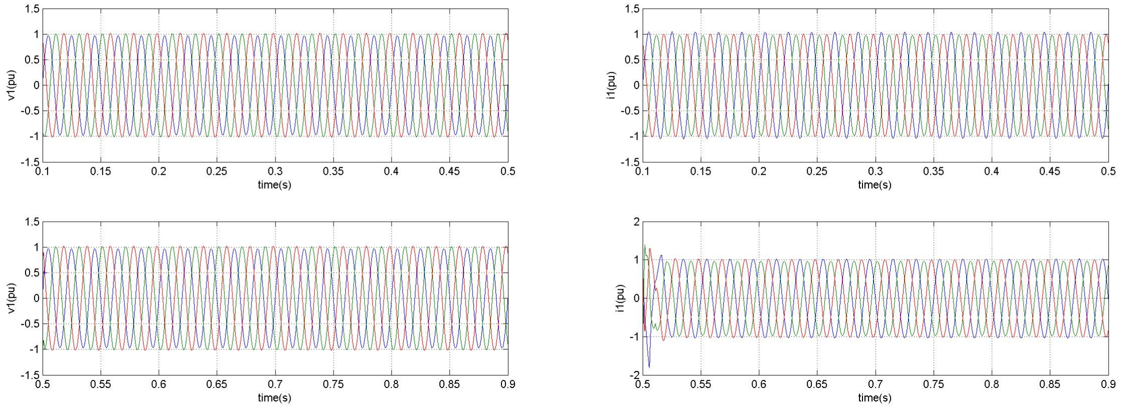

a) b)

Fig. 5.16. Simulation results in Port 1 for voltage unbalances:
a) voltages and b) currents.

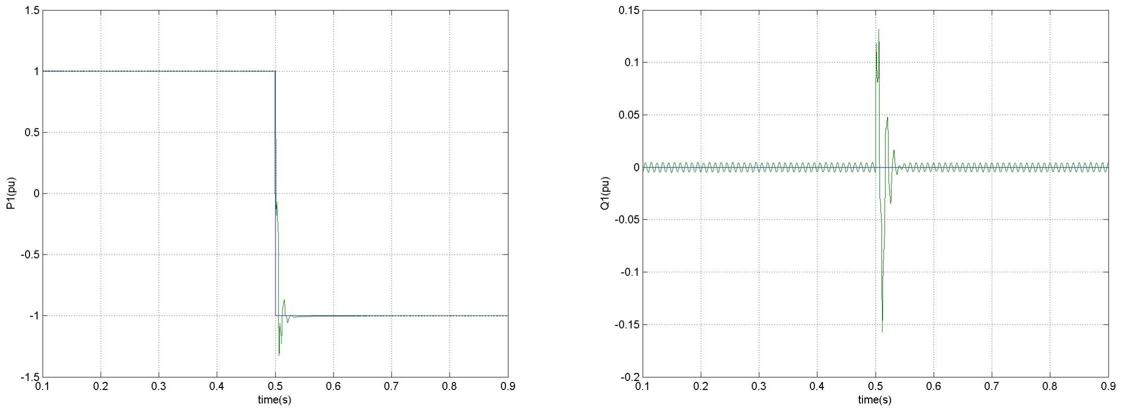

a) b)

Fig. 5.17. Simulation results in Port 1 for voltage unbalances:
a) active power and b) reactive power.

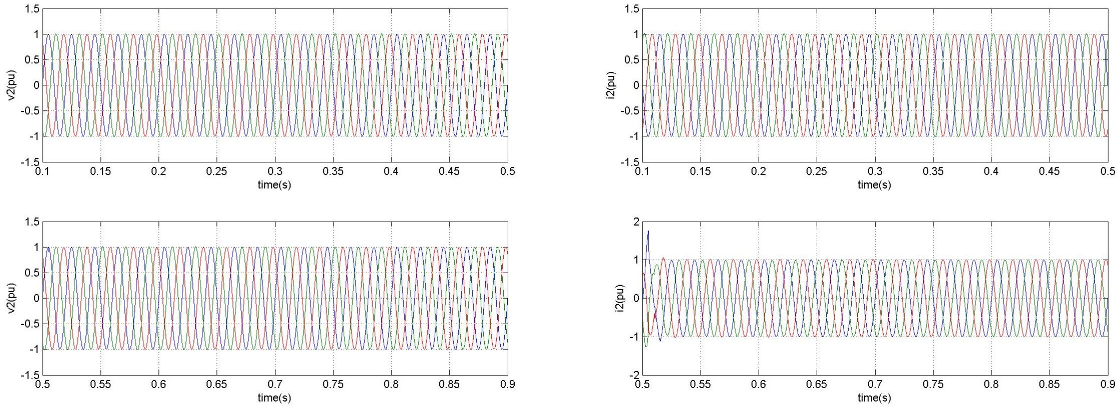

a) b)

Fig. 5.18. Simulation results in Port 2 for voltage unbalances:
a) voltages and b) currents.

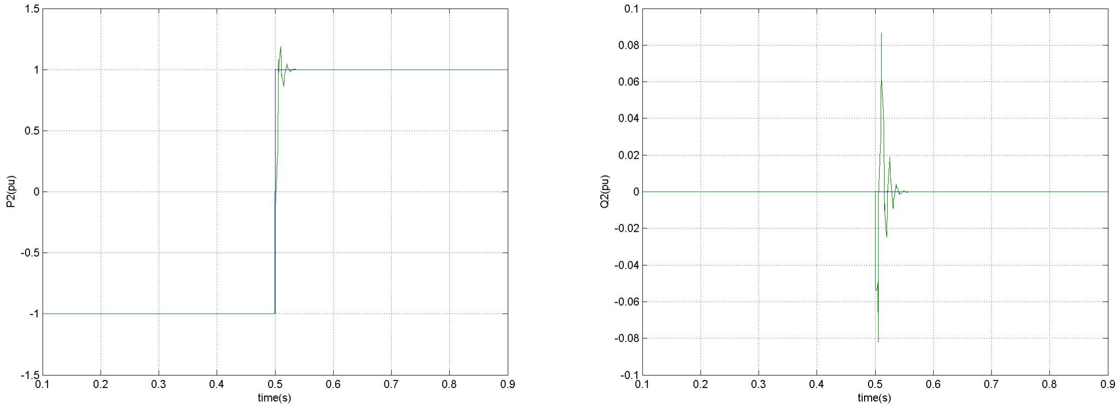

a) b)

Fig. 5.19. Simulation results in Port 2 for voltage unbalances:
a) active power and b) reactive power.

5.3.1.5 Phase jumps

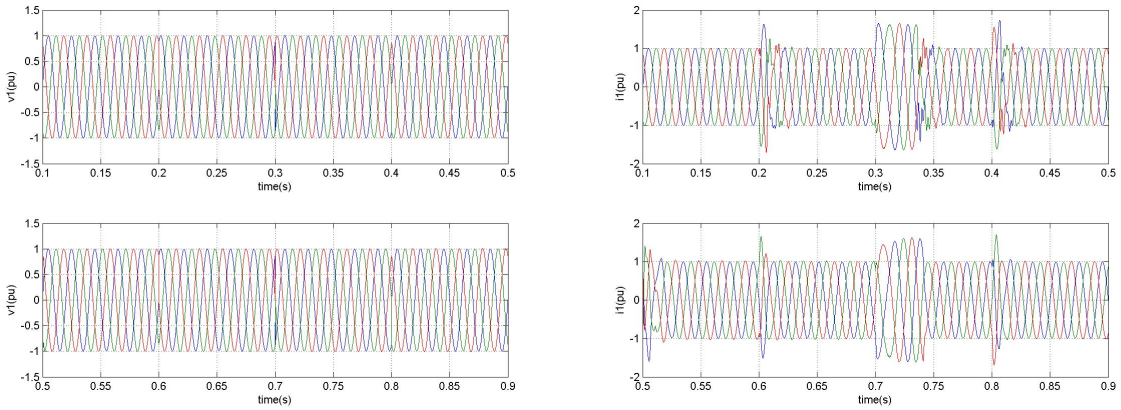

a) b)

Fig. 5.20. Simulation results in Port 1 for phase jumps:
a) voltages and b) current.

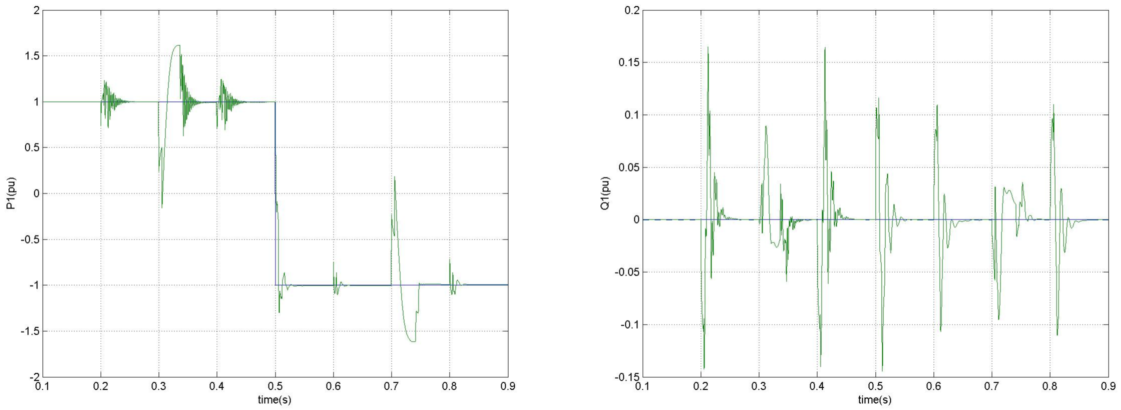

a) b)

Fig. 5.21. Simulation results in Port 1 for phase jumps:
a) active power and b) reactive power.

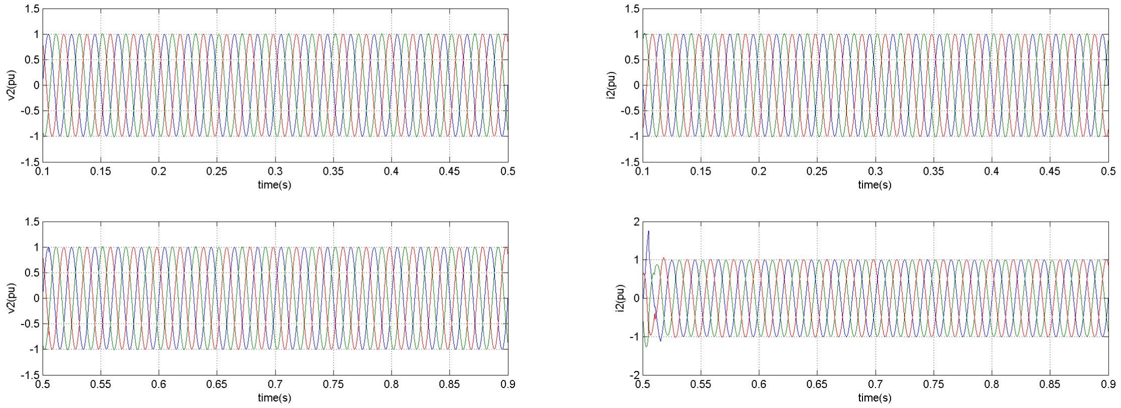

a) b)

Fig. 5.22. Simulation results in Port 2 for phase jumps:
a) voltages and b) current.

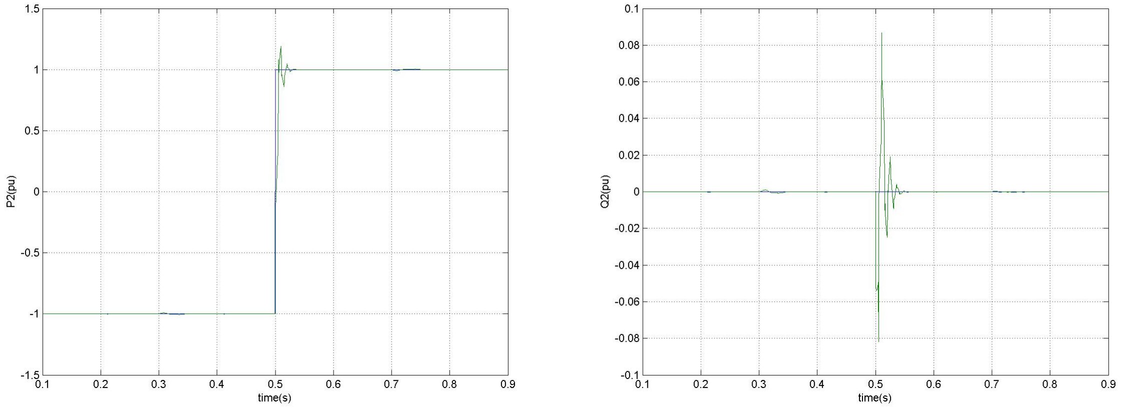

a) b)

Fig. 5.23. Simulation results in Port 2 for phase jumps:
a) active power and b) reactive power.

5.3.1.6 Frequency Excursions

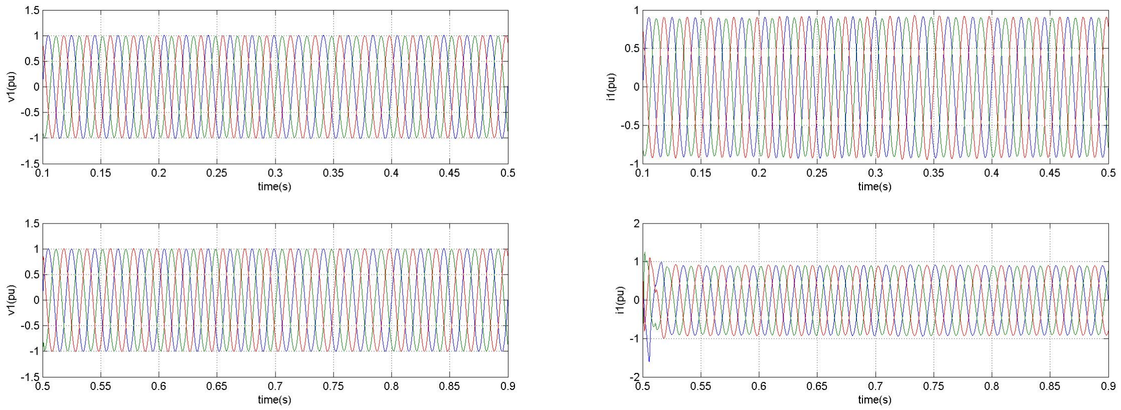

a) b)

Fig. 5.24. Simulation results in Port 1 for frequency excursions:
a) voltages and b) currents.

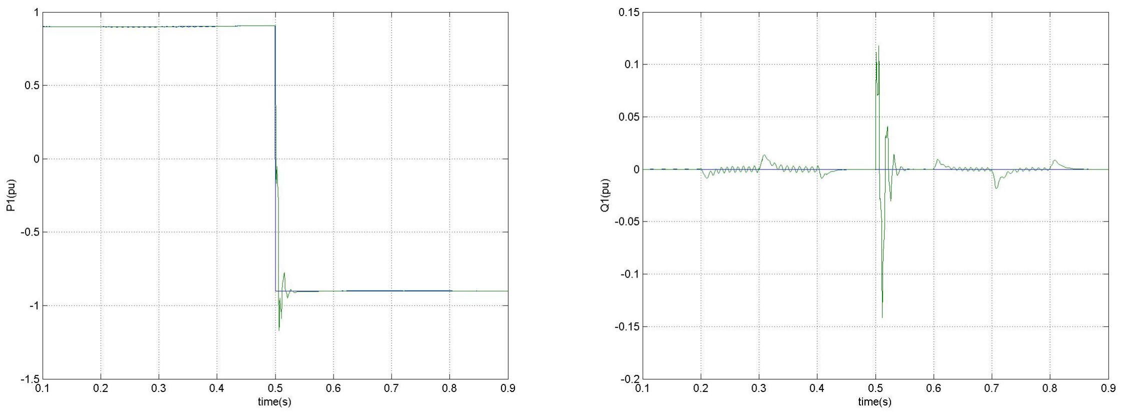

a) b)

Fig. 5.25. Simulation results in Port 1 for frequency excursions:
a) active power and b) reactive power.

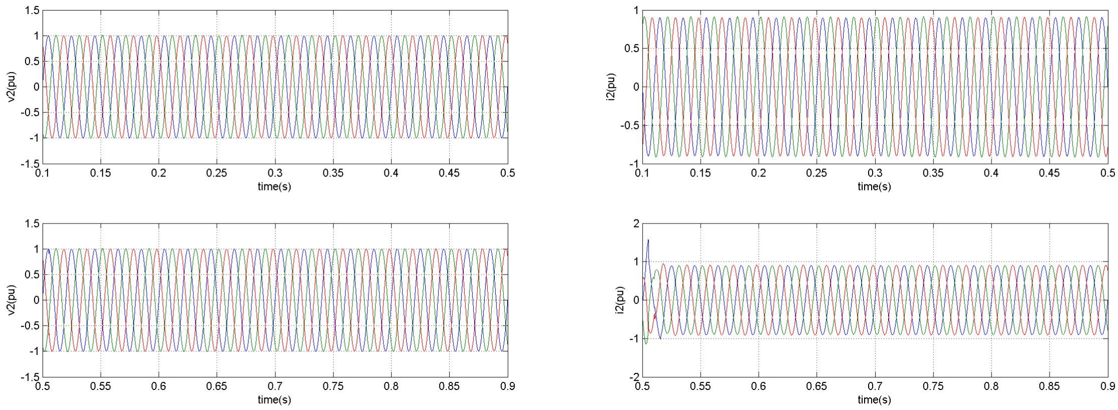

a) b)

Fig. 5.26. Simulation results in Port 2 for frequency excursions: a) voltages and b) currents.

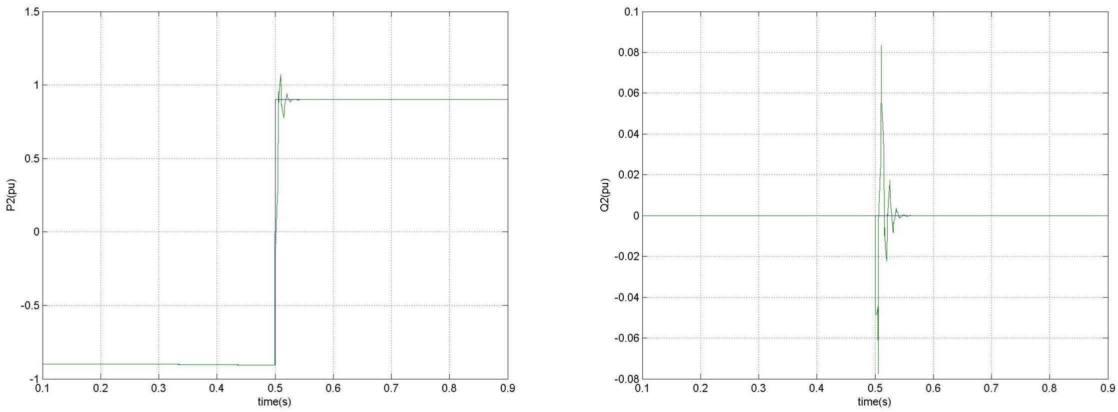

a) b)

Fig. 5.27. Simulation results in Port 2 for frequency excursions: a) active power and b) reactive power.

5.3.1.7 Single-phase short circuit

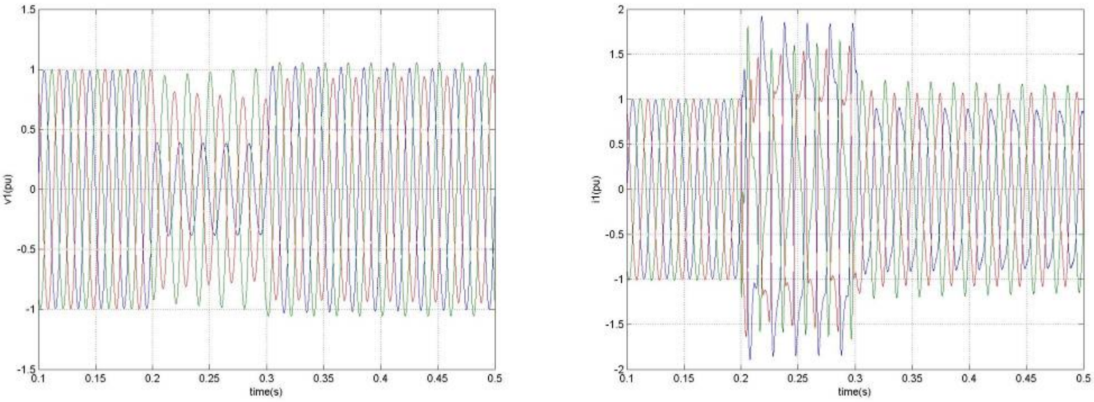

a) b)

Fig. 5.28. Simulation results in Port 1 for single phase short-circuit:
a) voltages and b) currents.

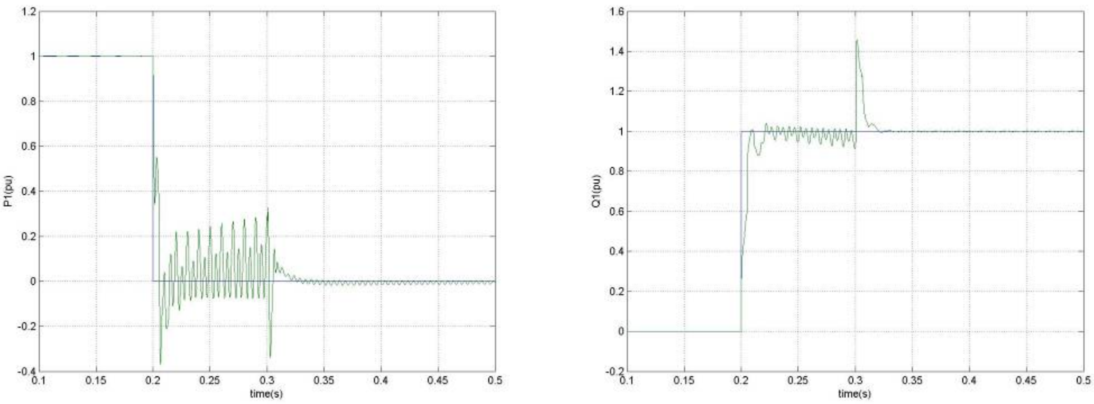

a) b)

Fig. 5.29. Simulation results in Port 1 for single phase short-circuit:
a) active power and b) reactive power.

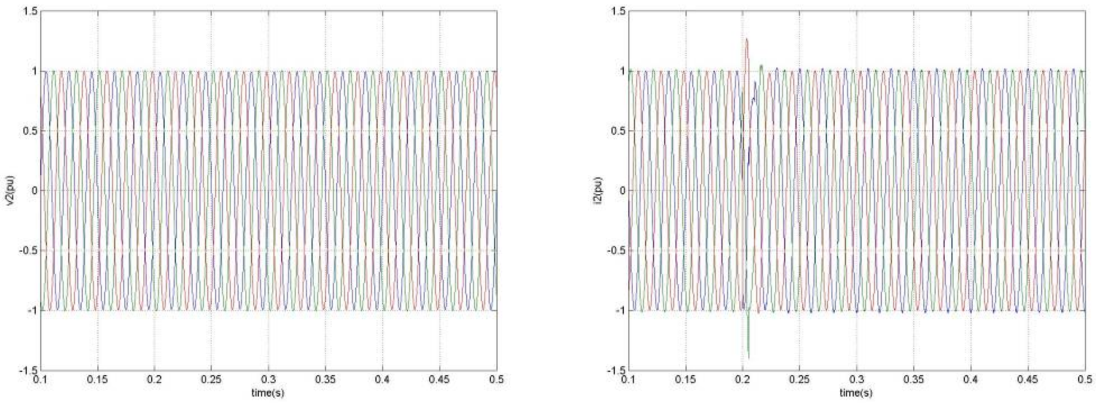

a) b)

Fig. 5.30. Simulation results in Port 2 for single phase short-circuit:
a) voltages and b) currents.

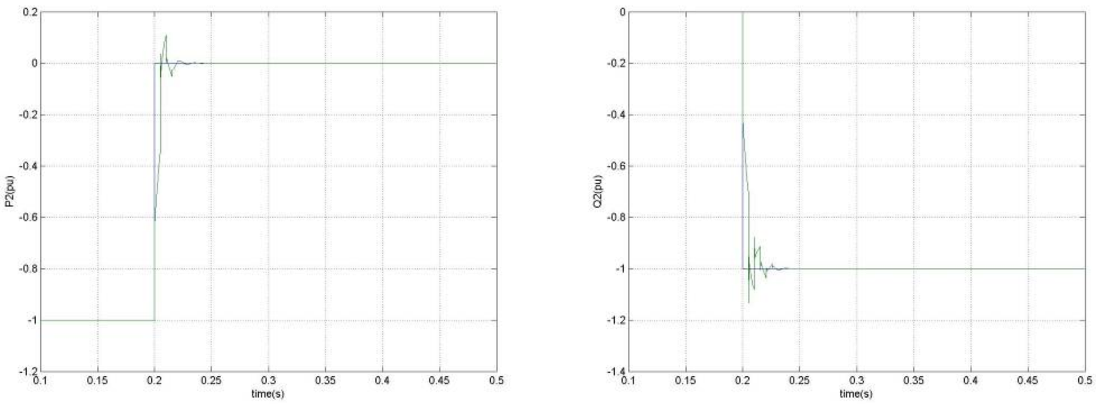

a) b)

Fig. 5.31. Simulation results in Port 2 for single phase short-circuit:
a) active power and b) reactive power.

5.3.1.8 Two-phase short-circuit

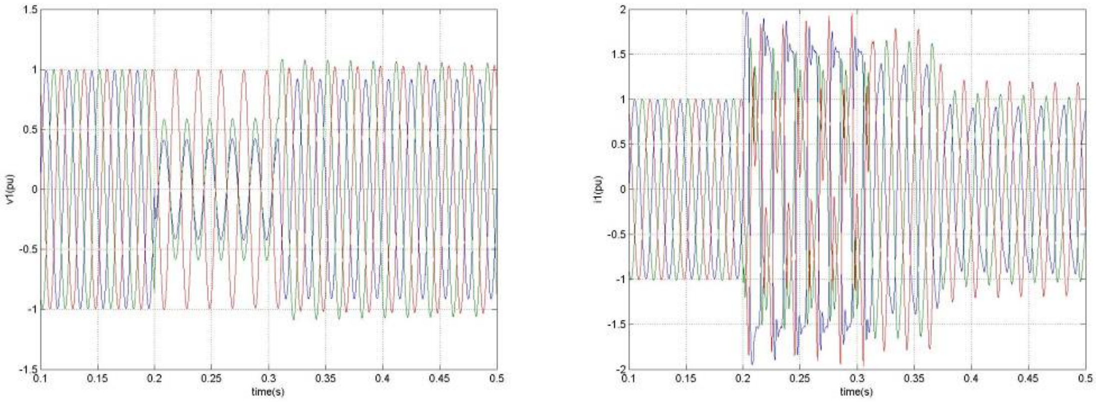

a) b)

Fig. 5.32. Simulation results in Port 1 for two- phase short-circuit: a) voltages and b) currents.

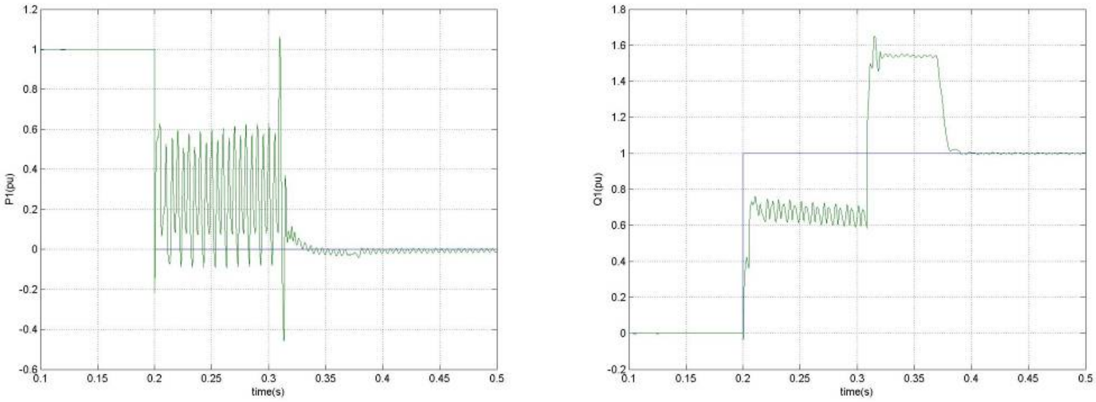

a) b)

Fig. 5.33. Simulation results in Port 1 for two- phase short-circuit: a) active power and b) reactive power.

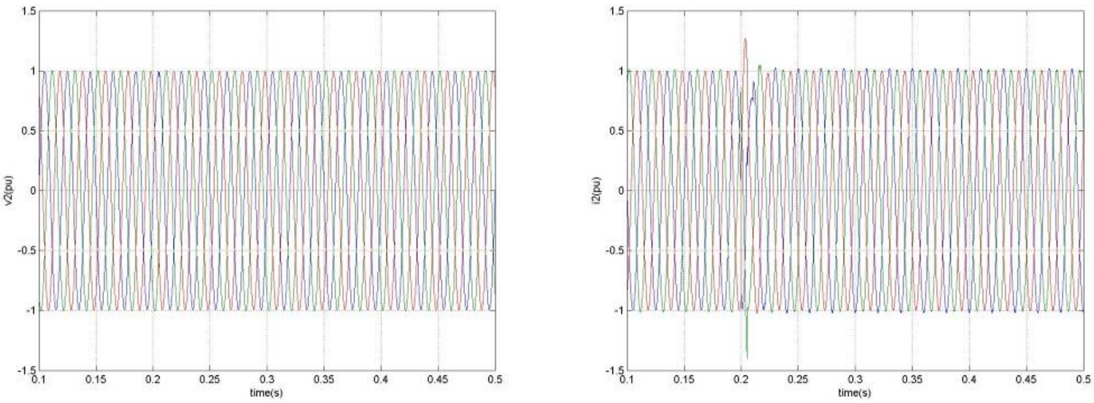

a) b)

Fig. 5.34. Simulation results in Port 2 for two- phase short-circuit:
a) voltages and b) currents.

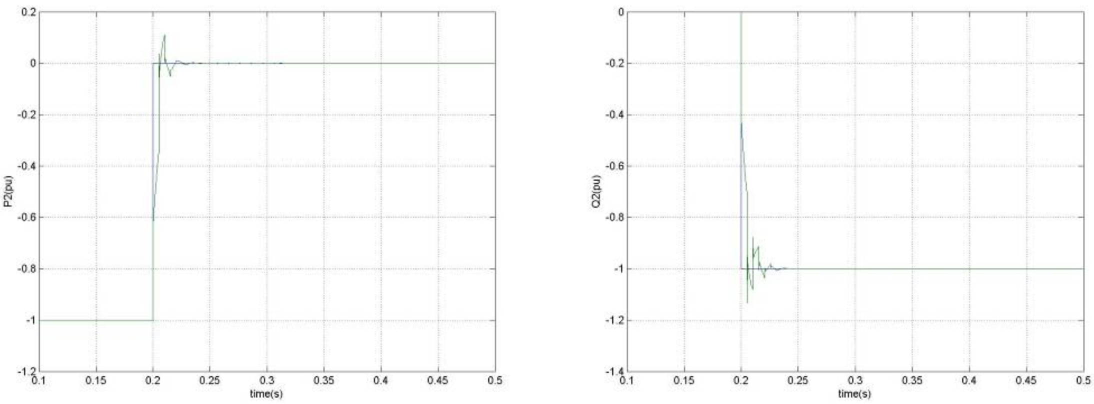

Fig. 5.35. Simulation results in Port 2 for two- phase short-circuit
a) active power and b) reactive power.

5.3.1.9 Two-phase with ground short-circuit

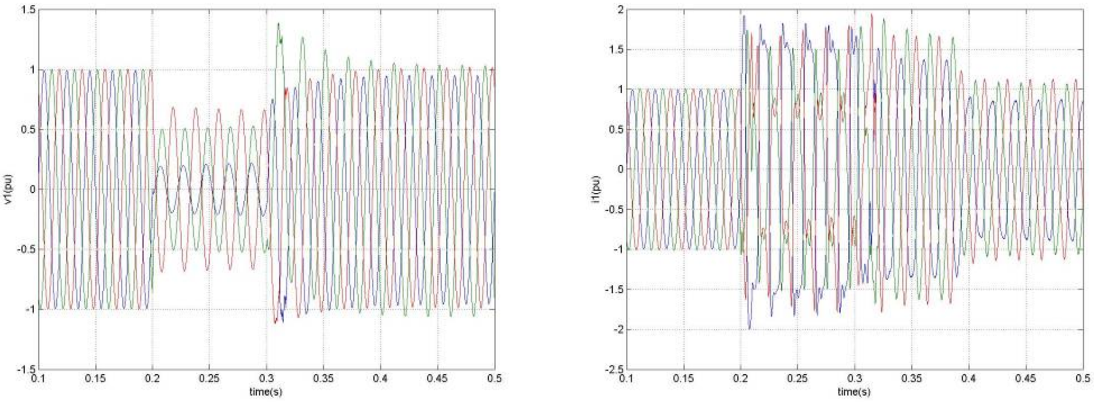

a) b)

Fig. 5.36. Simulation results in Port 1 for two- phase with ground short-circuit: a) voltages and b) currents.

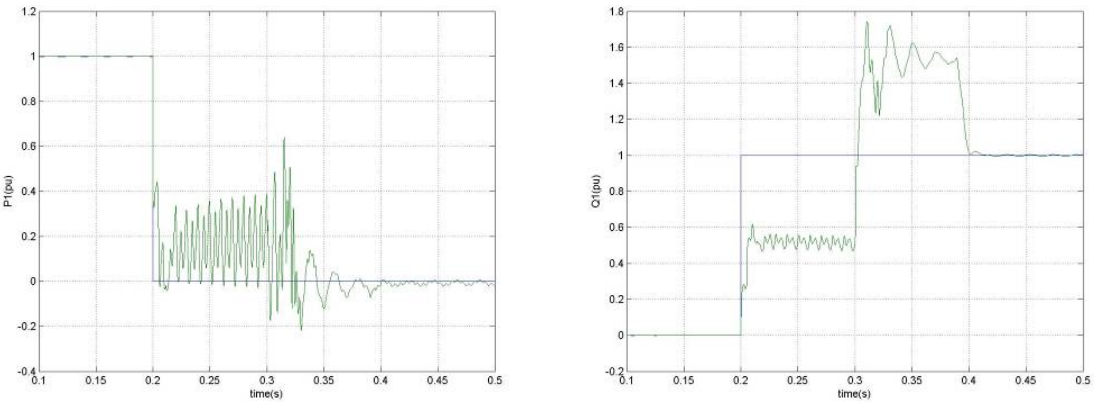

a) b)

Fig. 5.37. Simulation results in Port 1 for two- phase with ground short-circuit: a) active power and b) reactive power.

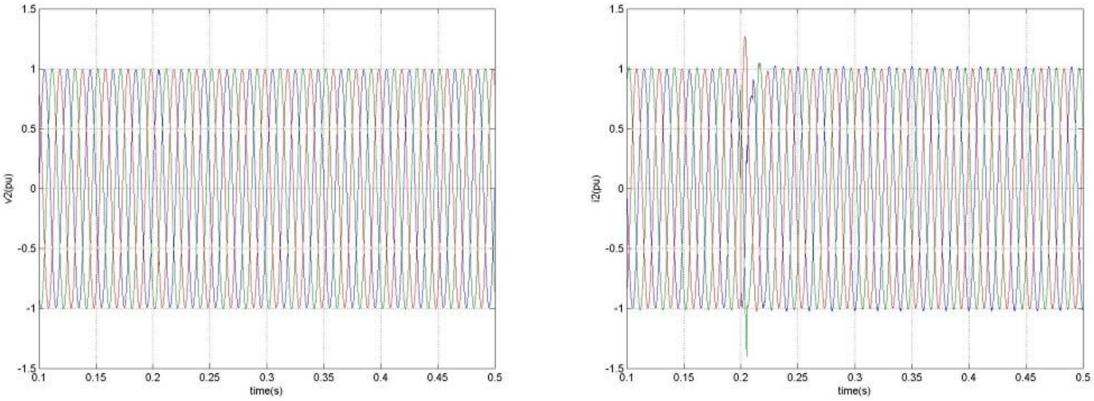

a) b)

Fig. 5.38. Simulation results in Port 2 for two- phase with ground short-circuit: a) voltages and b) currents.

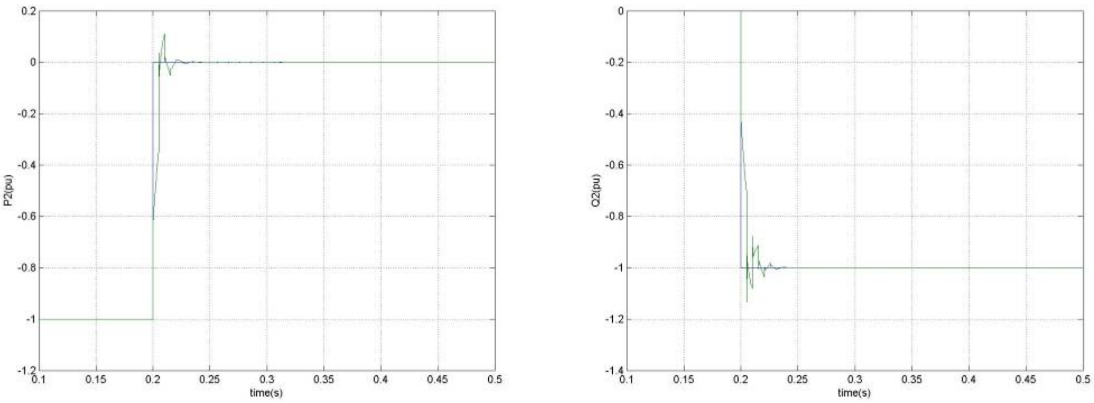

a) b)

Fig. 5.39. Simulation results in Port 2 for two- phase with ground short-circuit: a) active power and b) reactive.

5.3.1.10 Three-phase short-circuit

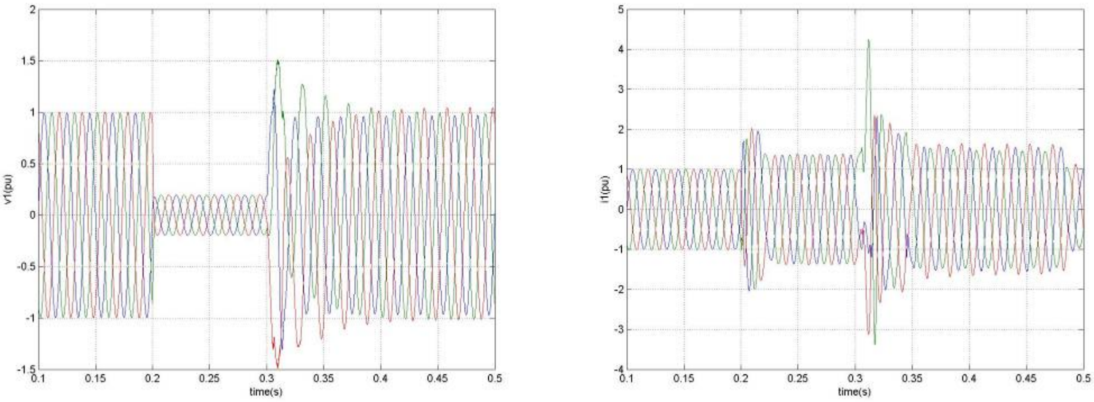

a) b)

Fig. 5.40. Simulation results in Port 1 for three- phase short-circuit: a) voltages and b) currents.

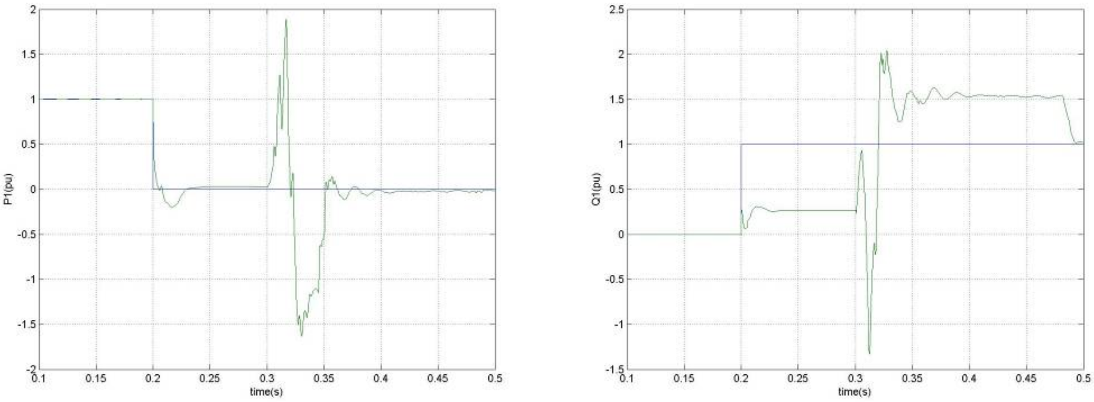

Fig. 5.41. Simulation results in Port 1 for three- phase short-circuit: a) active power and b) reactive power.

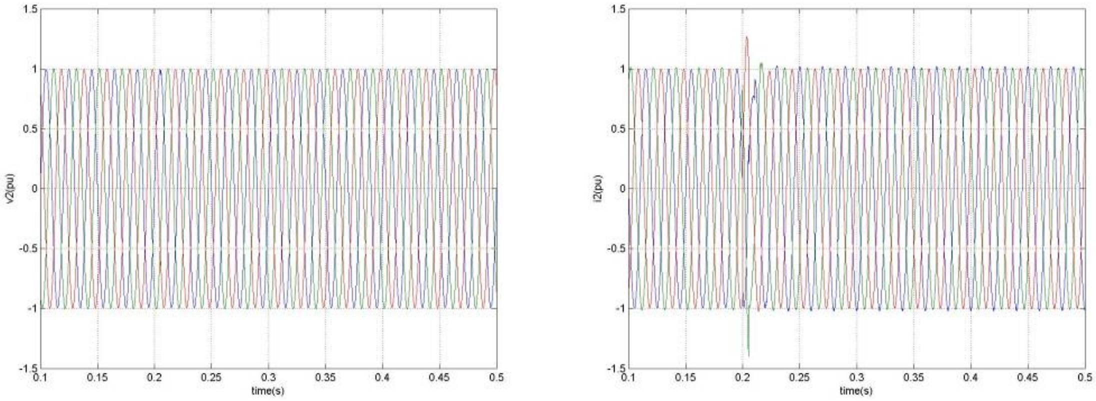

a) b)

Fig. 5.42. Simulation results in Port 2 for three- phase short-circuit: a) voltages and b) currents.

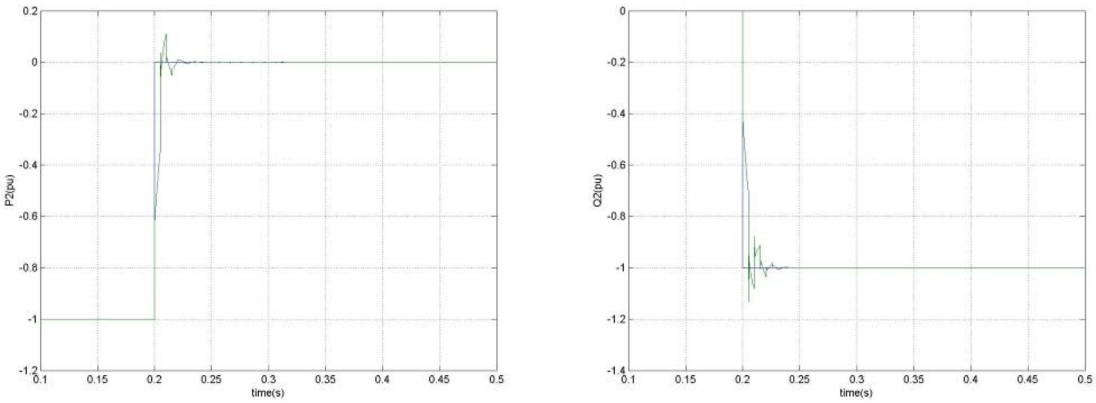

Fig. 5.43. Simulation results in Port 2 for three- phase short-circuit: a) active power and b) reactive power.

5.3.1.11 Conclusions

From the above simulation results, the effectiveness of the proposed PI controller-based method in dual synchronous reference frame is verified. It allows a good tracking of the active and reactive power references under different conditions. However, the reactive power control is not completely decoupled of the active power. Thus, transients in the reactive power can be observed when the power flow is changed between the two ports in all considered cases. The supply currents are essentially sinusoidal even under extreme unbalanced supply conditions.

Among all the study-cases, the phase excursions are the most difficult to control. Relatively large transients in both active and reactive power can be observed in this case especially when the phase changes from +60º to -60 º.

The system performance during short-circuits relies on the angular information, so the PLL is a key-element in the control. A reliable and fast PLL is expected to have deep effect on the controller bandwidth and reliability. Furthermore the delay signal cancellation method, which allows positive and negative signals extraction, also plays an important role to improve the controller bandwidth.

Thus, the currents in the faulted port exceed the rated values by a factor of two in all cases except the three-phase short circuit where this factor is approximately four during the clearance of the fault. A 100 Hz component is present in the active and reactive power of the faulted port in all cases. Also the active and reactive power are difficult to control during the all types of short-circuits.

Further developments must be made in order to improve the grid voltage angle detection as well as the extraction of the positive and negative sequences of the grid voltage.

5.3.2 Predictive current control

5.3.2.1 Current Harmonic Compatibility Levels

A comparison of the current harmonic compatibility levels with the standard is given in Fig. 5.44.

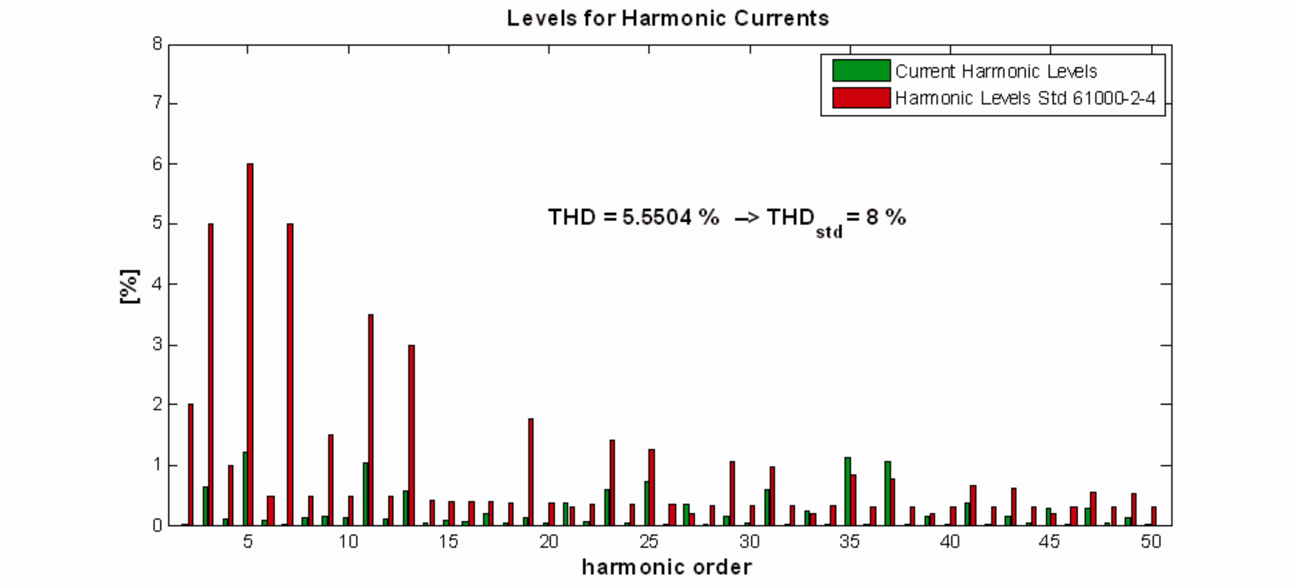

Fig. 5.44. Current harmonic compatibility levels for the predictive control.

The current harmonic levels are exceeding the standard values for harmonic orders around the switching frequency. It should be noticed that a global switching frequency of 1.8 kHz will correspond to the 36th harmonic in the spectrum. Important value of the 3rd harmonic is present due to the neutral connection required by this control strategy. Also, important values, however in the limits, are present for the 5th, 11th and 13th harmonics. Globally, a value of 5.55% is obtained for the current THD.

5.3.2.2 Bi-directional Power Flow

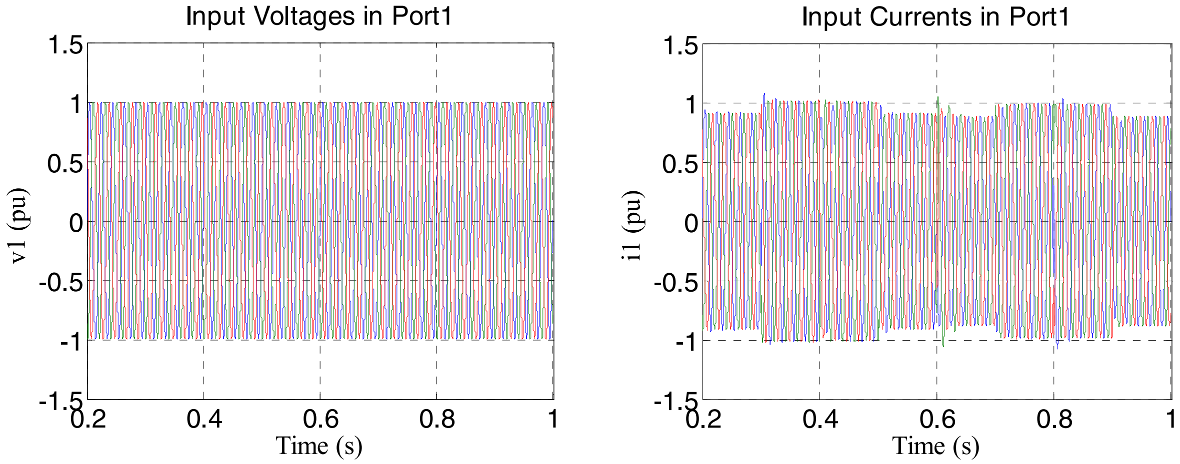

a) b)

Fig. 5.45. Simulation results in Port 1 for bi-directional power flow: a) voltages and b) currents.

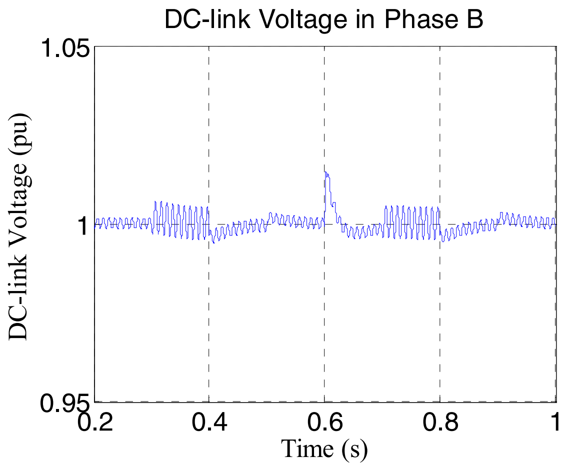

a) b)

Fig. 5.46. Average DC-link Voltage in Phase B for bi-directional power flow.

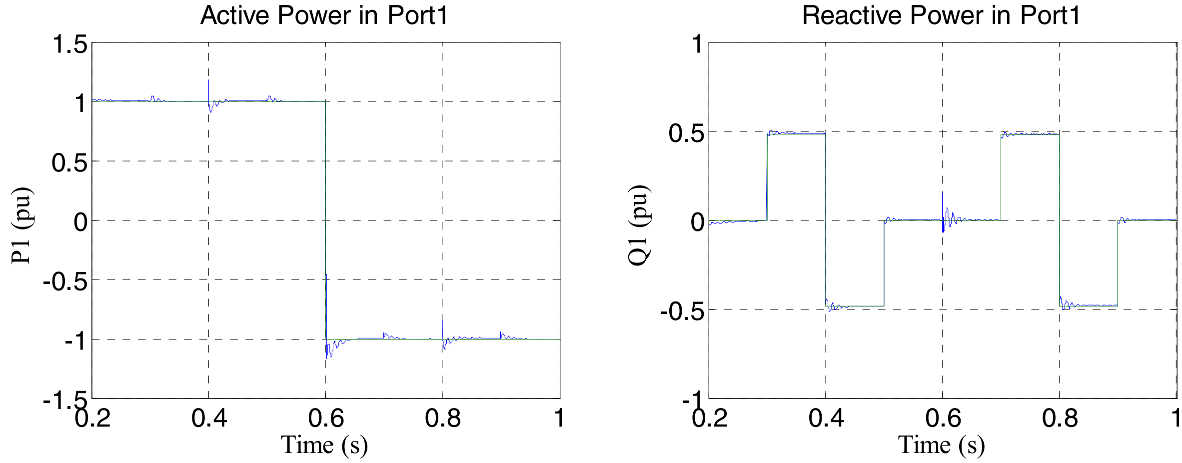

a) b)

Fig. 5.47. Simulation results in Port 1 for bi-directional power flow: a) active power and b) reactive power.

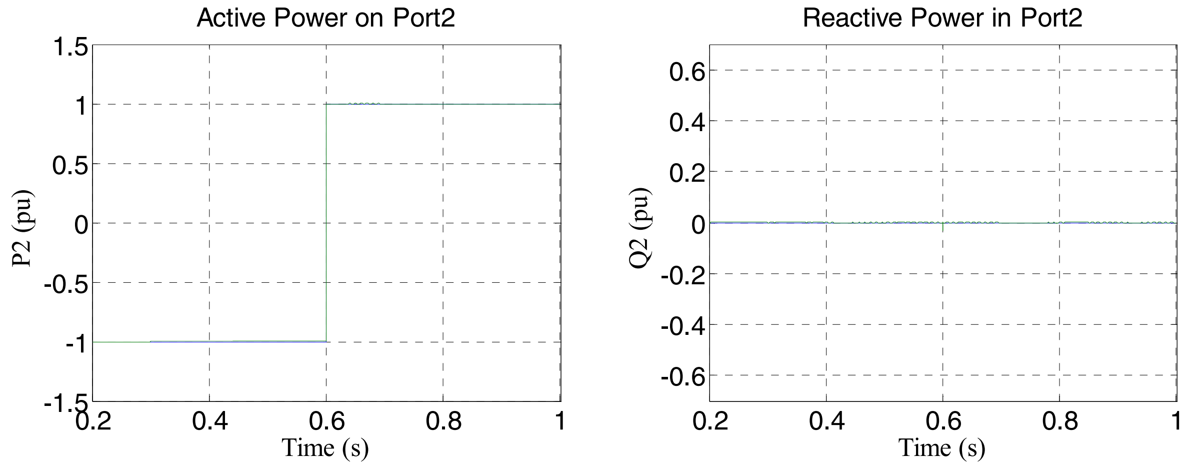

a) b)

Fig. 5.48. Simulation results in Port 2 for bi-directional power flow: a) active power and b) reactive power.

5.3.2.3 Voltage Excursions

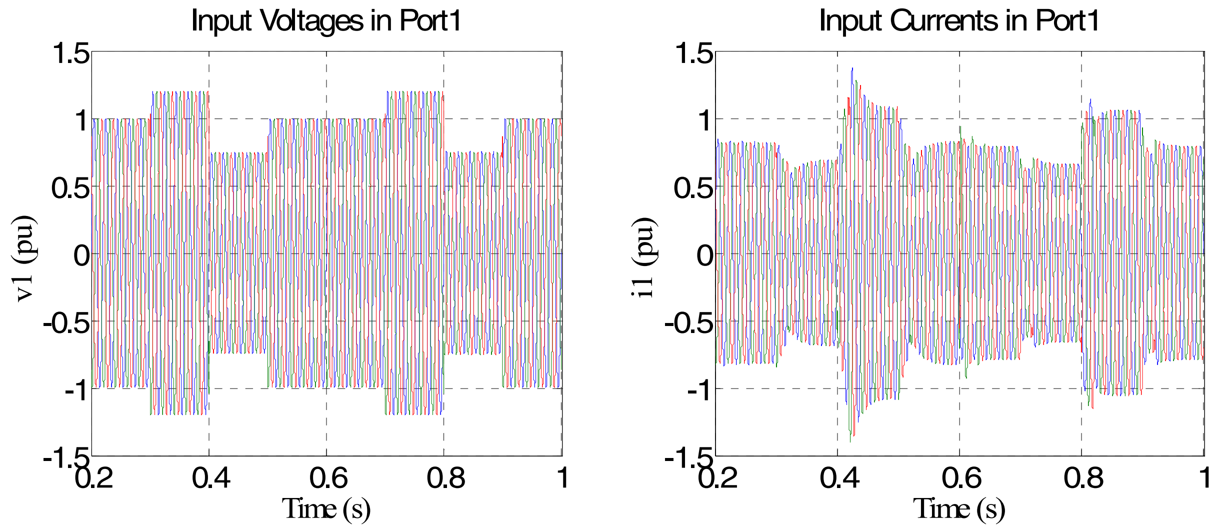

a) b)

Fig. 5.49. Simulation results in Port 1 for voltage excursions:
a) voltages and b) currents.

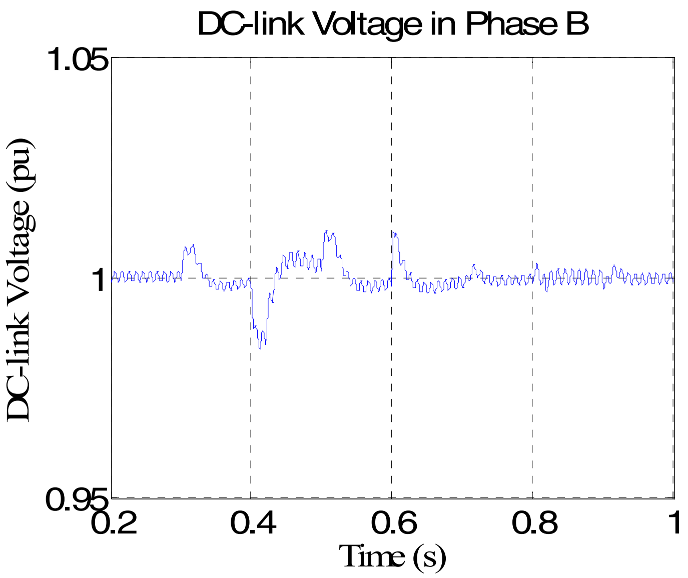

Fig. 5.50. Average DC-link voltage in Phase B for voltage excursions.

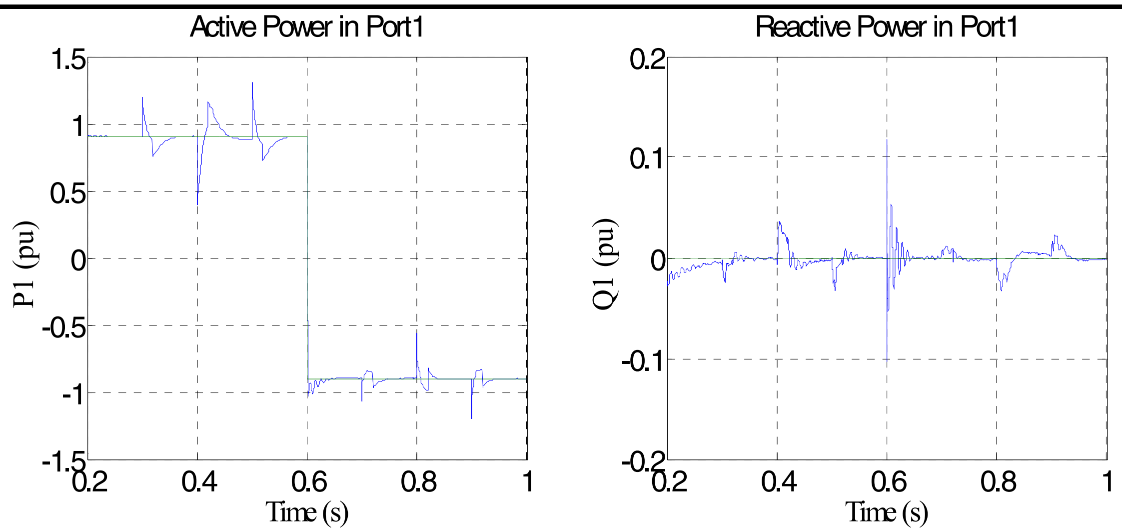

a) b)

Fig. 5.51. Simulation results in Port 1 for voltage excursions:
a) active power and b) reactive power.

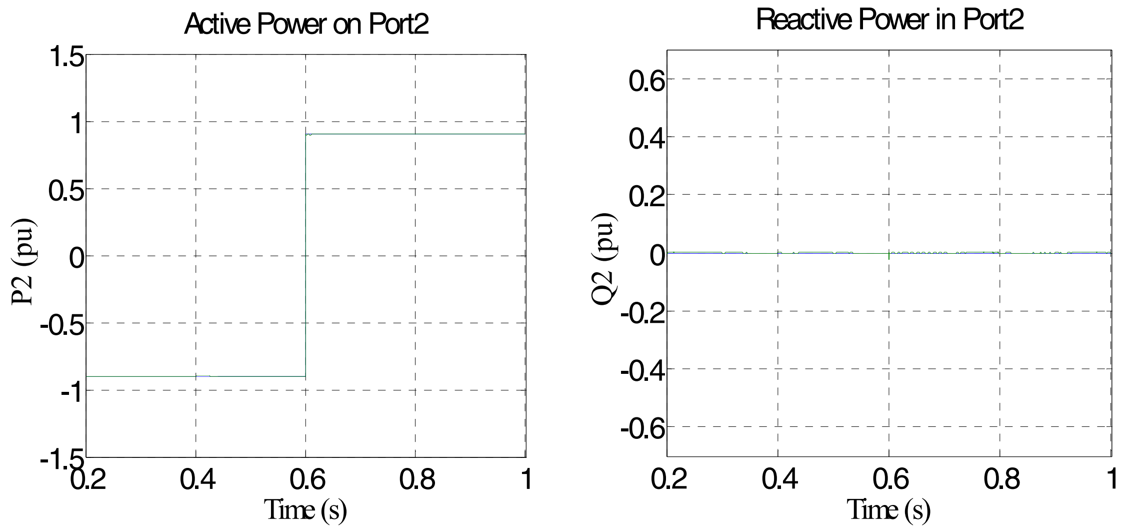

a) b)

Fig. 5.52. Simulation results in Port 1 for voltage excursions:
a) active power and b) reactive power.

5.3.2.4 Voltage Unbalances

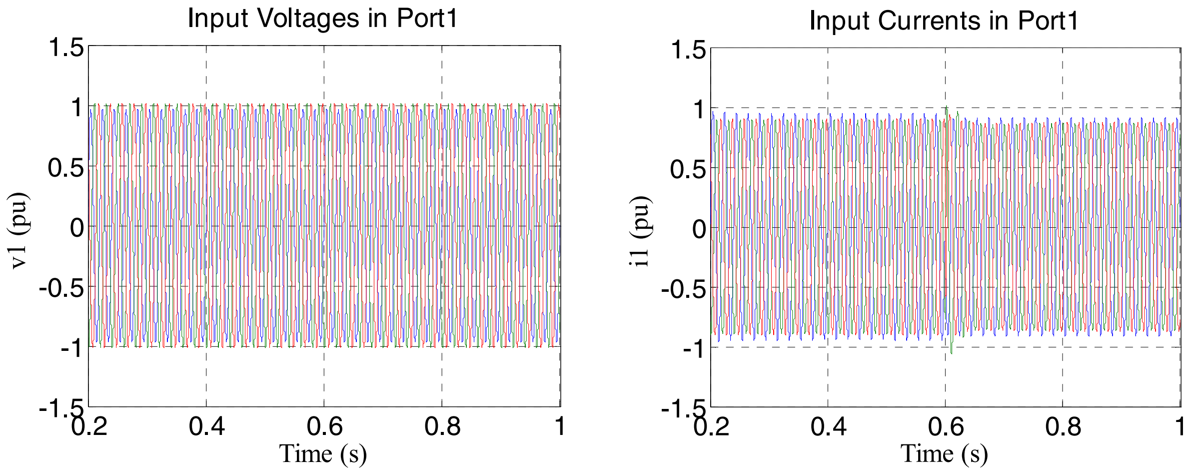

a) b)

Fig. 5.53. Simulation results in Port 1 for voltage unbalances:
a) voltages and b) currents.

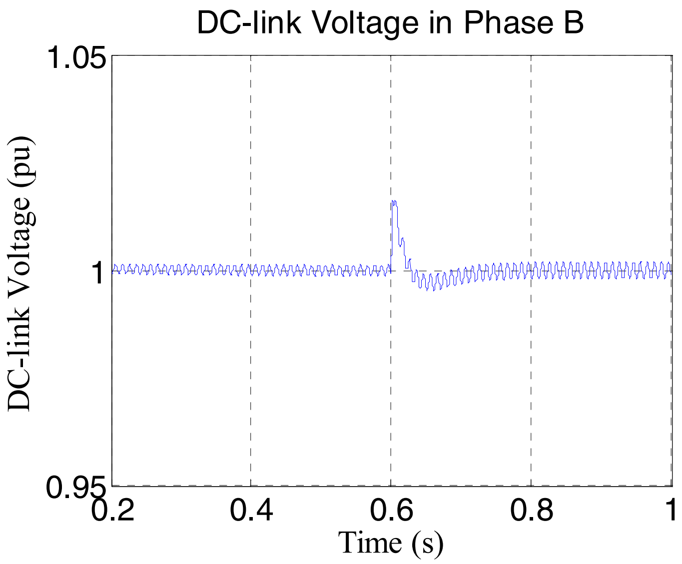

Fig. 5.54. Average DC-link voltage in Phase B for unbalanced voltages.

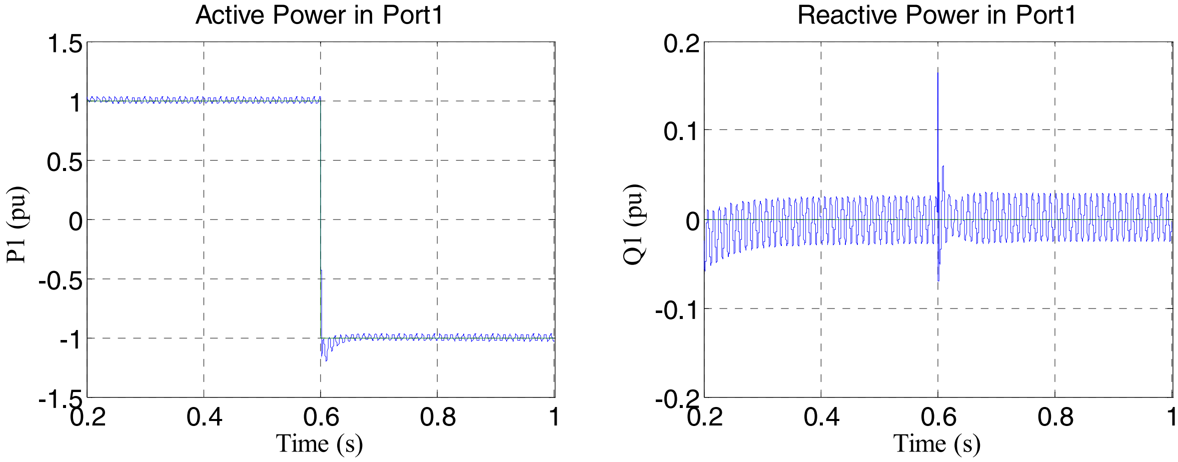

a) b)

Fig. 5.55. Simulation results in Port 1 for voltage unbalances:
a) active power and b) reactive power.

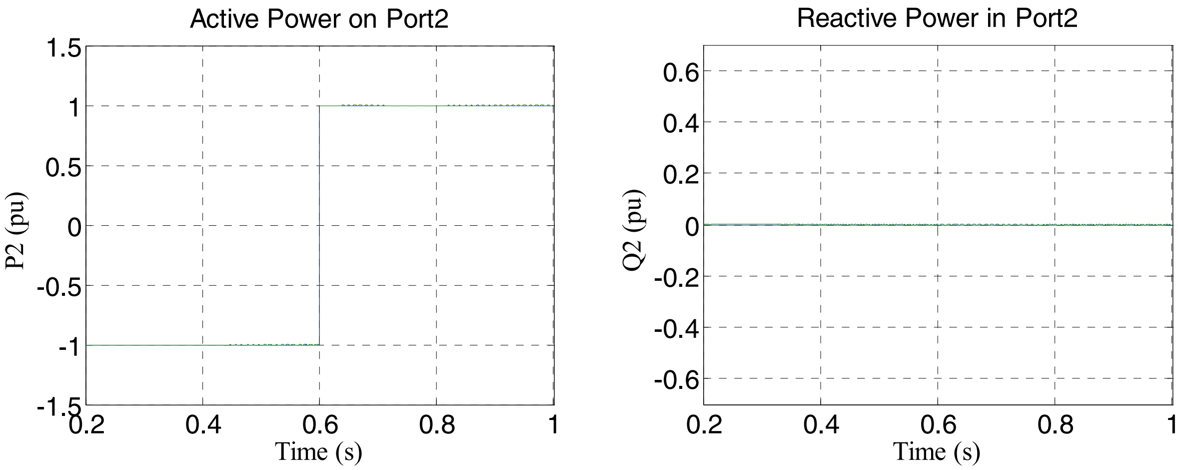

Fig. 5.56. Simulation results in Port 2 for voltage unbalances:
a) active power and b) reactive power.

5.3.2.5 Phase Jumps

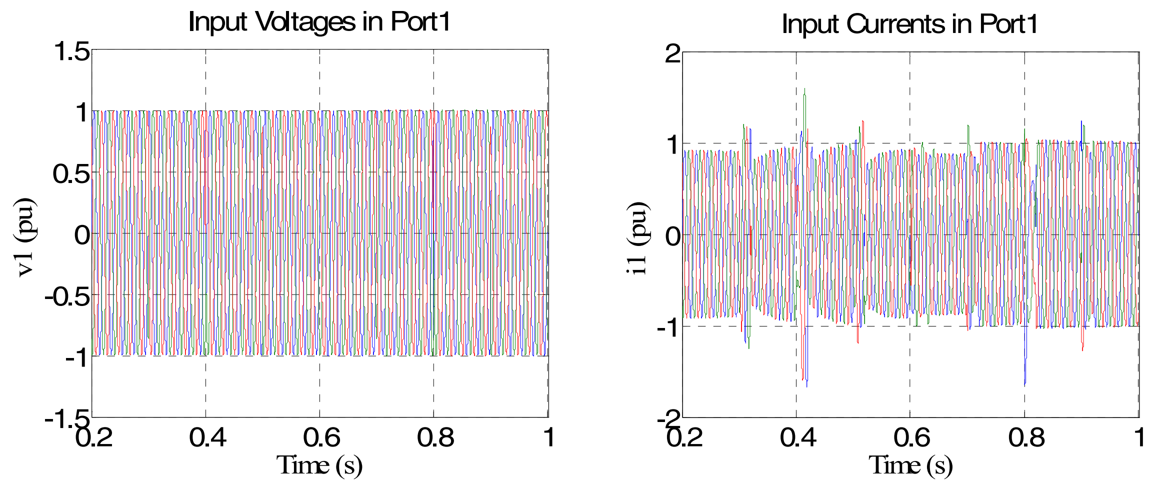

a) b)

Fig. 5.57. Simulation results in Port 1 for phase jumps: a) voltages and b) currents.

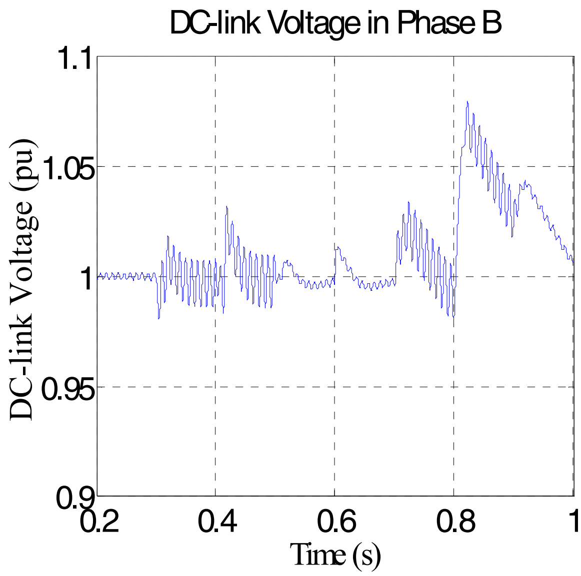

Fig. 5.58. Average DC-link voltage in Phase B during phase jumps.

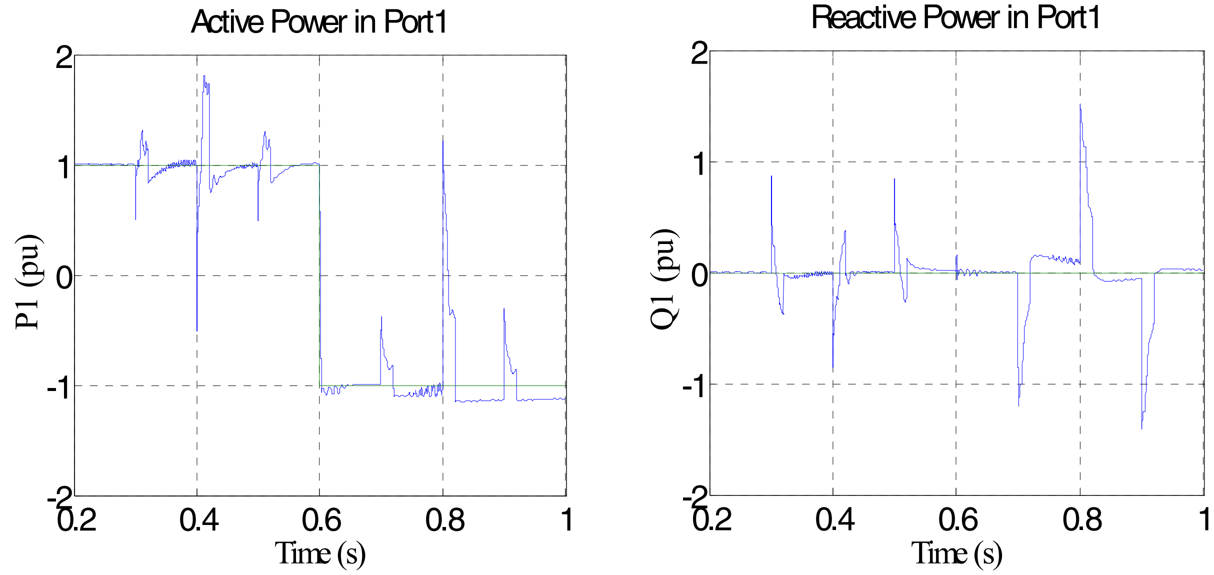

Fig. 5.59. Simulation results in Port 1 for phase jumps:
a) active power and b) reactive power.

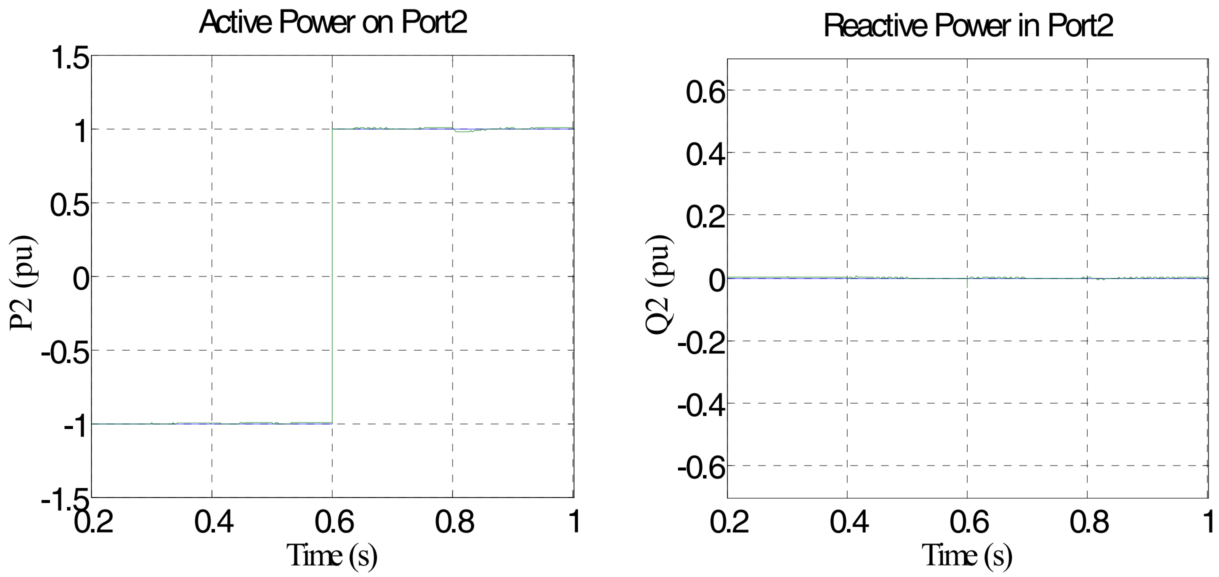

a) b)

Fig. 5.60. Simulation results in Port 2 for phase jumps:
a) active power and b) reactive power.

5.3.2.6 Frequency Excursions

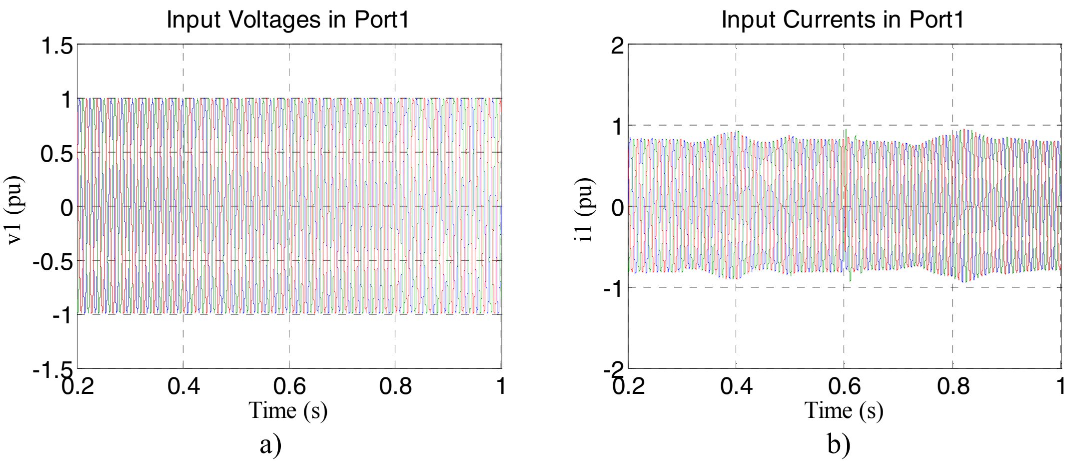

Fig. 5.61. Simulation results in Port 1 for frequency excursions: a) voltages and b) currents.

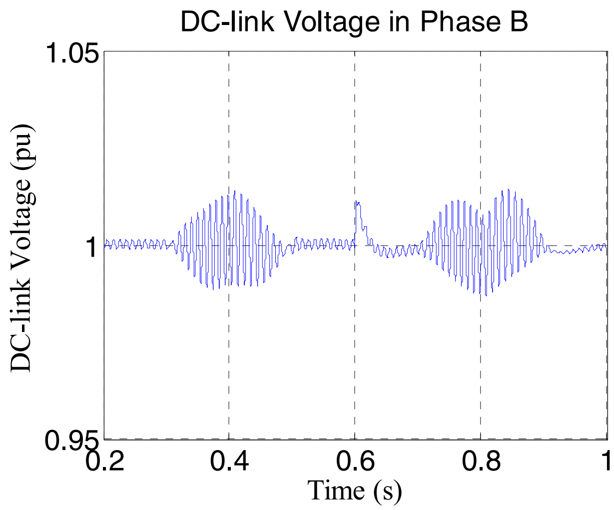

Fig. 5.62. Average DC-link voltage in Phase B during frequency excursions.

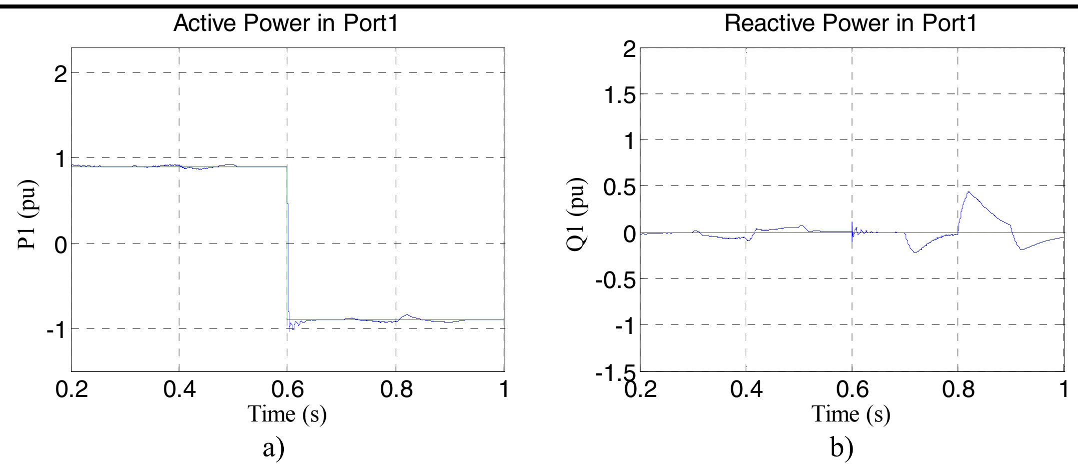

Fig. 5.63. Simulation results in Port 1 for frequency excursions:
a) active power and b) reactive power.

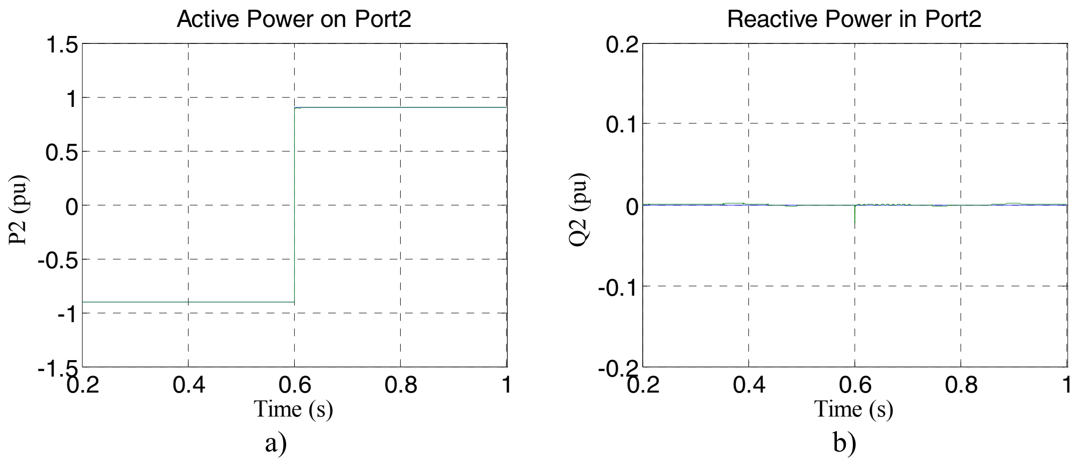

Fig. 5.64. Simulation results in Port 2 for frequency excursions:
a) active power and b) reactive power.

5.3.2.7 Single-Phase Short-Circuit

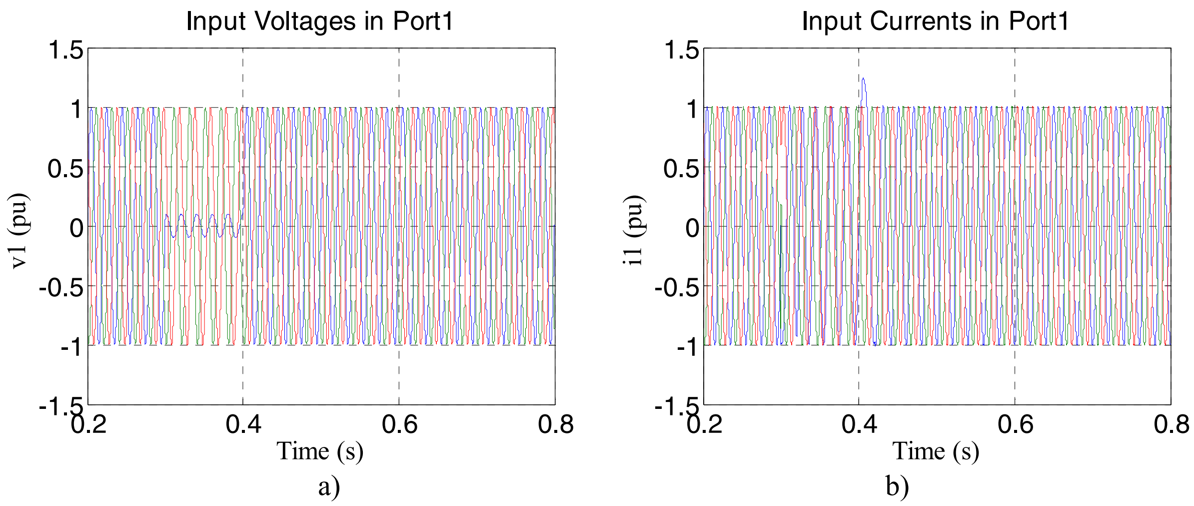

Fig. 5.65. Simulation results in Port 1 for single-phase short-circuit: a) voltages and b) current.

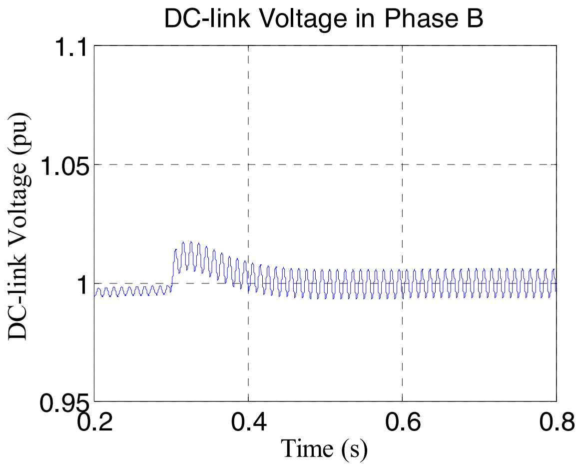

Fig. 5.66. Average DC-link voltage in Phase B during single-phase short-circuit.

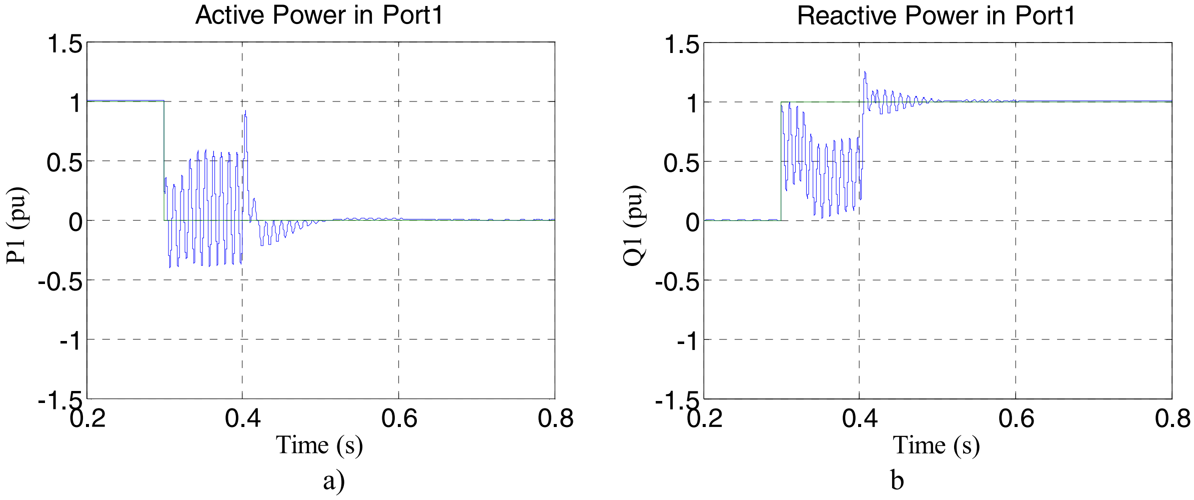

*Fig. 5.67. Simulation results in Port 1 for single-phase short-circuit:
a) active power and b) reactive power.*

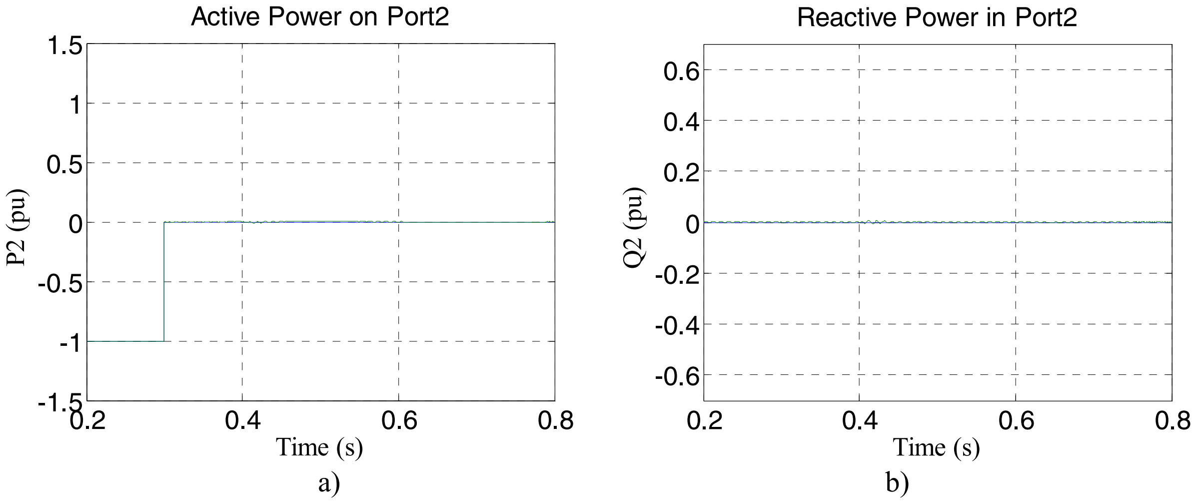

*Fig. 5.68. Simulation results in Port 1 for single-phase short-circuit:
a) active power and b) reactive power.*

5.3.2.8 Two-Phase Short-Circuit

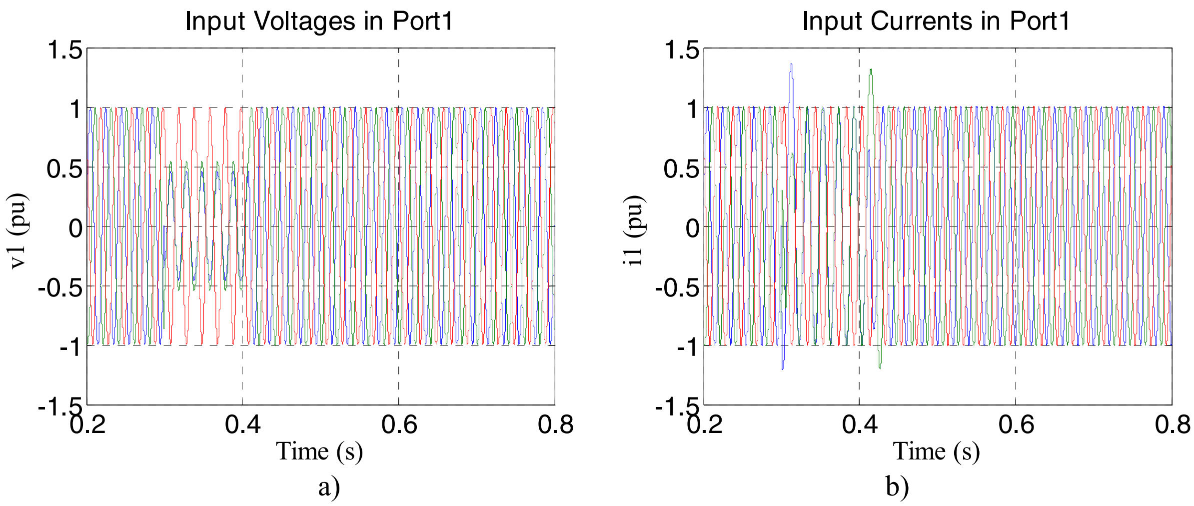

Fig. 5.69. Simulation results in Port 1 for two-phase short-circuit: a) voltages and b) current.

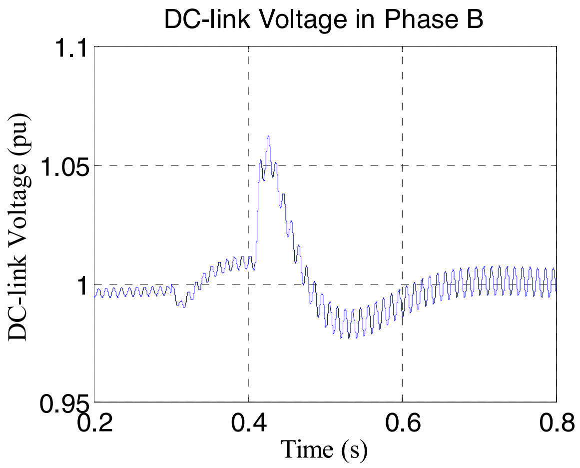

Fig. 5.70. Average DC-link voltage in Phase B during a two-phase short circuit.

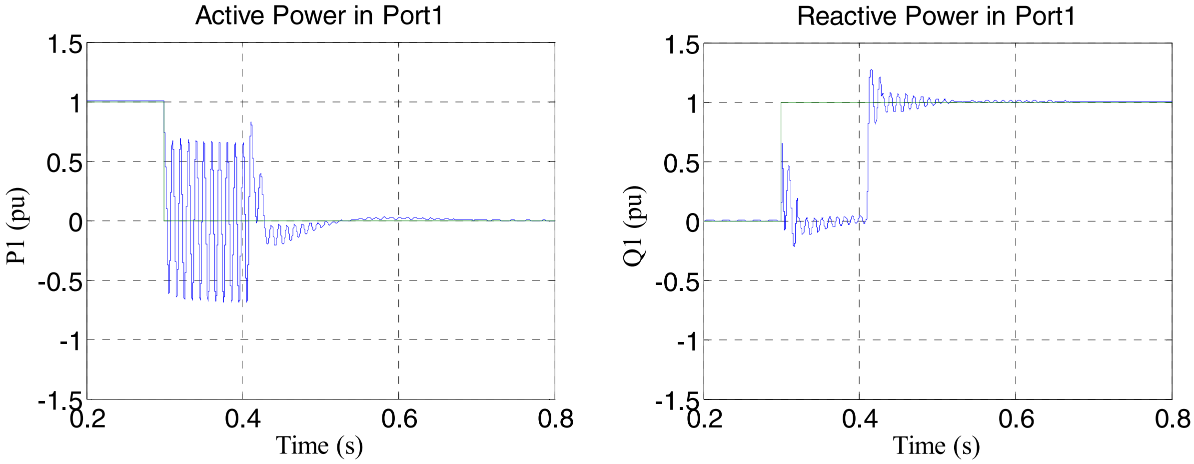

Fig. 5.71. Simulation results in Port 1 for two-phase short-circuit: a) active power and b) reactive power.

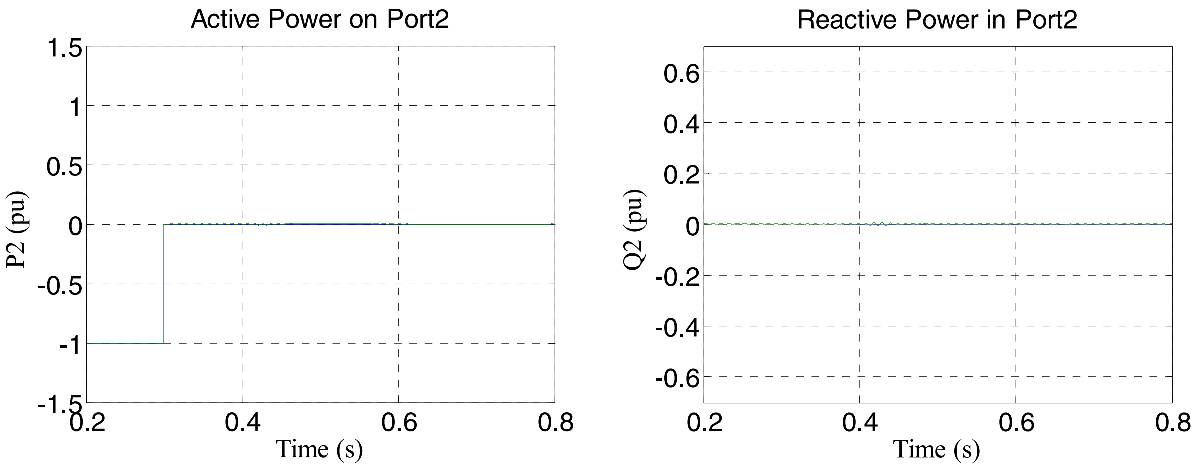

a) b)

Fig. 5.72. Simulation results in Port 2 for two-phase short-circuit: a) active power and b) reactive power.

5.3.2.9 Two-Phase with ground Short-Circuit

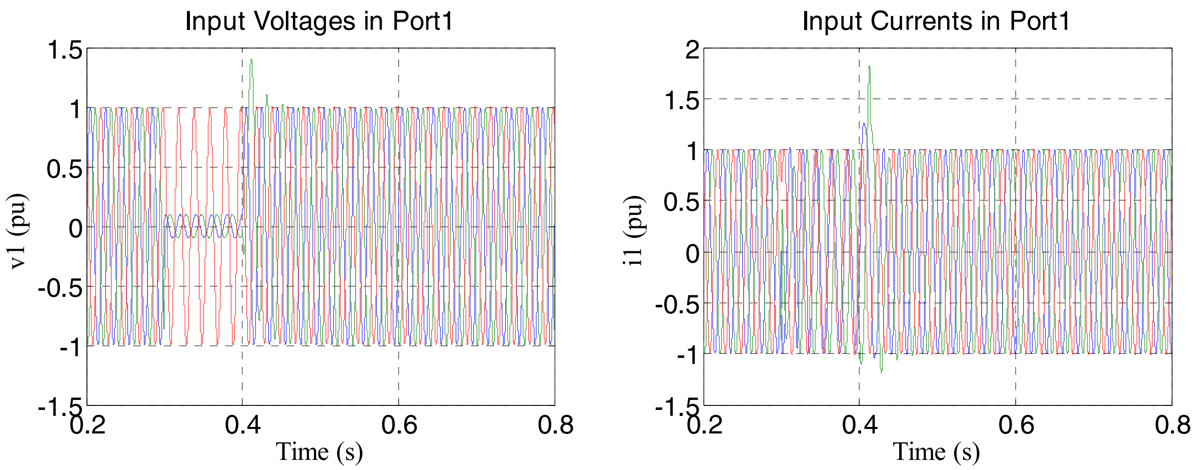

a) b)

Fig. 5.73. Simulation results in Port 1 for two-phase with ground short-circuit: a) voltages and b) current.

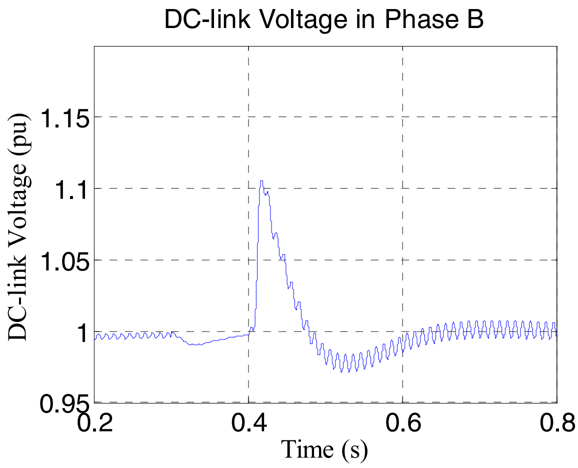

Fig. 5.74. Average DC-link voltage in Phase B during a two-phase with ground short-circuit.

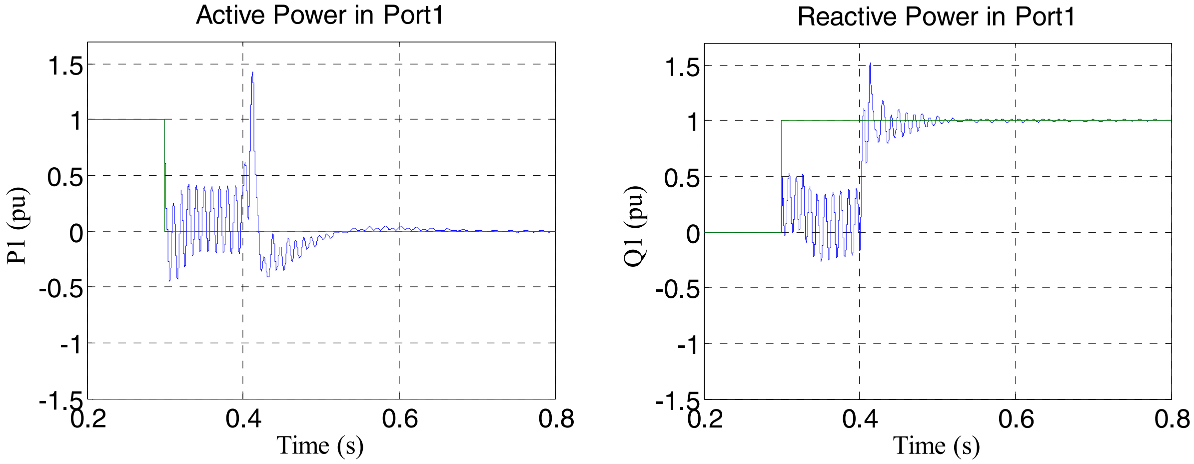

a) b)

Fig. 5.75 Simulation results in Port 1 for two-phase with ground short-circuit: active power and b) reactive power.

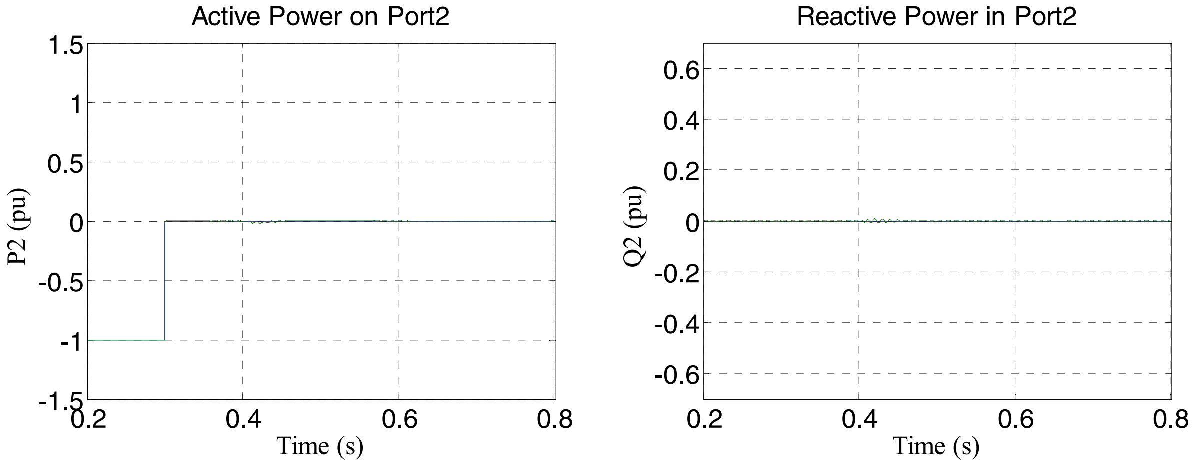

a) b)

Fig. 5.76. Simulation results in Port 1 for two-phase with ground short-circuit: a) active power and b) reactive power.

5.3.2.10 Three-Phase Short-Circuit

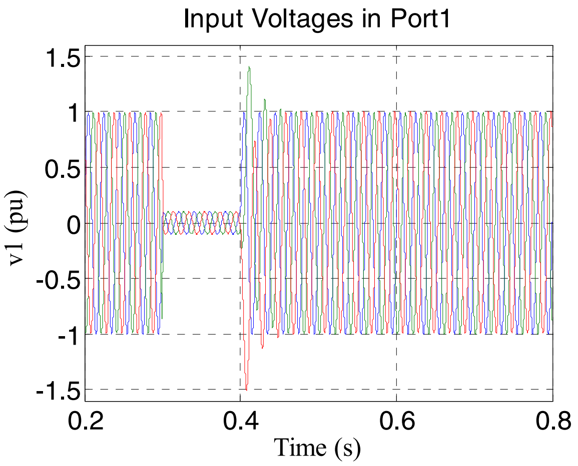

a)

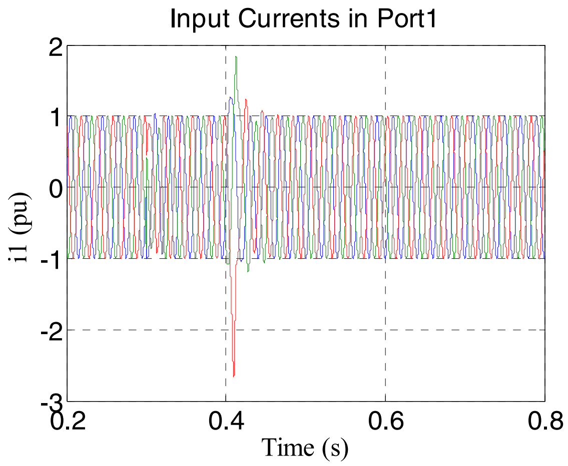

b)

Fig. 5.77. Simulation results in Port 1 for three-phase short-circuit: a) voltages and b) current.

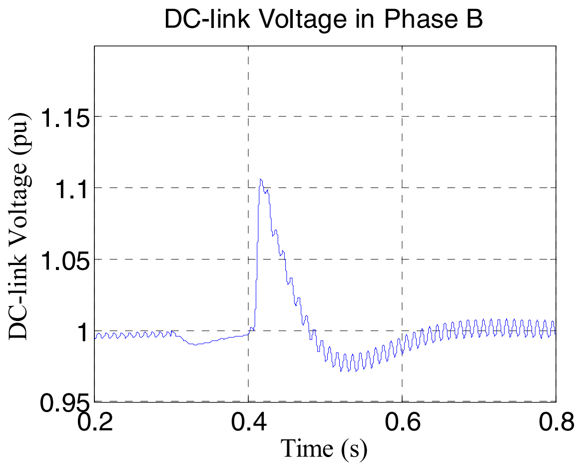

Fig. 5.78. Simulation results in Port 2 for three-phase short-circuit: a) voltages and b) current.

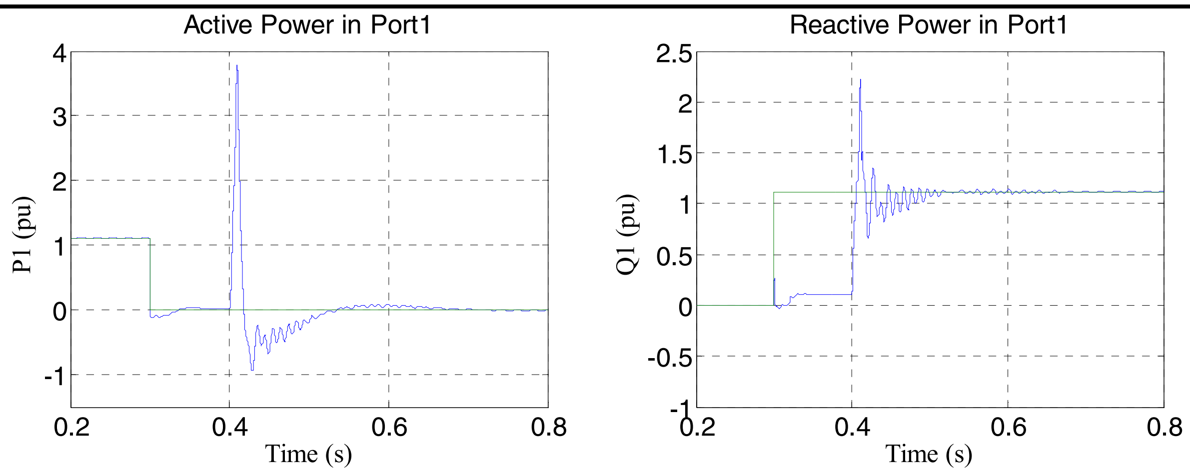

a) b)

Fig. 5.79. Simulation results in Port 1 for three-phase short-circuit: a) active power and b) reactive power.

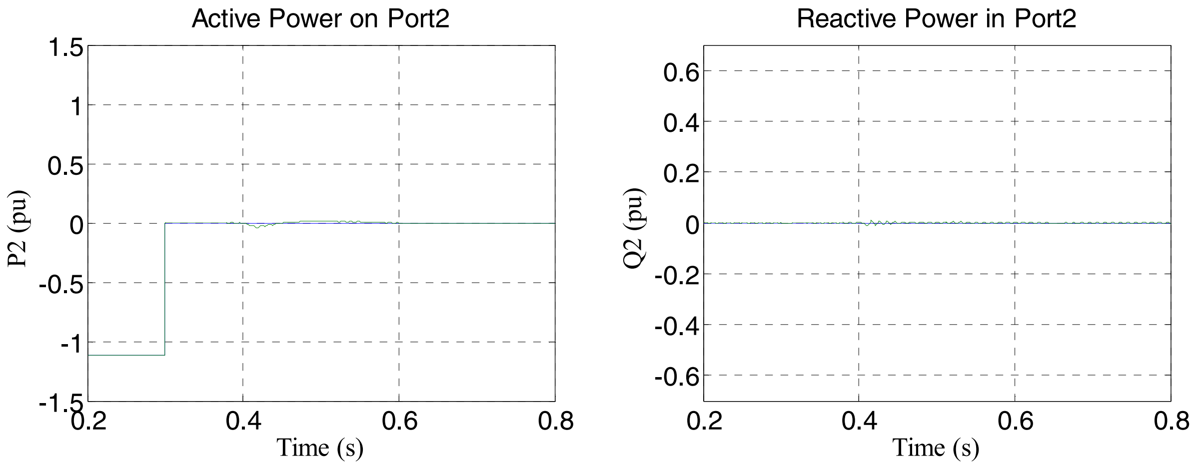

a) b)

Fig. 5.80. Simulation results in Port 2 for three-phase short-circuit: a) active power and b) reactive power.

5.3.2.11 Conclusions

The effectiveness of the Predictive controller applied to the Uniflex-PM system in dual natural reference frame is verified through different study cases. The simulation results have shown that the control system present a fast response and can trace the active and reactive power under different power reference profiles and grid operating conditions.

A good decoupling of the active and reactive power control is obtained in all considered cases. The supply currents are essential sinusoidal even under extreme unbalanced supply conditions.

Among all the study-cases, the phase excursions are the most difficult to control. Relatively large transients up to 2 times the rated power in both active and reactive power can be observed in this case especially when the phase changes from +60º to -60 º.

The overall system performance relies on the angular information. Thus the PLL is again a key-element in the control. A reliable and fast PLL is expected to have deep effect on the controller bandwidth and reliability. Predictive controller can reject significantly the harmonic distortion in the supply voltage without using any additional filter in the control loop; so, the produced currents present a good harmonic content.

The control sensitivity on the grid voltage angle can be observed very well during the short-circuit event. Large transients as well as the 100 Hz component are present in both active and reactive power especially after the fault clearance. The active power in the faulted port in the case of the three-phase short circuit has transients up to four times the rated power, while the currents exceed the rated values by a factor of two. Further investigations are needed to reduce the control sensitivity to fast grid voltage variations.

The average DC-link voltage in the considered phase has small variations except the single and the two-phase short-circuits where peaks of 10% from the rated value are observed.

5.3.3 Stationary reference frame control with PR current controllers

5.3.3.1 Current Harmonic Compatibility Levels

The harmonic compatibility levels for the synchronous reference frame control with PR controllers are given in Fig. 5.81.

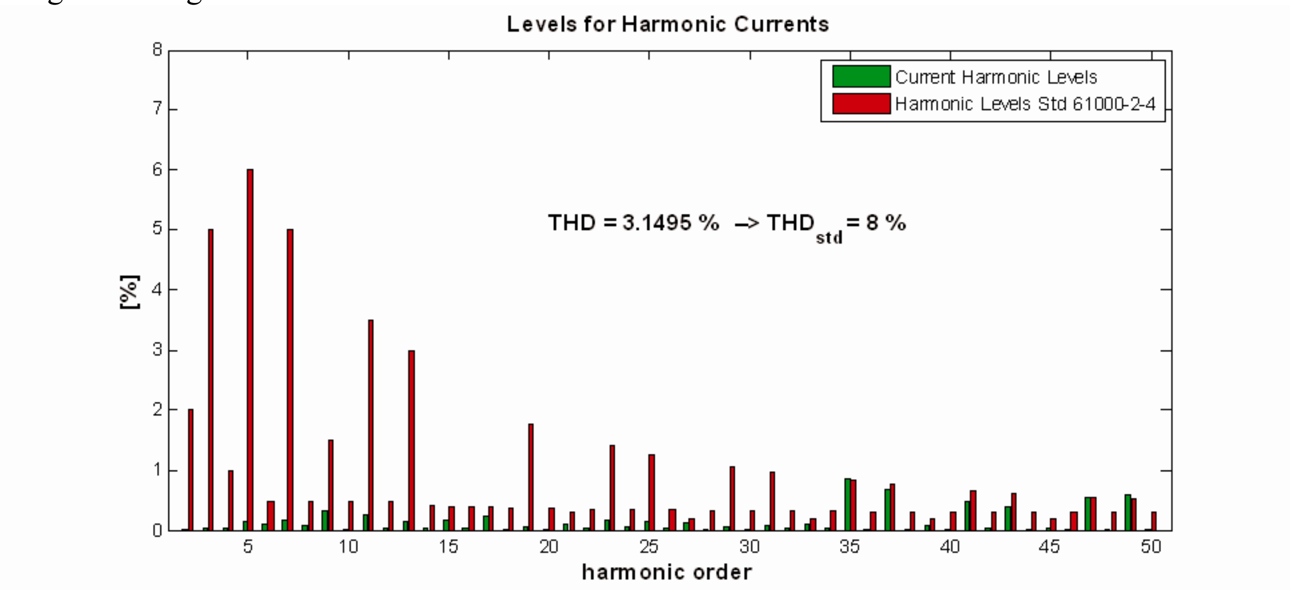

Fig. 5.81. Current harmonic compatibility levels for stationary reference frame control.

The spectrum up to the 35th harmonic presents very low values below the standard limits. The most important harmonic is related with the switching frequency; that is the 35th harmonic. All the harmonic levels are below the standard limits except the 49th which is a little higher than the standard limit. The current THD is around 3.15%.

5.3.3.2 Bi-directional Power Flow

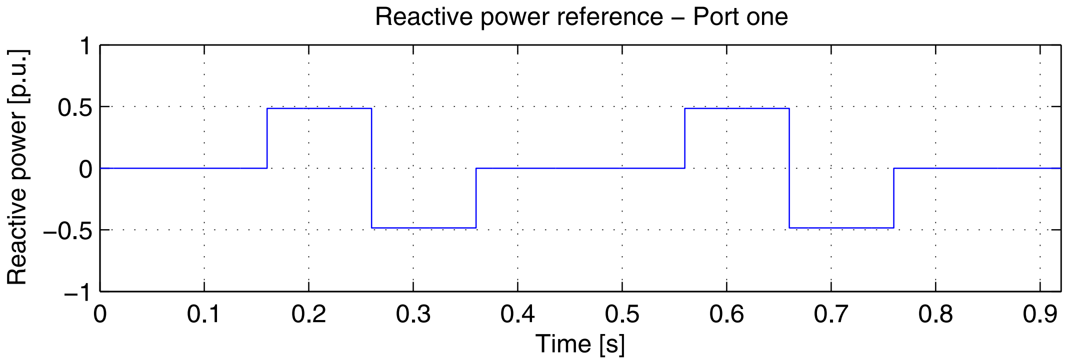

Fig. 5.82. Reactive power reference in Port 1.

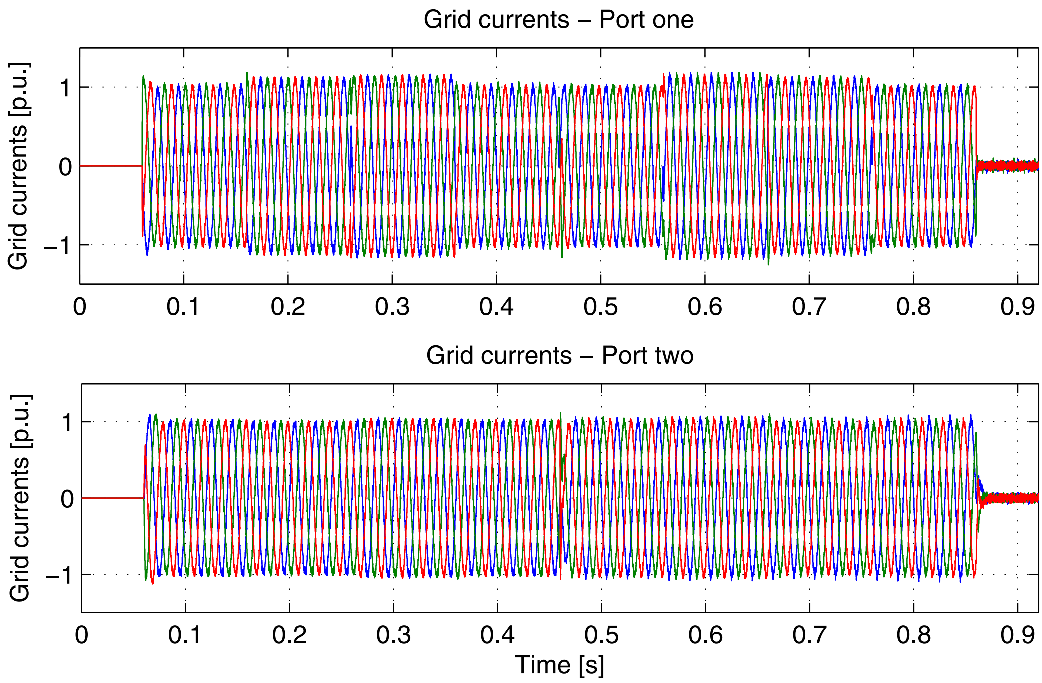

Fig. 5.83. Currents in Port 1 and Port 2 for bi-directional power flow.

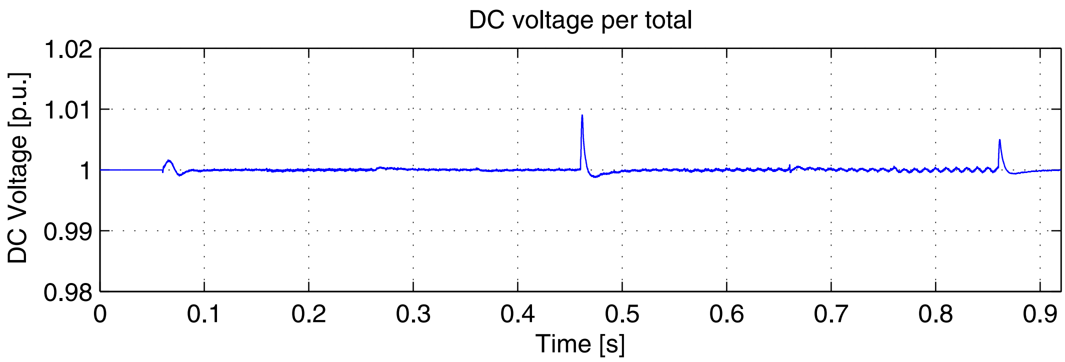

Fig. 5.84. Average DC-link voltage for bi-directional power flow.

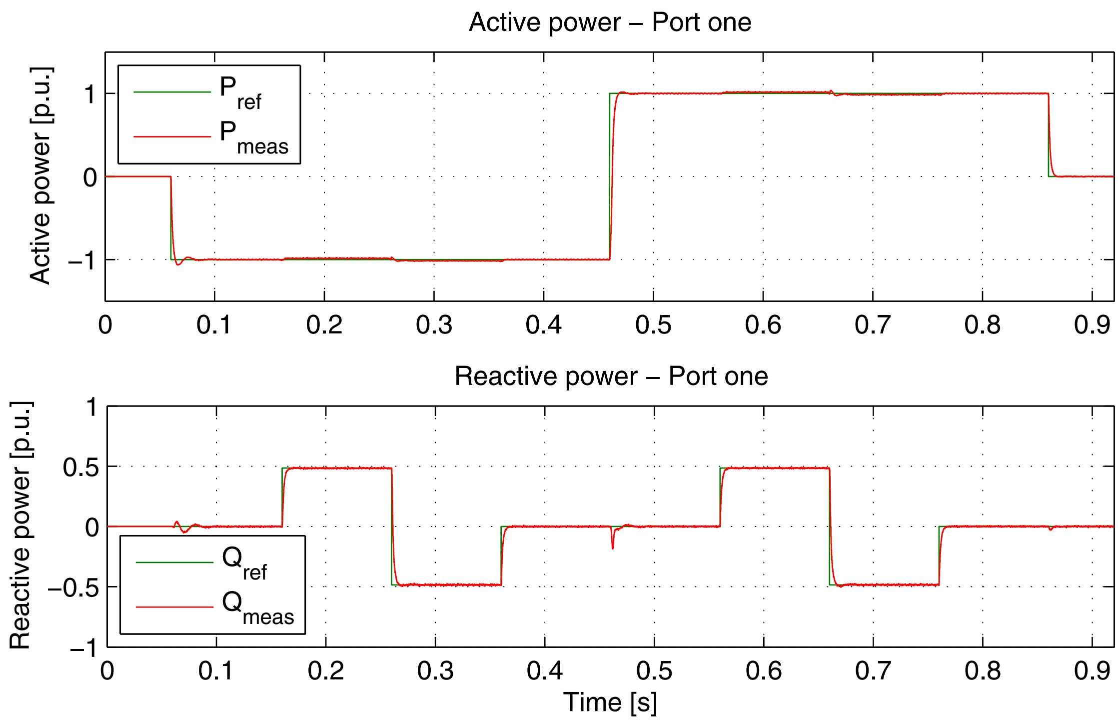

Fig. 5.85. Active and reactive power in Port 1 for bi-directional power flow.

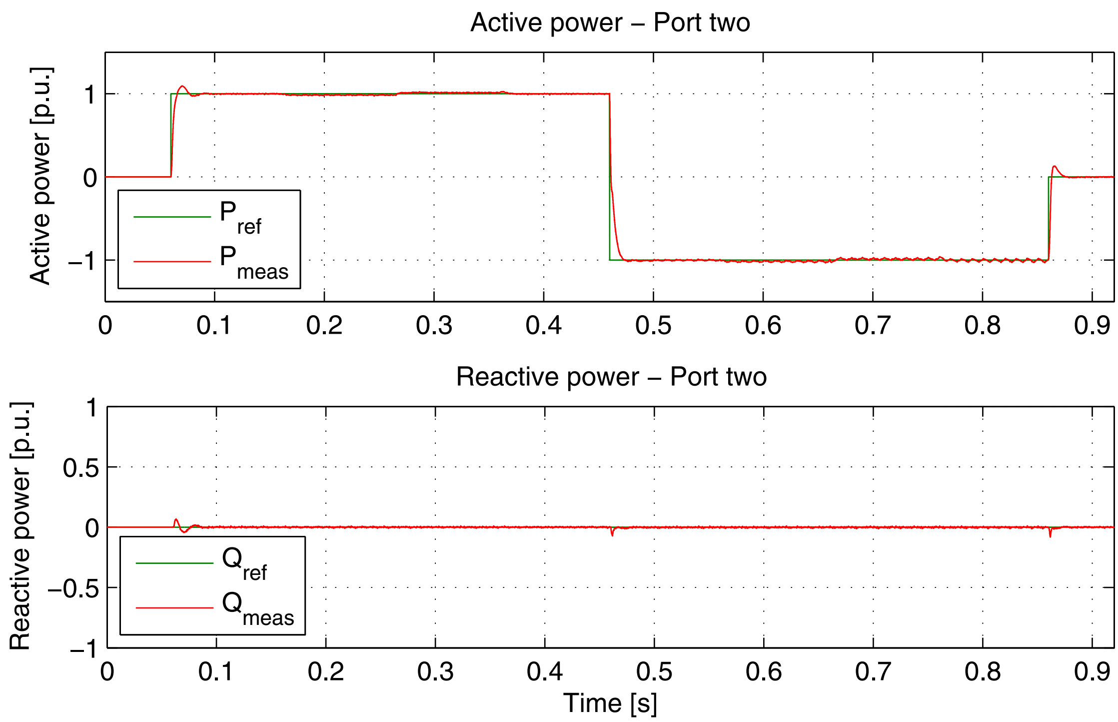

Fig. 5.86. Active and reactive power in Port 2 for bi-directional power flow.

5.3.3.3 Voltage Excursions

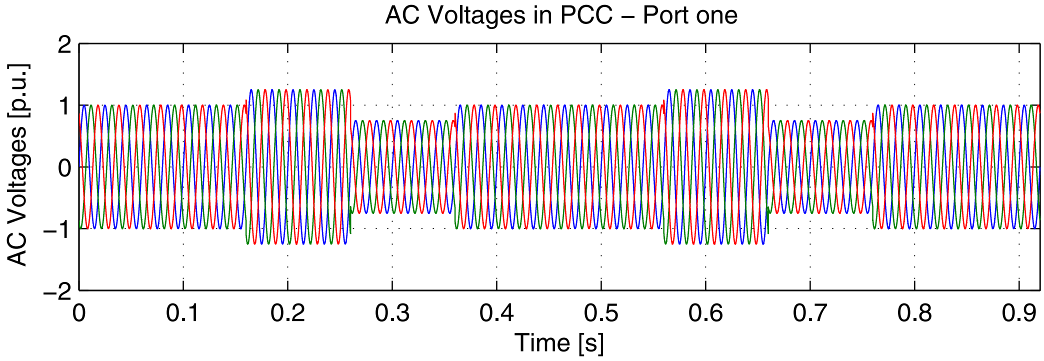

Fig. 5.87. Voltages in Port 1 during voltage excursions.

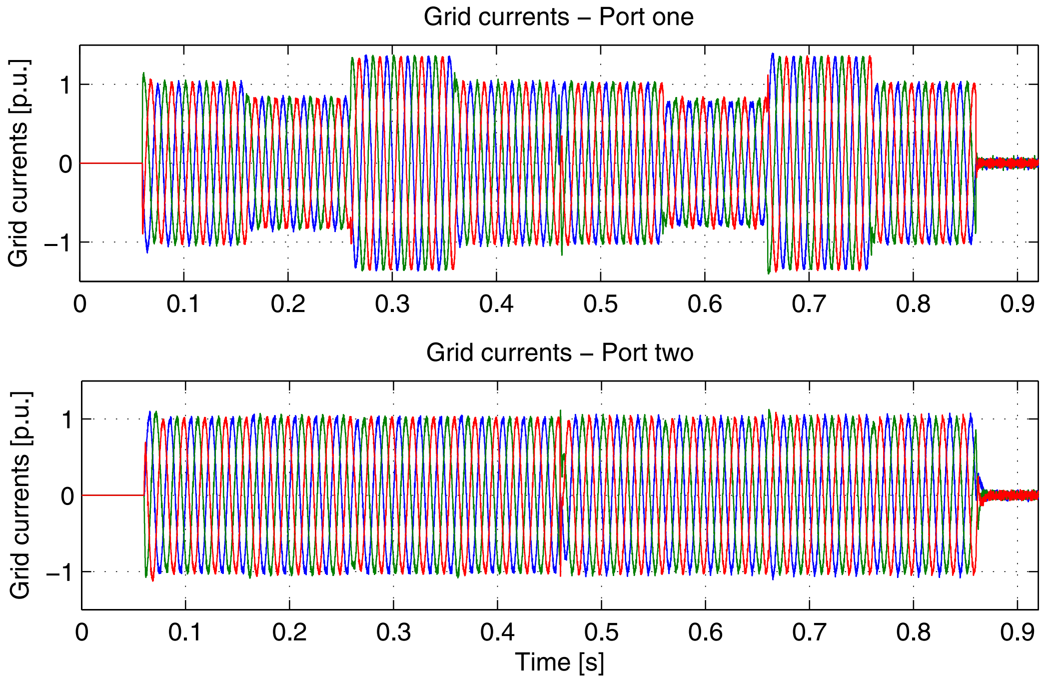

Fig. 5.88. Currents in Port 1 and Port 2 for voltage excursions.

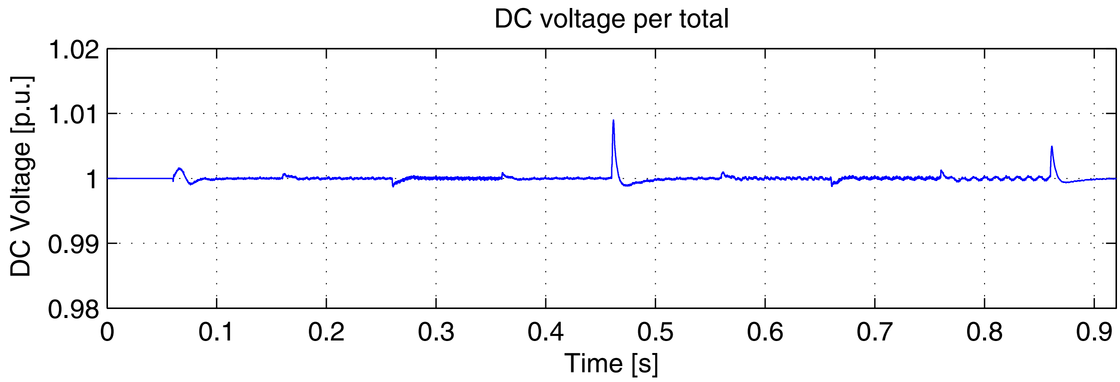

Fig. 5.89. Average DC-link voltage for voltage excursions.

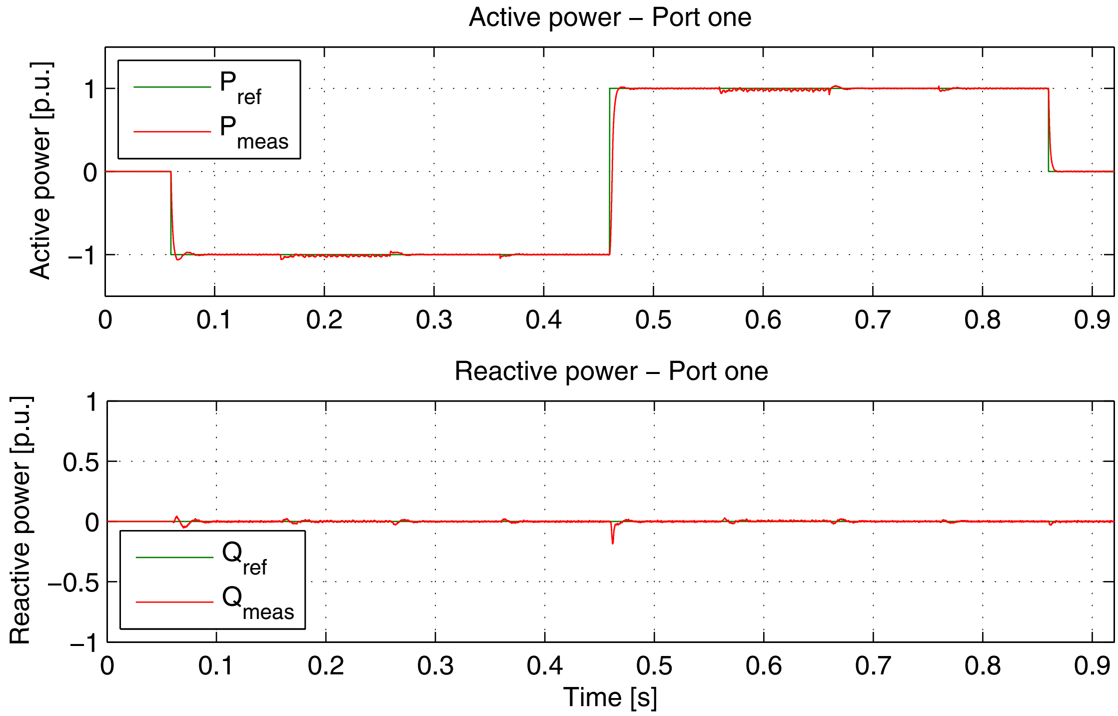

Fig. 5.90. Active and reactive power in Port 1 during voltage excursions.

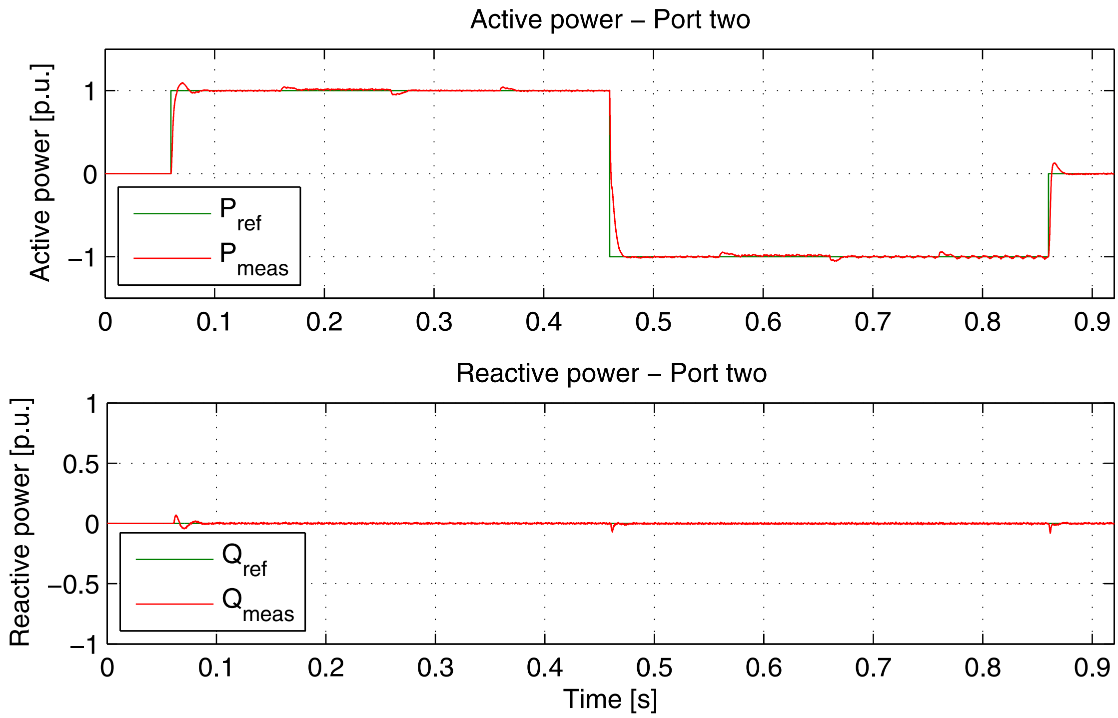

Fig. 5.91. Active and reactive power in Port 2 during voltage excursions.

5.3.3.4 Voltage Unbalances

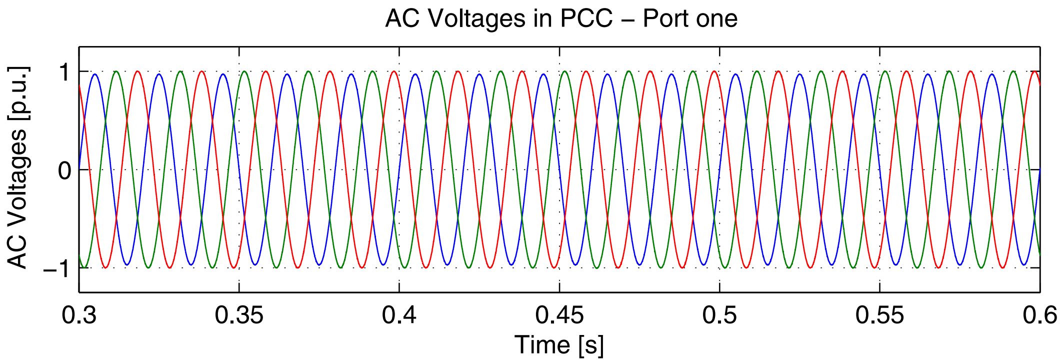

Fig. 5.92. Unbalanced voltages in Port 1.

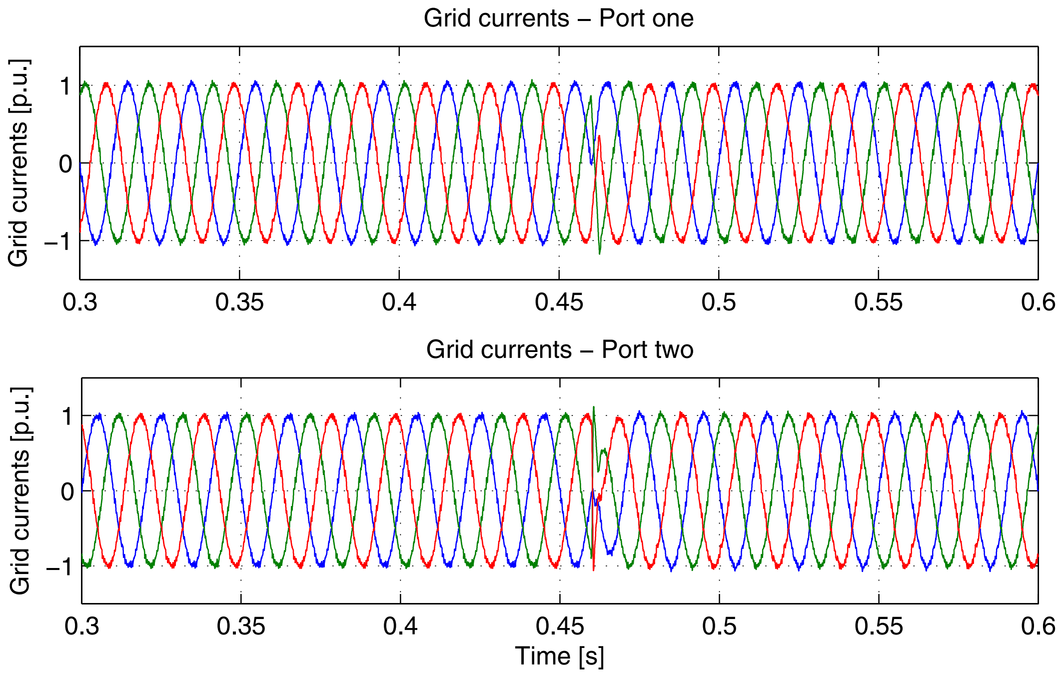

Fig. 5.93. Currents in Port 1 and Port 2 for unbalanced voltages.

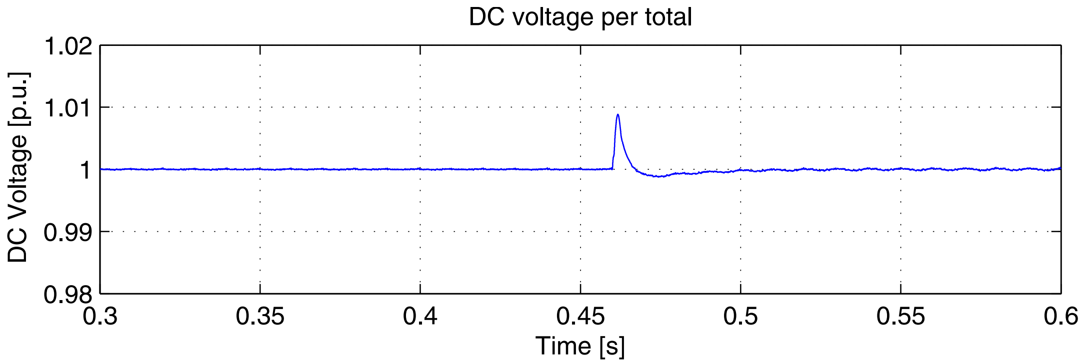

Fig. 5.94. Average DC-link voltage for unbalanced voltages.

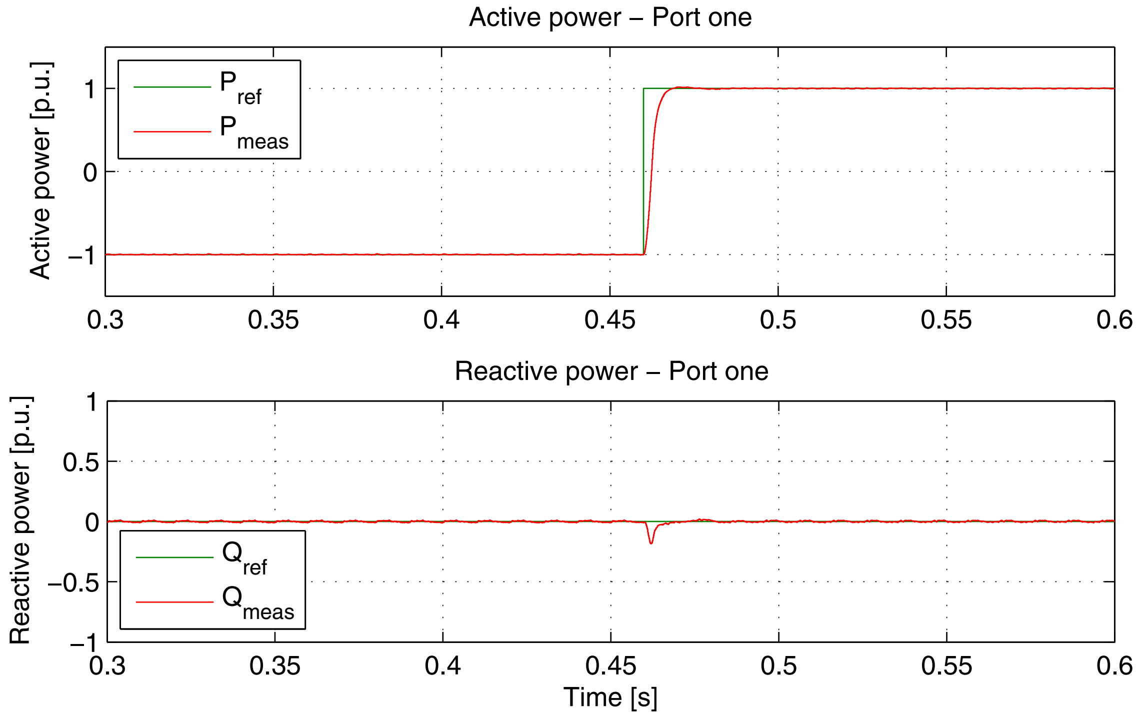

Fig. 5.95. Active and reactive power in Port 1 for unbalanced voltages.

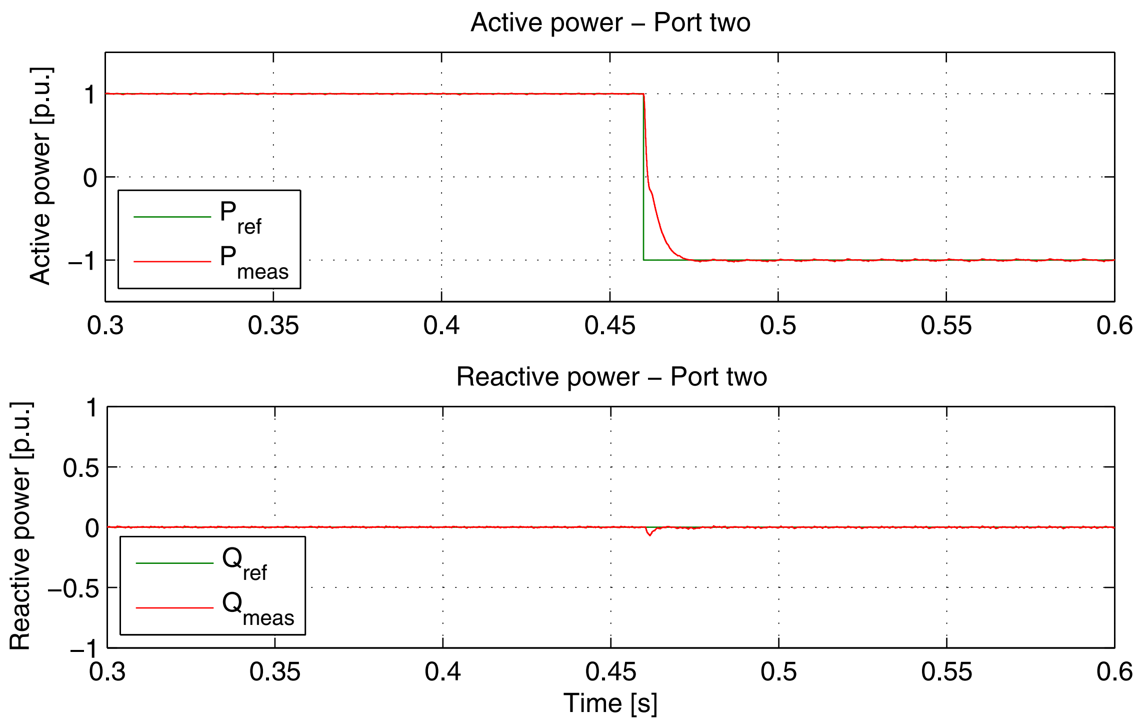

Fig. 5.96. Active and reactive power in Port 2 for unbalanced voltages.

5.3.3.5 Phase Jumps

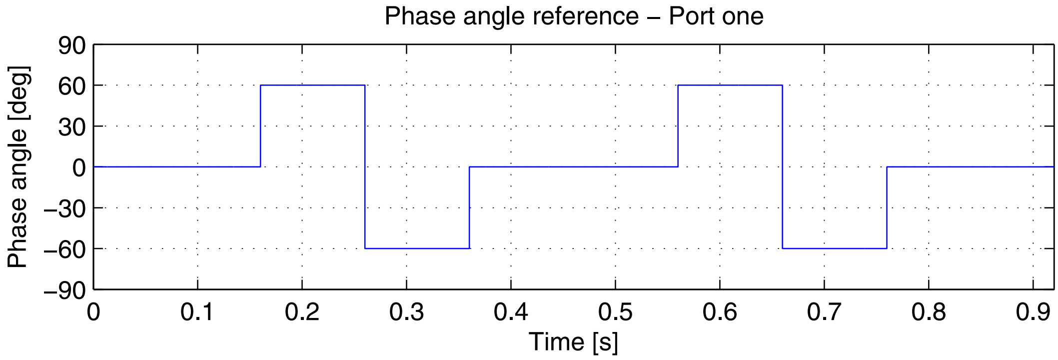

Fig. 5.97. Phase angle reference for voltages in port 1.

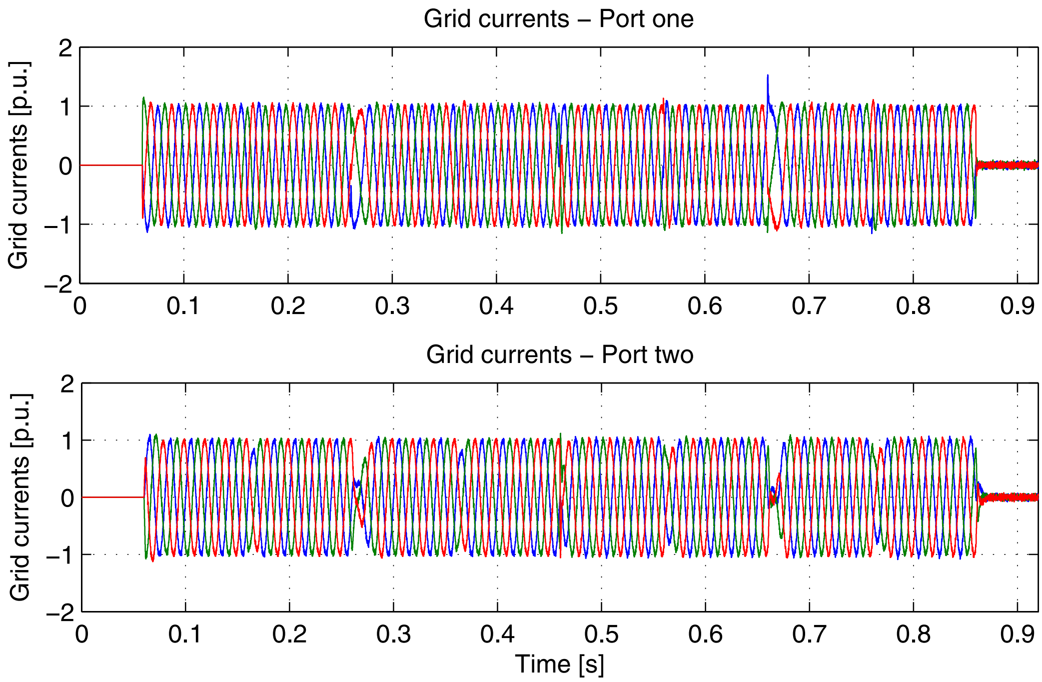

Fig. 5.98. Currents in Port 1 and Port 2 for phase jumps in Port 1.

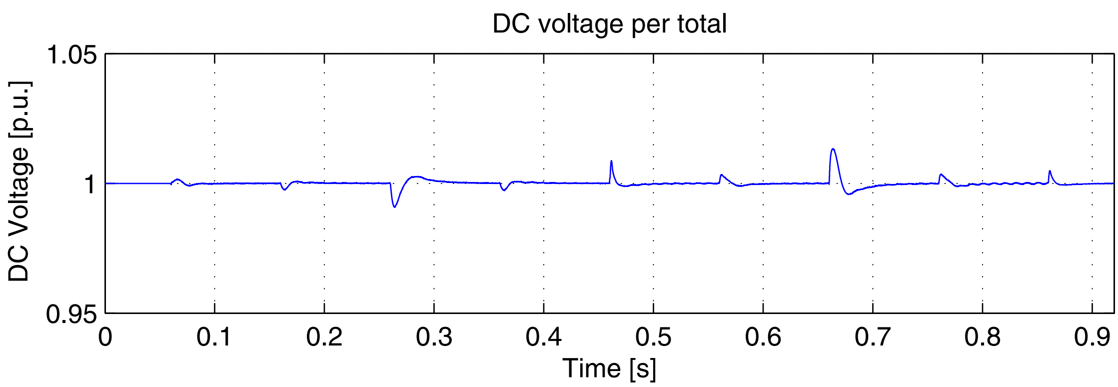

Fig. 5.99. Average DC-link voltage for phase jumps in Port 1.

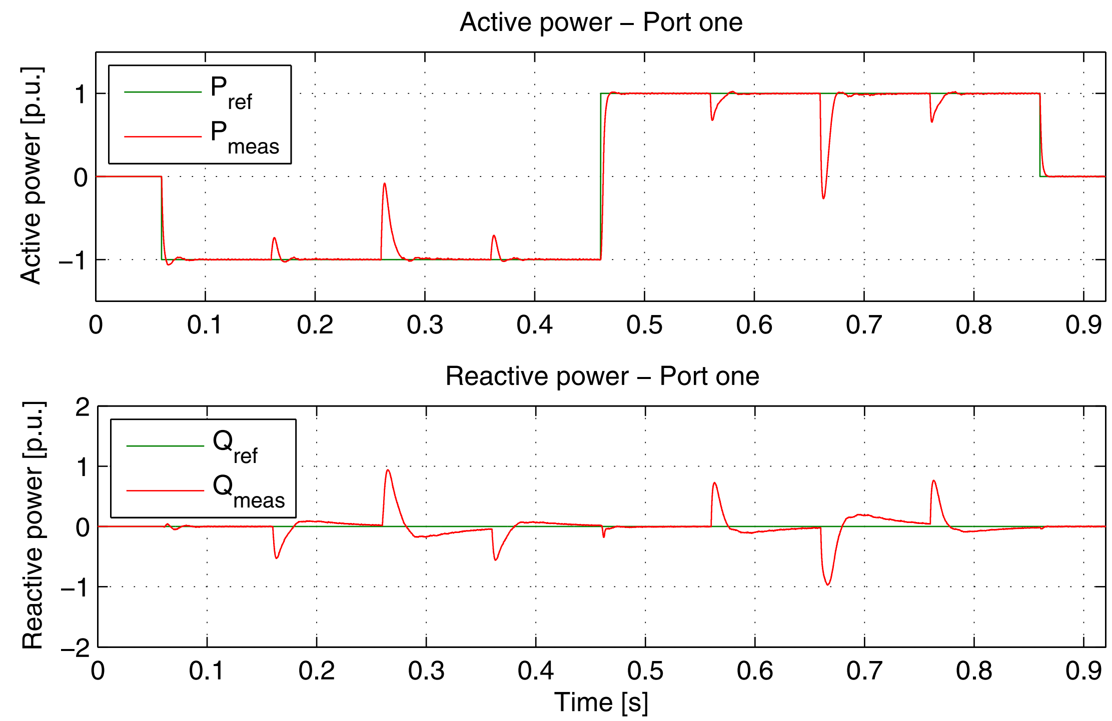

Fig. 5.100. Active and reactive power in Port 1 during phase jumps.

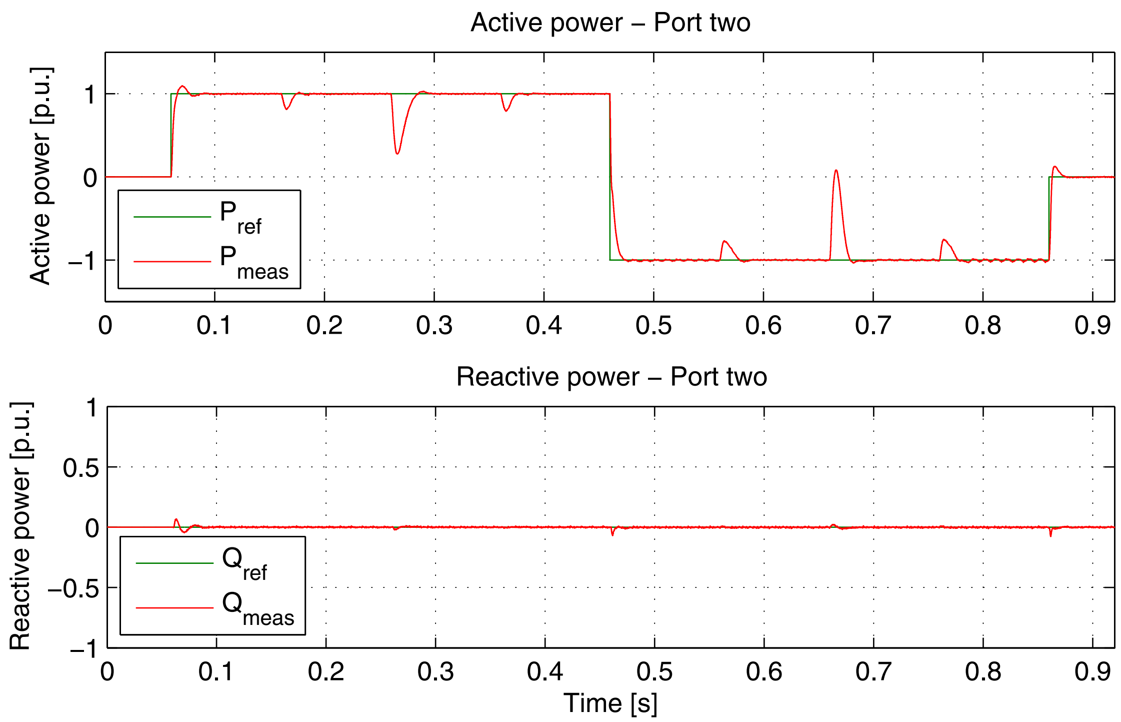

Fig. 5.101. Active and reactive power in Port 2 during phase jumps.

5.3.3.6 Frequency Excursions

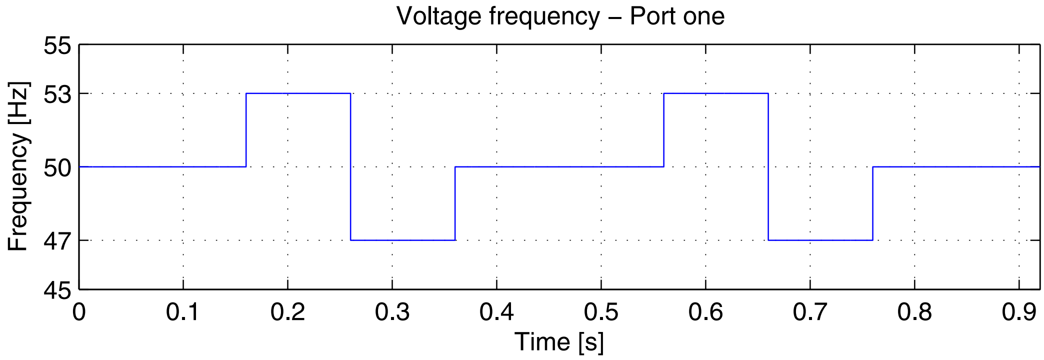

Fig. 5.102. Voltage frequency in Port 1.

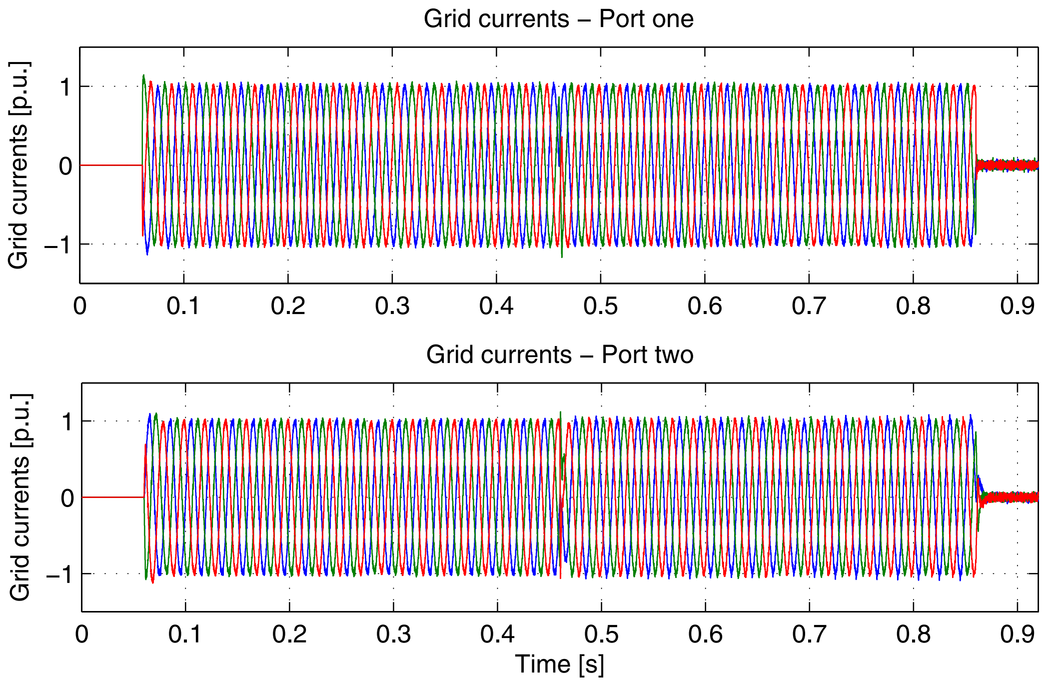

Fig. 5.103. Currents in Port 1 and Port 2 for frequency excursions in Port 1.

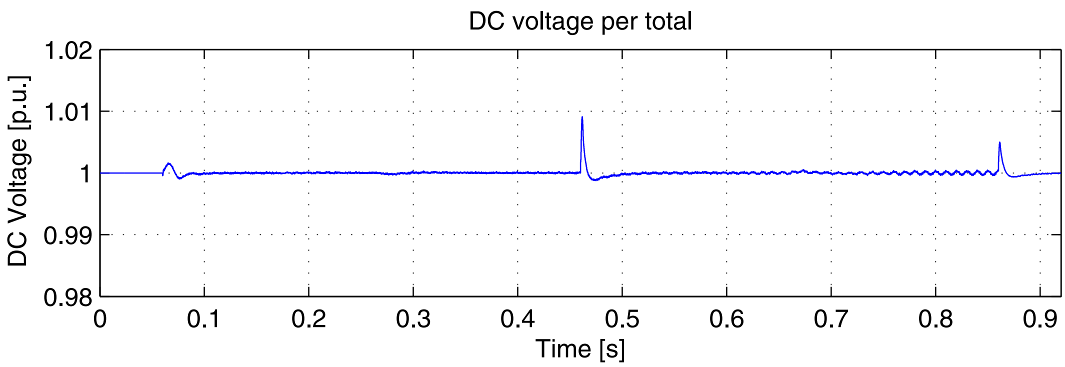

Fig. 5.104. Average DC-link voltage during frequency excursions in Port 1.

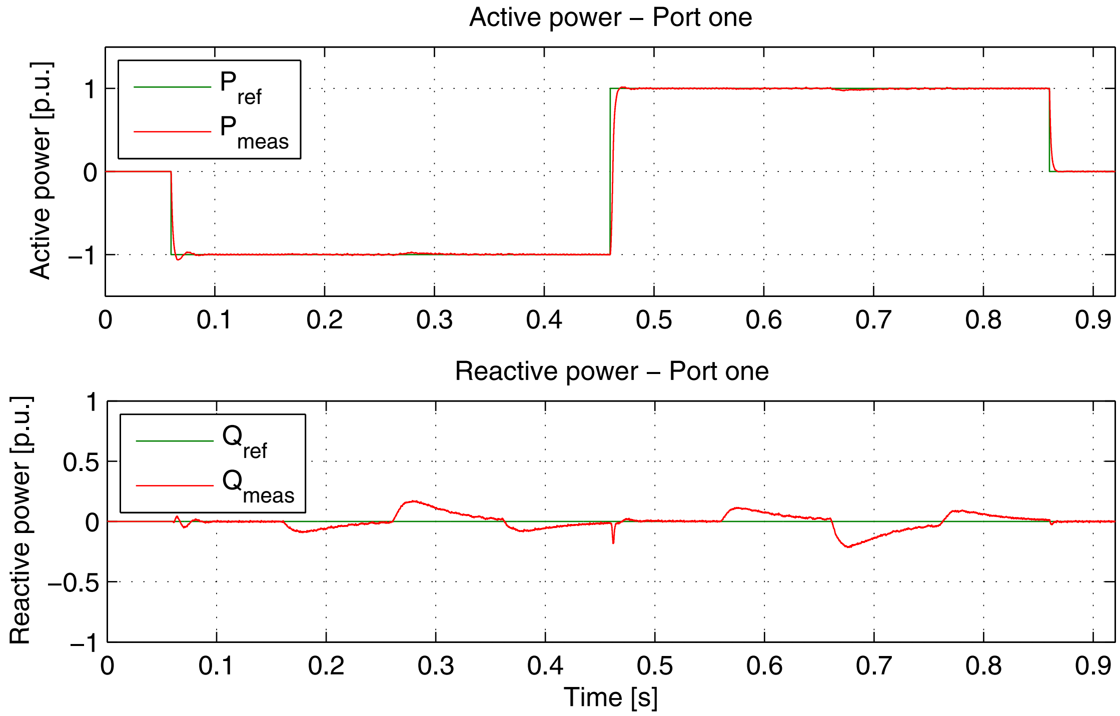

Fig. 5.105. Active and reactive power in Port 1 during frequency excursions in Port 1.

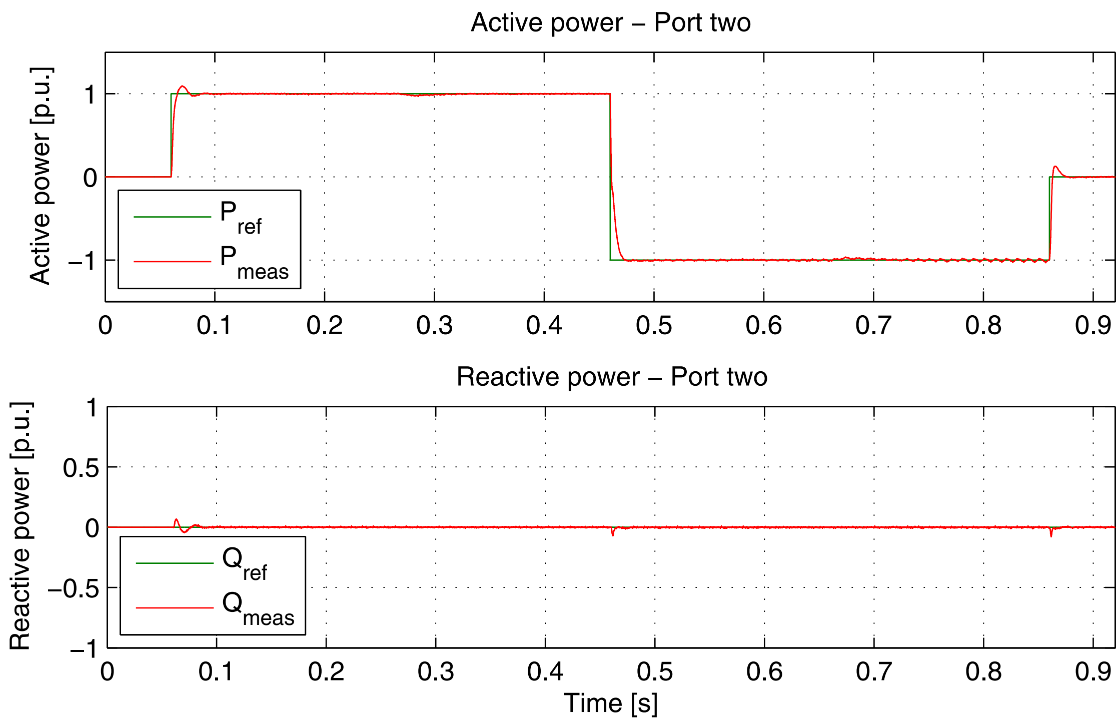

Fig. 5.106. Active and reactive power in Port 2 during frequency excursions in Port 1.

5.3.3.7 Single-Phase Short-Circuit

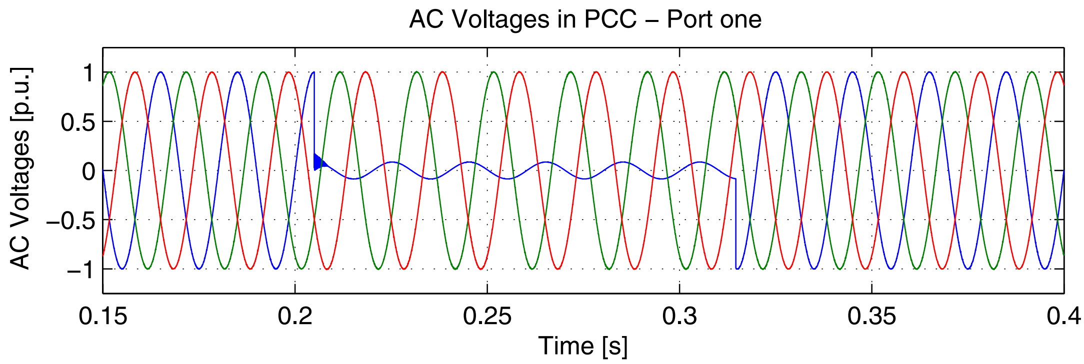

Fig. 5.107. Voltages in Port 1 during single-phase short-circuit.

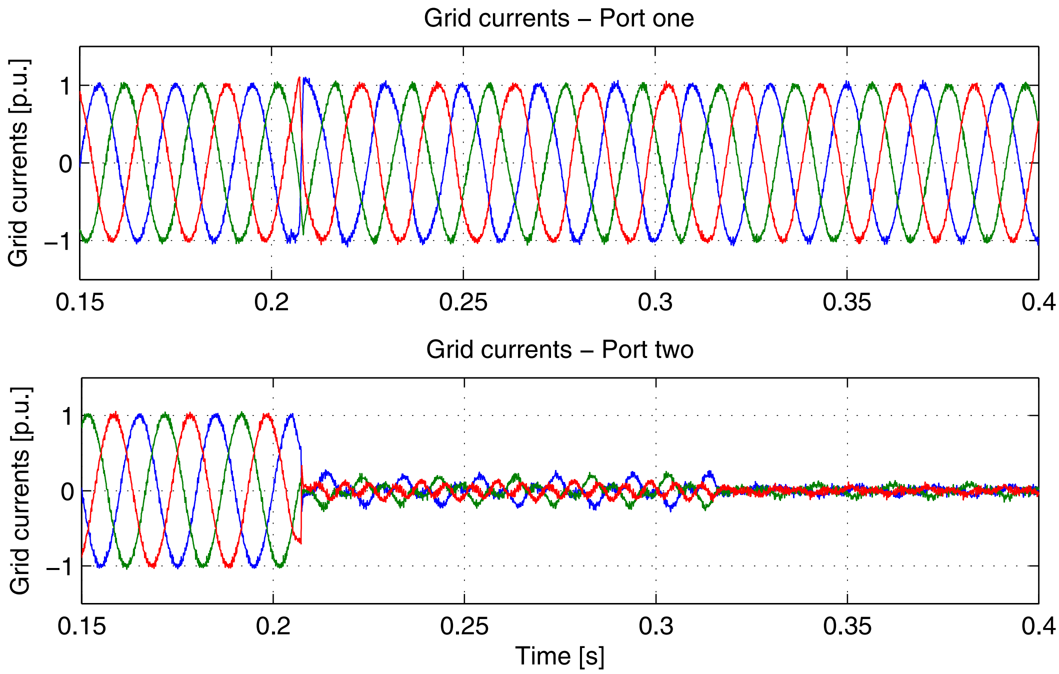

Fig. 5.108. Currents in Port 1 and Port 2 during single-phase short-circuit.

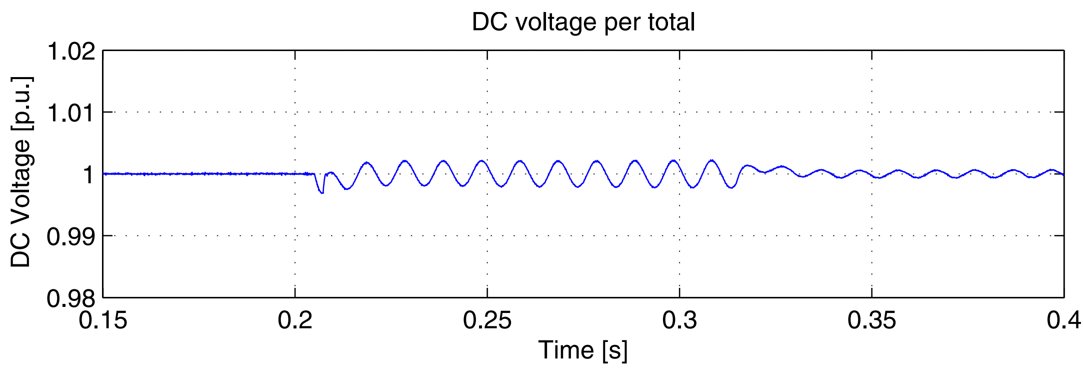

Fig. 5.109. Average DC-link voltage during single-phase short-circuit.

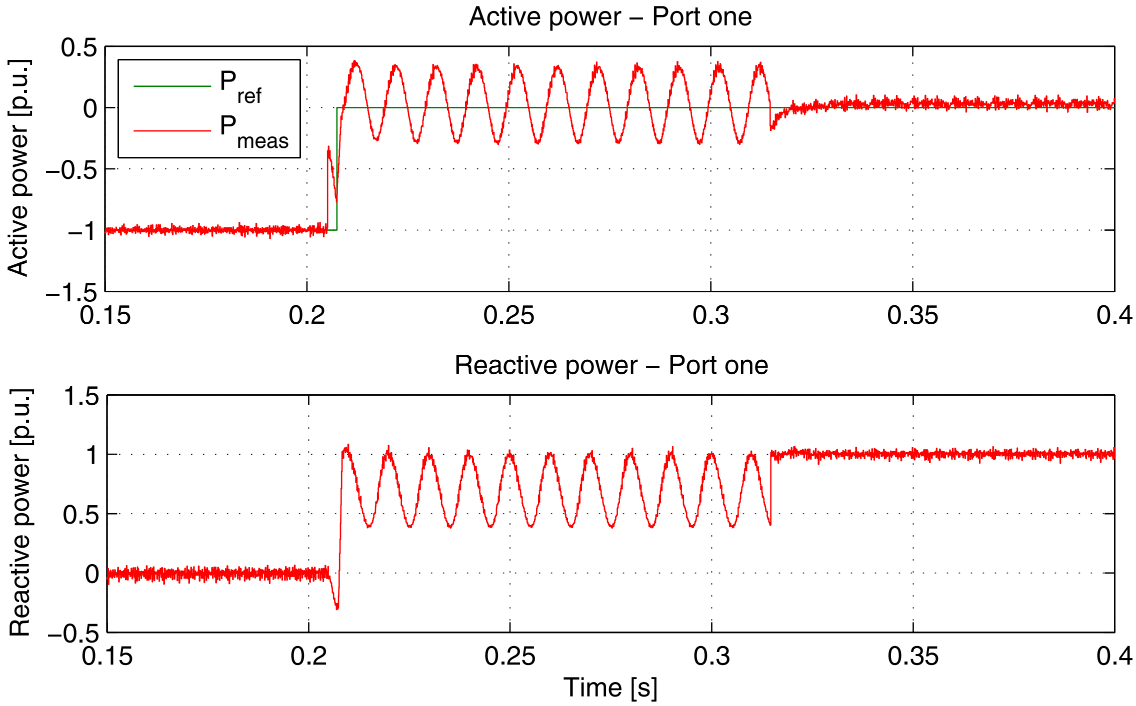

Fig. 5.110. Active and reactive power in Port 1 during single-phase short-circuit.

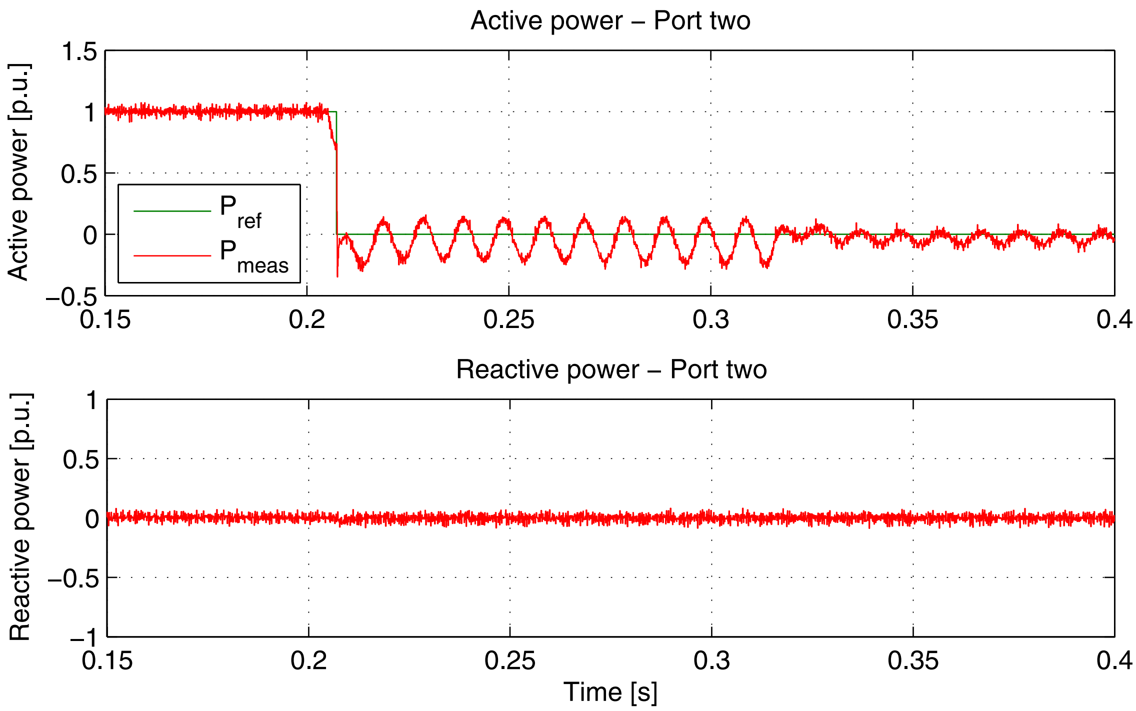

Fig. 5.111. Active and reactive power in Port 2 during single-phase short-circuit.

5.3.3.8 Two-Phase Short-Circuit

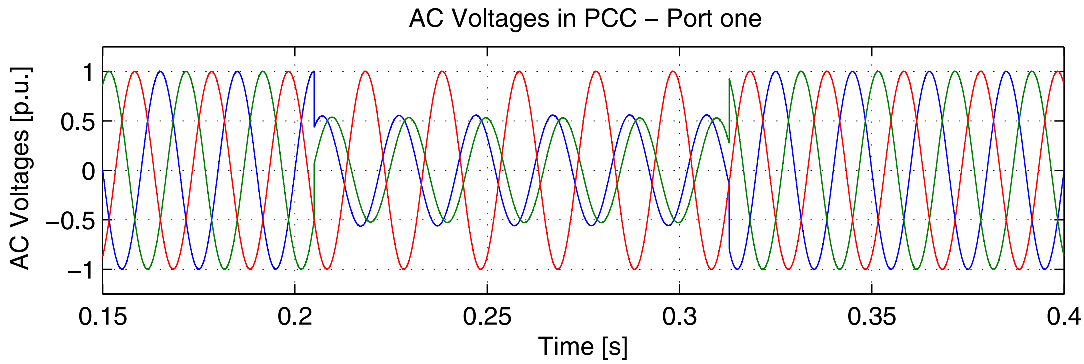

Fig. 5.112. Voltages in Port 1 during two-phase short-circuit without ground.

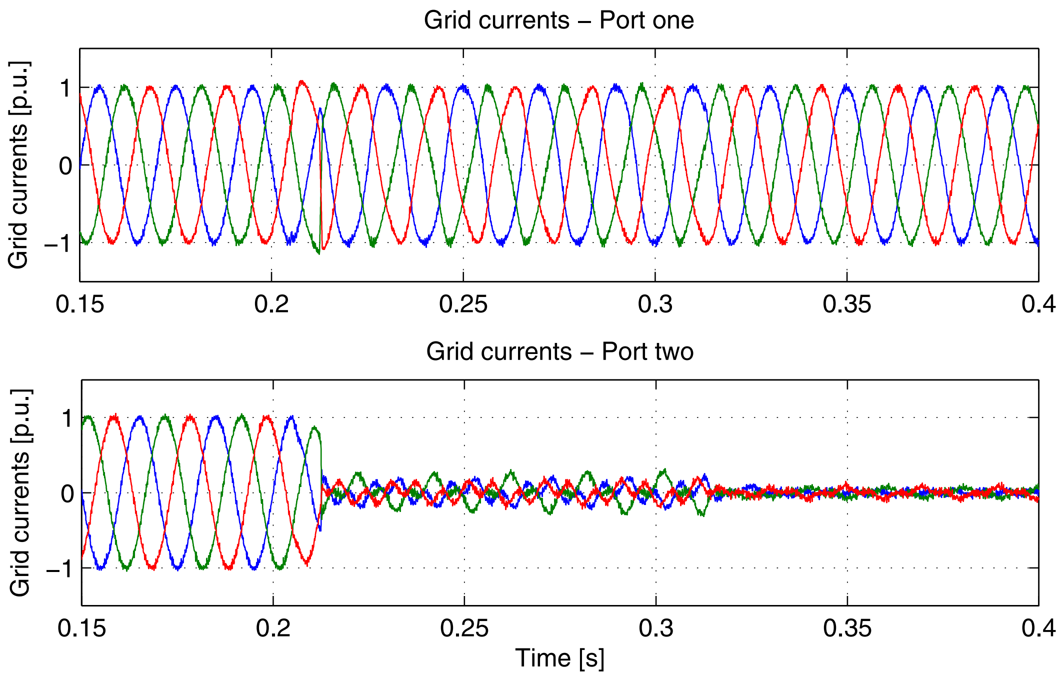

Fig. 5.113. Currents in Port 1 and Port 2 during two-phase short-circuit without ground.

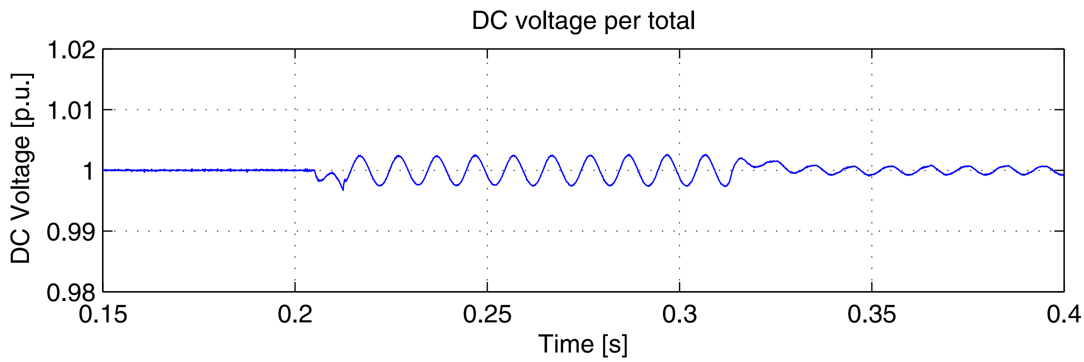

Fig. 5.114. Average DC-link voltage during two-phase short-circuit without ground.

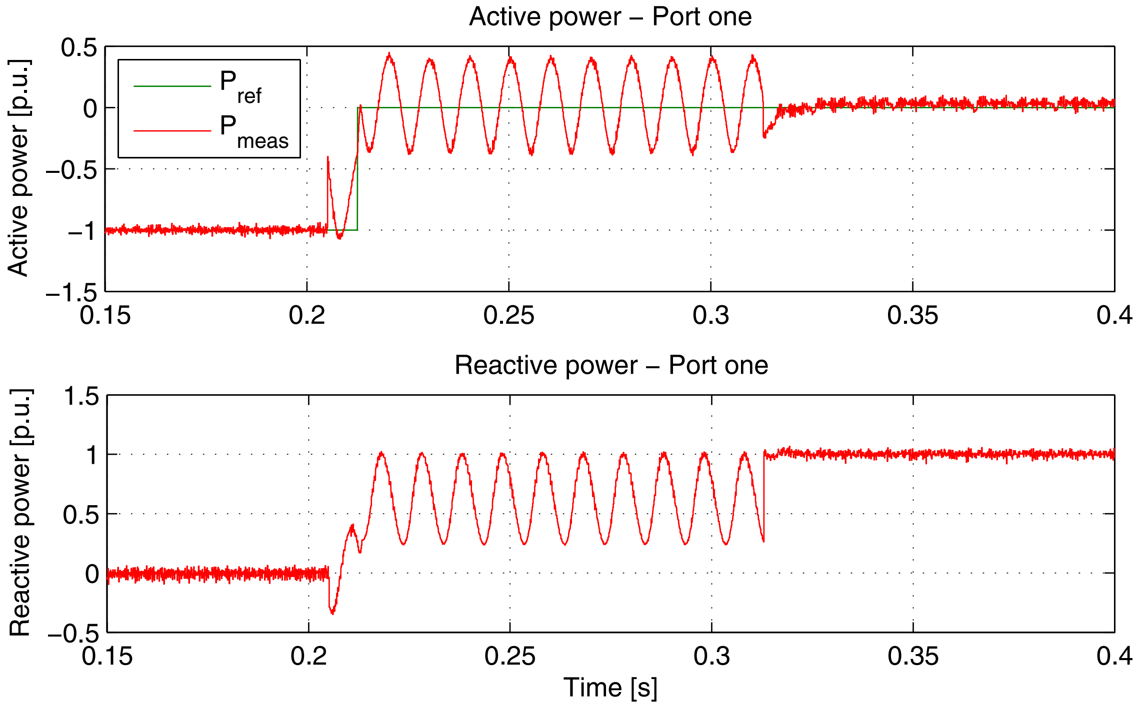

Fig. 5.115. Active and reactive power in Port 1 during two-phase short-circuit without ground.

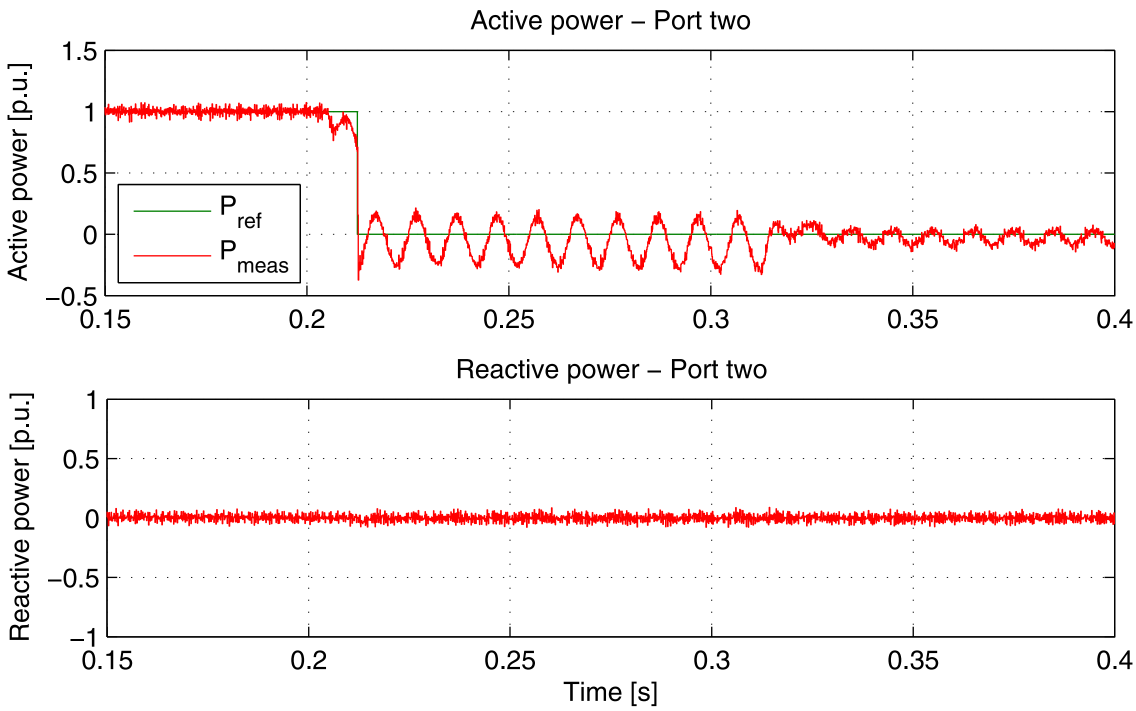

Fig. 5.116. Active and reactive power in Port 2 during two-phase short-circuit without ground.

5.3.3.9 Two-Phase with ground Short-Circuit

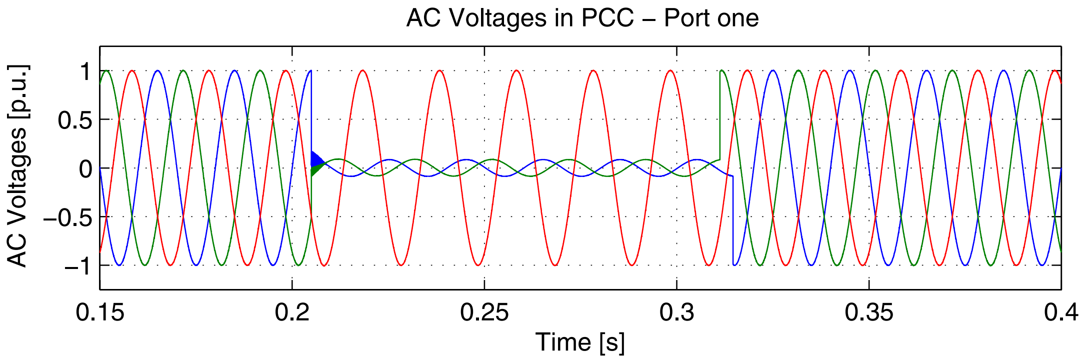

Fig. 5.117. Voltages in Port 1 during a two-phase short-circuit with ground.

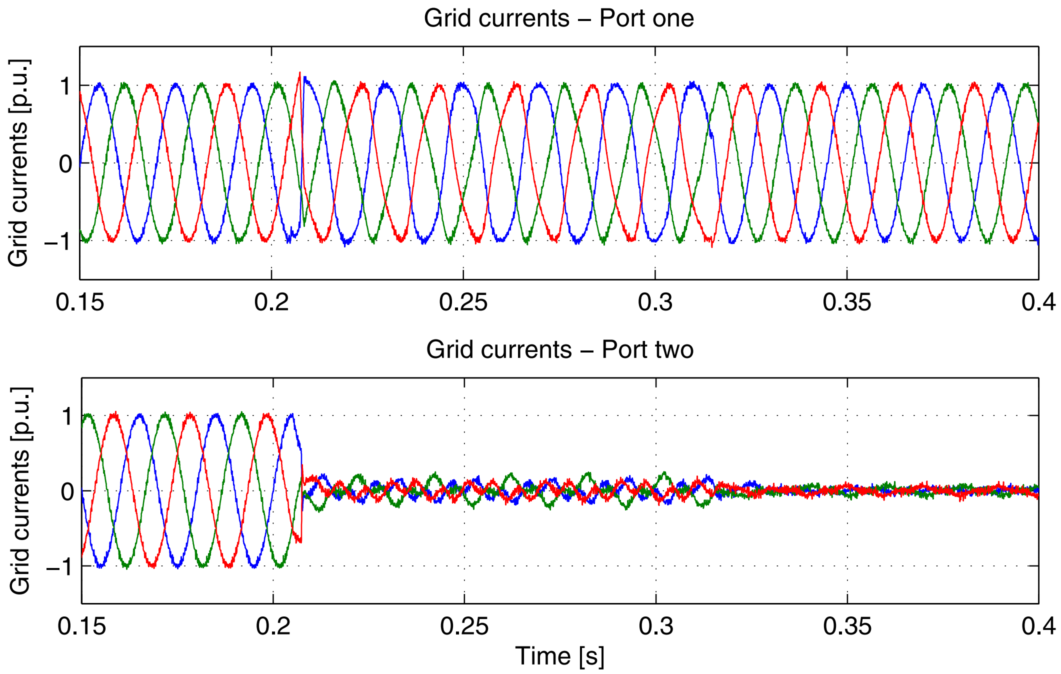

Fig. 5.118. Currents in Port 1 and Port 2 during a two-phase short-circuit with ground.

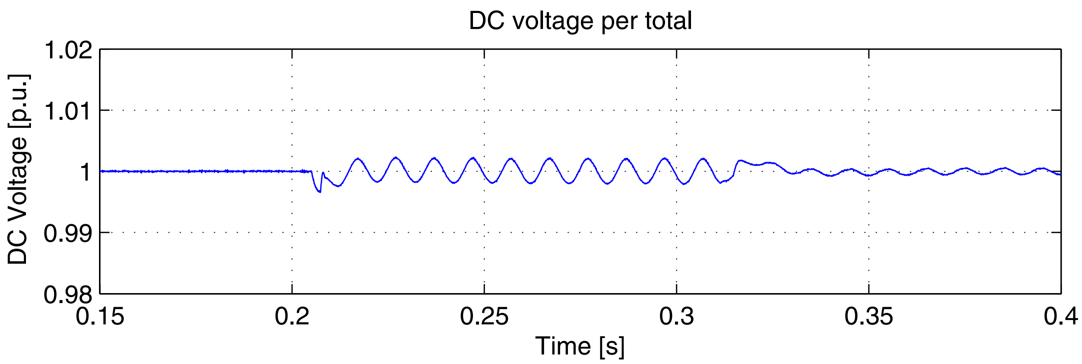

Fig. 5.119. Average DC-link voltage during a two-phase short-circuit with ground.

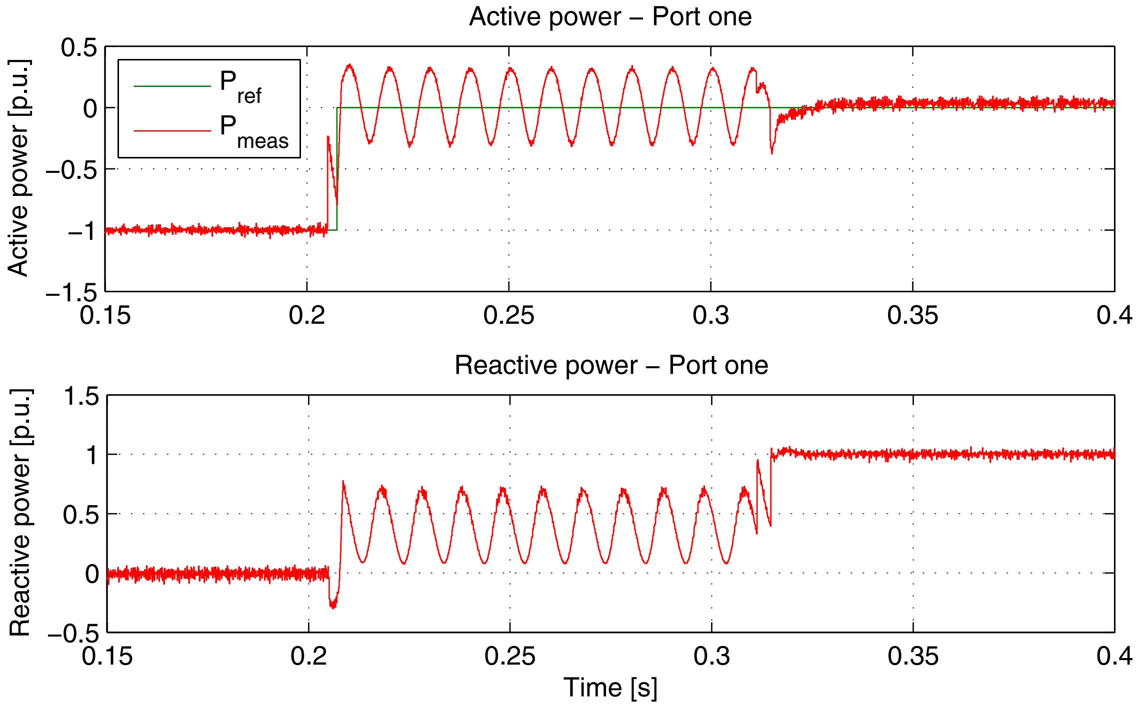

Fig. 5.120. Active and reactive power in Port 1 during a two-phase short-circuit with ground.

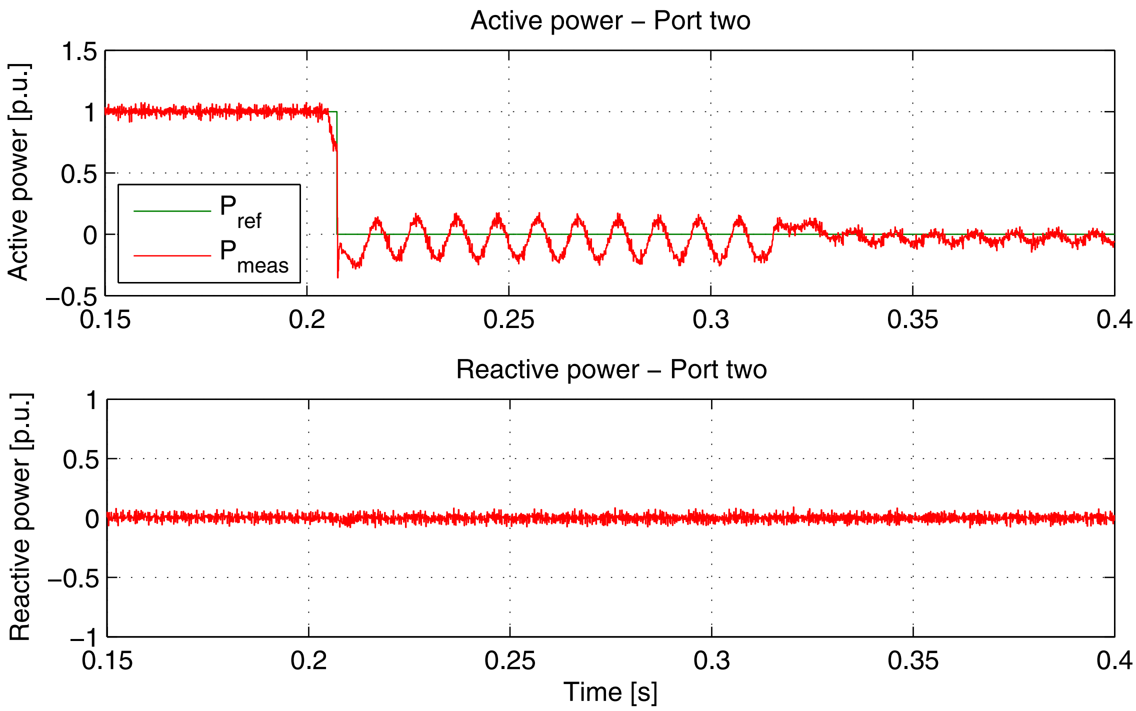

Fig. 5.121. Active and reactive power in Port 2 during a two-phase short-circuit with ground

5.3.3.10 Three-Phase Short-Circuit

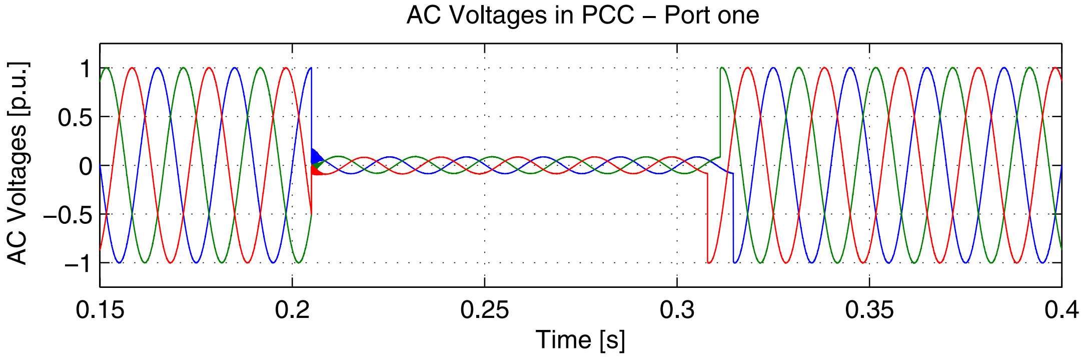

Fig. 5.122. Voltages in port 1 during a three-phase short-circuit.

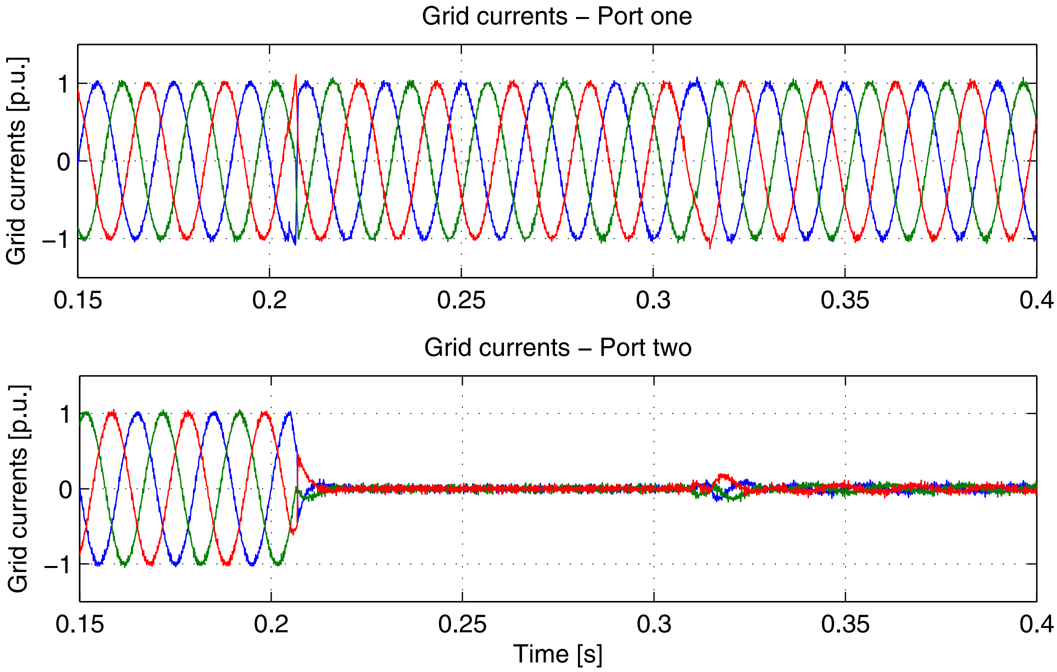

Fig. 5.123. Currents in Port 1 and Port 2 during a three-phase short-circuit.

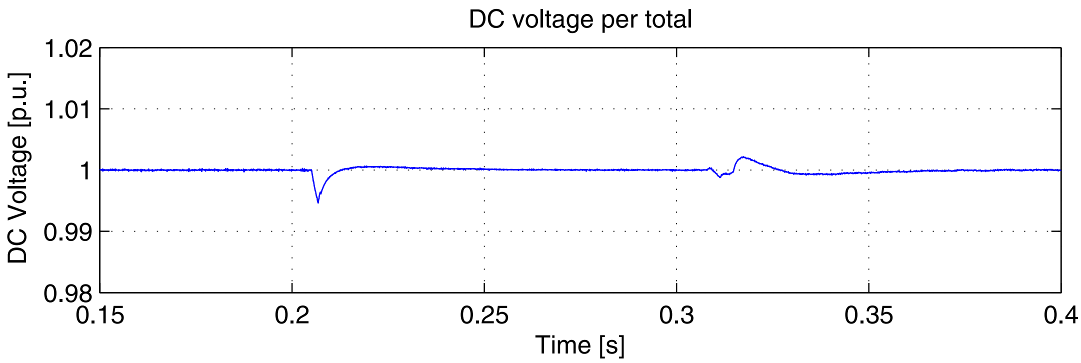

Fig. 5.124. Average DC-link voltage during a three-phase short-circuit.

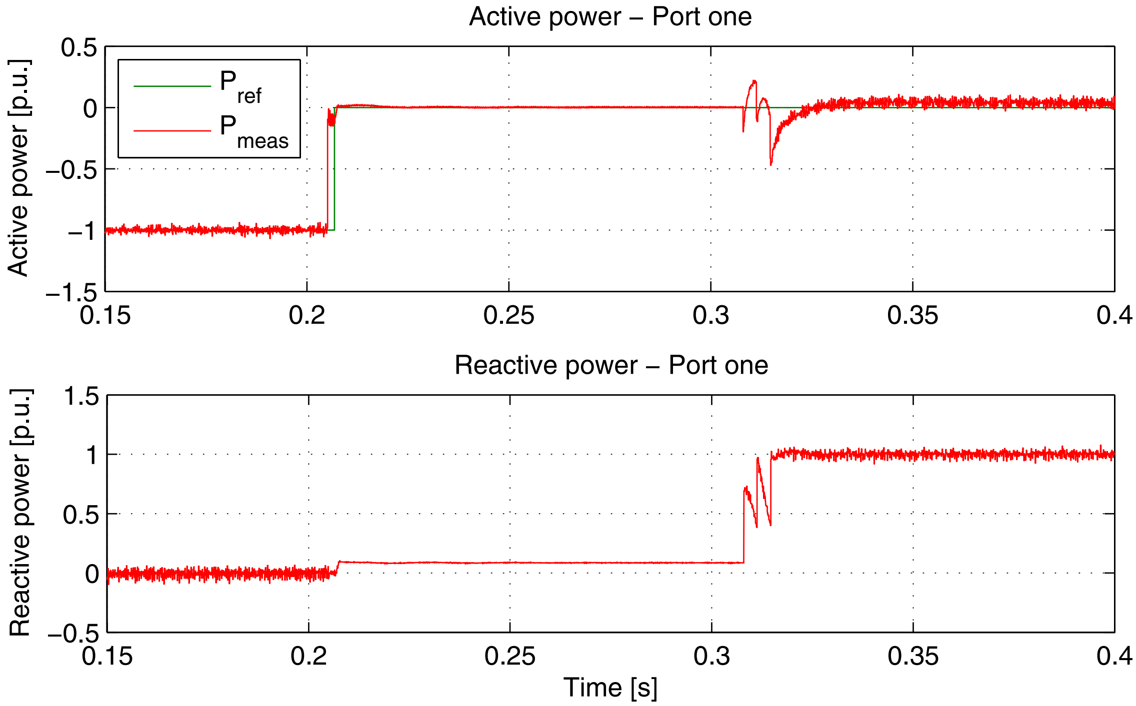

Fig. 5.125. Active and reactive power in Port 1 during a three-phase short-circuit.

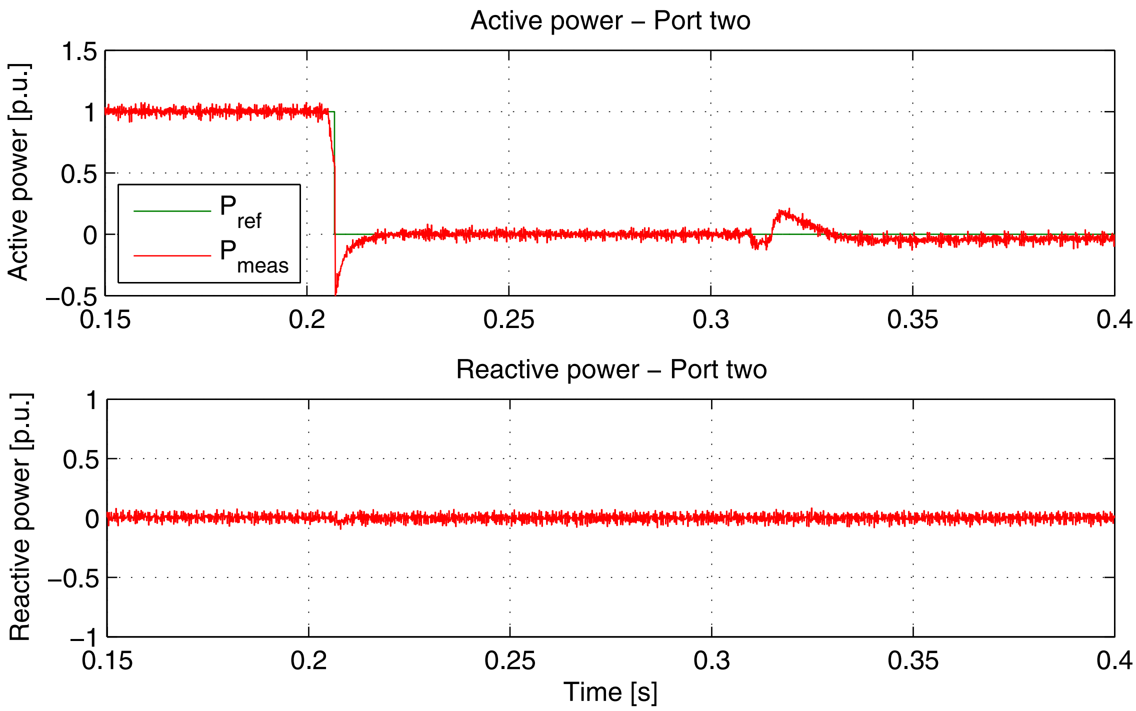

Fig. 5.126. Active and reactive power in Port 1 during a three-phase short-circuit.

5.3.3.11 Conclusions

Based on the above simulation results it can be concluded that the stationary reference frame control strategy with PR current controllers gives good results in all considered study cases.

Very fast reversal of power and a complete decoupling of active and reactive power are obtained. The control structure is insensitive to voltage excursions and unbalances being able to track accurately the references. The control is able to track the power references even during the phase jumps from +60º to -60º, without exceeding the rated currents. The excursions of active and reactive power in this case are also within the limits. All types of faults can be handled with good performances. The 100 Hz component is present in the active and reactive power output of the faulted port for the unsymmetrical faults due to the reference frame transformation for currents. However, improvements and different control strategies during the fault shall be investigated. The currents in the faulted port does not exceed the rated values in all considered short-circuits. Moreover, the currents are sinusoidal even during the fault duration. In all considered study cases the average DC-link voltage used in the control has variations below 1%.

Thus, the PR current controllers gives advantages such as: very fast reversal of power flow, robustness to voltage amplitude, phase and frequency excursions, short-circuits, good balancing of the DC-link voltages without any additional DC voltage compensators, small DC-link voltage overshoot during different disturbances are obtained.

5.3.4 Natural reference frame control

5.3.4.1 Current Harmonic Compatibility Levels

The current harmonic compatibility levels for the natural reference frame control are presented in Fig. 5.127.

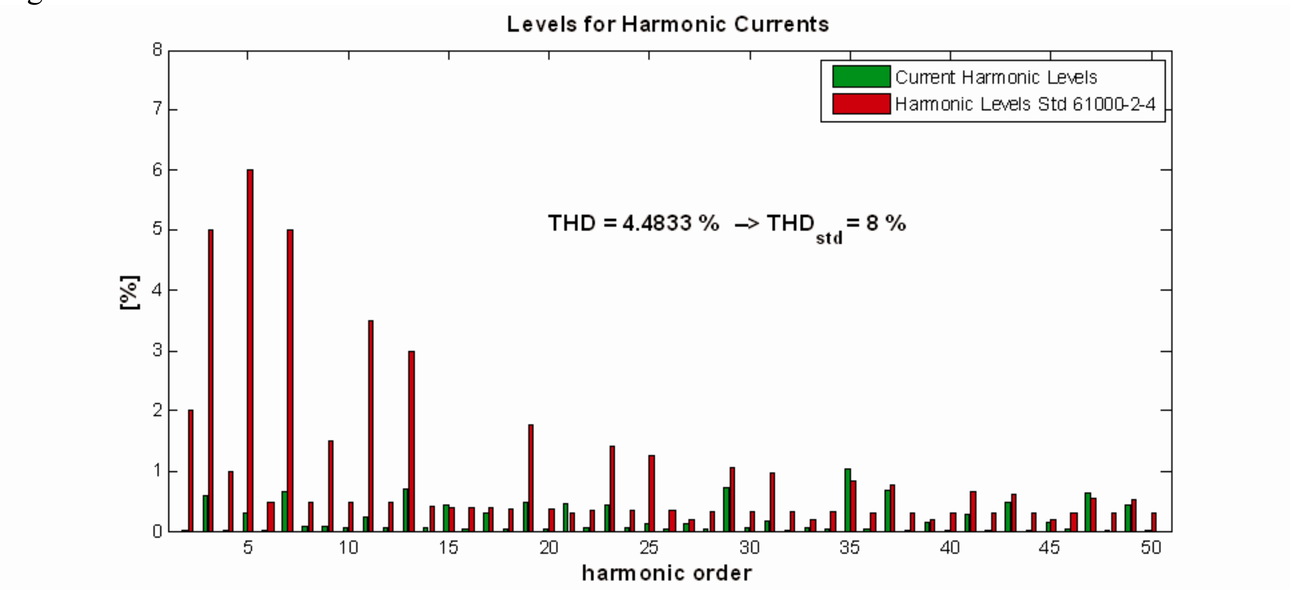

Fig. 5.127. Current harmonic compatibility levels in PCC for natural reference frame control.

Due to the neutral connection required by this control strategy the presence of the multiples of the 3rd harmonic can be observed in the spectrum. Also, noticeable levels are obtained for the 5th, 7th, 11th and 13th. The 35th harmonic corresponds to the switching frequency. The current THD is about 4.5%.

5.3.4.2 Bi-directional Power Flow

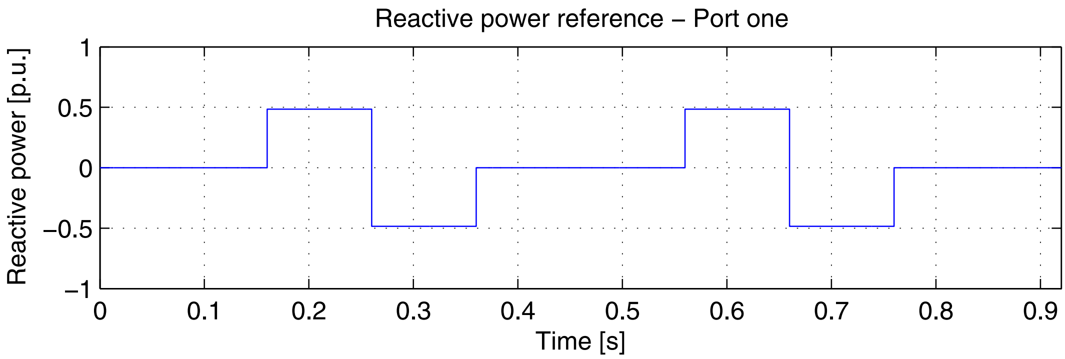

Fig. 5.128. Reactive power reference for bi-directional power flow.

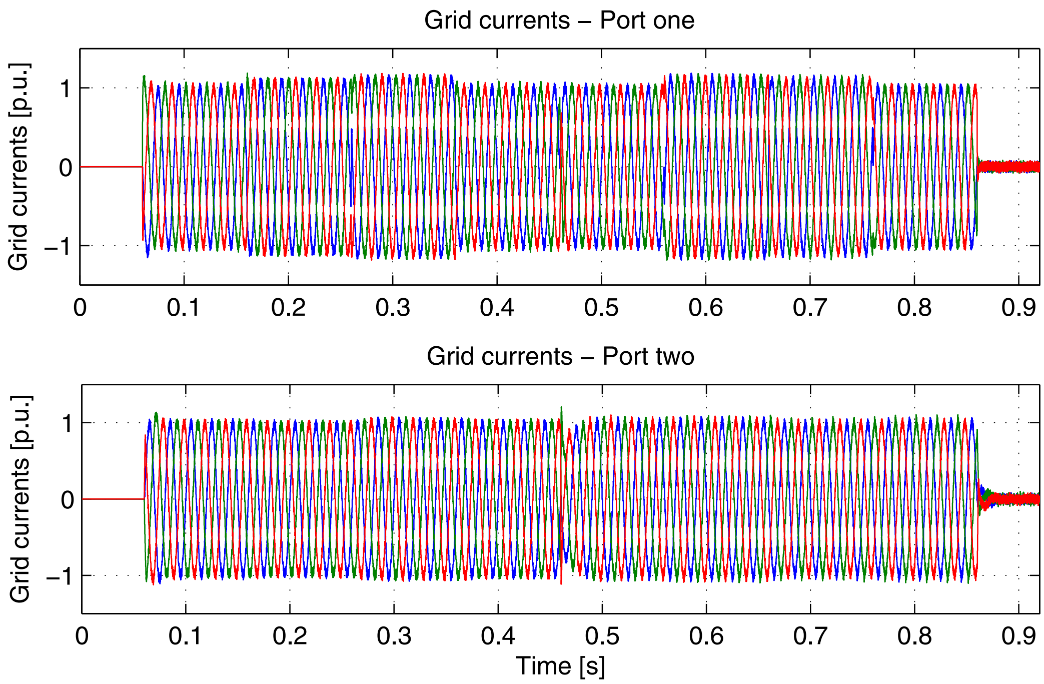

Fig. 5.129. Currents in Port 1 and Port 2 for bi-directional power flow.

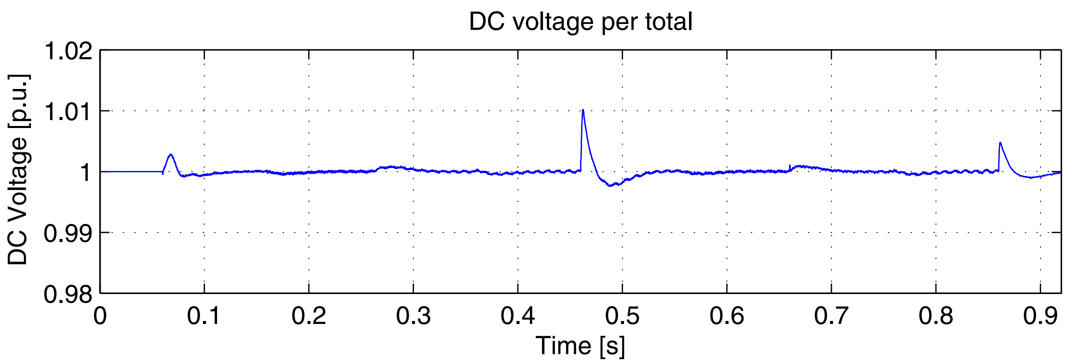

Fig. 5.130. Average DC-link voltage for bi-directional power flow.

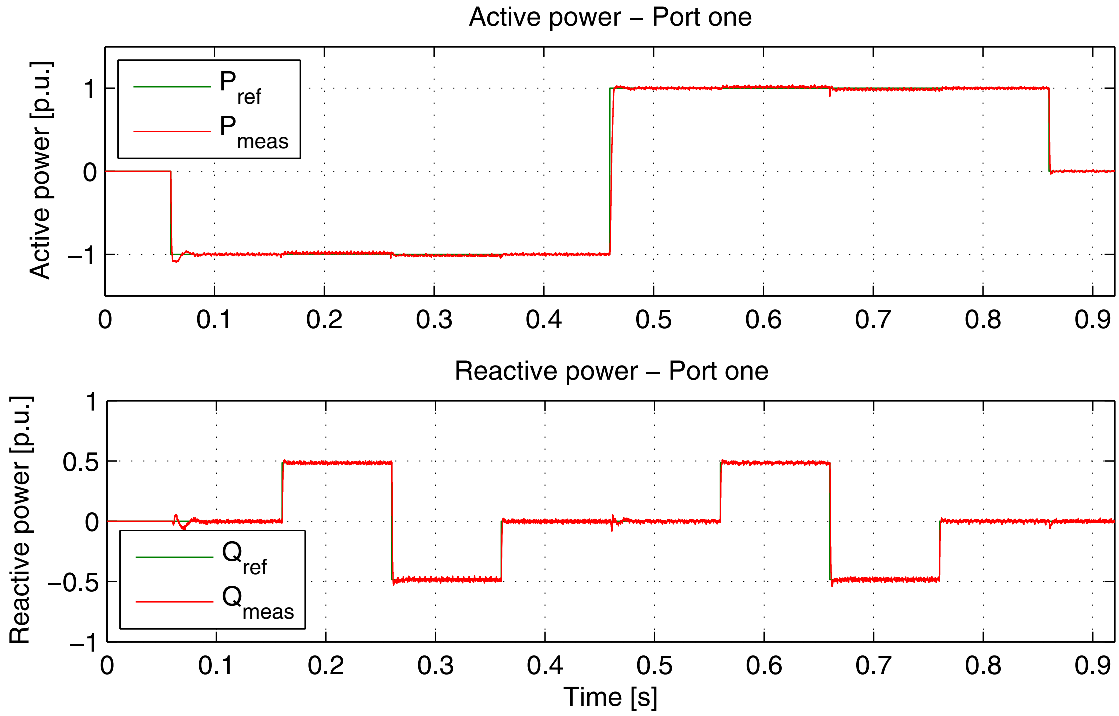

Fig. 5.131. Active and reactive power in Port 1 for bi-directional power flow.

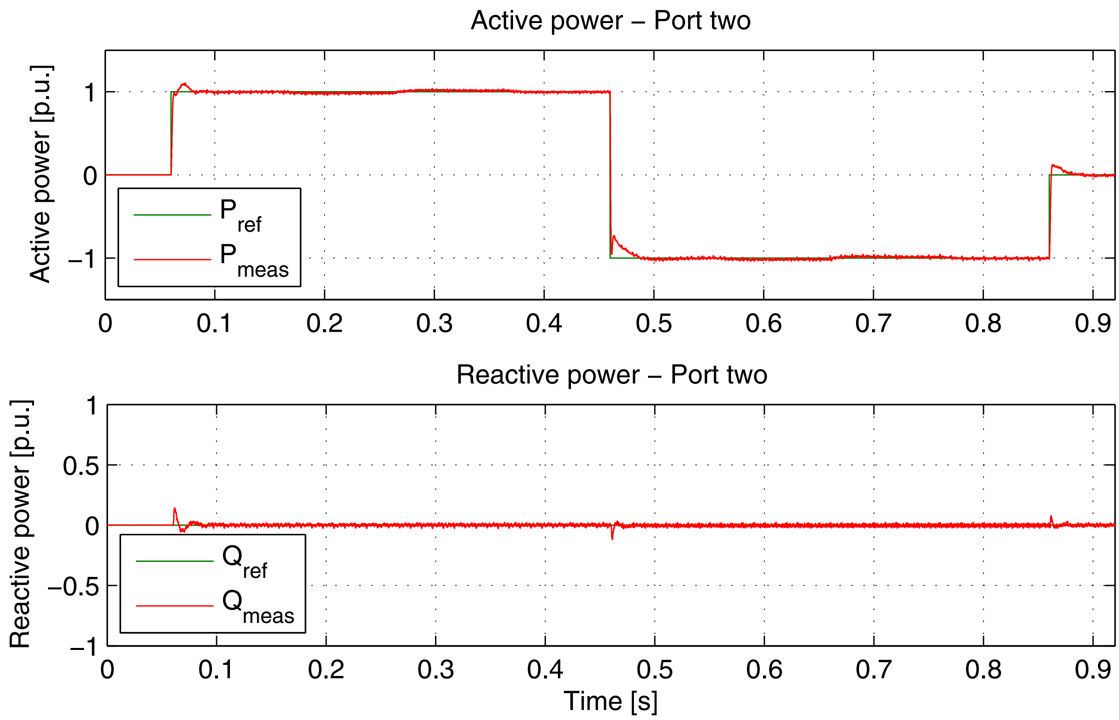

Fig. 5.132. Active and reactive power in Port 2 for bi-directional power flow.

5.3.4.3 Voltage Excursions

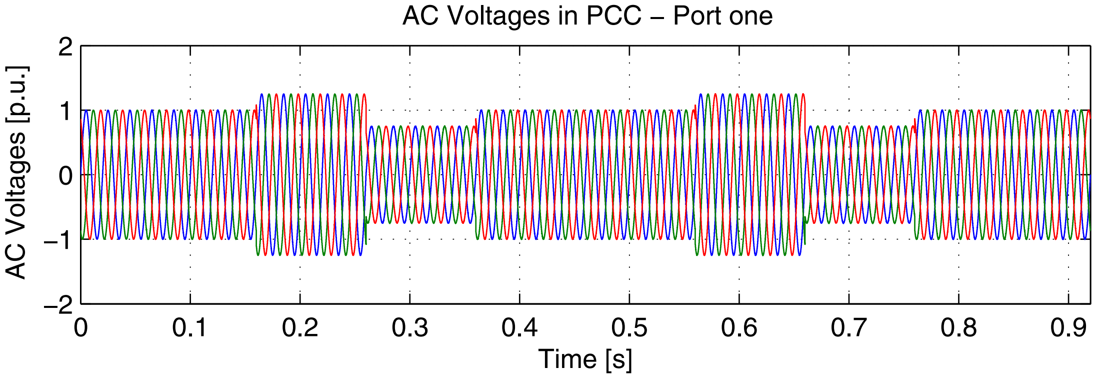

Fig. 5.133.Voltage excursions in Port 1.

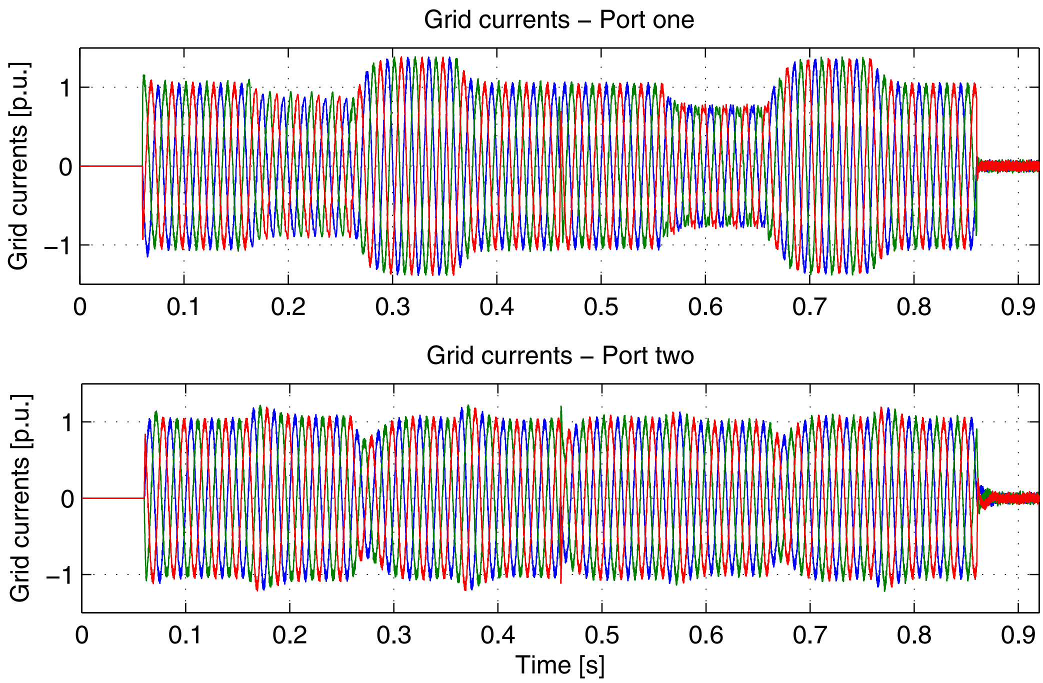

Fig. 5.134. Currents in Port 1 and Port 2 during voltage excursions.

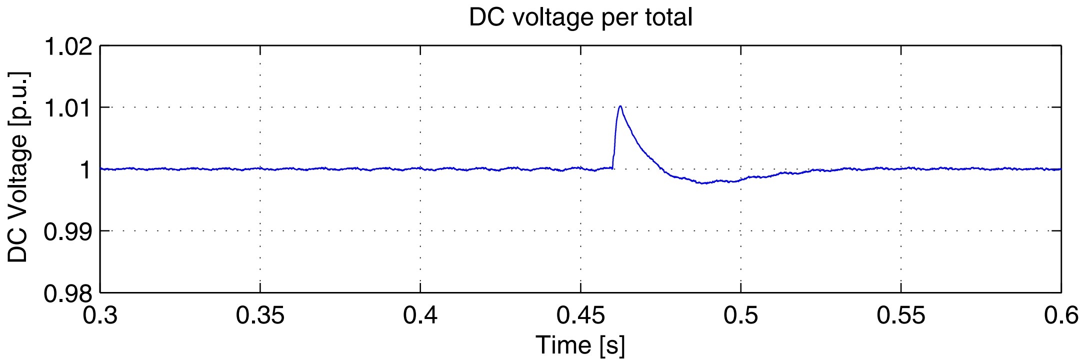

Fig. 5.135. Average DC-link voltage during voltage excursions.

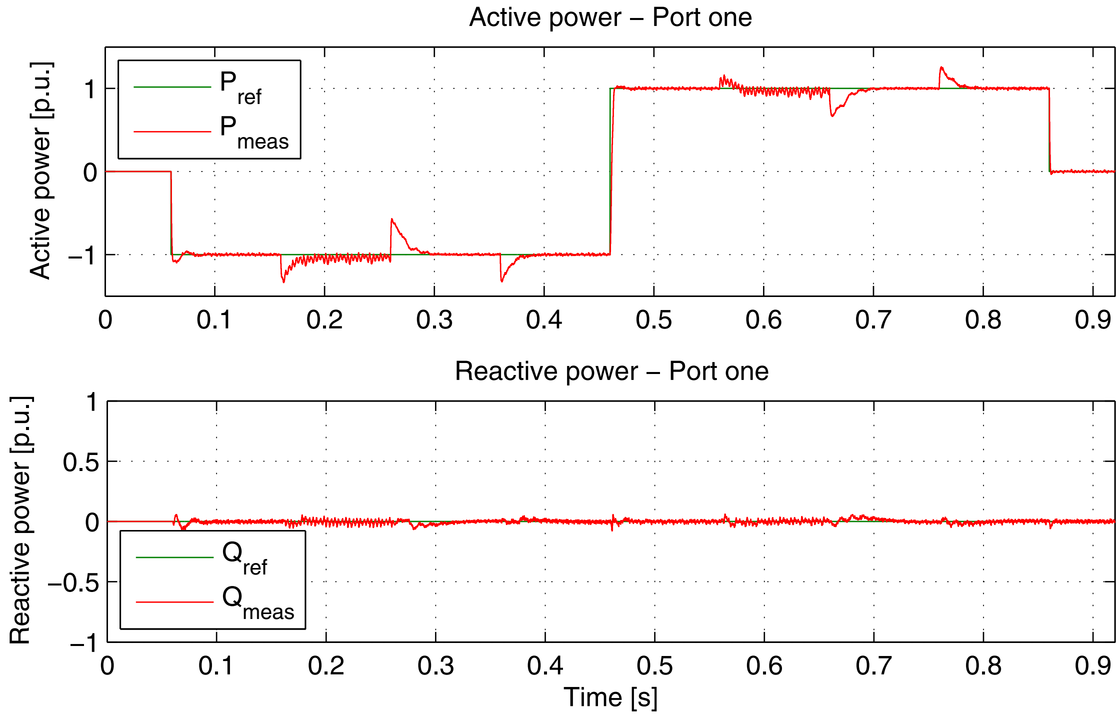

Fig. 5.136. Active and reactive power in Port 1 during voltage excursions.

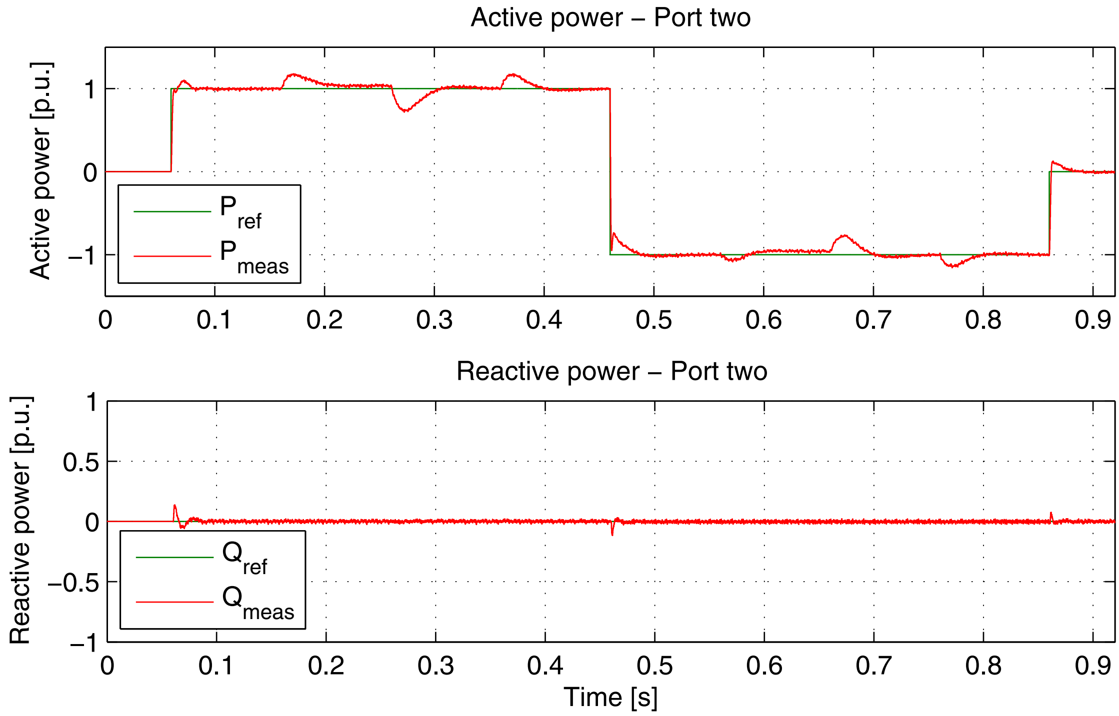

Fig. 5.137. Active and reactive power in Port 2 during voltage excursions.

5.3.4.4 Voltage Unbalances

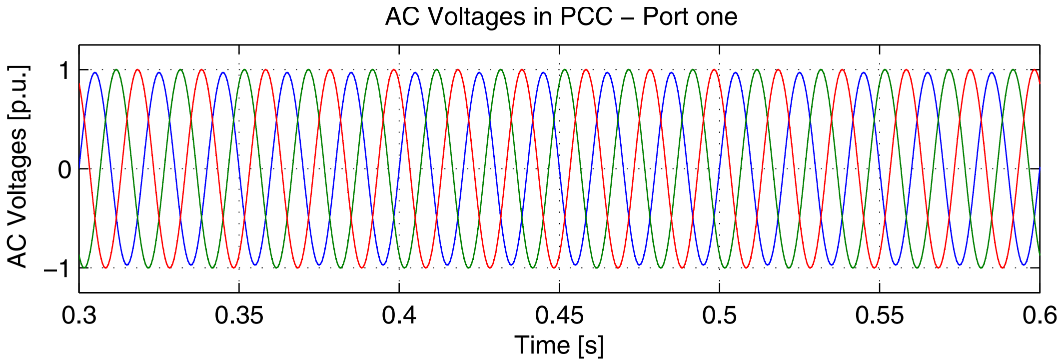

Fig. 5.138. Unbalance voltages in Port 1.

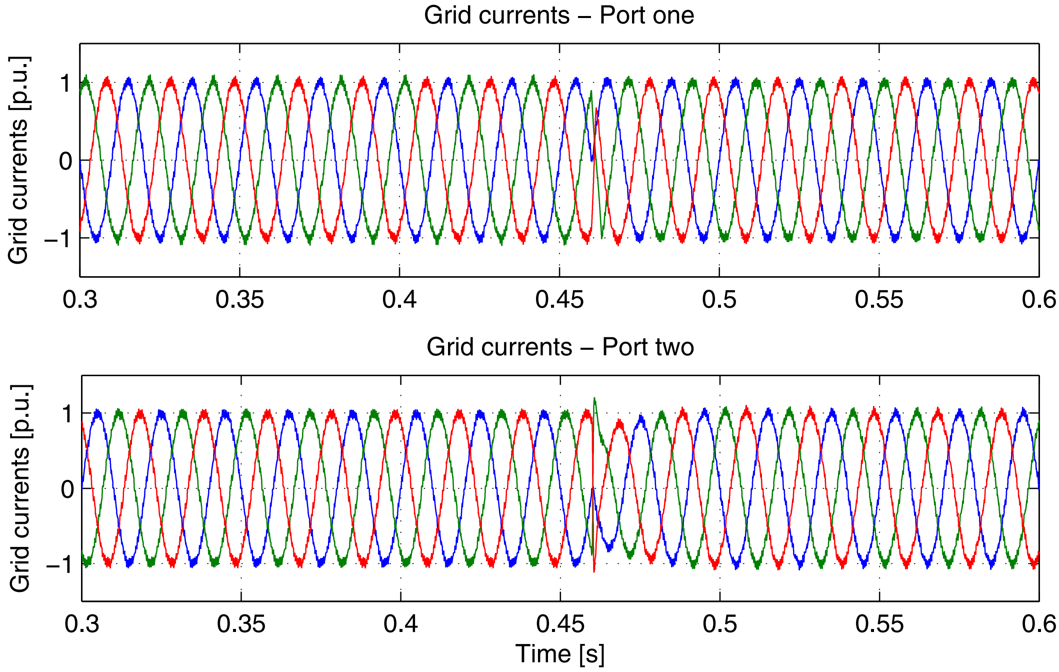

Fig. 5.139. Currents in Port 1 and Port 2 for voltage unbalances.

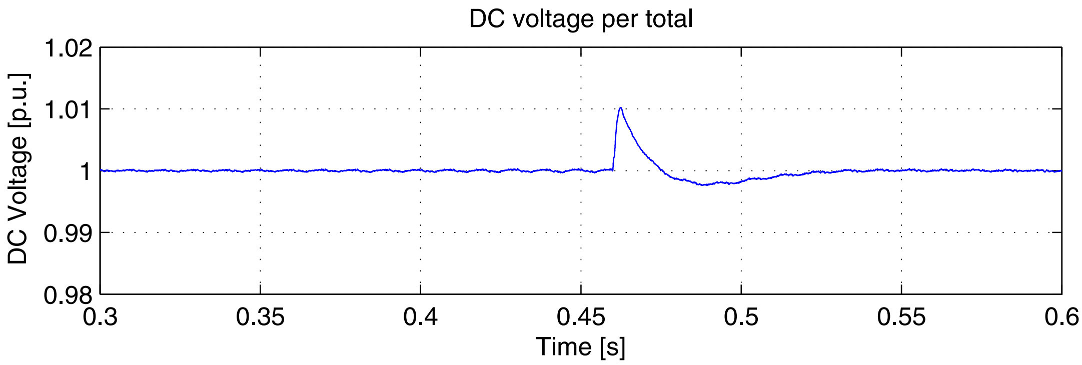

Fig. 5.140. Average DC-link voltage for voltage unbalances.

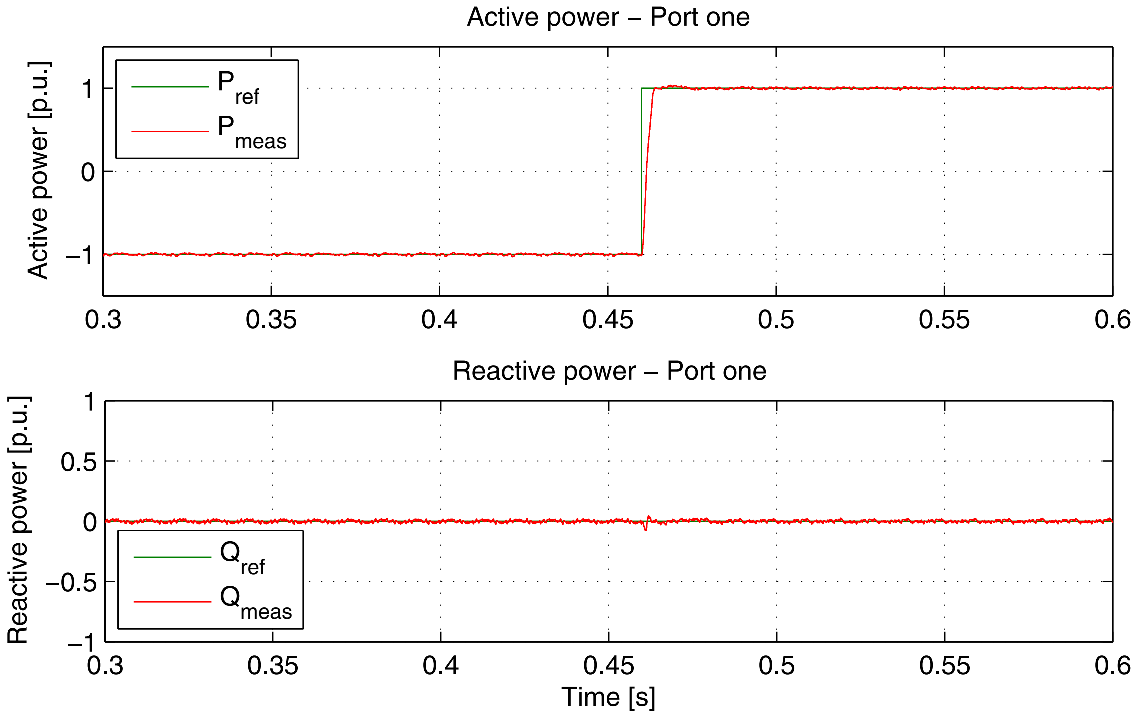

Fig. 5.141. Active and reactive power in Port 1 for unbalance voltages.

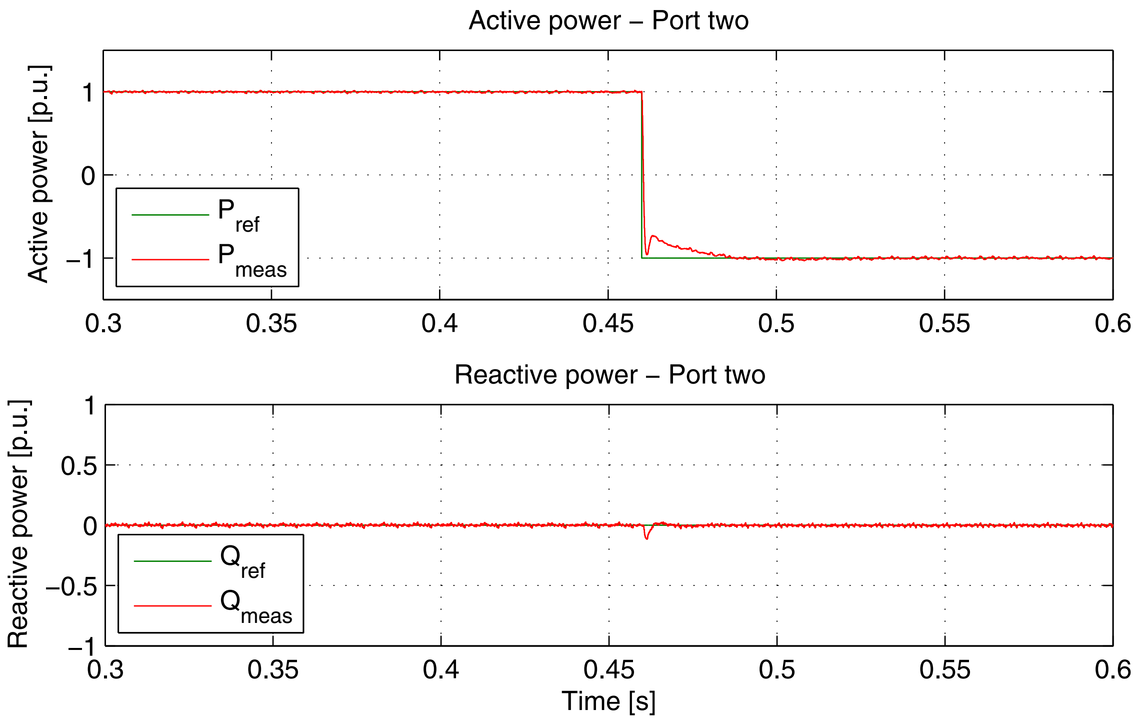

Fig. 5.142. Active and reactive power in Port 2 for unbalance voltages.

5.3.4.5 Phase Jumps

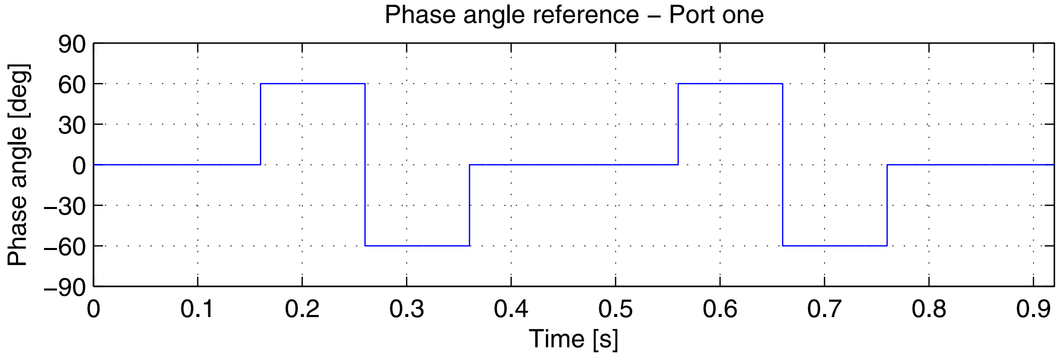

Fig. 5.143. Phase jumps in Port 1.

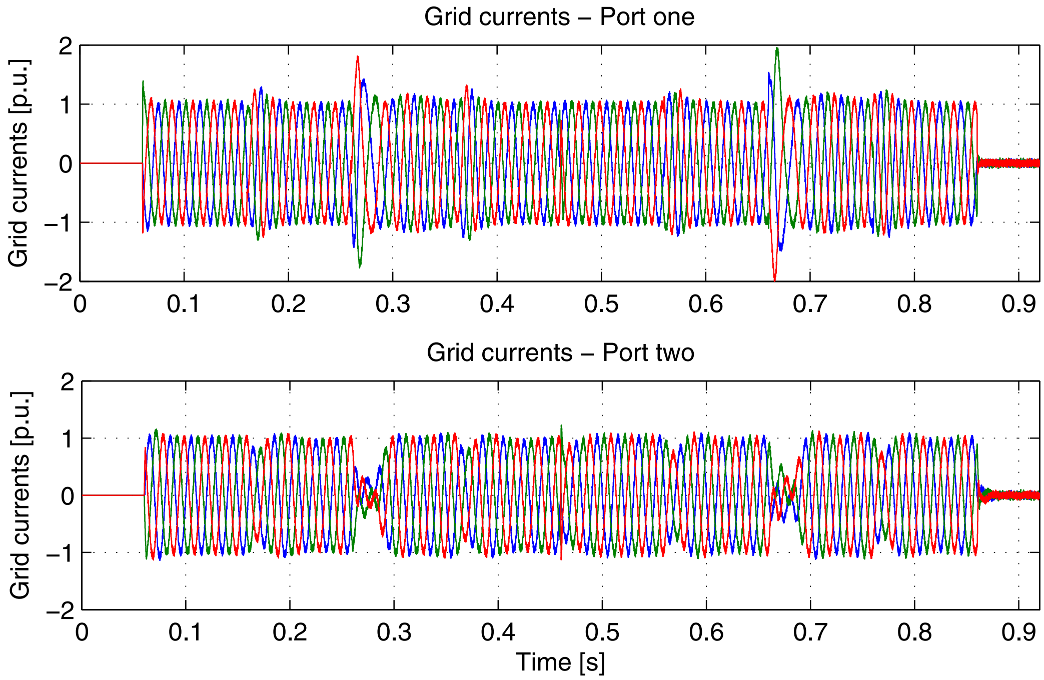

Fig. 5.144. Currents in Port 1 and Port 2 during phase jumps.

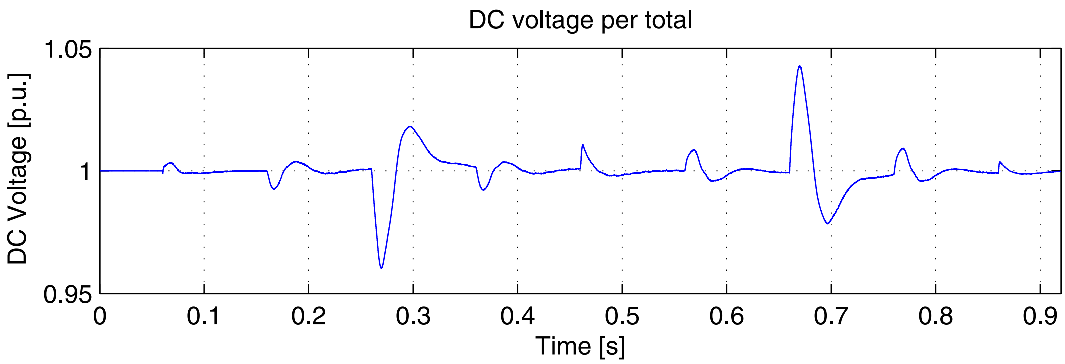

Fig. 5.145. Average DC-link during phase jumps.

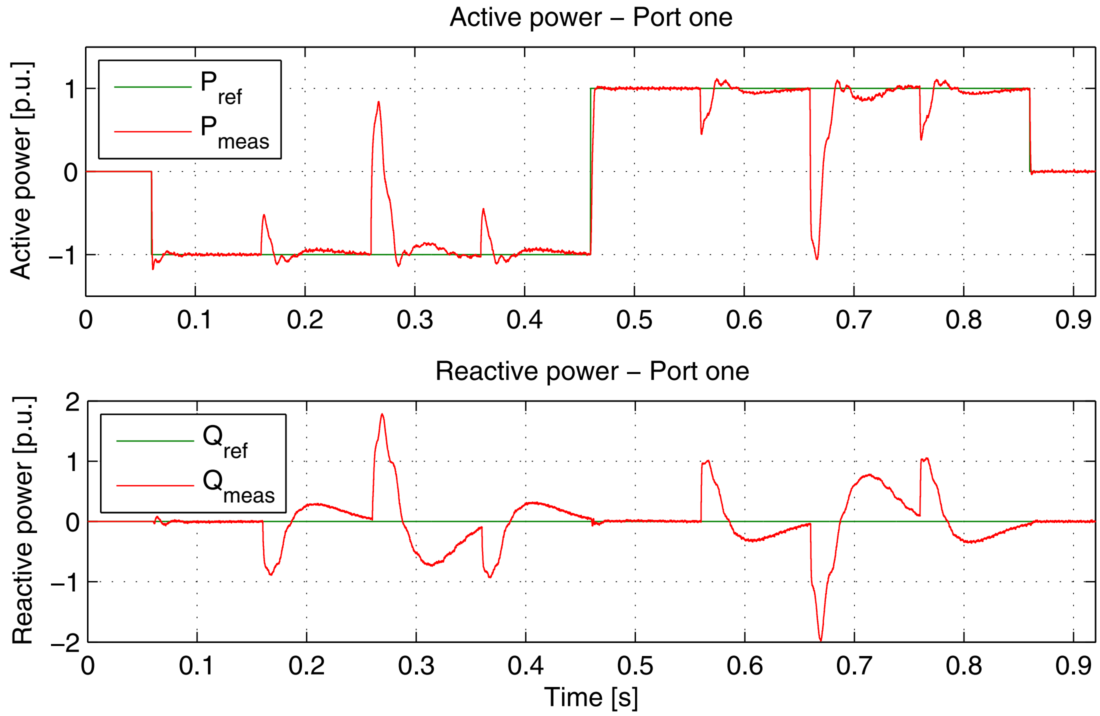

Fig. 5.146. Active and reactive power in Port 1 during phase jumps.

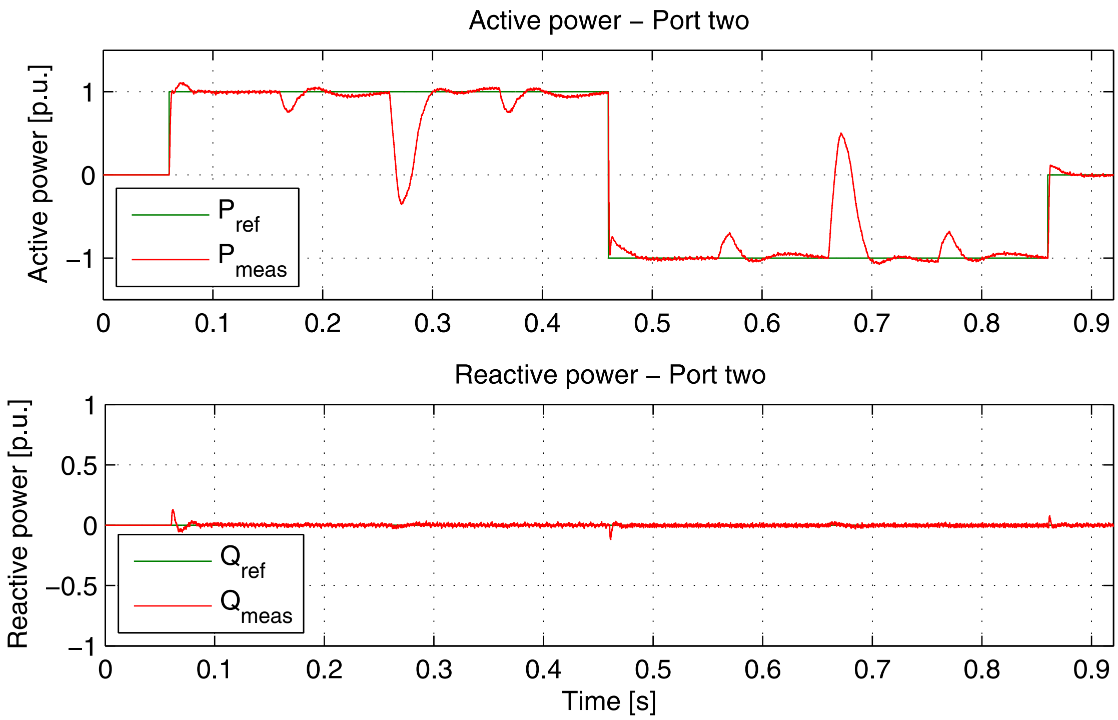

Fig. 5.147. Active and reactive power in Port 2 during phase jumps.

5.3.4.6 Frequency Excursions

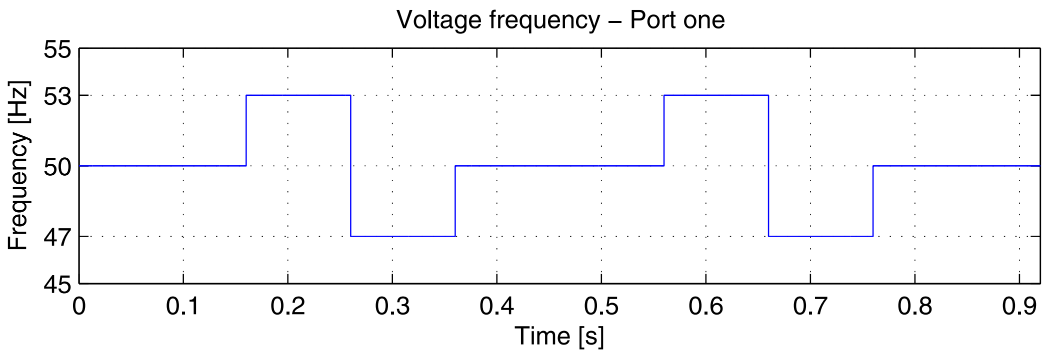

Fig. 5.148. Frequency excursions in Port 1.

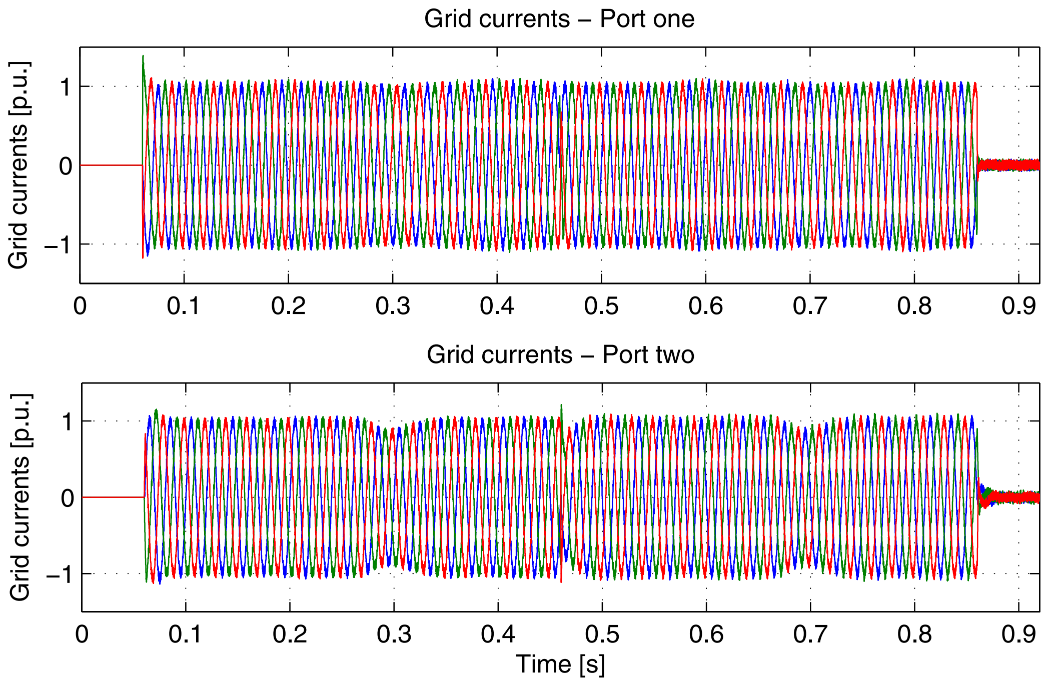

Fig. 5.149. Currents in Port 1 and Port 2 during frequency excursions.

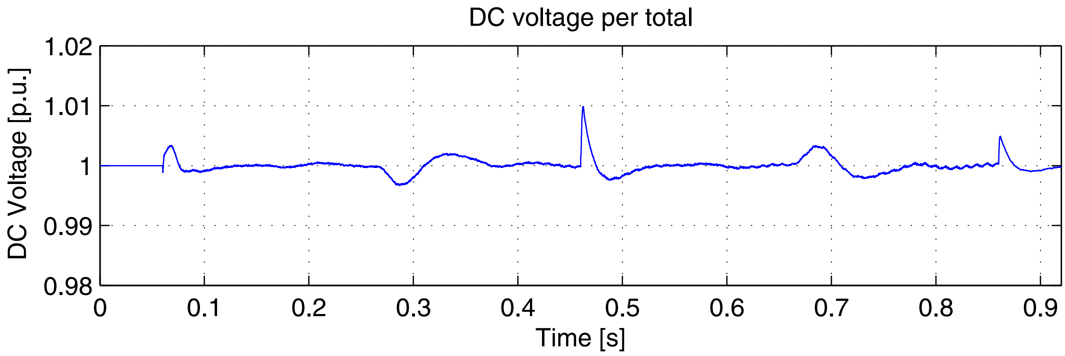

Fig. 5.150. Average DC-link voltage during frequency excursions.

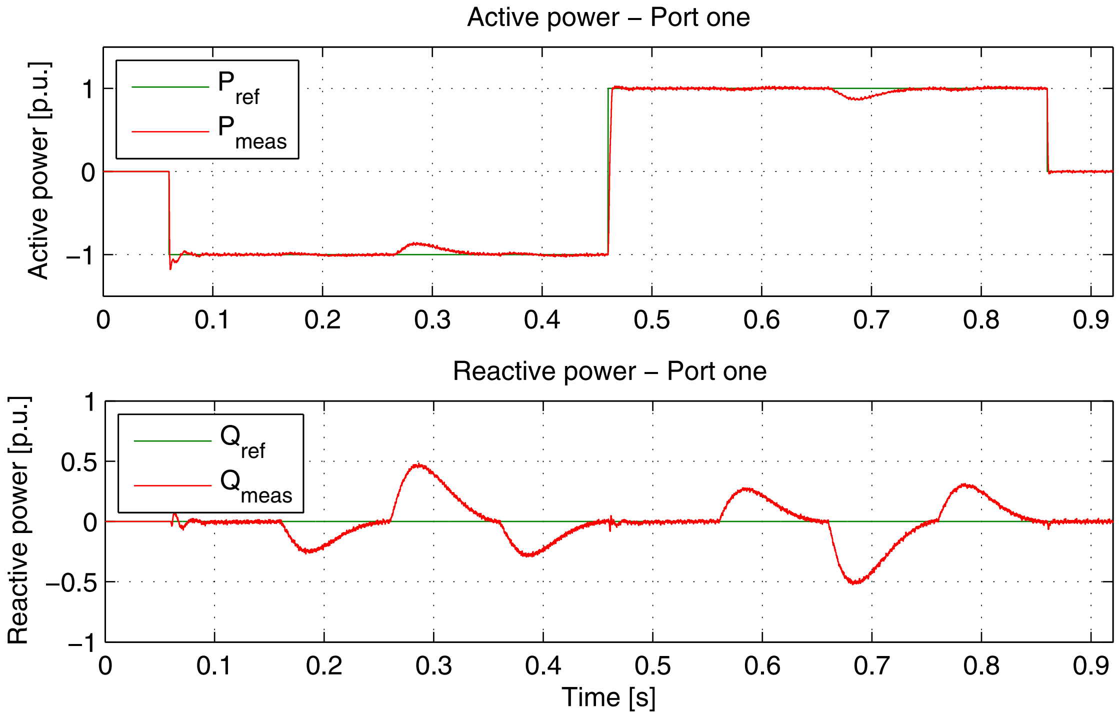

Fig. 5.151. Active and reactive power in Port 1 during frequency excursions.

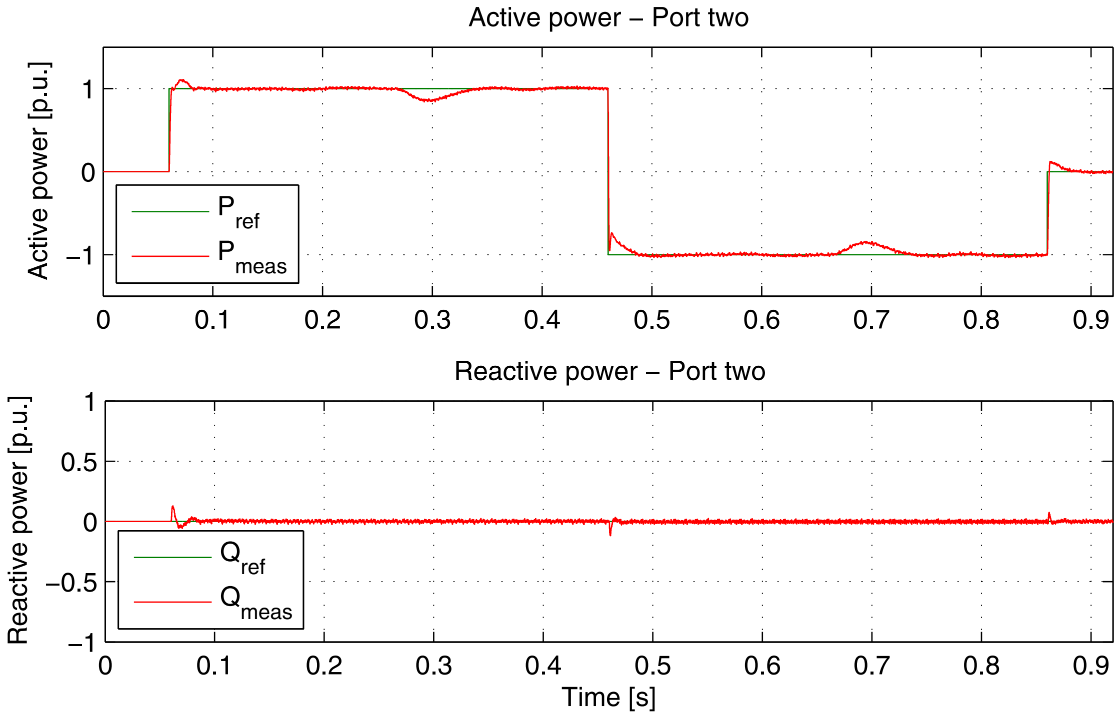

Fig. 5.152. Active and reactive power in Port 2 during frequency excursions.

5.3.4.7 Single-Phase Short-Circuit

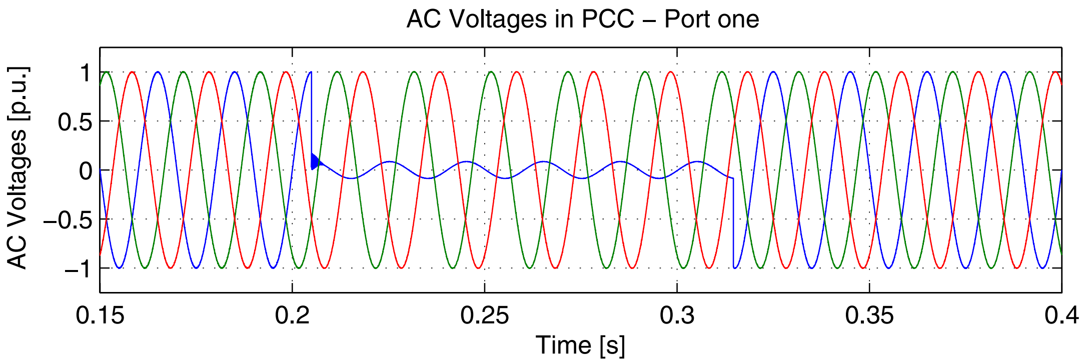

Fig. 5.153. Voltages in Port 1 during a single-phase short-circuit.

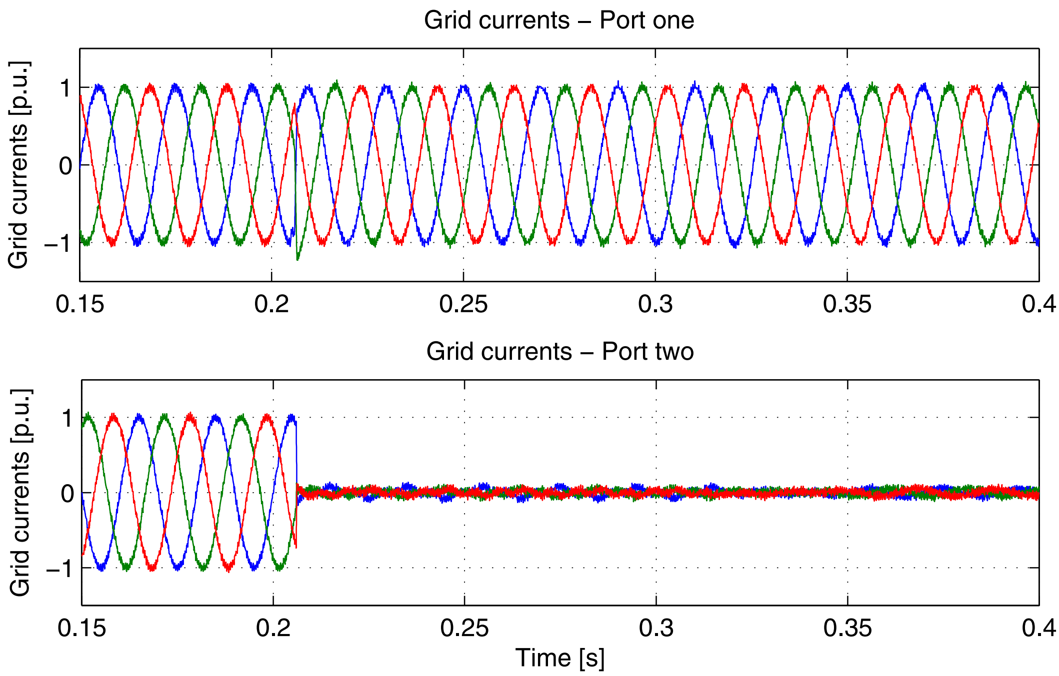

Fig. 5.154. Currents in Port 1 and Port 2 during a single-phase short-circuit.

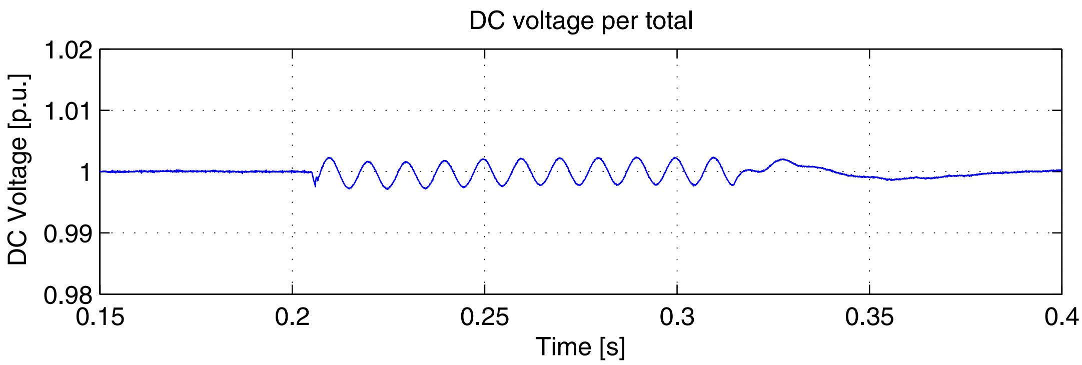

Fig. 5.155. Average DC-link voltage during a single-phase short-circuit.

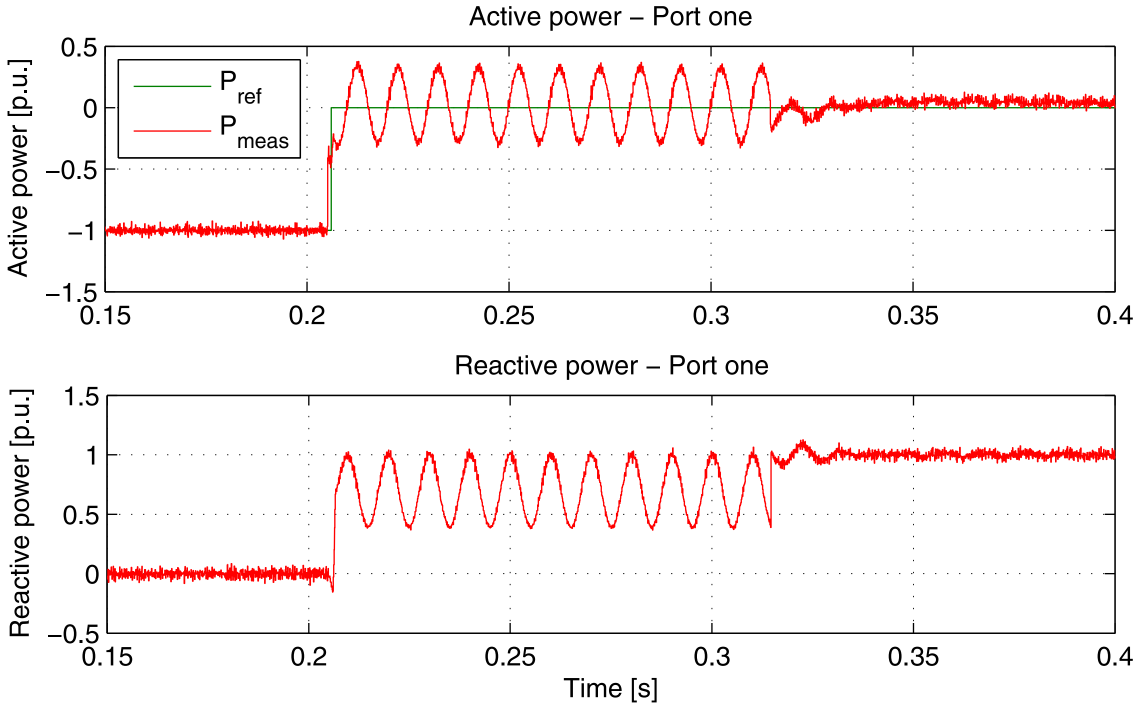

Fig. 5.156. Active and reactive power in Port 1 during a single-phase short-circuit.

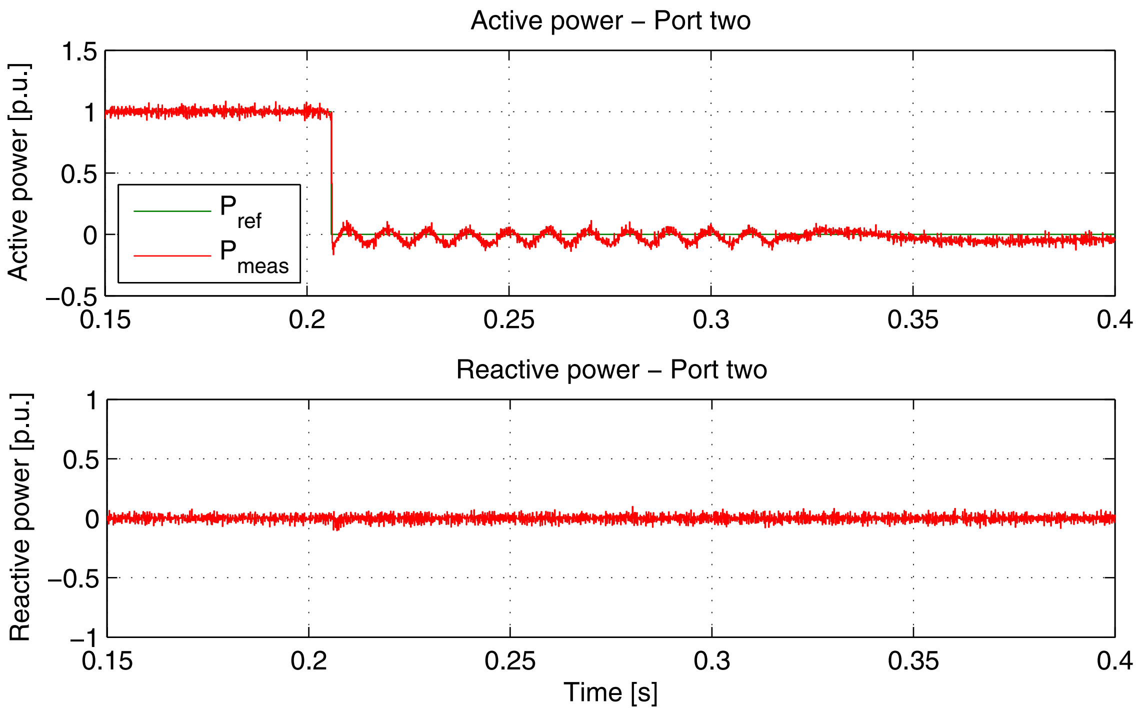

Fig. 5.157. Active and reactive power in Port 2 during a single-phase short-circuit.

5.3.4.8 Two-Phase Short-Circuit

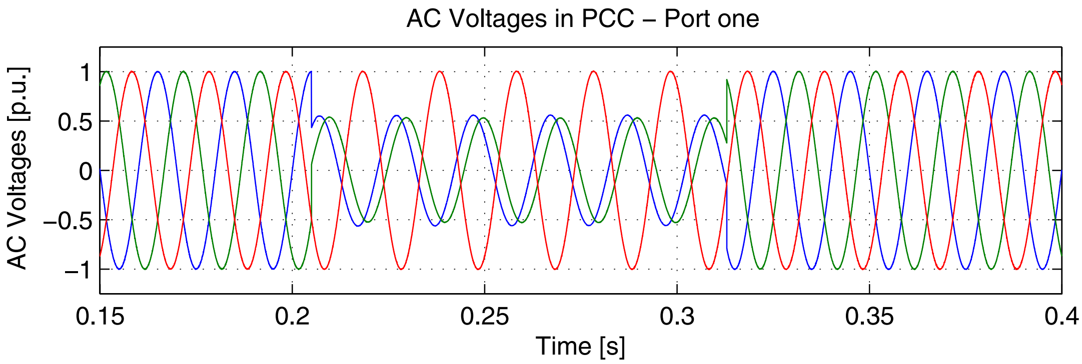

Fig. 5.158. Voltages in Port 1 during a two-phase short-circuit without ground.

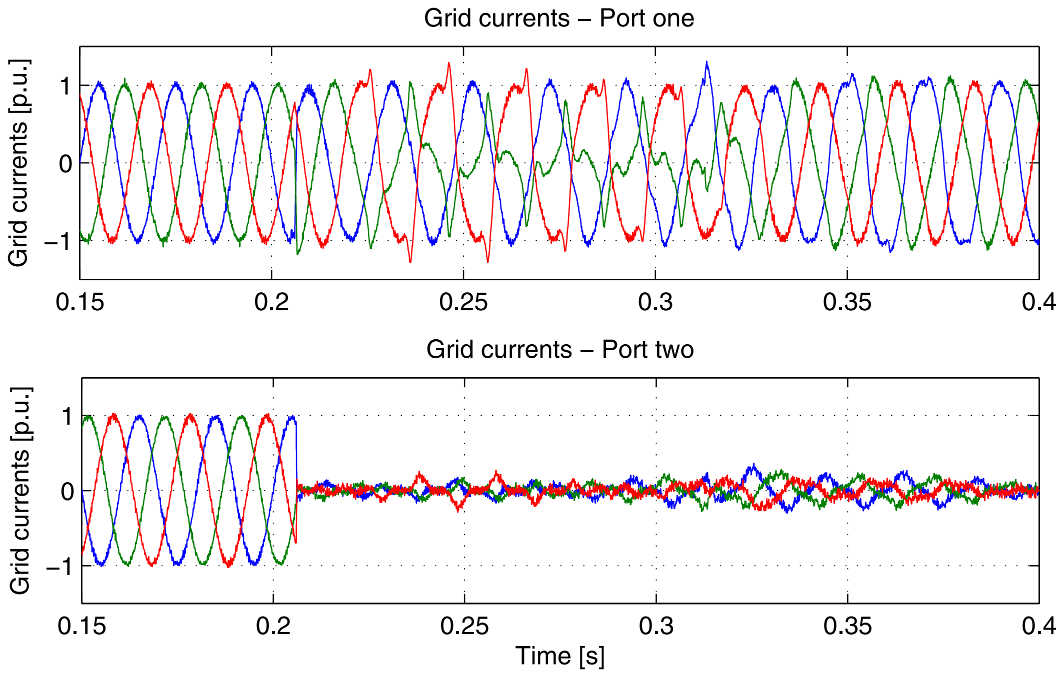

Fig. 5.159. Currents in port 1 and Port 2 during a two-phase short-circuit without ground.

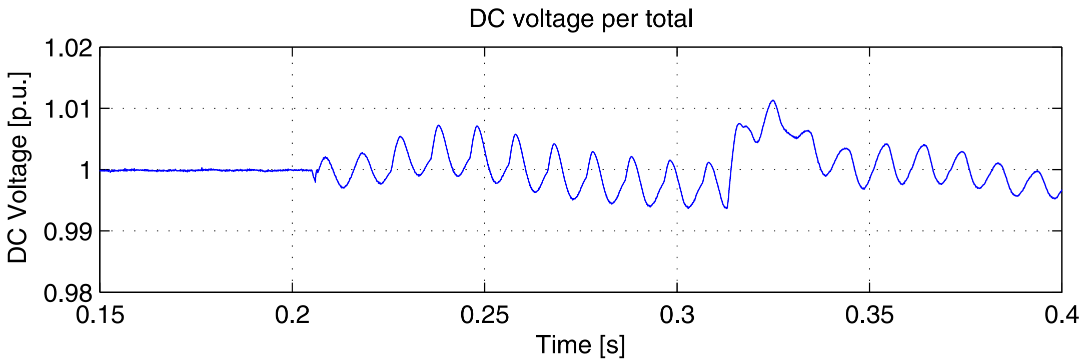

Fig. 5.160. Average DC-link voltage during a two-phase short-circuit without ground.

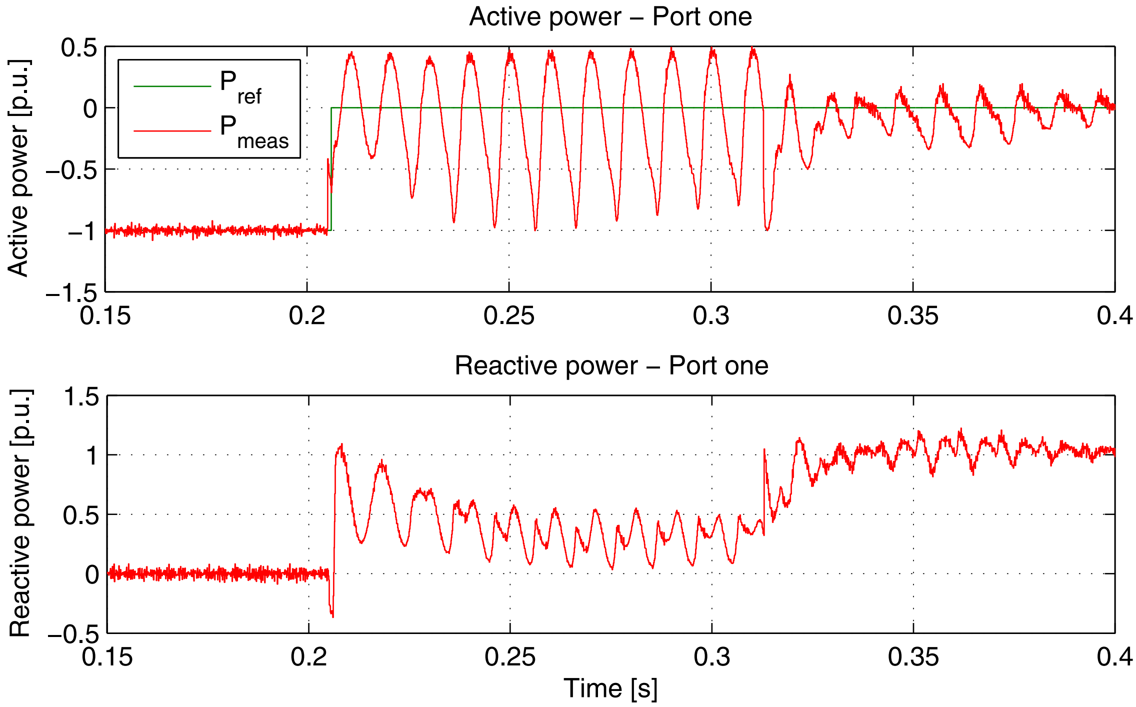

Fig. 5.161. Active and reactive power in Port 1 during a two-phase short-circuit without ground.

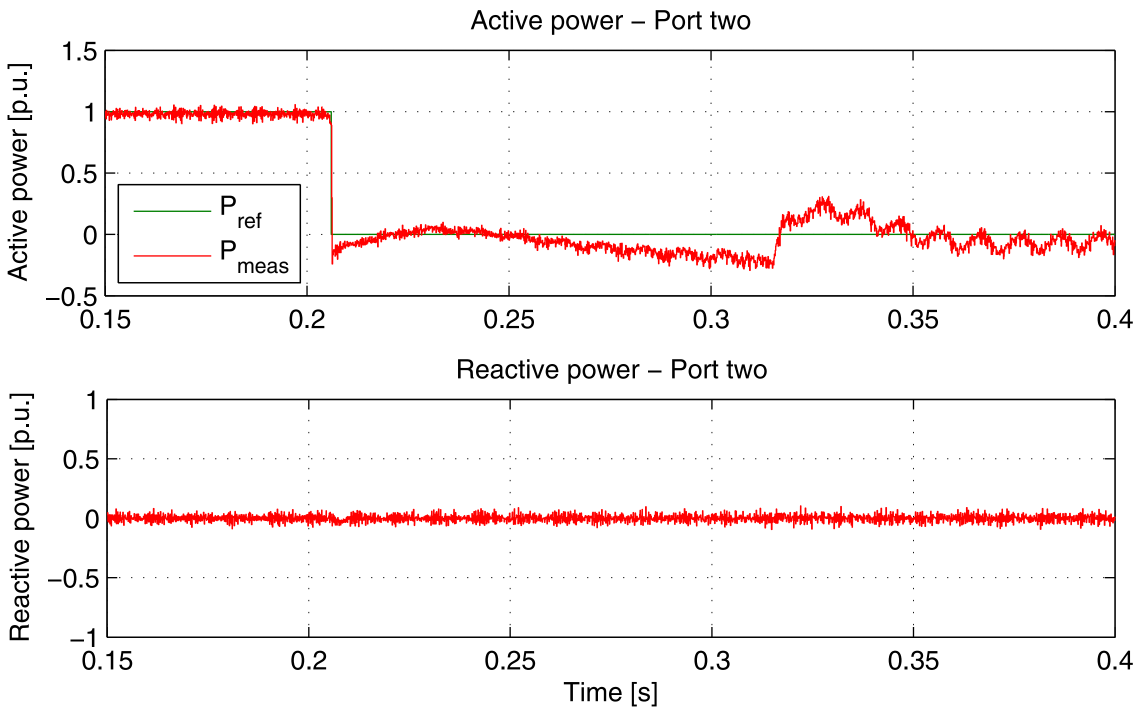

Fig. 5.162. Active and reactive power in Port 2 during a two-phase short-circuit without ground.

5.3.4.9 Two-Phase with ground Short-Circuit

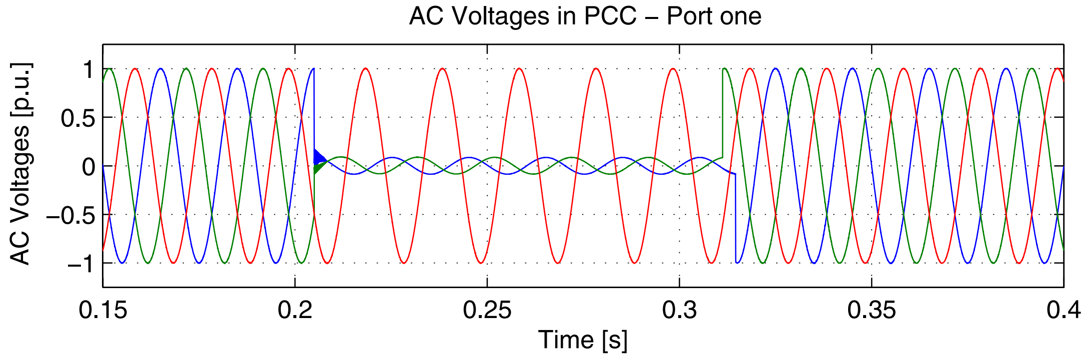

Fig. 5.163. Voltages in Port 1 during a two-phase short-circuit with ground.

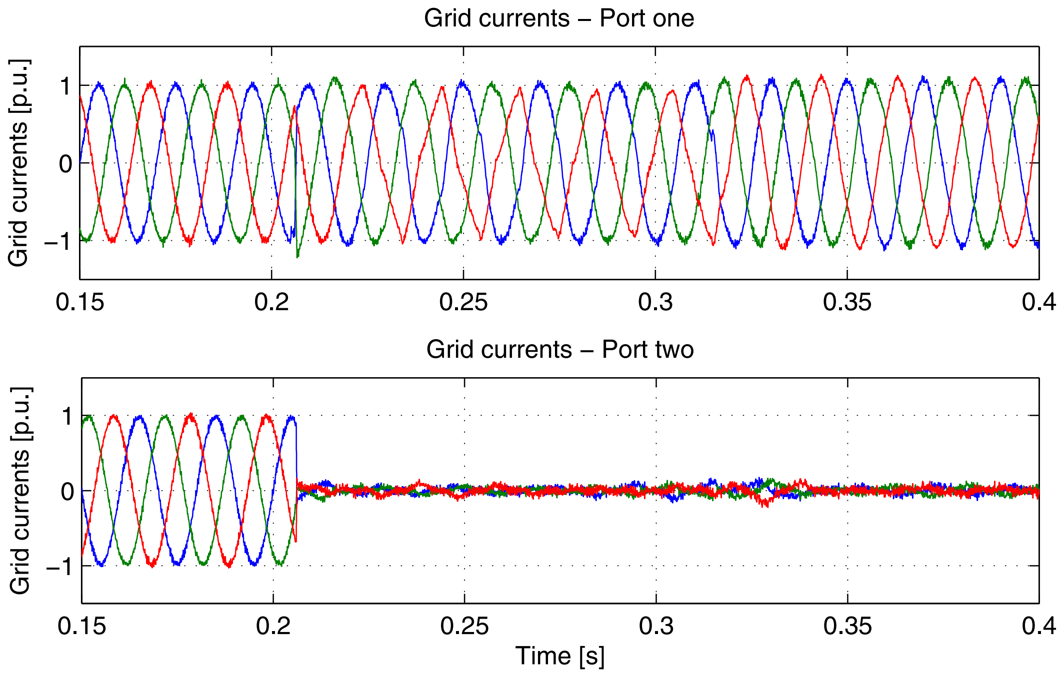

Fig. 5.164. Currents in Port 1 and Port 2 1 during a two-phase short-circuit with ground.

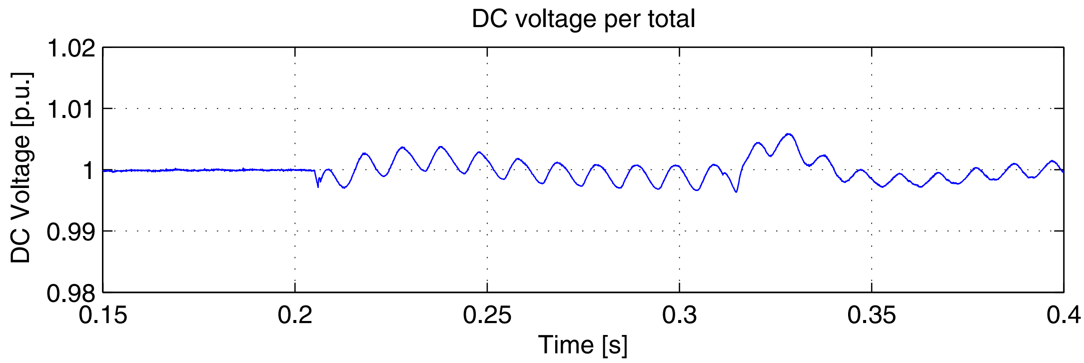

Fig. 5.165. Average DC-link voltage during a two-phase short-circuit with ground.

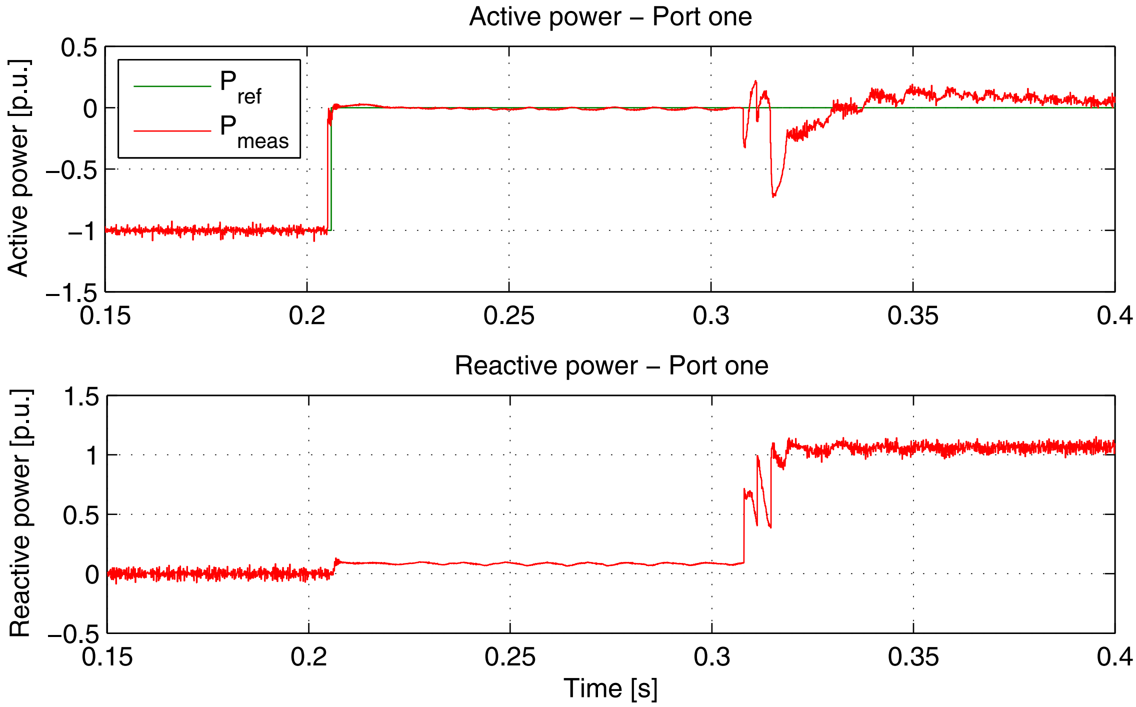

Fig. 5.166. Active and reactive power in port 1 during a two-phase short-circuit with ground.

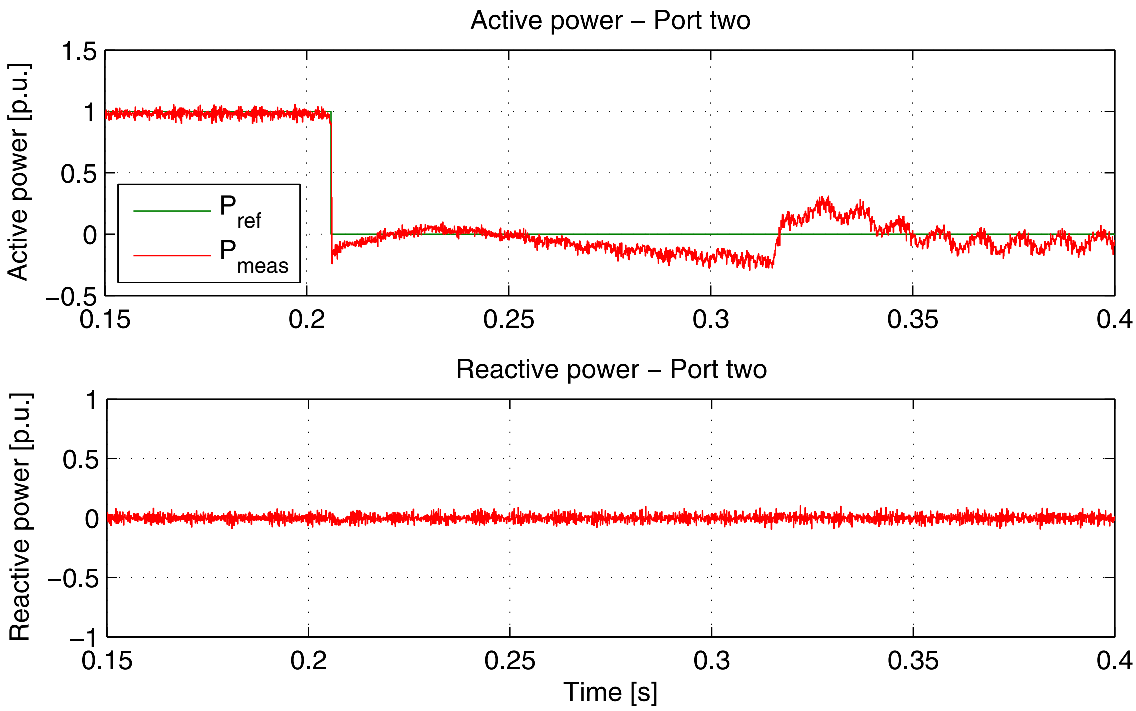

Fig. 5.167. Active and reactive power in port 2 during a two-phase short-circuit with ground.

5.3.4.10 Three-Phase Short-Circuit

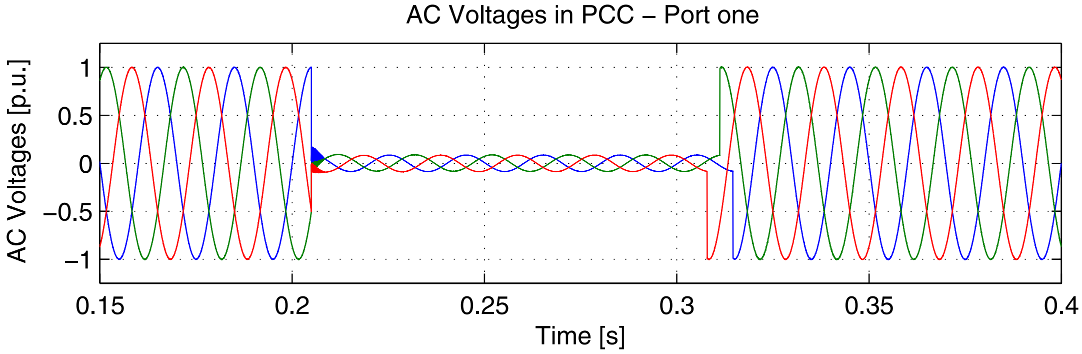

Fig. 5.168. Voltages in Port 1 during a three-phase short-circuit.

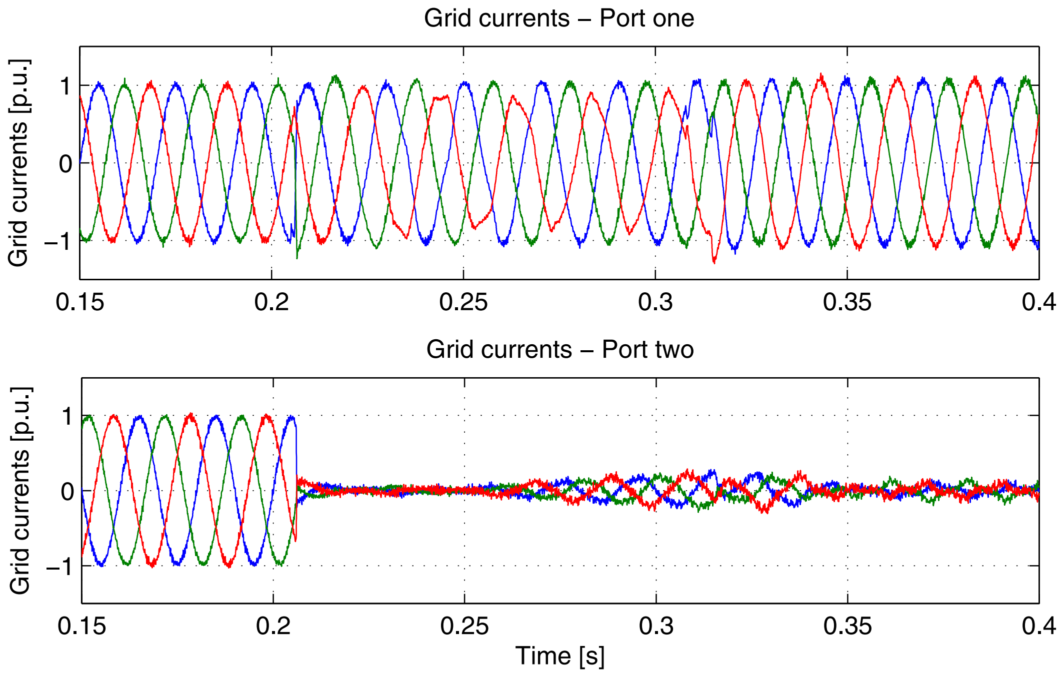

Fig. 5.169. Currents in Port 1 and Port 2 during a three-phase short-circuit.

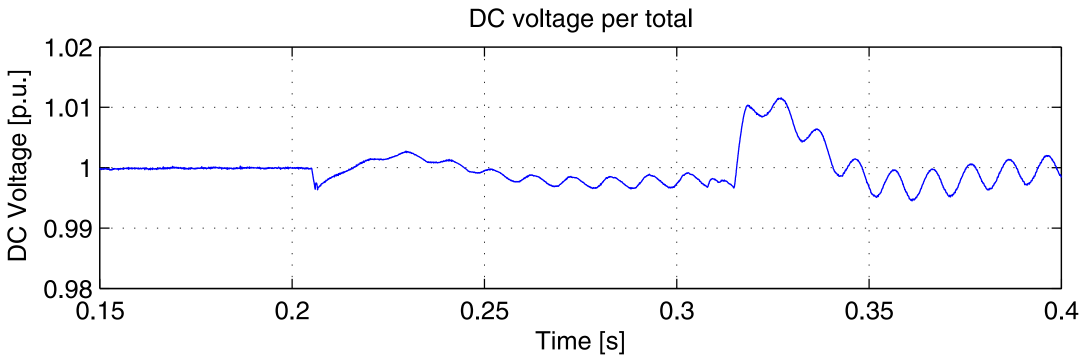

Fig. 5.170. Average DC-link voltage during a three-phase short-circuit.

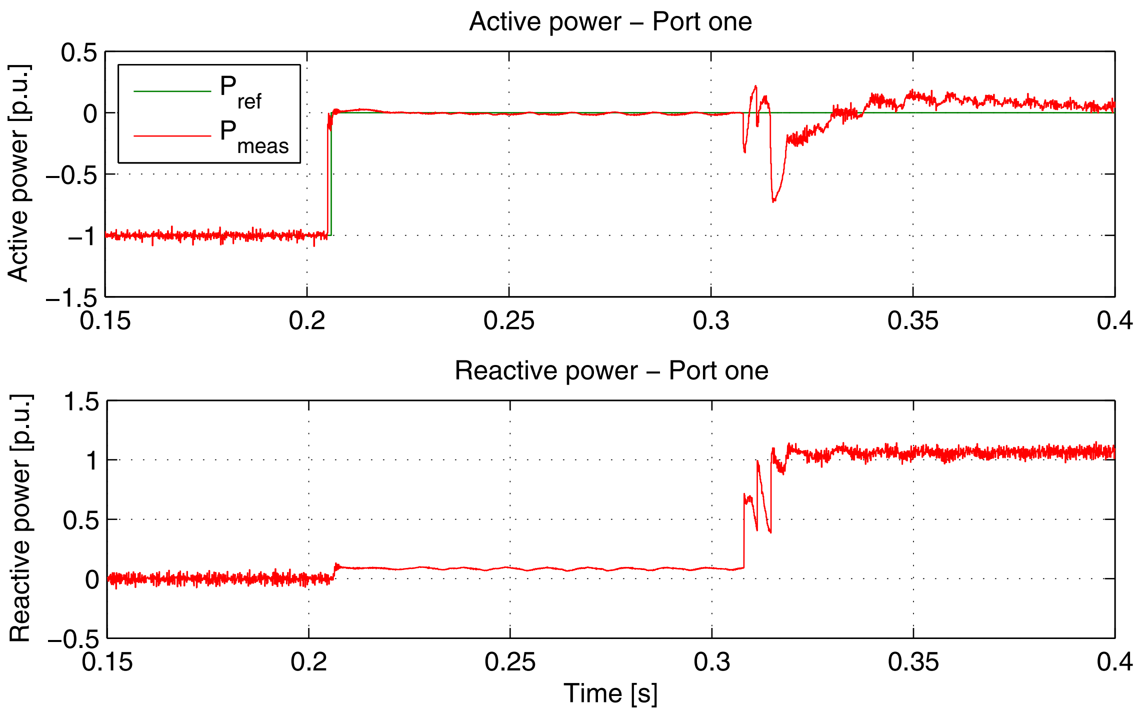

Fig. 5.171. Active and reactive power in Port 1 during a three-phase short-circuit.

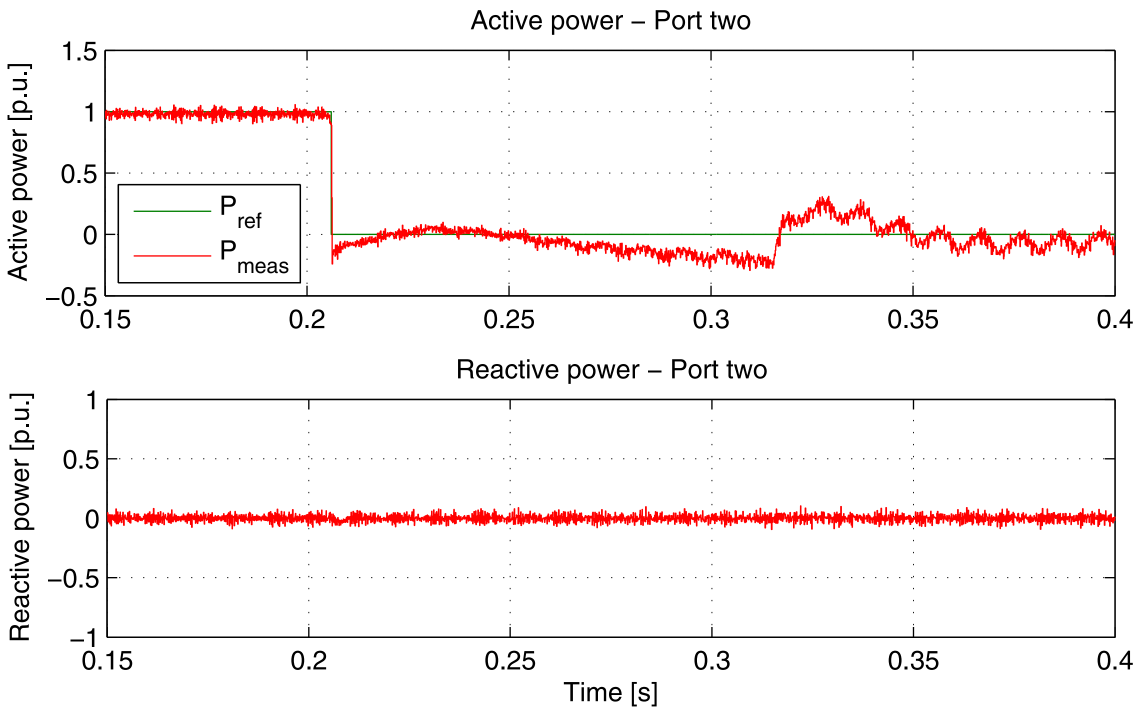

Fig. 5.172. Active and reactive power in Port 2 during a three-phase short-circuit

5.3.4.11 Conclusions

Based on the above simulation results it can be concluded that the natural reference frame control strategy with PR current controllers gives relatively good results in all considered study cases.

Very fast reversal of power and a complete decoupling of active and reactive power are obtained. The control structure is relatively insensitive to voltage excursions and unbalances being able to track the references. The control is able to "survive" the phase jumps from +60º to -60º. However, large excursions in the active and reactive power up to two times the rated power can be observed. Relatively large transients in the reactive power are obtained during the frequency excursions. All types of faults can be handled with good performances. The 100 Hz component is present in the active and reactive power output of the faulted port for the single-phase and two-phase without ground short-circuit. Also, large excursions in the active power can be observed especially for the two-phase without ground fault. The currents in the faulted port does not exceed the limits in all considered short-circuits. In all cases the currents in the faulted port are sinusoidal except the two-phase short-circuit without ground where they are distorted.

In all considered study cases the average DC-link voltage used in the control has variations below 1% except the phase-jumps case where the voltage overshoot is about 4%.

5.4 SUMMARY

A comprehensive analysis of four control strategies considered for the Uniflex-PM system was presented. Before drawing some conclusions regarding this analysis the following remarks must be made:

- No weighted limiter has been used in calculation of the reference currents;
- No limitations were imposed to the current controllers;
- Same parameters were used for the plant model as well as for the PLLs.

Using current limitations for the controllers as well as weighted limiters for calculation of the current references the current overshoot can be decreased for all control strategies.

Moreover the PLL parameters can be adjust for a better response in each case.

Based on the harmonic analysis the current THD for the considered control strategies is summarized in Fig. 5.173.

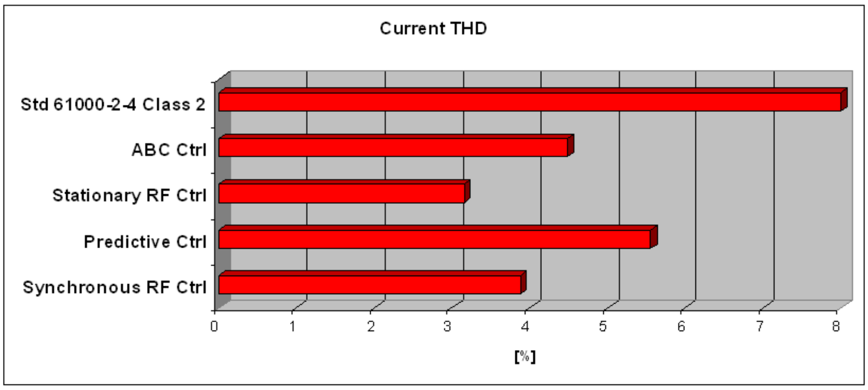

Fig. 5.173. Summary of the current THD for the control strategies under analysis.

Important values for low harmonic orders are present in the spectrum for the control strategies that consider a neutral connection i.e. the predictive control and the natural frame control with PR current controllers. Therefore, the THD is expected to be higher than the other two control strategies. However, considering a special neutral connection as well as harmonic compensation the THD is expected to be lower.

Regarding the control ability as well as the dynamic response under different grid conditions the selected control strategies have different performances.

A summary regarding the simulation studies for the selected control strategies under different grid condition is given in Table 5.3.

Table 5.3. Comparison of the control strategies under investigation.

Study case	**Synch Ref Frame**		**Predictive**		**Stationary Ref Frame**		**Natural Ref Frame**	
	PQ	Current	PQ	Current	PQ	Current	PQ	Current
Power flow	👍	👍	👍	👍	👍	👍	👍	👍
Voltage excursion	👍	👉	👉	👎	👍	👍	👍	👍
Voltage unbalances	👍	👍	👍	👍	👍	👍	👍	👍
Phase jumps	👉	👎	👎	👎	👉	👉	👎	👎
Frequency excursions	👍	👍	👍	👍	👍	👍	👍	👍
Single-phase Short-Circuit	👉	👎	👉	👎	👍	👍	👍	👍
Two-phase Short-Circuit	👉	👎	👉	👉	👍	👍	👉	👉
Two-phase SC with gnd	👉	👎	👎	👎	👍	👍	👍	👍
Three-phase Short-Circuit	👉	👎	👎	👎	👍	👍	👍	👍

In general the stationary reference frame ($\alpha\beta$) control has the best behaviour compared with the other control strategies while the synchronous reference frame control has the lowest performances especially during the faults.

All control strategies needs further attention especially regarding the tuning of the PLL parameters as well as the current limitation and weighting of current controllers;

6 CONCLUSIONS AND RECOMMENDATIONS

The present WP5 report assesses four control strategies for the Uniflex-PM system. These control strategies are evaluated under different grid condition and events though different study cases. It must be noticed that these study cases were designed to "push" the control to its limits. Most of the study cases cannot occur in the real operation of a power converter connected to MV networks. Therefore, these study cases must be considered as the "worst case scenario" as well as a benchmark of the control strategies.

It is not in the scope of this analysis to recommend the best control strategy. The main goal here was to identify the improvements that can be made so that the Uniflex-PM system can comply with any grid code and "survive" to any event into the electrical network.

Based on the analysis it can be concluded that the synchronous reference frame control needs further attention especially on the decomposition of the positive and negative sequences of the grid voltage. Also, the reactive power control for the sending end port must be improved. In order to comply with the power quality requirements some methods for harmonic cancellation especially for multiple of switching frequency must be investigated.

The predictive control that provides a fast current control on individual phases requires harmonic cancellation methods for harmonics up to the switching frequency. Special attention is needed for the 5th, 7th, 11th and 13th harmonics as well as for the neutral treatment. Further investigations are needed to improve the response when very fast variation of the grid voltage occurs.

The stationary reference frame control with PR current controllers seems to have the best performances compared to the other control strategies. However, harmonic cancelation methods for multiples of the switching frequency can be considered.

The natural reference frame control needs harmonic cancellation methods for harmonics up to the switching frequency as well as methods for neutral treatment. This control strategy seems to be very promising for separate control of power in each phase. Therefore, further investigations are necessary.

All control strategies needs further attention especially regarding the tuning of the PLL parameters as well as the current limitation and weighting of current controllers.

Handling of faults in the networks shall also be investigated. In the present analysis all control strategies provide 100% reactive current during and after the fault. Other control methods such as constant power factor, constant active power, etc. must be investigated.

The validation of the developed models and control strategies for the Uniflex-PM system is expected to be done in close cooperation with WP7.

7 REFERENCES

[1]. European Commission – New ERA for electricity in Europe. Distributed Generation: Key Issues, Challenges and Proposed Solutions, EUR 20901, 2003, ISBN 92-894-6262-0;

[2]. European Commission – Towards Smart Power Networks. Lessons learned from European research FP5 projects, EUR 21970, 2005, ISBN 92-79-00554-5;

[3]. Uniflex-PM – Deliverable D3.1 Report on Converter structures, November 2007

[4]. Bin Wu – "High-Power Converters and AC Drives", *IEEE Press, Wiley Interscience 2006, ISBN 10-0-471-73171-4*.

[5]. Uniflex-PM – Deliverable D 4.1 Report on isolation module efficiency, December 2007;

[6]. EnergiNet – Grid connection of wind turbines to networks with voltages below 100 kV, Regulation TF 3.2.6, May 2004, p. 29;

[7]. Energinet - Grid connection of wind turbines to networks with voltages above 100 kV, Regulation TF 3.2.5, December 2004, p. 25;

[8]. F. Iov, R. Teodorescu, F. Blaabjerg, B. Andresen, J. Birk, J. Miranda – *Grid code compliance of grid-side converter in wind turbine systems*, Proceed. of PESC 2006 Conference, 18-22 June 2006, Jeju, South-Korea, 7 p., IEEE Catalog Number: 06CH37819C, ISBN: 1-4244-9717-7, ISSN 02-75-9306;

[9]. DS/EN 50160 – Voltage characteristics of electricity supplied by public distribution systems, 2nd edition, June 2000.

[10]. DS/EN 61000 - *Electromagnetic compatibility – Compatibility levels in industrial plants for low-frequency conducted disturbances*. 2nd Edition, September 2002;

[11]. M. Ciobotaru, T. Kerekes, R. Teodorescu and A. Bouscayrol - PV inverter simulation using MATLAB/Simulink graphical environment and PLECS blockset

[12]. F. Iov, A.D. Hansen, P. Soerensen, N.A. Cutululis – *Mapping of grid faults and grid codes*, Risø-R-1617(EN) July 2007,41 p., ISSN 0106-2840, ISBN 978-87-550-3622-2.

[13]. M. H. J. Bollen – *Understanding Power Quality Problems. Voltage sags and interruptions*, IEEE Press Series on Power Engineering, 2000, ISBN 0-7803-4713-7.

[14]. IEEE Std. 1159/1995 – *IEEE Recommended Practice for Monitoring Electric Power Quality*, June 1995;

[15]. IEEE Std. 1250-1995 – *IEEE Guide for service to equipment sensitive to momentary voltage disturbances*, March 1995;

[16]. F. Iov, M. Ciobotaru, D. Sera, R. Teodorescu, F. Blaabjerg - *Power Electronics and Control of Renewable Energy Systems*, keynote paper in Proc. of The 7th International Conference on Power Electronics and Drives Systems, PEDS 07, 27-30 november 2007, Bangkok, Thailand, 23 p. ISBN 1-4244-0645-5

[17]. F. Iov, F. Blaabjerg - UNIFLEX-PM. *Advanced power converters for universal and flexible power management in future electricity network – Converter applications in future European electricity network*. Deliverable D2.1, EC Contract no. 019794(SES6), February 2007, p. 171,

[18]. Myo Thu Aung, Jovica Milanovic – *The influence of transformer winding connection on the propagation of voltage sags*, IEEE Trans on Power Delivery, vol. 21, no. 1, January 2006, pp.262-269;

[19]. D.S. Dorr – *Point of Utilization Power Quality Study results*, IEEE Trans on Industry Applications, vol. 3, no. 4, July/August 1995, pp. 658-666;
[20]. D.S. Dorr, M.B. Hughes, T.M. Gruzs, R.E. Jurewicz, J.L. McClaine – *Interpreting Recent Power Quality Surveys to Define the Electrical Environment*, IEEE Trans on Industry Applications, vol. 33, no. 6, November/December 1997, pp. 1480-1487;
[21]. CRISP – *Distributed Intelligence in Critical Infrastructures for Sustainable Power, Functional specifications of electric networks with high degrees of distributed generation*, Deliverable D1.1, ENK8-CT-2002-00673, June 2003.
[22]. www.nordel.org;
[23]. M.J. Voeten – *16 years of fault statistics in the Dutch LV, MV and HV distribution networks.*
[24]. F. Iov, M. Ciobotaru, F. Blaabjerg, *"Power Electronics Control of Wind Energy in Distributed Power Systems"*, keynote paper in Proc. of Optim'08, May 2008, Brasov, Romania, in press.
[25]. F. M. Gardner, *"Phase Lock Techniques*". New York: Wiley, 1979.
[26]. F. Mur, V. Cardenas, J. Vaquero, and S. Martinez, *"Phase synchronization and measurement digital systems of AC mains for power converters"*, Proc. of CIEP, 1998, pp. 188-194.
[27]. J. W. Choi, Y.K. Kim, and H.G. Kim*, "Digital PLL control for single-phase photovoltaic system"*, IEE Trans. on Electric Power Applications, 2006, Vol. 153, pp. 40-46..
[28]. S.-K. Chung, *"A phase tracking system for three phase utility interface inverters*" IEEE Trans. on Power Electronics, Vol. 15, No. 3, pp. 431–438, 2000.
[29]. C. T. Nguyen and K. Srinivasan, *"A New Technique for Rapid Tracking of Frequency Deviations Based on Level Crossings"* IEEE Trans. on Power Apparatus and Systems, 1984, Vol. PAS-103, pp. 2230-2236.
[30]. B.P. McGrath, D.G. Holmes, J.J.H. Galloway, *"Power converter line synchronization using a discrete Fourier transform (DFT) based on a variable sample rate"*, IEEE Trans. on Power Electronics, 2005, Vol. 20, pp. 877-884
[31]. O. Vainio, S. J. Ovaska, and M. Polla, *"Adaptive filtering using multiplicative general parameters for zero-crossing detection",* IEEE Trans. on Industrial Electronics, 2003, vol. 50, pp. 1340-1342.
[32]. S. Valiviita, S. J. Ovaska, and J. Kyyra, *"Adaptive signal processing system for accurate zero-crossing detection of cycloconverter phase currents"*, Proc. of PCC'97, 1997, Vol.1, pp. 467-472.
[33]. O. Vainio and S. J. Ovaska, "*Noise reduction in zero crossing detection by predictive digital filtering"*, IEEE Trans. on Industrial Electronics, 1995, vol. 42, pp. 58-62.
[34]. R.W. Wall, *"Simple methods for detecting zero crossing"*, Proc. of IECON, 2003, Vol.3, pp. 2477-2481.
[35]. S. Valiviita, *"Neural network for zero-crossing detection of distorted line voltages in weak AC-systems"*, Proc. of IMTC, 1998, Vol.1, pp. 280-285.
[36]. S. Das, P. Syam, G. Bandyopadhyay, and A.K. Chattopadhyay, *"Wavelet transform application for zero-crossing detection of distorted line voltages in weak AC-systems"*, Proc. of INDICON, 2004, pp. 464-467.
[37]. S. Valiviita, *"Zero-crossing detection of distorted line voltages using 1-b measurements"*, IEEE Trans. on Industrial Electronics, 1999, Vol. 46, pp. 917-922.

[38]. R. Weidenbrug, F. P. Dawson, and R. Bonert, *"New synchronization method for thyristor power converters to weak"*, IEEE Trans. on Industrial Electronics, 1993, Vol. 40, pp. 505-511.

[39]. D.M. Baker and V.G. Agelidis, *"Phase-locked loop for microprocessor with reduced complexity voltage controlled oscillator suitable for inverters"*, Proc. of PEDES, 1998, Vol.1, pp. 464-469.

[40]. D. Nedeljkovic, J. Nastran, D. Voncina, and V. Ambrozic, *"Synchronization of active power filter current reference to the network"*, IEEE Trans. on Industrial Electronics, 1999, vol. 46, pp. 333-339.

[41]. D. Nedeljkovic, V. Ambrozic, J. Nastran, and D. Hudnik, *"Synchronization to the network without voltage zero-cross detection"*, Proc. of MELECON, 1998, Vol. 2, pp. 1228-1232.

[42]. L. N. Arruda, S. M. Silva, and B. Filho, *"PLL structures for utility connected systems*," in Proc. of IAS'01, vol. 4, 2001, pp. 2655–2660.

[43]. S.-K. Chung, *"Phase-Locked Loop for grid-connected three-phase power conversion systems*," IEE Proceedings on Electronic Power Applications, vol. 147, no. 3, pp. 213–219, 2000.

[44]. V. Kaura and V. Blasko, *"Operation of a phase loop system under distorted utility conditions*," IEEE Trans. on Industry Applications, vol. 33, no. 1, pp. 58–63, 1997.

[45]. M. Karimi-Ghartemani and M. Iravani, *"A method for synchronization of power electronic converters in polluted and variable-frequency environments*," IEEE Trans. on Power Systems, vol. 19, no. 3, pp. 1263–1270, 2004.

[46]. P. Rodriguez, J. Pou, J. Bergas, I. Candela, R. Burgos, and D. Boroyevich, *"Double synchronous reference frame PLL for power converters"* in Proc. of PESC'05, 2005, pp. 1415–1421.

[47]. M. C. Benhabib and S. Saadate, *"A new robust experimentally validated Phase-Looked Loop for power electronic control,"* EPE Journal, vol. 15, no. 3, pp. 36–48, August 2005.

[48]. S. Lee, J. Kang, and S. Sul, *"A new phase detection method for power conversion systems considering distorted conditions in power system,"* in Proc. of IAS'99, vol. 4, 1999, pp. 2167–2172.

[49]. H.-S. Song, H.-G. Park, and K. Nam, *"An instantaneous phase angle detection algorithm under unbalanced line voltage condition"*, Proc. of PESC'99, vol. 1, 27 June-1 July 1999, pp. 533–537.

[50]. S. M. Silva, B. M. Lopes, B. J. C. Filho, R. P. Campana, and W. C. Bosventura, *"Performance evaluation of PLL algorithms for single-phase grid-connected systems"*, Proc. of IAS, 2004, Vol. 4, pp. 2259-2263.

[51]. J. Salaet, S. Alepuz, A. Gilabert, and J. Bordonau, *"Comparison between two methods of DQ transformation for single phase converters control. Application to a 3-level boost rectifier"*, Proc. of PESC, 2004, Vol.1, pp. 214-220.

[52]. M. Ciobotaru, R. Teodorescu, and F. Blaabjerg, *"Improved PLL structures for single-phase grid inverters"*, Proc. of PELINCEC, 2005, pp. 1-6.

[53]. M. Saitou, N. Matsui, and T. Shimizu, *"A control strategy of single-phase active filter using a novel d-q transformation"*, Proc. of IAS'03, 2003, Vol. 2, pp. 1222-1227.

[54]. L. N. Arruda, B. J. Cardoso Filho, S. M. Silva, S. R. Silva, and A. S. A. C. Diniz, *"Wide bandwidth single and three-phase PLL structures for grid-tied"*, Proc. of Photovoltaic Specialists Conference, 2000, pp. 1660-1663.

[55]. M. Ciobotaru, R. Teodorescu, and F. Blaabjerg, *"A New Single-Phase PLL Structure Based on Second Order Generalized Integrator"*, Proc. of PESC, 2006, pp. 1-6.

[56]. K. De Brabandere, T. Loix, K. Engelen, B. Bolsens, J. Van den Keybus, J. Driesen, and R. Belmans, *"Design and Operation of a Phase-Locked Loop with Kalman Estimator-Based Filter for Single-Phase Applications"*, Proc. of IECON, 2006, pp. 525-530.

[57]. A. Timbus, P. Rodriguez, R. Teodorescu and F. Blaabjerg, *"Grid monitoring for distribution power generation systems to comply with grid codes"*, Proc. of ISIE'06, pp. 1601-1607, 2006.

[58]. A. Timbus, M. Liserre, R. Teodorescu, P. Rodriguez and F. Blaabjerg, *"PLL algorithm for power generation systems robust to grid voltage faults"*, Proc. of PESC'06, pp. 1-7, 2006.

[59]. M.P. Kazmierkowski, R. Krishnan, F. Blaabjerg, *"Control in Power Electronics-Selected problems"*, Academic Press, 2002. ISBN 0-12-402772-5.

[60]. long-Seok Song; Kwanghee Nam, *Dual current control scheme for PWM converter under unbalanced input voltage conditions*, IEEE Transactions on Industrial Electronics, Volume 46, Issue 5, Oct. 1999 Page(s):953 – 959.

[61]. Yongsug Suh; Lipo, T.A. - *Modeling and analysis of instantaneous active and reactive power for PWM AC/DC converter under generalized unbalanced network*; IEEE Transactions on Power Delivery, Volume 21, Issue 3, July 2006 Page(s):1530 – 1540

[62]. Lenwari, Wanchak; Sumner, Mark; Zanchetta, Pericle; Culea, Mihai - *A High Performance Harmonic Current Control for Shunt Active Filters Based on Resonant Compensators*; IECON 2006, Nov. 2006 Page(s):2109 – 2114

[63]. Monopoli, V.G.; Gerry, D.; Zanchetta, P.; Clare, J.C.; Wheeler, P.W.; A low frequency predictive current control for multilevel active rectifiers Power Electronics Specialists Conference, 2004. PESC 04. 2004 IEEE 35th Annual Volume 5, 20-25 June 2004 Page(s):3553 - 3558 Vol.5